Sulfur Polymers as Antibacterial Particles and Surfaces

Thesis submitted in accordance with the requirements of the University of Liverpool for the degree of Doctor in Philosophy by:

Romy Ambretta Dop

April 2023

Supervisor: Dr Thomas Hasell

Secondary supervisor: Dr Daniel Neill

Acknowledgements

First of all I would like to express my gratitude to my supervisors, Dr Tom Hasell and Dr Daniel Neill. It goes without saying that I am extremely grateful to have had a great supervision team behind me throughout this PhD, without which I wouldn't have got this far. During meetings and catch ups I have only ever been met with positivity and encouragement, which has made studying for this PhD an enjoyable experience.

I would like to thank everyone in the Hasell group for all of the encouragement and support, and more importantly for being great company whenever I was in spells of procrastination. The laughs and positivity made trying times seem a breeze! I definitely would not have survived the heatwave at YRM to be able to write this without you guys. Thank you to everyone at the Ronald Ross for helping me navigate a new field and lab, and for always being so willing to help me out whenever I have needed it. Sydney, Ellie, Lauren and Robyn thank you for all the lunch breaks and bottomless brunches, those breaks were the boost my one remaining brain cell needed to get going again!

I am grateful for my very supportive family. Thank you to my Mam and Dad who have always encouraged me and always had a door open when I have needed a break. Dad, I think I can now answer yes to all the "have you finished your course yet?" questions. Thank you Suzanne and Kevin for also always having a door open for me, literally, letting us gate crash for 6 months and for when I have been stranded after snapping my house key(!).

Finally, thank you Will for being an incredible partner. Your encouragement and love throughout the years got me through the toughest of times, and has seen me through the best. Thank you for always giving me the motivation to carry on.

List of Publications

Publications discussed in this thesis:

1. **Dop, R. A.**; Neill, D. R.; Hasell, T. Antibacterial Activity of Inverse Vulcanized Polymers. *Biomacromolecules*, 2021, *22* (12), 5223–5233 **– Discussed in Chapter 2**
2. **Dop, R. A.**; Neill, D. R.; Hasell, T. Sulfur-polymer Nanoparticles: Preparation and Antibacterial Activity. *ACS Appl. Mater. Interfaces*, 2023, *15* (17), 20822-20832**– Discussed in Chapter 3**

Other publications:

1. Upton, R. L.; **Dop, R. A.**; Sadler, E.; Lunt, A. M.; Neill, D. R.; Hasell, T.; Crick, C. R. Investigating the Viability of Sulfur Polymers for the Fabrication of Photoactive, Antimicrobial, Water Repellent Coatings. *J. Mater. Chem. B*, 2022, *10* (22), 4153–4162.
2. Wang, H.; Zhang, B.; **Dop, R.**; Yan, P.; Neale, A. R.; Hardwick, L. J.; Hasell, T. Oxygen Heteroatom Enhanced Sulfur-Rich Polymers Synthesized by Inverse Vulcanization for High-Performance Lithium-Sulfur Batteries. *J. Power Sources*, 2022, *545*, 231921.
3. Zhang, B.; Petcher, S.; **Dop, R. A.**; Yan, P.; Zhao, W.; Wang, H.; Dodd, L. J.; McDonald, T. O.; Hasell, T. Inverse Vulcanised Sulfur Polymer Nanoparticles Prepared by Antisolvent Precipitation. *J. Mater. Chem. A*, 2022, *10* (26), 13704–13710.

Abstract

Antimicrobial resistance has become a global health threat due to the emergence and persistence of multidrug-resistant bacteria, therefore the discovery and development of novel antimicrobial agents is of utmost importance. Sulfur containing compounds such as cephalosporins and sulphonamides are amongst the most important antimicrobial agents used clinically. More recently, there is growing interest in polysulfides as novel antimicrobial agents inspired by the antimicrobial activity of natural polysulfides found in garlic and onions.

In 2013, a new class of high sulfur content polymers coined 'inverse vulcanised polymers' were reported by Pyun and co-workers. Inverse vulcanised polymers can be synthesised sustainably using elemental sulfur, a by-product of the petrochemical industry, stabilised with other waste or naturally derived products. High sulfur content polymers have been investigated for use as novel optical devices, cathode materials for Li-S batteries, smart fertilisers and as sorbents for environmental remediation. One potential application of high sulfur content polymers that has been overlooked is their potential as novel antibacterial materials.

The work presented in this thesis discusses the antibacterial properties of high sulfur content polymers synthesised by inverse vulcanisation, and their potential applications as antibacterial polymer nanoparticles and surface coatings. Sulfur polymers have been found to have antibacterial activity against both Gram-negative and Gram-positive pathogens, where the sulfur content, comonomer type and the glass transition temperature of the materials were found to impact these properties. Sulfur polymer nanoparticles can be prepared by antisolvent based methods, which were found to have antibacterial activity, low cytotoxicity and potential applications as combination therapies with other antibiotics. Superhydrophobic surfaces can also be fabricated from spray deposition of sulfur polymer composites with potential applications as antibacterial surface coatings.

Contents

Abbreviations

ANOVA	Analysis of variance
DADS	Diallyldisulfide
DAS	Diallylsulfide
DATS	Diallyltrisulfide
DCPD	Dicyclopentadiene
DIB	1,3-diisopropenylbenzene
DLS	Dynamic light scattering
DMF	Dimethylformamide
DSC	Differential scanning calorimetry
DVB	Divinylbenzene
EDS	Energy-dispersive X-ray spectroscopy
EPS	Extracellular polymeric matrix
FT-IR	Fourier transform-infrared
HMDS	Hexamethyldisilazane
ICP-OES	Inductively Coupled Plasma Optical Emission Spectroscopy
LB	Luria-Bertani
LPS	Lipopolysaccharide
MIC	Minimum inhibitory concentration
MTT	3-[4,5-dimethylthiazole-2-yl]-2,5-diphenyltetrazolium bromide
NMR	Nuclear magnetic resonance
PABA	*para*-aminobenzoic acid
PBS	Phosphate buffered saline
ROS	Reactive oxygen species

SEM	Scanning electron microscopy
T_g	Glass transition temperature
THF	Tetrahydrofuran
TLC	Thin layer chromatography
WCA	Water contact angle
XPS	X-ray photoelectron spectroscopy

Chapter 1

Introduction

1.1 Background

Element 16 of the periodic table, sulfur, also known as “brimstone” (“burning stone”) is the 16th most abundant element in nature. Sulfur occurs mainly as sulfides (S^{2-}) an example of such being iron sulfide, also known as “fool’s gold”, and sulfates (SO_4^{2-}) such as calcium sulfate. Documented throughout history and featuring in the book of Genesis, sulfur is one of the key elements in modern society.[1] The Claus process, utilised in the petrochemical industry has become one of the main production pathways of elemental sulfur. In recent years, where the negative impact of the chemical industry upon the environment is unable to be ignored, there has been a growing focus on sustainability across all areas of chemistry. Also known as ‘Green Chemistry’, sustainable chemistry aims to reduce the detrimental effects of some processes by replacing hazardous feedstocks with safer alternatives, conserving energy and reducing waste.[2] The petrochemical industry have focussed on the hydrodesulfurisation and the Claus process in effort to move towards the improved production of petroleum products. Hydrodesulfurisation involves the removal of unwanted sulfur atoms in petroleum feedstocks by employing high temperatures and pressures with heterogeneous catalysis (Equation 1.1). High sulfur content petroleum is particularly problematic for the pipelines used in the processing plants due to corrosion which increases the cost of process.[3] Furthermore, the combustion of sulfur containing compounds in petroleum fuels produces sulfur oxides such at sulfur dioxide which are emitted into the atmosphere and are responsible for the generation of acid rain.[4]

$$[\text{R-S}] + \text{H}_2 \xrightarrow{\text{cat}} [\text{R-H}] + \text{H}_2\text{S} \qquad (1.1)$$

The by-product of the hydrodesulfurization process is hydrogen sulfide (H_2S),is a highly toxic gas that can be used as a source of elemental sulfur, which is non-hazardous. The Claus process,

patented in 1883 by C. F. Claus is the most significant sulfur recovery process from hydrogen sulfide, it is a two-step process that requires temperatures exceeding 1100 ºC (Equations 1.2).[5]

$$2H_2S + 3O_2 \longrightarrow 2SO_2 + 2H_2O$$
$$4H_2S + 2SO_2 \longrightarrow 3S_2 + 4H_2O \qquad (1.2)$$

According to the U.S. Geological Survey, in 2019 the worldwide annual production of elemental sulfur exceeded 80 million tonnes, with the majority produced *via* the Claus process. The production of elemental sulfur far exceeds its consumption, where it is mainly used for the production of sulfuric acid, a commodity chemical used for the synthesis of phosphoric fertilizers, and responsible for terming the 19th century as the "Sulfur Age".[1,6] Another notable use of elemental sulfur is for the vulcanisation of rubber, discovered in 1839 by Charles Goodyear. Vulcanisation refers to the addition of sulfur to the production of rubbers such as polyisoprene. The addition of sulfur to the process leads to highly crosslinked networks which manifests itself as hardened rubber, used for the manufacture of car tyres.[7] The carbon-carbon double bonds in rubber act as the reactive sites for the crosslinking process whereby sulfur atoms can add across forming 3-dimensional polymer networks.[8] Although the vulcanisation of rubber was discovered more than a 180 years ago, the detailed mechanism of this process is still unknown. Whether the reactions proceed *via* a free-radical mechanism (Figure 1.1), an ionic mechanism (Figure 1.2), or both, remains an uncertainty.[9–11] The difficulty in underpinning the mechanistic pathways of vulcanisation with sulfur are partly due to the insolubility of such highly crosslinked materials and the number of reagents used during vulcanisation.[12,13]

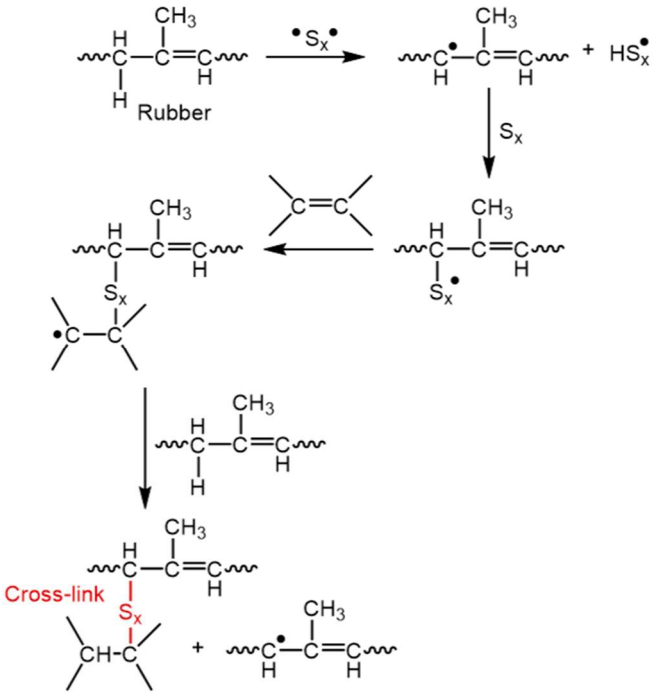

Figure 1.1: Free radical mechanism for vulcanisation as proposed by Farmer and Shipley (1946).[10,11]

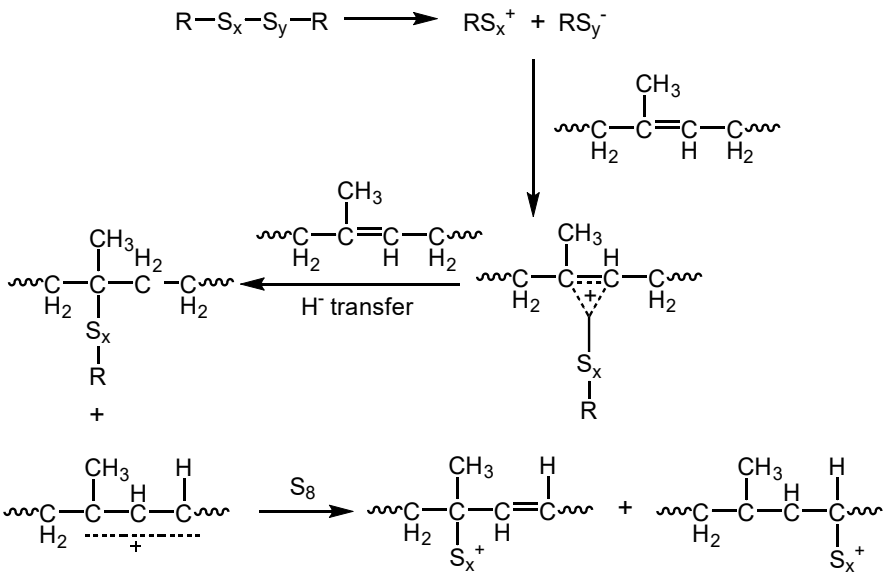

Figure 1.2: Ionic mechanism for vulcanisation as proposed by Bateman *et al.* (1958).[9]

1.2 Inverse Vulcanisation

Sulfur has the highest number of solid allotropes amongst all of the elements, most of which consist of cyclic molecules. The most common form of elemental sulfur is 8-membered sulfur rings (S_8), which can exist as several allotropes.[14] At ambient temperature, the main form of S_8 is the orthorhombic (S_α) allotrope. The solid melts at a temperature around 115 ºC to give a clear yellow liquid. Upon cooling of the molten sulfur, sulfur can exist in its monoclinic (S_β) form which reverts back to the thermodynamically favoured S_α allotrope, an observation first made in 1825 by Eilhard Mitscherlich.[15] At temperatures exceeding 159 ºC, known as the floor temperature of sulfur, ring opening polymerisation of the S_8 rings can occur giving viscous orange solutions followed by deep-red coloured polymeric sulfur upon continued heating (Figure 1.3).[16,17]

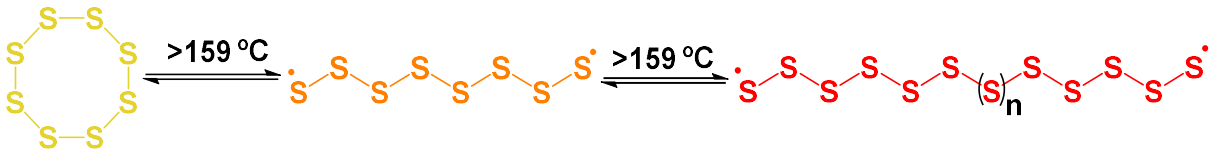

Figure 1.3: Thermally initiated ring-opening polymerisation of elemental sulfur. The colours are representative of the different states of sulfur during polymerisation. Figure adapted from "Sulfur Chemistry in Polymer and Materials Science" by Theato *et al.* [17]

The terminal sulfur radicals on the ends of polymeric sulfur can promote backbiting depolymerisation back to the thermodynamically favoured cyclic form of elemental sulfur. As a result, polymeric sulfur cannot be processed into useful materials. In 2013 Pyun and co-workers demonstrated that the copolymerisation of elemental sulfur with the vinylic monomer 1,3-diisopropenylbenzene (DIB) (Figure 1.4) allowed for the synthesis of stable high sulfur content materials.

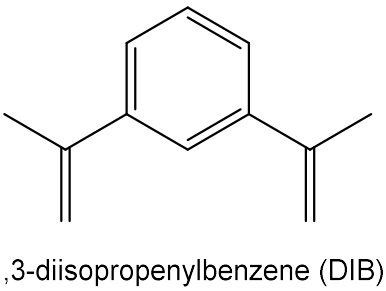

Figure 1.4: The chemical structure of 1,3-diisopropenylbenzene (DIB).

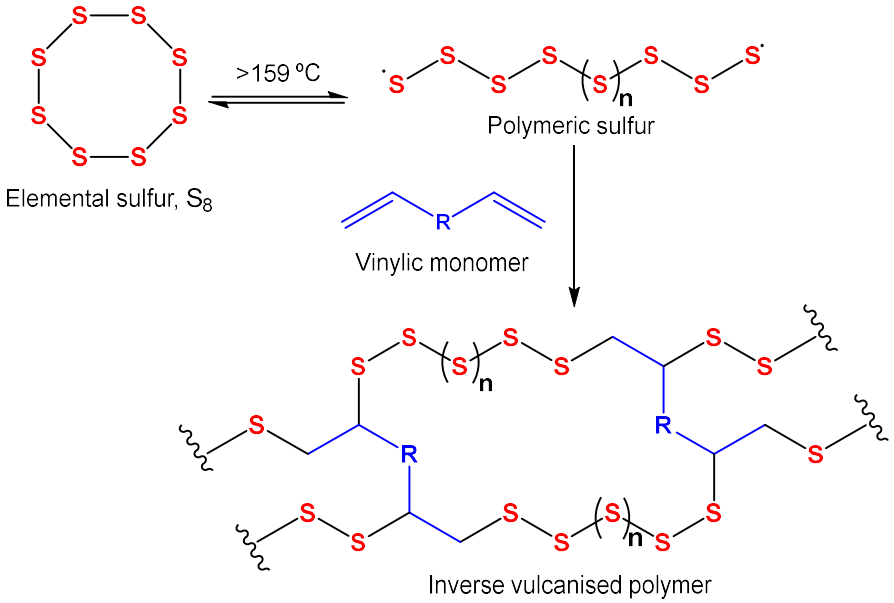

Figure 1.5: A general scheme for the inverse vulcanisation of sulfur with a vinylic monomer.[18]

This experimental method, coined 'inverse vulcanisation' demonstrates the ability to form polymers from elemental sulfur and a small amount of vinylic comonomer, the converse of conventional vulcanisation which implements sulfur as a minor component of the reaction feedstock (Figure 1.5).[19] The novel polymer synthesised by Pyun and coworkers termed poly(sulfur-*random*-1,3-diisopropenylbenzene) (S-DIB) containing 70 wt% sulfur showed interesting optical properties and maintained electrochemical activity showing potential applications in lithium-sulfur (Li-S) batteries. Since 2013, research and interest in inverse vulcanisation has increased due to the worldwide problem of excess sulfur, evident from the so-called 'great sulfur pyramid of Alberta' in Canada which continues to increase in size

(Figure 1.6).[20] The products of inverse vulcanisation are often referred to as inverse vulcanised polymers[21], sulfur polymers, thiopolymers[22] and organically modified chalcogenides.[23] All terms relate to the same class of material derived from the polymerisation of elemental sulfur.[24] Inverse vulcanisation allows for the synthesis of cheap functional materials from elemental sulfur, whilst simultaneously tackling the problem of sulfur stockpiles. In addition to this, it is a solvent-free method with high atom-economy allowing for large-scale synthesis of sulfur based polymers.

Figure 1.6: Photograph of the large blocks of sulfur, a by-product of crude oil refining at the Syncrude Mildred Lake site, Alberta, Canada.[18] Credit: Alex MacLean

It is proposed that inverse vulcanisation is initiated by the ring-opening polymerisation of sulfur generating diradical polymeric sulfur species. The diradical polysulfides can subsequently be trapped by vinylic monomers, further generating new free-radical sites which allow for propagation of the reaction (Figure 1.7). It has been reported that hydrogen sulfide has been produced as a by-product of some inverse vulcanisation reactions, especially at elevated temperatures, which suggests that the mechanism of inverse vulcanisation may also proceed *via* hydrogen abstraction rather than or alongside radical addition across C=C double bonds.[25–27]

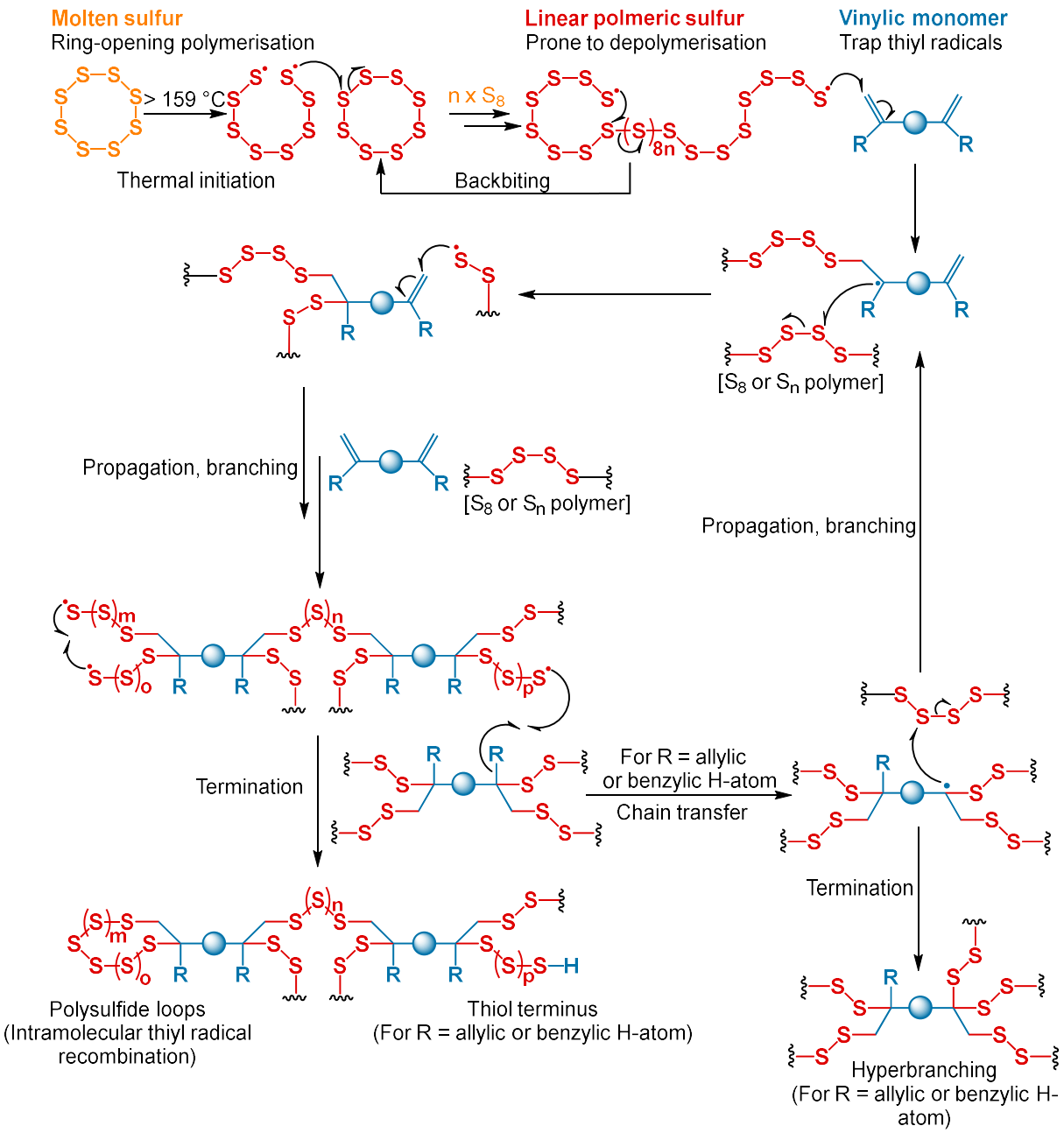

Figure 1.7: The mechanistic aspects of inverse vulcanisation as depicted by Chalker and co-workers.[31]

Investigations to prevent the generation of hydrogen sulfide gas include employing catalysis in order to reduce the reaction temperatures required for inverse vulcanisation.[22] Lowering the temperature of inverse vulcanisation has important safety implications. Inverse vulcanisation has been reported to be prone to the Trommsdorff-Norrish effect.[18] The Trommsdorff-Norrish effect is commonly observed in solvent-free syntheses and is caused by an increase in the viscosity of polymerisation systems. The increase in viscosity reduces the

frequency of termination steps from taking place during polymerisation, whilst initiation and propagation steps continue, which leads to auto-acceleration and an excessive exothermic reaction.[18] Therefore, lowering the reaction temperature of inverse vulcanisation could prevent the occurrence of the Trommsdorff-Norrish effect during the reaction.[22] It has also been found that catalytic inverse vulcanisation allows for a wider range of vinylic monomers to be used, specifically monomers that are unreactive in uncatalysed inverse vulcanisation such as ethylene glycol dimethacrylate (Figure 1.8).[22]

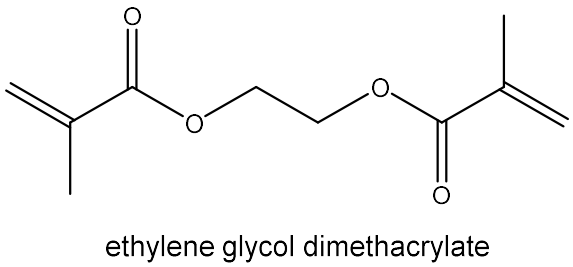

ethylene glycol dimethacrylate

Figure 1.8: Chemical structure of ethylene glycol dimethacrylate.

More recently, Yan *et al.* reported the mechanochemical synthesis of inverse vulcanised polymers using a ball mill.[28] Mechanochemistry refers to chemical syntheses that are enabled by mechanical force.[29] The method has been reported to allow inverse vulcanisation to take place at room temperature, with low reaction times of 3 hours.[28] Due to the milder temperature conditions of the mechanochemical synthesis in comparison to conventional inverse vulcanisation, the method has allowed the use of comonomers that have been previously incompatible with inverse vulcanisation due to their low boiling points.[28] Inverse vulcanisation has also been reported to occur under photochemical conditions, rather than the conventional thermal conditions.[30] Photoinduced inverse vulcanisation has been found to proceed at room temperature in the absence of a catalyst, no H_2S was formed and the method inhibits auto-acceleration from taking place. Similarly to mechanochemical inverse vulcanisation, photoinduced inverse vulcanisation allows for low boiling point comonomers to be reacted with sulfur, such as isoprene, ethylene, propyne and diallylamine.[30]

1.3 The Potential Applications of Inverse Vulcanised Polymers

Substituting carbon backbones of polymeric chains with sulfur backbones has the potential to synthesise polymers that have different properties to conventional carbon-based materials. For example, the refractive indices of sulfur polymers (reported up to 1.86) tend to be higher than those of carbon polymers (region of 1.5-1.6), demonstrating that substituting carbon with sulfur can alter the optical properties of a material.[22,32] Furthermore, inverse vulcanisation is compatible with a library of vinylic monomers, allowing for the synthesis and discovery of polymers with tunable properties such as mechanical strength and thus different potential applications.[33] Many potential applications have been investigated (Figure 1.9), amongst the most extensively researched are the use of inverse vulcanised polymers for novel cathode materials for Li-S batteries,[34,35] and for environmental remediation by means of mercury capture[18,36,37], water purification and oil spill recovery.[38] Other investigated potential applications include the development of novel optical devices,[39,40] smart fertilisers,[41,42] cement additives,[43] antimicrobial surfaces,[44] improved solar cell components and photocatalysts for water-splitting.[45] Sections 1.3.1-1.3.4 will discuss some of the most commonly reported applications of inverse vulcanised polymers, of which include; environmental remediation, cathode materials for Li-S batteries, smart fertilisers and dynamic materials

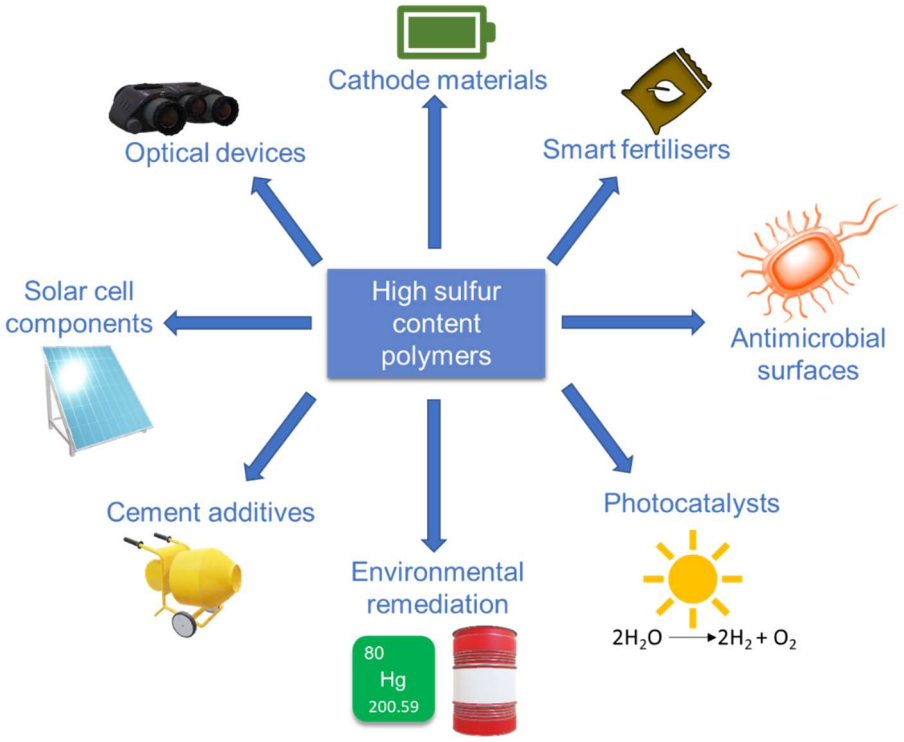

Figure 1.9: A summary of some of the reported potential applications of inverse vulcanised polymers.

1.3.1 Environmental Remediation

Poly(S-r-DIB) is widely reported in the literature, and has been investigated for its use in the removal of inorganic mercury (II) salts, however, DIB is a relatively expensive monomer, and efforts have been made to find cheaper alternatives.[37, 36] One alternative reported is limonene, a by-product of the citrus industry isolated from fruit peels (Figure 1.10).[46]

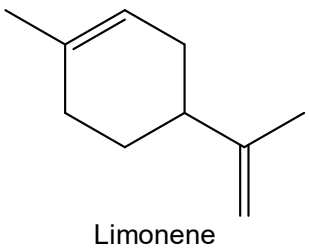

Figure 1.10: The chemical structure of limonene.

In 2016 Chalker and co-workers reported the copolymerisation of elemental sulfur and D-limonene giving a polysulfide that can be processed into coatings and solid materials with

possible applications in the remediation of heavy metal salts such as mercury and palladium (II) from water and soil.[47] Upon exposure of the novel sulfur-limonene polysulfide to mercury (II) chloride ($HgCl_2$), a chromogenic response was observed. This response was not observed when testing other metal ions such as Li^+, Ca^{2+} amongst many others, which opened up the possibility of synthesising polysulfides for the selective capture of heavy metal salts such as mercury (II).[47] Mercury is the third most toxic element on the planet to arsenic and lead, ranked by the US Government Agency for Toxic Substances and Disease. Therefore, the remediation of heavy metals such as mercury is an important area of research, where contaminated soil or water has the potential to allow mercury to enter food chains where it can bioaccumulate and subsequently cause adverse health effects.[48] The impact of mercury exposure is widespread across low-income countries due to the higher prevalence of processes such as artisanal and small-scale gold mining which often have little or no regulations on mercury emissions.[49] Inverse vulcanised polymers are therefore attractive for the remediation of inorganic heavy metal salts, especially in low-income countries, as the polymers can be produced inexpensively at large-scale. However, inorganic mercury salts are not the only problematic forms of mercury, organomercury compounds, especially those with short aliphatic chains are amongst the most hazardous forms of mercury. Methylmercury is the most studied alkylmercury, following the outbreak of Minamata disease and the poisoning in Iraq in the early 70's.[50,51] Research into organomercury uptake by inverse vulcanised polymers has also been conducted by Chalker and co-workers using canola oil as a monomer while Parker *et al.* investigated bio-derived terpenes such as farnesol, myrcene and farnesene (Figure 1.11) as monomers. [18, 52]

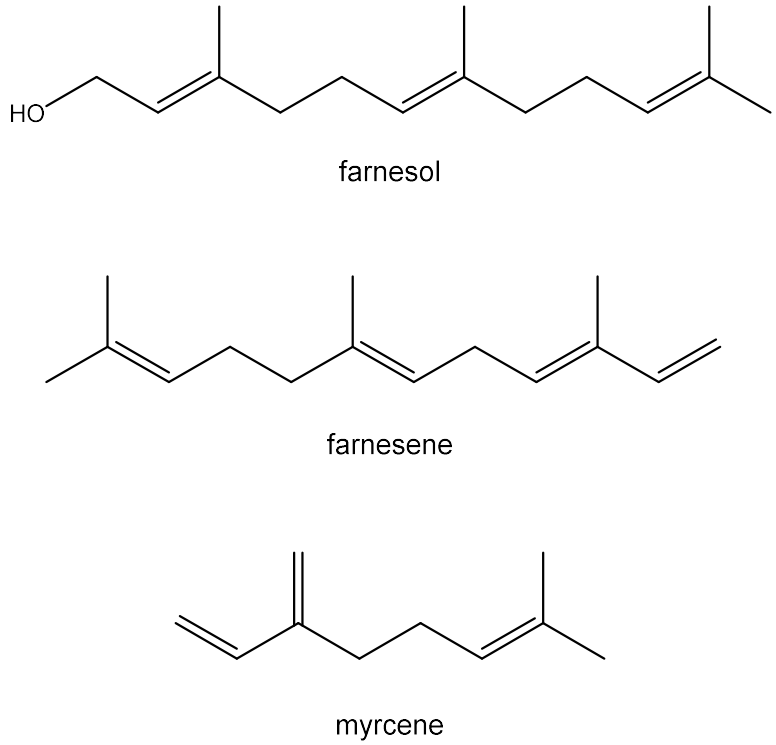

Figure 1.11: Chemical structures of the farnesol, farnese and myrcene, all of which are known as terpenes.

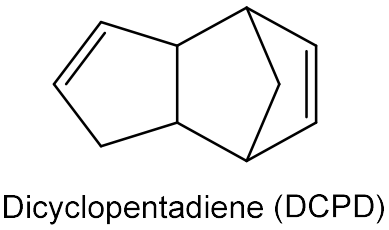

Figure 1.12: The chemical structure of dicyclopentadiene (DCPD).

A study by Hasell *et al.* showed the ability to synthesise porous polymers by supercritical CO_2 foaming and by salt templating, all of which were able to uptake mercury. One interesting polymer synthesised during this study is the copolymer of elemental sulfur and the crosslinker dicyclopentadiene (DCPD) (Figure 1.12).[36] DCPD is an attractive crosslinker for inverse vulcanised polymers, as it is also relatively cheap and is a by-product of the manufacture of ethylene.[53] The polymer containing 50 wt% sulfur was a glossy black and rigid material with a glass transition temperature (T_g) of 115 ºC, higher than that of S-DIB.[18] The T_g of a polymer is an important property as it is the temperature at which the polymer changes from its hard,

glassy state to a rubbery, soft state.[54] In another study, it has been shown that by polymerising sulfur in the presence of both limonene and DCPD, a shape persistent polymer can be synthesised.[55] This has also been done by blending canola oil and linseed oil separately with DCPD, the polymers obtained have different physical properties which vary with different ratios of the reaction feedstocks. To date, little is known about the origin of the colour of inverse vulcanised polymers, however, efforts have been made to understand some of their physical properties and how these can be tuned using different crosslinkers and different ratios of sulfur to crosslinker.[55]

The polysulfide reported by Chalker and co-workers synthesised from sulfur and canola oil has also been investigated for oil spill remediation.[38] Oil spills have devastating effects on the environment where hydrocarbon contamination can persist for many years meaning many ecosystems can take decades to recover.[56] Cost effective sorbents that can be produced on a large scale are of particular interest in tackling oil contaminants. Many reports have demonstrated the ability to synthesise inverse vulcanised sulfur polymers at kilogram scale and at low cost, which makes these materials appealing for such applications. A porous canola oil polysulfide was found to bind approximately twice their mass in crude oil by forming oil-polymer aggregates, which were easily recovered from water. It was also found that the oil could be removed from the porous polysulfide by mechanical compression, allowing the polysulfide to be reused in oil spill remediation.[38]

1.3.2 Novel Cathode Materials for Li-S Batteries

Another application of inverse vulcanised polymers that is being extensively researched is for the improvement of Li-S batteries. Due to the demand for more sustainable energy, the development of batteries with high energy densities is of importance. Traditional Li-ion batteries have a maximum energy density of approximately 300 W h kg^{-1}, which is not sufficient to meet energy output demands.[57,58] Li-S batteries are attractive candidates to provide

such high energy densities, and could become commercially available for use in electric vehicles and other future devices due to the high theoretical specific capacity of lithium (3860 mA h g^{-1}) and sulfur (1675 mA h g^{-1}).[59] Sulfur is an ideal material for batteries because it is one of the most abundant elements on earth, it is inexpensive and its theoretical capacity is much higher than the cathode materials in traditional Li-ion batteries. The Li-S rechargeable battery is based on the reversible redox reaction between lithium and sulfur (E^o = 2.20 V vs. Li/Li^+) (Equation 1.3).[60]

$$S_8 + 16Li^+ + 16e^- \rightleftharpoons 8Li_2S \quad (1.3)$$

The commercialisation of the Li-S battery has not yet been successful due to several factors such as low charging efficiency, short cycle life and high self-discharge rate. All of these factors are related to the dissolution of lithium polysulfides (Li_2S_x, $1 \leq x \leq 8$) which are intermediates of the sulfur reduction reaction.[61, 62] The discharge process of the Li-S battery forms both long chain polysulfides (Li_2S_x, $4 \leq x$) which are soluble in the electrolyte, and insoluble Li_2S_2 and Li_2S. The main issue caused by these discharge products is the "polysulfide shuttle" which consists of the transfer of the polysulfides between the anode and the cathode. The polysulfides can react with the lithium anode, forming deposits of insoluble Li_2S and subsequently loss of active anode material. The soluble polysulfides are also problematic as they lead to the redistribution of sulfur within the cell which results in a lower cycle life of the battery. Another challenge for the commercialisation of the Li-S battery is that sulfur and lithium sulfides are insulating which results in low utilisation of the sulfur cathode, this can be improved by using conducting polymers.[60] As an attempt to improve the performance of Li-S batteries, efforts have been made to use nanocomposites as cathode materials in order to encapsulate elemental sulfur to mitigate any unwanted reactions at the anode.[63,64] In 2014 Pyun and co-workers demonstrated that inverse vulcanised polymers could be used as potential cathode materials for Li-S batteries. In their study, S-DIB copolymers with varying ratios of sulfur to DIB were

fabricated into 2032 type coin cells using lithium foil as the anode. S-DIB synthesised with a composition of 90 wt% sulfur was found to be optimum and showed improved battery performance such as reduced capacity loss per cycle. It was shown that upon discharge of the copolymer, soluble organosulfur species such as thiolated DIB monomers were formed. These discharge products can deposit onto the cathode along with other insoluble polysulfides, it was proposed that the organosulfur compounds plasticise the insoluble polysulfides, which allows for improved battery cycling. The study found that inverse vulcanised polymers can be used to fabricate high capacity electrodes that can also suppress capacity fading after extending the battery performance to 500 cycles.[34] Further research on the use of inverse vulcanised polymers for novel Li-S battery cathode materials has focused on identifying the best performing polymer which can be synthesised using a cheap crosslinker. Naturally derived vinylic monomers are attractive for the fabrication of functional materials due to their low-cost and sustainability. In 2016, Mecerreyes and co-workers reported the synthesis of high sulfur content polymers *via* inverse vulcanisation with two natural diene monomers. The two natural dienes investigated were diallyl sulfide (DAS), a major organosulfur compound present in garlic, and myrcene, a monoterpene found in numerous plants such as lemon grass, basil, thyme and ylang-ylang fruit amongst others.[65–67] Polymers synthesised containing 90 wt% sulfur were investigated as active cathode materials in coin cells versus Li/Li^+ at various C-rates, which is the rate at which a battery is fully charged or discharged, ranging from C/10 (0-100% charging in 10 hours) to 1C (0-100% charging in 1 hour). Poly(S-DAS) performed the best having slightly higher discharge capacities at moderate and high C-rates compared to poly(S-myrcene). Charge-discharge profiles and long-term cycling profiles of both materials indicated good stability during cycling and therefore were shown to be suitable candidates for Li-S batteries.[68]

1.3.3 Smart Fertilisers

It has been estimated that the worlds' population will rise beyond 9 billion by 2050, this increase of nearly 2 billion in the next 30 years has raised several questions. How agriculture is going to meet the increased global food demand and how this can be done sustainably are arguably the most important questions raised.[69] Fertilisers are one of the main components of agriculture that allow the current food demands to be met, by increasing the achieved average crop yields and their quality.[70] Nitrogen (N), phosphorus (P) and potassium (K) are vital components of a well-fertilised crop and the so-called NPK fertilisers are widely used, however, the role of sulfur as an important fertiliser component has been largely neglected. Sulfur is one of the 16 essential elements for plant life where it plays an important role in the biosynthesis of cysteine and methionine and thus is essential for crop growth.[71, 72] Sulfur is normally administered to crops indirectly *via* NPK fertilisers, its main forms are as ammonium sulfate (24 % S), gypsum (14-18 % S) and potassium sulfate (18 % S), all of which are required in large amounts due to the relatively low percentages of sulfur present.[73] Elemental sulfur is the most concentrated form of sulfur and can be added to soils, however, plants are unable to uptake S^0. Plants can only uptake elemental sulfur once it has been microbially oxidised in the soil to SO^{4-} ions, this process can take some time and depends on the soil conditions that affect microbial activity such as temperature and aeration amongst others. The oxidation to SO^{4-} means there is a lag phase before the sulfur is available for uptake, this has rendered elemental sulfur ineffective as a sulfur source for fertilisers.[74]

Research has been conducted to investigate the potential of using inverse vulcanisation as means of converting crystalline S_8 to amorphous polymers. In a study by Ribeiro *et al.*, the fungus *Aspergillus niger* was used to investigate the effect of the structure of inverse vulcanised polymers on sulfur oxidation. The crosslinking agent used was soybean oil, polymers with 50 and 70 wt% sulfur content were compared against elemental sulfur to study the amount of

released sulfate per initial total sulfur. It was found that the 50 wt% sulfur polymer performed optimally, attributed to the differences in the structures of the polymers. The 50 wt% sulfur polymer contained a higher proportion of polymeric sulfur compared to the 70 wt% sulfur polymer which was richer in residual elemental sulfur. The improved oxidation by the 50 wt% sulfur polymer was therefore attributed to the higher polymeric sulfur content compared to that of the 70 wt% sulfur polymer.[42] More recently, Ribeiro *et al.* reported the co-application of a porous polysulfide with the S-oxidising bacterium *Acidithiobacillus thiooxidans* (*A. thiooxidans*) to improve the sulfate availability of soil.[75] The application of *A. thiooxidans* with the porous sulfur polymer was found to result in greater sulfate delivery compared with S_8 pellets.[75]

Along with the expected increase in the world population, the demand for fertilisers is also expected to increase.[76] Not only will there be pressure on agriculture to provide food security for a larger population, there will also be a pressure to do this sustainably with minimal impacts on the environment. Mineral deposits such as calcium phosphate, are the main supply of phosphorus for fertilisers, however, there is concern that the mineral deposit reserves are becoming scarce and thus threatening food security.[77] Traditional phosphorus fertilisers are highly inefficient, mainly due to their high solubility in water which results in losses to water and their ability to become immobilised. The immobilisation of phosphorus in the soil occurs due to interactions with calcium in alkaline soils and components such as iron in acidic soils, this results in unavailability for uptake by plants.[78–80] In order to improve the efficiency of phosphorus fertilisers and aid their conservation, so-called 'smart' fertilisers have been investigated. Smart fertilisers have focused on the use of microorganisms and enzymes for the production of biofertilisers, and the use of nanotechnology for nanofertilisers. One of the widely reported uses of smart fertilisers is for the development of slow- and controlled-release fertilisers. Slow- and controlled-release fertilisers delay the availability of the nutrients to the

plant, allowing uptake after application of the fertiliser, they also allow the nutrients to be available to the plant for prolonged periods of time compared to traditional fertilisers. Slow- and controlled-release fertilisers have mainly been achieved through the use of coatings to control the solubility of the fertiliser, a classical example being sulfur coated urea ,which can be additionally coated with other polyolefins or resins.[81, 82] Chalker and co-workers demonstrated that inverse vulcanised polymers can be used as controlled-release fertilisers. In this study, elemental sulfur was copolymerised with canola oil in the presence of three components of NPK fertilisers, including ammonium sulfate, calcium hydrogen phosphate and potassium chloride. A small-scale plant growth study was conducted using tomato plants (*Lycopersicom esculentum*) as a model. The results at the end of the 10 week study showed that the plants treated with the sulfur polymer composite were significantly taller, greener and produced more fruit compared to the plants treated with free NPK. Preliminary studies on the biodegradability of the polymers were also conducted, the results of which suggest that the triglyceride backbone of the polymer can hydrolyse slowly in basic water, producing glycerol as a by-product. This study demonstrated the potential for inverse vulcanised polymers to be used as smart fertilisers, a vital application in sustaining global food security.[41]

1.3.4 Repairable and Dynamic Materials

Disulfide bonds in polysulfide chains are dynamic and can be broken and reformed.[83] The dynamic nature of disulfide bonds has important implications on the repairability and recyclability of inverse vulcanised polymers. Griebel *et al.* demonstrated that S-DIB has dynamic behaviour which can be controlled by altering the sulfur:comonomer ratio in the reaction feedstock, which alters the length of the dynamic polysulfide chains within the formed material.[39] S-DIB was found to have applications for mid-IR imaging, where current mid-IR imaging lenses are prepared from semiconductors such as germanium zinc selenide. The imaging capability of materials such as germanium zinc selenide can become compromised if damages such as scratches occur. It was found that S-DIB could be thermally healed after causing surface defects (Figure 1.13). The healing of the material also restored the quality of the mid-IR images obtained, demonstrating that inverse vulcanised polymers could be used to circumvent the issue of loss of imaging capability in conventional mid-IR imaging materials after applying surface defects such as scratches.[39]

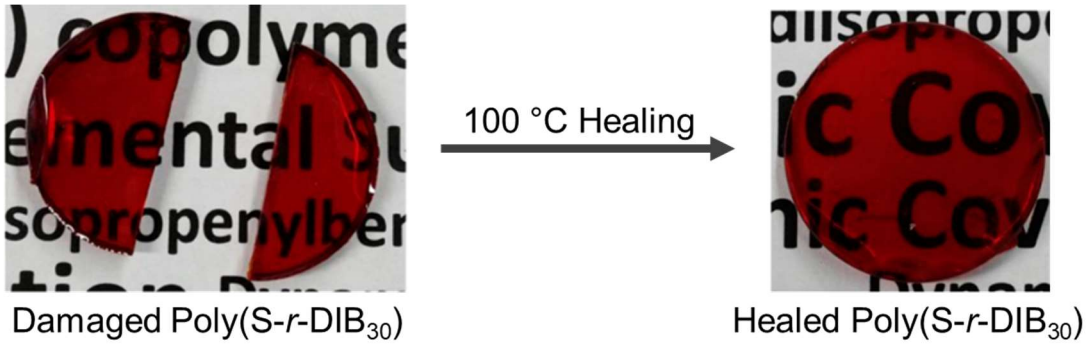

Figure 1.13: Damaged Poly(S-r-DIB30) polymer lens can be healed by thermal annealing at 100 °C demonstrated by Griebel *et al*.[39]

The dynamic nature of S-S bonds in inverse vulcanised polymers has also allowed the investigation of the polymers as novel adhesives.[84] Herrera *et al.* reported the development of novel adhesives from renewable monomers. The adhesives were prepared by inverse vulcanisation of sulfur with garlic essential oil, and other garlic derived monomers. The prepared materials were found to be viscous liquids which became solids upon curing. At the

optimum sulfur:comonomer ratios found to have the best adhesion strength, the materials demonstrated adhesion 3 times greater than that of commercial hide glue.[84]

Inverse vulcanised polymers have also been shown to undergo repair by phosphine or amine-catalysed S-S bond exchange.[85] Tonkin *et al.* demonstrated that two surfaces of inverse vulcanised polymers could be chemically joined at room temperature using nucleophiles such as pyridine. No polymer repair was found when common solvents such as acetone, ethanol, chloroform, tetrahydrofuran (THF) or dimethylformamide (DMF) was applied to the polymer surfaces, showing that the repair mechanism could not be due to polymer dissolution and re-entanglement of polymeric chains. It was proposed that the nucleophile could react and break S-S bonds, inducing S-S bond metathesis.[85]

1.4 The Antimicrobial Properties of Sulfur

The era of chemotherapy began with the discovery of the first modern antimicrobial in 1910, Salvarsan, by Paul Ehrlich, and his search for a "magic bullet". Subsequent discoveries such as that of penicillin by Alexander Fleming in 1928, sulphanilamide by Gerhard Domagk in 1935 and streptomycin in 1943 by Selman Waksman revolutionised modern day medicine. Despite such revolutionary discoveries, antimicrobial pathogens, especially multi-resistant strains, pose one of the main health challenges of the 21st century. The demand for novel antimicrobial agents is vital for the fight against antimicrobial resistance in pathogens. Sulfur has been familiar throughout the history of medicine, for the treatment of granular eyelids reported in the medical record *Ebers Papyrus* dated from 1550 B.C., and for the treatment of skin diseases by the ancient Greeks.[86] During the early 20th century, the antimicrobial properties of elemental sulfur were investigated by several scientists. In 1934 Lawson and co-workers found that elemental sulfur had an inhibitory effect on the growth of *tubercle bacilli*, but noted that no inhibitory effect was observed for some common pathogenic bacteria. In 1947 Weld and Gunther reported that saturated solutions of sulfur in carbowax and in alcohol showed inhibitory effects against some Gram-positive bacteria such as *Staphylococcus aureus* (*S. aureus*).[87,88]

1.4.1 Heterocyclic Compounds

Nowadays, sulfur is present in many clinically used antimicrobial agents, especially in heterocyclic drug compounds. The most used class of hetereocyclic antimicrobials that often contain sulfur are the β-lactams such as penicillins and cephalosporins (Figure 1.14) amongst many others. These antimicrobial agents operate by binding to specific penicillin-binding proteins which inhibits the formation of the peptidoglycan layer of the cell wall subsequently leading to cell death. [89,90]

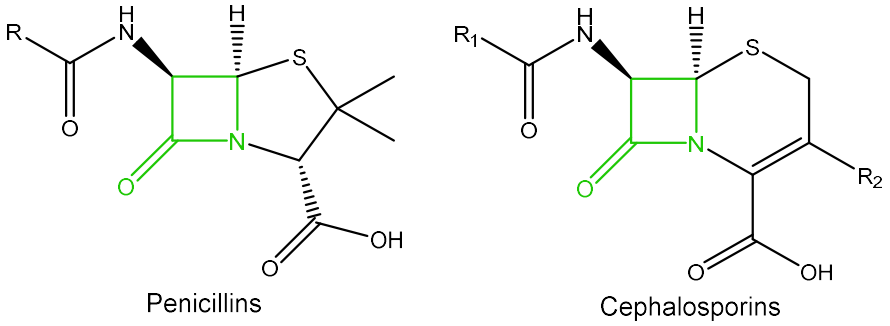

Figure 1.14: The general structures of penicillins and cephalosporins, with the beta lactam ring highlighted in green.

Despite being one of the most important classes of chemotherapeutic agents against bacterial pathogens, the β-lactams are being outsmarted by the development of resistance mechanisms amongst many bacterial strains. After only 4 years of penicillin G being used clinically, penicillin resistant strains of *S. aureus* were reported in 1944. One of the most common forms of resistance methods that have been employed by bacteria are the synthesis of β-lactamases, a group of enzymes that inactivate the antibiotic by hydrolysis of the β-lactam ring. Other resistance mechanisms include expression of low affinity penicillin-binding proteins.[91] In order to overcome these resistance mechanisms, several approaches have been investigated such as the development of β-lactamase stable antimicrobials and β-lactamase inhibitors such as clavulanic acid.[92] Another important class of sulfur containing antimicrobial agents are the sulfonamides such as sulfamethoxazole (Figure 1.15) for the treatment of urinary tract infections and bronchitis amongst other infections. The sulfonamides are known as folate inhibitors which act as competitive antagonists for dihydropteroate synthase, an important enzyme folate biosynthesis (Figure 1.15) which is essential for the synthesis of bacterial nucleic acids. The natural substrate of this enzyme is *para*-aminobenzoic acid (PABA), when competitively inhibited by sulfonamides a bacteriostatic effect is exerted by inhibiting the production of folic acid. Sulfonamides were the first drugs to selectively target bacterial cells by selectively targeting dihydropteroate synthase, which is absent in mammalian cells as they do not produce their own folic acid.[93] Trimethoprim also prohibits the synthesis of folate by

inhibiting dihydrofolate reductase which is the bacterial enzyme utilised in the last step of folate biosynthesis. Trimethoprim is seldom used alone, it is normally administered alongside sulfonamides, the advantages of this is broad spectrum activity against both Gram-positive and Gram-negative pathogens.[94]

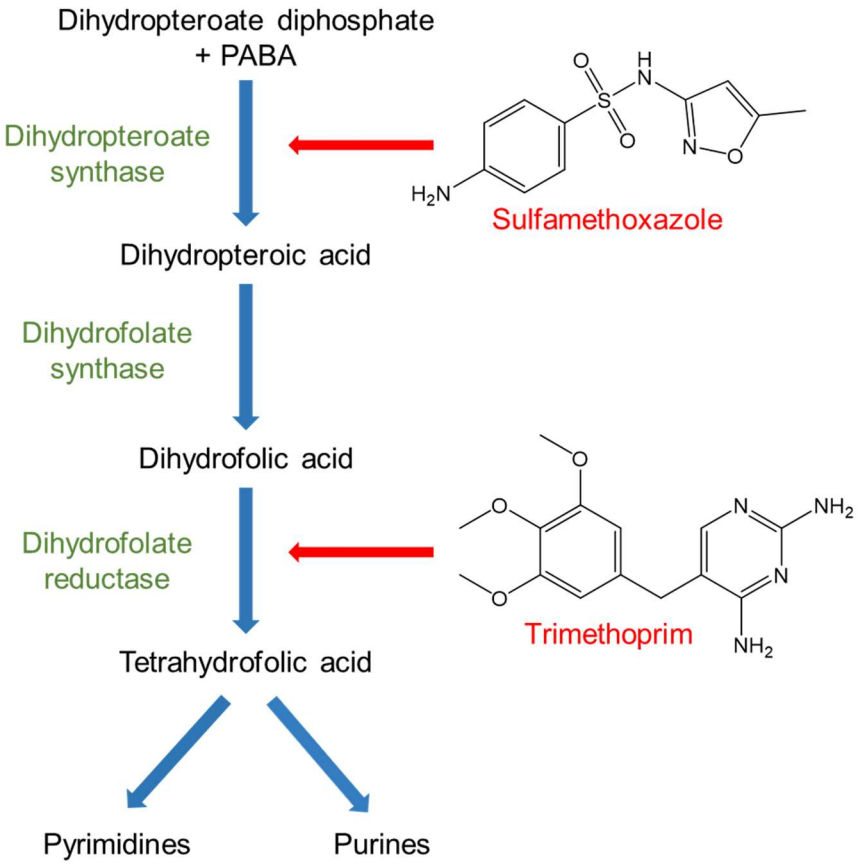

Figure 1.15: A summary of the folate biosynthetic pathway highlighting the steps inhibited by sulfamethoxazole and trimethoprim.

Despite having a very different mechanism of action compared to the β-lactams, bacteria have also evolved mechanisms of resistance towards trimethoprim and the sulfonamides. One mechanism of resistance shown by bacterial cells are the expression of dihydropteroate synthases which are highly resistant to sulfonamides.[95] Acquired resistance to trimethoprim has also been reported, where mutations in bacteria allow the production of a dihydrofolate reductase enzyme which is less susceptible to inhibition by trimethoprim.[96]

1.4.2 Polysulfides

More recently, polysulfides have been investigated for their antimicrobial properties. The antimicrobial activity of natural polysulfides found in garlic (*Allium sativum L.*) and onions (*Allium cepa L.*) has been known since the 16th century and in recent years efforts have been made to elucidate their modes of action.[97] One of the major components of garlic oil, isolated from steam distillations of crushed garlic over a century ago is allicin (Figure 1.16), which shows broad spectrum antimicrobial activities against Gram-positive and Gram-negative bacteria. Allicin has also been found to exhibit antifungal activity against fungi including *Candida albicans*, antiprotozoal activity against protozoa such as *Entamoeba histolytica* and antiviral activity.[98] The thiosulfinate functional group plays a vital role in the antimicrobial activity of allicin, the electron withdrawing nature of the oxygen atom induces an electrophilic sulfur centre which can subsequently react with thiol groups. Many enzymes with important thiol groups can thus be oxidised and inhibited in the presence of allicin, examples of which include alcohol dehydrogenase and RNA polymerase.[98] In 1951 Stoll and Seebeck found that allicin was not the main component of uncrushed garlic cloves, and is only found in substantial quantities in crushed garlic. The main compound present in uncrushed garlic is alliin which itself has no antimicrobial activity, but is converted to antimicrobial allicin by the enzyme alliinase (Figure 1.16). Alliinase is thought to be an important defence enzyme in garlic to protect the plant from pathogenic microbes in the soil by converting the precursor alliin to allicin. The antimicrobial activity of allicin is of interest as the mechanism of action is different to that of conventional antimicrobial agents, and it seems that many pathogens have been unable to develop resistance against allicin.[98,99] Allicin exhibits sulfhydryl-modifying activity and thus inhibits sulfhydryl enzymes.[100] The antibacterial properties of allicin has inspired the synthesis of heterocyclic disulfides as novel antimicrobial compounds.[101]

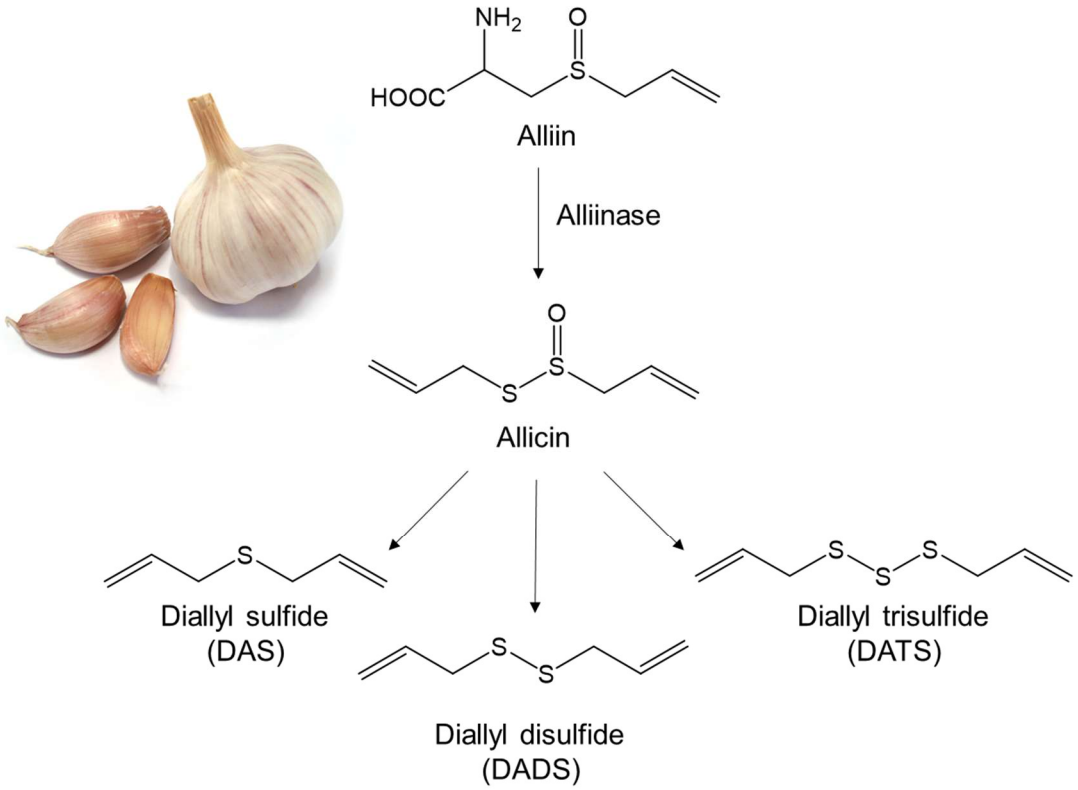

Figure 1.16: A summary of some of the sulfur containing compounds found in garlic.

Due to its instability, allicin can be converted into lipid soluble diallyl sulfides such as diallyl sulfide (DAS), diallyl disulfide (DADS) and diallyl trisulfide (DATS) and other higher order diallyl polysulfides (Figure 1.16). These diallyl sulfides are also thought to have antimicrobial properties and other health benefits. Several studies have been conducted and have found that the diallyl sulfides show an antimicrobial effect on both Gram-positive and Gram-negative pathogens, and that the antimicrobial effect increases with an increasing number of sulfur atoms in a chain (antimicrobial effect of DATS > DADS > DAS).[102–104] This suggests that other polysulfides could also have antimicrobial activity, and that higher order polysulfides could have an enhanced antimicrobial effect compared to lower order polysulfides. Inverse vulcanisation provides a method to synthesise high sulfur content polymers, that are likely to contain high order polysulfides, that is, a high sulfur rank. In 2017, Deng *et al.* reported the first study on the antimicrobial activity of inverse vulcanised polymers, where they studied poly(S-DIB) and its surface properties by studying thin films of the polymer.[44] The study

concluded that poly(S-DIB) showed significant antimicrobial activity against *E. coli*, killing up to 72 % of the bacteria with a polymer containing 50 wt% sulfur. DIB was the only crosslinker studied and therefore the effect of the crosslinker structure on the antimicrobial properties of the sulfur polymer could not be elucidated.[44] More recently, Smith *et al.* conducted a study aiming to elucidate the antibacterial properties of inverse vulcanised polymers.[105] The study conducted investigated the antibacterial activity of S-DIB and S-DCPD against *E. coli* and *S. aureus*. It was found that S-DIB exhibited greater antimicrobial activity compared to S-DCPD, and was suggested that this could be attributed to S-DIB having a greater sulfur rank (length of polysulfide segments R-$(S)_n$-R) and thus a weaker central S-S bond that allows for homolysis and formation of sulfur radicals.[105] The antimicrobial properties of inverse vulcanised polymers have received little attention compared to other possible applications such as for novel cathode materials in Li-S batteries, however, the studies by both Deng *et al.* and Smith *et al.* warrant further investigation of the antimicrobial properties of high sulfur content polymers.[44,105]

1.5 Thesis Overview

Inverse vulcanisation, reported by Pyun *et al.* allows the synthesis of high sulfur content polymers, allowing the properties of poly(sulfur) to be applied, where it has been previously inaccessible due to depolymerisation back to crystalline S_8.[19] Polysulfides have reported antibacterial activity, as demonstrated by the garlic-derived small molecules such as DAS, DADS and DATS. It is thought that longer polysulfide chains have greater antibacterial activity compared to shorter polysulfides. Sulfur polymers prepared by inverse vulcanisation are expected to have polysulfide segments of various lengths. The antibacterial activity of sulfur polymers synthesised by inverse vulcanisation has been reported by Deng *et al.* and Smith *et al.*[44,105] The overall conclusions of both studies were that inverse vulcanised polymers do have antibacterial properties, however, further work is required to understand why they have such properties.

The aim of the research discussed in this thesis is to investigate the antibacterial activity of sulfur polymers prepared by inverse vulcanisation to improve the current understanding reported in the literature.[44,105] The potential biological applications of inverse vulcanised polymers will also be investigated by formulating nanoparticles and fabricating surface coatings. Some aims and questions that were set out to be investigated included:

1. To improve the current understanding of the antibacterial properties of inverse vulcanised polymers

    Gaps in understanding of the antibacterial properties of inverse vulcanised polymers reported by Deng *et al.* and Smith *et al.* require further investigation. Both studies were limited in terms of the number of polymers studied, large error margins and conclusions as to what effects the antibacterial properties of inverse vulcanised polymers.

2. Can sulfur polymers prepared by inverse vulcanisation be formulated into nanoparticles by post-polymerisation methods to improve their water dispersibility and potential biological applications?

    At the start of this study, nanoparticles of inverse vulcanised polymers prepared by post-polymerisation methods had not been reported and had not been investigated for their antibacterial activity.

3. Can sulfur polymers prepared by inverse vulcanisation be used to prepare superhydrophobic surface coatings that inhibit bacterial adhesion?

    At the start of this study, superhydrophobic surface coatings of inverse vulcanised polymers had not been reported or investigated for their use as antibiofilm surface coatings.

1.6 References

1 G. Kutney, ed. G. B. T.-S. Second E. Kutney, ChemTec Publishing, Oxford, 2013.

2 P. T. Anastas and J. C. Warner, *Green chemistry : theory and practice*, Oxford University Press, Oxford [England]; New York, 1998.

3 J. Alaei Kadijani and E. Narimani, *Appl. Petrochemical Res.*, 2016, **6**, 25–34.

4 R. A. Sánchez-Delgado, *Organometallic Modeling of the Hydrodesulfurization and Hydrodenitrogenation Reactions.*, Springer Netherlands, 2002.

5 F. Manenti, D. Papasidero, G. Bozzano, S. Pierucci, E. Ranzi and G. Buzzi-Ferraris, in *23 European Symposium on Computer Aided Process Engineering*, eds. A. Kraslawski and I. B. T.-C. A. C. E. Turunen, Elsevier, 2013, vol. 32, pp. 811–816.

6 N. P. Cheremisinoff and P. E. Rosenfeld, eds. N. P. Cheremisinoff and P. E. B. T.-H. of P. P. and C. P. Rosenfeld, William Andrew Publishing, Oxford, 2010, pp. 179–259.

7 Y. Ikeda, eds. S. Kohjiya and Y. B. T.-C. Ikeda Manufacture and Applications of Natural Rubber, Woodhead Publishing, 2014, pp. 119–134.

8 W. K. Lewis, L. Squires and R. D. Nutting, *Rubber Chem. Technol.*, 1938, **11**, 107–130.

9 L. Bateman, C. G. Moore and M. Porter, *J. Chem. Soc.*, 1958, 2866–2879.

10 M. J. E. R. M. C. Erman Burak, *Sci. Technol. Rubber 4th Ed.*, 2013.

11 E. H. Farmer and F. W. Shipley, *J. Polym. Sci.*, 1946, **1**, 293–304.

12 N. P. Cheremisinoff, ed. N. P. B. T.-C. E. of P. E. T. Cheremisinoff, Butterworth-Heinemann, Boston, 2001, pp. 268–300.

13 M. Akiba and A. S. Hashim, *Prog. Polym. Sci.*, 1997, **22**, 475–521.

14 R. Steudel and B. Eckert, in *Elemental Sulfur and Sulfur-Rich Compounds I*, ed. R. Steudel, Springer Berlin Heidelberg, Berlin, Heidelberg, 2003, pp. 1–80.

15 G. Kutney, ed. G. B. T.-S. Second E. Kutney, ChemTec Publishing, Oxford, 2013, pp. 1–41.

16 B. R. Currell and A. J. Williams, *Thermochim. Acta*, 1974, **9**, 255–259.

17 H. Mutlu, E. B. Ceper, X. Li, J. Yang, W. Dong, M. M. Ozmen and P. Theato, *Macromol. Rapid Commun.*, 2019, **40**, 1800650.

18 D. J. Parker, H. A. Jones, S. Petcher, L. Cervini, J. M. Griffin, R. Akhtar and T. Hasell, *J. Mater. Chem. A*, 2017, **5**, 11682–11692.

19 W. J. Chung, J. J. Griebel, E. T. Kim, H. Yoon, A. G. Simmonds, H. J. Ji, P. T. Dirlam, R. S. Glass, J. J. Wie, N. A. Nguyen, B. W. Guralnick, J. Park, Á. Somogyi, P. Theato, M. E. Mackay, Y.-E. Sung, K. Char and J. Pyun, *Nat. Chem.*, 2013, **5**, 518–524.

20 D. Grossman, Environmental impact of Alberta tar sands 'horrible,' expert says, https://www.pri.org/stories/2014-07-10/environmental-impact-alberta-tar-sands-horrible-expert-says-photos, (accessed 8 June 2020).

21 Y. Wei, X. Li, Z. Xu, H. Sun, Y. Zheng, L. Peng, Z. Liu, C. Gao and M. Gao, *Polym.*

Chem., 2015, **6**, 973–982.

22 X. Wu, J. Smith, S. Petcher, B. Zhang, D. Parker, J. Griffin and T. Hasell, *Nat. Commun.*, 2019, **10**, 647.

23 D. A. Boyd, C. C. Baker, J. D. Myers, V. Q. Nguyen, G. A. Drake, C. C. McClain, F. H. Kung, S. R. Bowman, W. Kim and J. S. Sanghera, *Chem. Commun.*, 2017, **53**, 259–262.

24 Y. Zhang, R. S. Glass, K. Char and J. Pyun, *Polym. Chem.*, 2019, **10**, 4078–4105.

25 M. Arslan, B. Kiskan and Y. Yagci, *Macromolecules*, 2016, **49**, 767–773.

26 J. J. Griebel, G. Li, R. S. Glass, K. Char and J. Pyun, *J. Polym. Sci. Part A Polym. Chem.*, 2015, **53**, 173–177.

27 J. A. Smith, X. Wu, N. G. Berry and T. Hasell, *J. Polym. Sci. Part A Polym. Chem.*, 2018, **56**, 1777–1781.

28 P. Yan, W. Zhao, F. McBride, D. Cai, J. Dale, V. Hanna and T. Hasell, *Nat. Commun.*, 2022, **13**, 4824.

29 J.-L. Do and T. Friščić, *ACS Cent. Sci.*, 2017, **3**, 13–19.

30 J. Jia, J. Liu, Z.-Q. Wang, T. Liu, P. Yan, X.-Q. Gong, C. Zhao, L. Chen, C. Miao, W. Zhao, S. (Diana) Cai, X.-C. Wang, A. I. Cooper, X. Wu, T. Hasell and Z.-J. Quan, *Nat. Chem.*, 2022, **14**, 1249–1257.

31 M. J. H. Worthington, R. L. Kucera and J. M. Chalker, *Green Chem.*, 2017, **19**, 2748–2761.

32 J. J. Griebel, S. Namnabat, E. T. Kim, R. Himmelhuber, D. H. Moronta, W. J. Chung, A. G. Simmonds, K.-J. Kim, J. van der Laan, N. A. Nguyen, E. L. Dereniak, M. E. Mackay, K. Char, R. S. Glass, R. A. Norwood and J. Pyun, *Adv. Mater.*, 2014, **26**, 3014–3018.

33 J. M. Chalker, M. J. H. Worthington, N. A. Lundquist and L. J. Esdaile, *Top. Curr. Chem.*, 2019, **377**, 16.

34 A. G. Simmonds, J. J. Griebel, J. Park, K. R. Kim, W. J. Chung, V. P. Oleshko, J. Kim, E. T. Kim, R. S. Glass, C. L. Soles, Y.-E. Sung, K. Char and J. Pyun, *ACS Macro Lett.*, 2014, **3**, 229–232.

35 F. Zhao, Y. Li and W. Feng, *Small Methods*, 2018, **2**, 1800156.

36 T. Hasell, D. J. Parker, H. A. Jones, T. McAllister and S. M. Howdle, *Chem. Commun.*, 2016, **52**, 5383-5386.

37 M. Thielke, L. Bultema, D. Brauer, B. Richter, M. Fischer and P. Theato, *Polymers (Basel).*, 2016, **8**, 266.

38 M. J. H. Worthington, C. J. Shearer, L. J. Esdaile, J. A. Campbell, C. T. Gibson, S. K. Legg, Y. Yin, N. A. Lundquist, J. R. Gascooke, I. S. Albuquerque, J. G. Shapter, G. G. Andersson, D. A. Lewis, G. J. L. Bernardes and J. M. Chalker, *Adv. Sustain. Syst.*, 2018, **2**, 1800024.

39 J. J. Griebel, N. A. Nguyen, S. Namnabat, L. E. Anderson, R. S. Glass, R. A. Norwood, M. E. Mackay, K. Char and J. Pyun, *ACS Macro Lett.*, 2015, **4**, 862–866.

40 S. Park, D. Lee, H. Cho, J. Lim and K. Char, *ACS Macro Lett.*, 2019, **8**, 1670–1675.

41 M. Mann, J. E. Kruger, F. Andari, J. McErlean, J. R. Gascooke, J. A. Smith, M. J. H. Worthington, C. C. C. McKinley, J. A. Campbell, D. A. Lewis, T. Hasell, M. V Perkins and J. M. Chalker, *Org. Biomol. Chem.*, 2019, **17**, 1929–1936.

42 S. F. Valle, A. S. Giroto, R. Klaic, G. G. F. Guimarães and C. Ribeiro, *Polym. Degrad. Stab.*, 2019, **162**, 102–105.

43 B. Gutarowska, R. Kotynia, D. Bieliński, R. Anyszka, J. Wręczycki, M. Piotrowska, A. Koziróg, J. Berłowska and P. Dziugan, *Mater. (Basel, Switzerland)*, 2019, **12**(16), 2602.

44 Z. Deng, A. Hoefling, P. Théato and K. Lienkamp, *Macromol. Chem. Phys.*, 2018, **219**, 1700497.

45 S. Zhuo, Y. Huang, C. Liu, H. Wang and B. Zhang, *Chem. Commun.*, 2014, **50**, 11208–11210.

46 C. Sun, C. Theodoropoulos and N. S. Scrutton, *Bioresour. Technol.*, 2020, **300**, 122666.

47 M. P. Crockett, A. M. Evans, M. J. H. Worthington, I. S. Albuquerque, A. D. Slattery, C. T. Gibson, J. A. Campbell, D. A. Lewis, G. J. L. Bernardes and J. M. Chalker, *Angew. Chem. Int. Ed. Engl.*, 2016, **55**, 1714–1718.

48 K. M. Rice, E. M. Walker Jr, M. Wu, C. Gillette and E. R. Blough, *J. Prev. Med. Public Health*, 2014, **47**, 74–83.

49 R. A. Kampalath and J. A. Jay, *J. Heal. Pollut.*, 2015, **5**, 33–51.

50 C. Sanfeliu, J. Sebastià, R. Cristòfol and E. Rodríguez-Farré, *Neurotox. Res.*, 2003, **5**, 283–305.

51 S. B. Skerfving and J. F. Copplestone, *Bull. World Health Organ.*, 1976, **54**, 101–112.

52 M. J. H. Worthington, R. L. Kucera, I. S. Albuquerque, C. T. Gibson, A. Sibley, A. D. Slattery, J. A. Campbell, S. F. K. Alboaiji, K. A. Muller, J. Young, N. Adamson, J. R. Gascooke, D. Jampaiah, Y. M. Sabri, S. K. Bhargava, S. J. Ippolito, D. A. Lewis, J. S. Quinton, A. V Ellis, A. Johs, G. J. L. Bernardes and J. M. Chalker, *Chem. – A Eur. J.*, 2017, **23**, 16219–16230.

53 T. T. P. Cheung, *Kirk-Othmer Encycl. Chem. Technol.*, 2001.

54 V. Pacáková and J. Virt, in *Encyclopedia of Analytical Science (Second Edition)*, eds. P. Worsfold, A. Townshend and C. Poole, Elsevier, Oxford, Second Edi., 2005, pp. 180–187.

55 J. A. Smith, S. J. Green, S. Petcher, D. J. Parker, B. Zhang, M. J. H. Worthington, X. Wu, C. A. Kelly, T. Baker, C. T. Gibson, J. A. Campbell, D. A. Lewis, M. J. Jenkins, H. Willcock, J. M. Chalker and T. Hasell, *Chem. – A Eur. J.*, 2019, **25**, 10433–10440.

56 P. F. Kingston, *Spill Sci. Technol. Bull.*, 2002, **7**, 53–61.

57 K. Zhu, C. Wang, Z. Chi, F. Ke, Y. Yang, A. Wang, W. Wang and L. Miao, *Front. Energy Res.*, 2019, **7**, 123.

58 X. Fan, W. Sun, F. Meng, A. Xing and J. Liu, *Green Energy Environ.*, 2018, **3**, 2–19.

59 Y. Wang, E. Sahadeo, G. Rubloff, C.-F. Lin and S. B. Lee, *J. Mater. Sci.*, 2019, **54**, 3671–3693.

60 Z. Lin and C. Liang, *J. Mater. Chem. A*, 2015, **3**, 936–958.

61 S. S. Zhang, *J. Power Sources*, 2013, **231**, 153–162.

62 L. Wang, Y. Wang and Y. Xia, *Energy Environ. Sci.*, 2015, **8**, 1551–1558.

63 F. Wu, J. T. Lee, E. Zhao, B. Zhang and G. Yushin, *ACS Nano*, 2016, **10**, 1333–1340.

64 X. Ji, K. T. Lee and L. F. Nazar, *Nat. Mater.*, 2009, **8**, 500–506.

65 J. Chen and X. Xu, in *Epigenetics and Cancer, Part B*, eds. Z. Herceg and T. B. T.-A. in G. Ushijima, Academic Press, 2010, vol. 71, pp. 237–255.

66 A. Behr and L. Johnen, *ChemSusChem*, 2009, **2**, 1072–1095.

67 J. A. Hartsel, J. Eades, B. Hickory and A. Makriyannis, ed. R. C. B. T.-N. Gupta, Academic Press, Boston, 2016, pp. 735–754.

68 I. Gomez, D. Mecerreyes, O. Leonet and J. A. Blazquez, *ChemSusChem*, 2016, **9**, 3419–3425.

69 D. Tilman, C. Balzer, J. Hill and B. L. Befort, *Proc. Natl. Acad. Sci.*, 2011, **108**, 20260 LP – 20264.

70 C. Hera, *Fertil. Res.*, 1995, **43**, 63–81.

71 F. A. Gilbert, *Bot. Rev.*, 1951, **17**, 671–691.

72 S. Kopriva, *Plant Signal. Behav.*, 2015, **10**, e1055436–e1055436.

73 A. R. Lucheta and M. R. Lambais, *Rev. Bras. Ciência do Solo* , 2012, **36**, 1369–1379.

74 J. J. Germida and H. H. Janzen, *Fertil. Res.*, 1993, **35**, 101–114.

75 S. F. Valle, A. S. Giroto, R. Klaic, D. Bevilaqua and C. Ribeiro, *J. Polym. Environ.*, 2022, **30**, 4571–4579.

76 W. Zhang and X. Zhang, *Environ. Monit. Assess.*, 2007, **133**, 427–434.

77 L. Reijnders, *Resour. Conserv. Recycl.*, 2014, **93**, 32–49.

78 D. L. Childers, J. Corman, M. Edwards and J. J. Elser, *Bioscience*, 2011, **61**, 117–124.

79 F. Hellal, S. El-Sayed, R. Zewainy and A. Amer, *Bull. Natl. Res. Cent.*, 2019, **43**, 11.

80 P. S. Bindraban, C. O. Dimkpa and R. Pandey, *Biol. Fertil. Soils*, 2020, **56**, 299–317.

81 M. Calabi-Floody, J. Medina, C. Rumpel, L. M. Condron, M. Hernandez, M. Dumont and M. de la L. Mora, ed. D. L. B. T.-A. in A. Sparks, Academic Press, 2018, vol. 147, pp. 119–157.

82 K. Mikula, G. Izydorczyk, D. Skrzypczak, M. Mironiuk, K. Moustakas, A. Witek-Krowiak and K. Chojnacka, *Sci. Total Environ.*, 2020, **712**, 136365.

83 M. Arslan, B. Kiskan and Y. Yagci, *Sci. Rep.*, 2017, **7**, 5207.

84 C. Herrera, K. J. Ysinga and C. L. Jenkins, *ACS Appl. Mater. Interfaces*, 2019, **11**, 35312–35318.

85 S. J. Tonkin, C. T. Gibson, J. A. Campbell, D. A. Lewis, A. Karton, T. Hasell and J. M. Chalker, *Chem. Sci.*, 2020, **11**, 5537–5546.

86 S. Gianfaldoni, G. Tchernev, U. Wollina, M. G. Roccia, M. Fioranelli, R. Gianfaldoni and T. Lotti, *Open Access Maced. J. Med. Sci.*, 2017, **5**, 566–568.

87 J. T. Weld and A. Gunther, *J. Exp. Med.*, 1947, **85**, 531–542.

88 L. Libenson, F. P. Hadley, A. P. McIlroy, V. M. Wetzel and R. R. Mellon, *J. Infect. Dis.*, 1953, **93**, 28–35.

89 P. R. Murray, K. S. Rosenthal and M. A. Pfaller, *Medical microbiology.*, Elsevier, 8th edition.

90 M. M. D'Andrea, M. Fraziano, M. C. Thaller and G. M. Rossolini, *Antibiot.*, 2019, **8**, 254.

91 R. J. Worthington and C. Melander, *J. Org. Chem.*, 2013, **78**, 4207–4213.

92 D. Rawat and D. Nair, *J. Glob. Infect. Dis.*, 2010, **2**, 263–274.

93 M. Kester, K. D. Karpa and K. E. Vrana, eds. M. Kester, K. D. Karpa and K. E. B. T.-E. I. R. P. Second E. Vrana, W.B. Saunders, Philadelphia, 2012, pp. 41–78.

94 M. G. Papich, ed. M. G. B. T.-S. H. of V. D. Fourth E. Papich, W.B. Saunders, St. Louis, 2016, pp. 820–822.

95 O. Skold, *Drug Resist. Updat.*, 2000, **3**, 155–160.

96 R. Gleckman, N. Blagg and D. W. Joubert, *Pharmacotherapy*, 1981, **1**, 14–20.

97 J. C. Harris, S. L. Cottrell, S. Plummer and D. Lloyd, *Appl. Microbiol. Biotechnol.*, 2001, **57**, 282–286.

98 S. Ankri and D. Mirelman, *Microbes Infect.*, 1999, **1**, 125–129.

99 R. Leontiev, N. Hohaus, C. Jacob, M. C. H. Gruhlke and A. J. Slusarenko, *Sci. Rep.*, 2018, **8**, 6763.

100 C. B. Oosthuizen, A.-M. Reid and N. Lall, in *Medicinal Plants for Holistic Health and Well-Being*, ed. N. Lall, Academic Press, 2018, pp. 277–295.

101 J.-R. Wang, Y.-M. Hu, H. Zhou, A.-P. Li, S.-Y. Zhang, X.-F. Luo, B.-Q. Zhang, J.-X. An, Z.-J. Zhang and Y.-Q. Liu, *J. Agric. Food Chem.*, 2022, **70**, 11782–11791.

102 P. RATTANACHAIKUNSOPON and P. PHUMKHACHORN, *Biosci. Biotechnol. Biochem.*, 2008, **72**, 2987–2991.

103 M. Nakamoto, K. Kunimura, J.-I. Suzuki and Y. Kodera, *Exp. Ther. Med.*, 2020, **19**, 1550–1553.

104 S.-M. Tsao and M. –. Yin, *J. Antimicrob. Chemother.*, 2001, **47**, 665–670.

105 J. A. Smith, R. Mulhall, S. Goodman, G. Fleming, H. Allison, R. Raval and T. Hasell, *ACS Omega*, 2020, **5**, 5229–5234.

Chapter 2

Antibacterial Activity of Sulfur Polymers

2.1 Abstract

There is growing interest in polysulfides as novel antimicrobial agents due to the antimicrobial activity of natural polysulfides found in garlic and onions. In this chapter we discuss the antibacterial properties of several inverse vulcanised polymers (also termed high sulfur content polymers) against Gram-positive *Staphylococcus aureus* and Gram-negative *Pseudomonas aeruginosa*, two common causes of nosocomial infection and pathogens identified by the World Health Organisation as priorities for antimicrobial development. High sulfur content polymers were synthesised with different comonomers and at different sulfur/comonomer ratios, to determine their effect on the antibacterial properties of the resulting materials. Polymers were tested for their potential as antibacterial materials at different temperatures to establish whether the glass transition temperature of the polymer has an influence on their antibacterial actvities. The findings presented in this chapter provide further understanding of the antibacterial properties of high sulfur content polymers and show that such polymers have the potential to be used as antibacterial surfaces.

2.2 Introduction

The antimicrobial properties of sulfur, sulfur-containing small molecules and polysulfides was introduced in Chapter 1. There is growing interest in polysulfides as novel antimicrobial agents due to the antimicrobial activity of natural polysulfides found in garlic and onions as the mechanism of action is thought to be different to that of conventional antimicrobial agents.[1–4] Several studies have reported that the diallyl sulfides show an antimicrobial effect against both Gram-positive and Gram-negative pathogens, and that the antimicrobial effect increases with an increasing number of sulfur atoms in a chain (antimicrobial effect of DATS > DADS > DAS).[1,2,5] Ajoene (Figure 2.1), another disulfide containing compound found in garlic oil has been found to inhibit quorum sensing, an important communication system used by bacteria including *P. aeruginosa* to achieve coordinated expression of genes involved in pathogenicity. It is thought that the disulfide bond present in ajoene is vital for its antivirulence activity.[6] Recently, thiol and disulfide containing vancomycin derivatives have been shown to improve the antibacterial and antibiofilm activity of vancomycin. Vancomycin is commonly known as the "last resort" antibiotic to tackle complicated methicillin-resistant *S. aureus* infections. The thiol and disulfide derivatives were shown to have improved antibacterial activity against vancomycin-resistant bacterial strains, showing that sulfide and thiol containing compounds may be important in medicinal chemistry.[7]

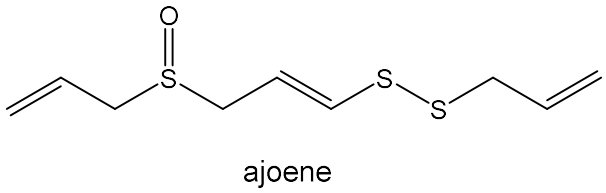

ajoene

Figure 2.1: The chemical structure of ajoene.

Inverse vulcanised polymers are also expected to have chains of sulfur of varying lengths, and thus may exhibit antimicrobial activity. In 2017, a study by Deng *et al.* found that thin layers of poly(sulfur-co1,3-diisopropenyl benzene) (S-DIB) spin-coated onto silicon substrates were able to kill *Escherichia coli* (*E. coli*). Several S-DIB polymers with different ratios of sulfur/DIB (between 50 and 70 wt % sulfur) were prepared and it was found that there were no significant differences in the antibacterial activity of each polymer.[8] Large error margins (~30-40 % error) associated with the antibacterial activity results meant that the antibacterial activity of S-DIB films prepared by Deng *et al.* could not be assessed quantitatively.[8] Although not synthesised by inverse vulcanisation, linear sulfur-nylon composites have been found to show an inhibitory effect against *Staphylococcus epidermidis*, *Klebsiella pneumoniae* and *E. coli* whereas pure nylon was found to have little to no inhibitory effect against the same bacterial strains.[9] In 2020, Smith *et al.* aimed to further elucidate the antibacterial properties of inverse vulcanised polymers by studying the antibacterial properties of S-DIB and S-DCPD, both synthesised with 50 wt % sulfur, against *S. aureus* and *E. coli*.[10] The study found that S-DIB showed a >99.9 % reduction in viable *S. aureus* and *E. coli* relative to a control.S-DCPD synthesised at the same sulfur:comonomer ratio, showed a 99 % reduction in *E coli*, but no inhibitory effect against *S. aureus*. It was suggested that the differences in the antibacterial activity of S-DIB and S-DCPD could be attributed to the higher sulfur rank (length of polysulfide segments -R-(S)n-R-) of S-DIB compared to S-DCPD.[10] It is thought that polysulfides can react with thiol-containing cellular proteins, and thus, higher sulfur ranks are expected to give more labile central S−S bonds, which could react with thiol groups of bacterial proteins.[10,11] More recently, Cubero-Cardoso *et al.* investigated the antimicrobial and antioxidant activity of terpolymers synthesised from sulfur, castor oil and a third monomer of which included styrene, imidazole and cinnamic acid amongst others. It was found that the presence of a third monomer could improve the antimicrobial and antioxidant activity of the

material compared to the copolymer of sulfur and castor oil alone.[12] Inverse vulcanised polymers have also been investigated for their use as antimicrobial adhesives, as demonstrated by Shen *et al.* by the synthesis of a self-repairable, high-strength adhesive through inverse vulcanisation of plant-derived urushiol and sulfur.[13]

2.3 Aims of Chapter

This chapter will focus on the investigation of the antimicrobial properties of inverse vulcanised polymers to improve the current understanding of the properties reported in the literature. Studies by Deng *et al.* and Smith *et al.* show that inverse vulcanised polymers do show antimicrobial activity.[8,10] Deng *et al.* investigated one type of comonomer at various sulfur:comonomer ratios, whereas Smith *et al.* investigated two different comonomers at the same sulfur:comonomer ratios.[8,10] The studies warrant a much more comprehensive investigation into the antibacterial activity, to bridge the gaps in understanding of the origin of the properties reported in both studies. Elucidation of the antimicrobial activity of inverse vulcanised polymers at a more in-depth level will require testing of polymers with different properties. The antimicrobial study conducted by Smith *et al.* showed that the crosslinker type is likely to impact the antimicrobial properties of the polymers, therefore testing polymers synthesised with various crosslinkers will be important.[14] Studies on natural polysulfides such as those present in garlic suggest that the antimicrobial properties of polysulfides is also dependent on the sulfur rank [1,3], it will therefore be essential to test polymers synthesised with different sulfur:crosslinker ratios as higher sulfur feeds are expected to give higher order polysulfides. Deng *et al.* investigated the effect of the sulfur:comonomer ratio within the polymers on the antibacterial properties by preparing thin films of S-DIB containing 50-70 wt.%. Films containing different sulfur:comonomer ratios were found to have similar antibacterial activity, with large error margins in the results.[8] Smith *et al.* demonstrated that S50-DCPD showed no inhibitory effect against Gram-positive *S. aureus*, but did show an inhibitory effect against Gram-negative *E. coli*.[10] This demonstrates that the polymers investigated in this study will need to be tested against both Gram-positive and Gram-negative species. Materials synthesised will be tested against Gram-positive methicillin resistant *S.*

aureus and Gram-negative *P. aeruginosa* to investigate if the polymers are able to inhibit both types of bacteria which have different cell wall structures.

Aims in summary:-

- Synthesise a small library of polymers with different comonomers and varying the sulfur:comonomer ratio. Polymers which have not been previously reported for their antibacterial activity will be investigated, in addition to polymers that have been previously investigated, namely S-DCPD and S-DIB, to bridge the gaps in studies done by Deng *et al.* and Smith *et al.* [8,10]
- Evaluate the antibacterial activity of bulk polymers prepared by inverse vulcanisation against methicillin-resistant *S. aureus* and *P. aeruginosa*. This study will be the first to investigate if inverse vulcanised polymers have an inhibitory effect against *P. aeruginosa*, which is an important nosocomial pathogen
- Evaluate the antibiofilm activity of inverse vulcanised polymers, which has not been previously investigated

2.4 Results and Discussion

The experimental details related to the results of this chapter are detailed in section 2.6.

2.4.1 Synthesis of High-Sulfur Content Polymers

The properties of inverse vulcanised polymers have been shown to be affected by the type of comonomer used. For example, high-sulfur content polymers synthesised using DIB as a comonomer results in polymers that are glass like materials and shape-persistent with reported Young moduli ranges of 260-460 MPa by Pyun and co-workers.[15]Polymers formed from the reaction of sulfur and limonene have been shown to form materials that do not retain their shape and have properties similar to that of highly viscous liquids.[15,16] Furthermore vegetable oils such as sunflower and canola oil as comonomers have been shown to produce polymeric materials with flexibility and compressibility with reported Young's modulus of ~90 MPa for the product of copolymerisation of sulfur and canola oil.[17] On the converse, using DCPD as a comonomer results in hard, rigid materials that have been reported to be too brittle to assess their tensile properties.[14,18,19] In addition to this, the sulfur:comonomer ratio employed in the reaction feedstock has been shown to influence the properties of the resultant materials. Parker *et al.* demonstrated that increasing the amount of DCPD in the reaction feedstock resulted in polymers with higher glass transition temperatures (115 °C for 50 wt.% sulfur), whereas a higher sulfur content resulted in a lower observed T_g (~ -20 °C for 90 wt.% sulfur).[18] As briefly mentioned in Chapter 1, the T_g is an important property of polymers. As the temperature rises above the T_g, polymers undergo a phase change from a glassy, rigid state to a rubbery, flexible state.[37] The T_g of a polymer is an important property that often dictates the applicability of materials.[20] The T_g is commonly determined by differential scanning calortimetry (DSC).

Since the comonomer type and sulfur:comonomer ratio influence the polymer properties, it is fair to assume that these variables will also influence the antibacterial properties

of the resultant materials. As mentioned above, Smith *et al.* demonstrated that the comonomer type does indeed effect the antibacterial properties of inverse vulcanised polymers where it was shown that the polymer synthesised from the copolymerisation of sulfur and DIB showed an increased antibacterial effect against *E. coli* and *S. aureus* compared to the polymer formed from sulfur and DCPD.[10] Therefore, for this study, polymers were synthesised (denoted S-comonomer) with different comonomers, sulfur:comonomer ratios and thus different T_g (Table 2.1) to further understand the antibacterial properties of inverse vulcanised polymers.

Table 2.1: Summary of the polymers synthesised, detailing the comonomer and the ratio of sulfur/comonomer employed in the reaction feedstock, the T_g of the resultant materials, and their solubility in chloroform. [a]S: soluble, SS: sparingly soluble, IS: insoluble. [b]Theoretical average sulfur rank given by (moles of S atoms/moles of alkene units).

Polymer	Comonomer	wt.% sulfur	wt.% comonomer	T_g (°C)	Solubility[a]	Average sulfur rank[b]
S50-PA	Perillyl alcohol	50	50	34	S	2.4
S70-PA	Perillyl alcohol	70	30	14	S	5.5
S50-DIB	DIB	50	50	27	S	2.5
S70-DIB	DIB	70	30	10	S	5.7
S50-DCPD	DCPD	50	50	88	IS	2.1
S70-DCPD	DCPD	70	30	45	IS	4.8
S50-DVB	DVB	50	50	72	IS	2
S70-DVB	DVB	70	30	52	IS	4.7
S30-RO	Rapeseed oil	30	70	-31	SS	-
S50-RO	Rapeseed oil	50	50	-30	SS	-
S30-LO	Linseed oil	30	70	-12	SS	-
S50-LO	Linseed oil	50	50	-12	SS	-

As introduced in Chapter 1, high-sulfur content polymers with a sulfur content of >50 wt.% can be synthesised by inverse vulcanisation.[15] The reaction involves heating elemental sulfur until molten, and adding a comonomer which has reactive vinylic groups which can undergo reaction with sulfur. Due to the molten state of sulfur at temperatures exceeding 115 °C, the process does not require a solvent.[21] Therefore, high sulfur content polymers were synthesised by adding the vinylic comonomer to molten sulfur at 135 °C and further heating

between 135 °C and 175 °C, depending on the comonomer used, until the mixture became homogeneous and viscous. The reaction mixture was poured into 1 cm^3 cube shaped silicone moulds and transferred to an oven to be cured overnight at 140 °C. Following curing, the polymers molded into 1 cm^3 cubes were removed from the silicone moulds and used for characterisation and antibacterial testing.

Three sets of materials differing by their T_g range were chosen to assess whether antibacterial activity was isolated to individual comonomers, or, if similar antibacterial activity was seen within a given set, and therefore dependent upon the T_g. The first set of comonomers chosen included DCPD and divinylbenzene (DVB) (Figure 2.2), as they result in insoluble crosslinked polymers with high T_g far exceeding room temperature (>45 °C) when reacted with elemental sulfur.

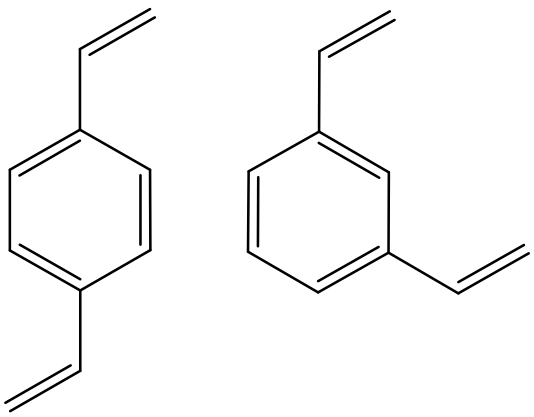

Figure 2.2: The chemical structure of divinylbenzene (DVB), which normally exists as a mixture of *p*-DVB and *m*-DVB.

DCPD is a by-product of ethylene production and thus is a relatively cheap monomer.[22] The synthesis of S-DCPD was carried out as mentioned above, firstly DCPD was added to molten sulfur under stirring at 135 °C, and the temperature was increased to 160 °C. The reaction mixture was biphasic, with an orange molten sulfur layer and a clear DCPD top layer. With continued stirring and heating the mixture became dark brown/black in colour and viscous. Once the mixture was deemed homogenous, the mixture was poured into a silicone mould and

the polymer was cured overnight at 140 °C. The homogeneity of the reaction mixture was determined by placing a clean spatula into the reaction mixture. The absence of precipitated elemental sulfur onto the spatula, and that the reaction mixture remained monophasic indicated that the mixture was homogeneous and suitable for curing. The reaction was carried out at 50 and 70 wt.% sulfur, forming S50-DCPD (50 wt.% sulfur) and S70-DCPD (70 wt.% sulfur). Both solids were dark, rigid and hard materials. DSC analysis of S50-DCPD (Figure 2.3) and S70-DCPD (Appendix 2.1) show glass transition temperatures of 88 and 45 °C (Table 2.1) respectively. The higher the sulfur content in S-DCPD, the lower the T_g of the polymer, likely due to the presence of longer sulfur chains within the polymeric material resulting in greater chain flexibility. The thermograms obtained by DSC show no traces of crystalline elemental sulfur for both S50-DCPD and S70-DCPD, which would be detected by the presence of sulfur melting peaks at around 115 °C, and crystallisation peaks at lower temperatures.

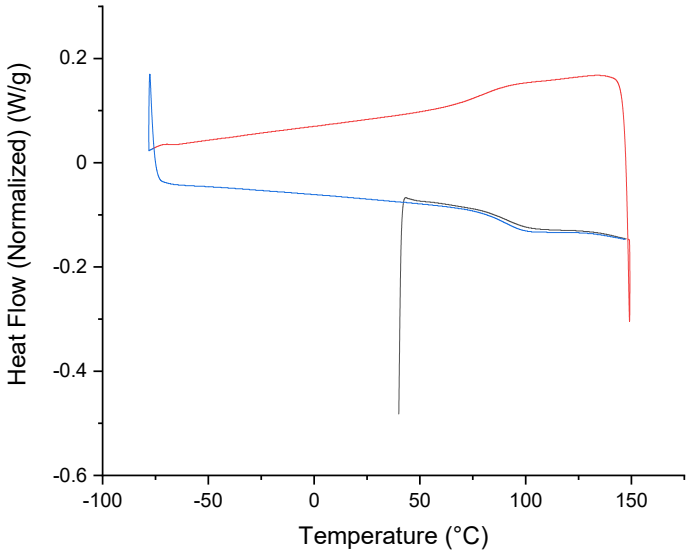

Figure 2.3: DSC traces for S50-DCPD showing the first heating cycle to 150 °C (black), cooling to -80 °C (red), and the second heating cycle to 150 °C (blue).

Fourier-transform infrared (FT-IR) spectroscopy was used to assess if DCPD had been fully consumed during the reactions to form S50-DCPD and S70-DCPD. Based on the proposed mechanism of inverse vulcanisation whereby reaction occurs across C=C bonds (Figure 1.7),

reaction of sulfur with the monomer can be assessed by evaluating the consumption of C=C units based on the presence/absence of signals corresponding to alkene units within the product. The resulting FT-IR spectra (Figure 2.4) show a loss of peaks corresponding to =C-H stretching and C=C stretching, indicating that DCPD units have been consumed during the reaction.

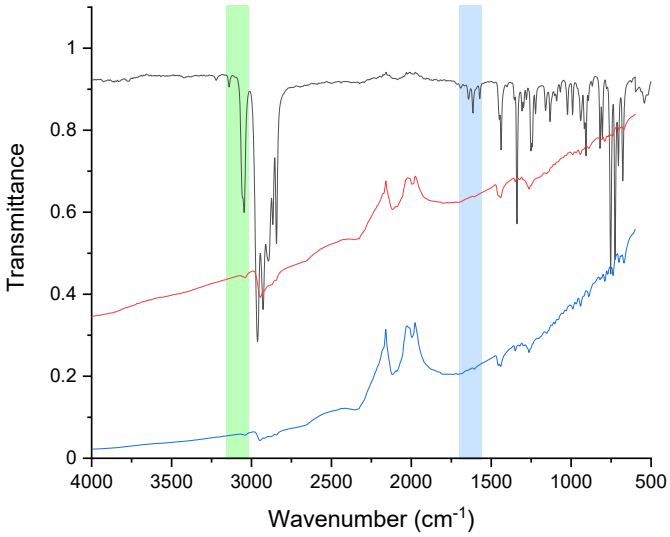

Figure 2.4: FT-IR spectra for DCPD (black), S50-DCPD (red) and S70-DCPD (blue). Highlighted in green at ca. 3100 cm^{-1} is the signal corresponding to =C-H stretch, and highlighted in blue at ca. 1640 cm^{-1} is the signal corresponding to an alkene C=C stretch. Both signal intensities are reduced in the polymer spectra compared to the monomer suggesting alkene consumption during the reaction.

Combustion analysis of the materials was conducted to evaluate how much sulfur is present in the resulting polymers (

Table 2.2). Both S50-DCPD and S70-DCPD were found to have an approximately 10 % higher sulfur content than expected. This could be due to the volatility of DCPD that may have evaporated during the reaction. Differences between the expected and actual sulfur content may also arise due to accuracy issues where the sulfur standards used during combustion analysis may not be suitable for such high sulfur content materials. Despite the differences between the calculated and obtained sulfur content, it can be concluded that the synthesised materials contain sulfur. The calculated and obtained C/H ratios can also be compared, which may give further mechanistic information. If sulfur radical addition occurs exclusively on the double

bonds, the C/H ratio is expected to remain the same. It has been reported that H_2S can form during inverse vulcanization, and is thought to be produced *via* H-abstraction.[23] Hydrogen abstraction by radicals would result in a higher than expected C/H ratio. This may explain the higher than expected C/H ratio obtained for S50-DCPD. The C/H ratio of S70-DCPD was lower than expected, this means that carbon atoms have been lost, or, hydrogen atoms have been gained, however, the origin of this result is not understood, and may be due to errors in combustion analysis.

Table 2.2: *Calculated and obtained elemental analysis of S-DCPD and S-DVB.*

Sample	Calc. % carbon	Calc. % hydrogen	Calc. % sulfur	**C/H ratio**	Actual % carbon	Actual % hydrogen	Actual % sulfur	**C/H ratio**
S50-DCPD	45.43	4.57	50	**9.9**	34.71	3.4	61.8	**10.2**
S70-DCPD	27.25	2.75	70	**9.9**	20.8	2.22	78.94	**9.37**
S50-DVB	46.13	3.87	50	**11.9**	27.1	2.67	71	**10.15**
S70-DVB	27.68	2.32	70	**11.9**	24.68	2.47	74	**9.99**

Both S50-DCPD and S70-DCPD were found to be insoluble in common solvents such as THF, chloroform, toluene, acetonitrile and methanol. Due to the insolubility of the materials in organic solvents, it is likely that both polymers are fully crosslinked materials.[24] It has been reported that the product of the reaction of sulfur and DCPD is influenced by the reaction temperature.[18] At temperatures below 140 °C, it has been found that only the norbornene alkene unit of DCPD reacts with sulfur, whereas the cyclopentene alkene unit remains intact, resulting in the formation of a linear polymer which was found to be soluble.[18] At elevated temperatures, it has been found that both the norbornene and cyclopentene alkenes of DCPD react with sulfur, allowing the formation of a 3D polymer network and thus a crosslinked polymer which is insoluble in common organic solvents.[18] Similarly to DCPD, DVB was also found to form high T_g polymers when reacted with sulfur *via* inverse vulcanisation where S50-DVB and S70-DVB had T_g's of 72 and 52 °C (Table 2.1) respectively, with the absence of remaining unreacted crystalline sulfur according to the thermograms obtained by DSC (Appendix 2.2 andAppendix

2.3). The resultant materials were hard, glassy black solids that were insoluble in common organic solvents, indicative of the formation of a crosslinked polymer. Consumption of DVB alkene units was confirmed by FT-IR spectroscopy (Appendix 2.4). The sulfur content of the polymers were determined by combustion analysis (Table 2.2), where both polymers were found to have an approximate sulfur content of 70 %. The reason that S50-DVB polymer contains a higher than expected sulfur content may be due to the volatility of DVB.

The second set of polymers synthesised used perillyl alcohol and DIB as comonomers, their respective sulfur polymers result in polymers with lower T_g (0-40 °C). In addition to this they are not fully crosslinked polymers as they are soluble in organic solvents such as chloroform and THF. Perillyl alcohol (Figure 2.5) is a naturally derived monocyclic terpene that is found in the essential oils of lavender and peppermint amongst others and, has received interest as a potential anti-cancer agent.[25]

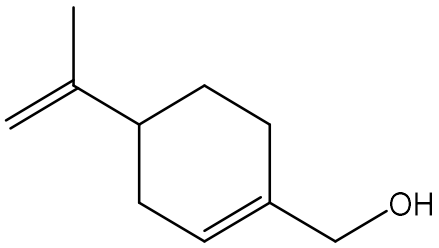

perillyl alcohol

Figure 2.5: The chemical strucure of perillyl alcohol.

The product of the copolymerization of perillyl alcohol and sulfur yielded red glassy materials. S50-PA and S70-PA were analysed by DSC and were found to have T_g's of 34 °C and 14 °C respectively (Table 2.1). Crystalline sulfur was not found to be present in the materials as shown by the lack of a melting transition at 115 °C in the thermograms of both S50-PA and S70-PA (Figure 2.6 and Appendix 2.5).

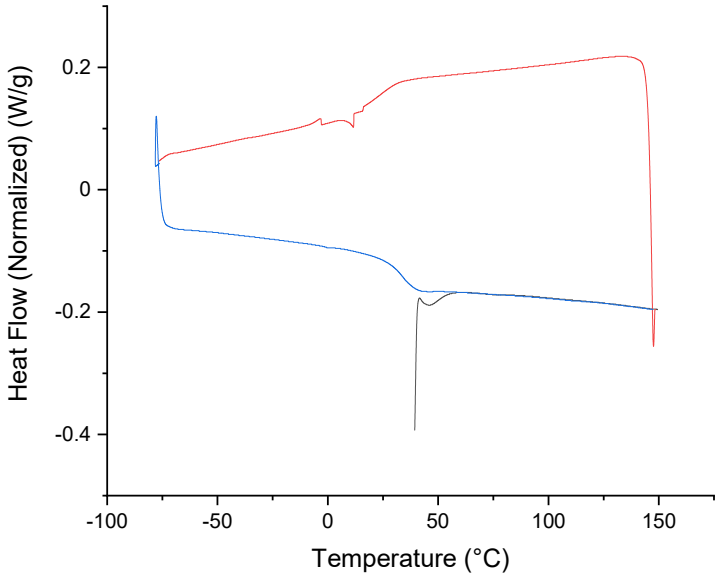

Figure 2.6: DSC traces for S50-PA showing the first heating cycle to 150 °C (black), cooling to -80 °C (red), and the second heating cycle to 150 °C (blue).

FT-IR analysis of both S50-PA and S70-PA (Figure 2.7) confirm consumption of the alkene units of perillyl alcohol due to the disappearance of the peaks at ca. 3100 cm^{-1} and 1640 cm^{-1} due to the =C-H and C=C stretching vibrations. New peaks are present in the fingerprint region of the spectra of both S50-PA and S70-PA which are not present in the spectra of perillyl alcohol at ca. 750 cm^{-1} which may be attributed to the C-S stretching vibration. This vibration is often very weak in infrared spectroscopy but may appear stronger in raman spectroscopy.[26]

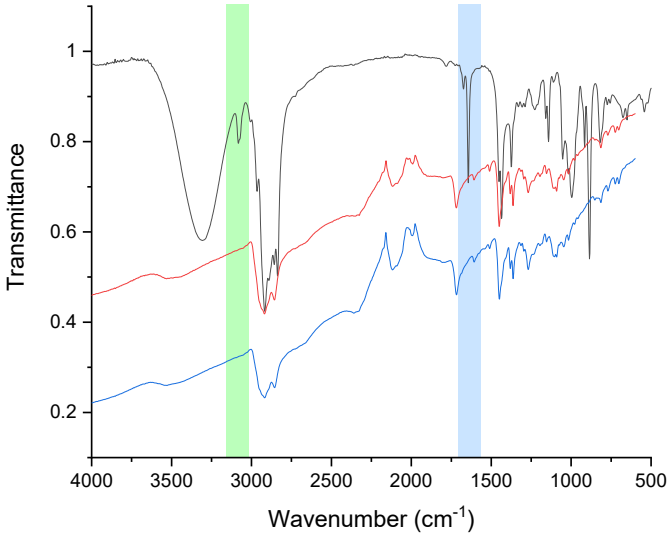

Figure 2.7: FT-IR spectra for perillyl alcohol (black), S50-PA (red) and S70-PA (blue). Highlighted in green at ca. 3100 cm^{-1} is the signal corresponding to =C-H stretch, and highlighted in blue at ca. 1640 cm^{-1} is the signal corresponding to an alkene C=C stretch. Both signals are visible in the spectrum of the monomer but are not visible in the spectra of the polymers suggesting alkene consumption during the reaction.

Table 2.3: Calculated and obtained elemental analysis of S-PA and S-DIB.

Sample	Calc. % carbon	Calc. % hydrogen	Calc. % sulfur	**C/H ratio**	Actual % carbon	Actual % hydrogen	Actual % sulfur	**C/H ratio**
S50-PA	39.45	5.29	50	**7.46**	40.07	4.92	51.58	**8.14**
S70-PA	23.67	3.17	70	**7.46**	23.22	3.11	73.23	**7.47**
S50-DIB	45.54	4.46	50	**10.2**	43.78	4.11	52	**10.65**
S70-DIB	27.32	2.67	70	**10.2**	27.2	2.84	71	**9.58**

Elemental analysis of S50-PA and S70-PA showed that both materials have sulfur contents similar to theoretical values of 50 and 70 % (Table 2.3). The C/H ratio of S70-PA was consistent with the expected ratio, whereas the C/H ratio of S50-PA was slightly increased. This may be due to loss of hydrogen due to hydrogen abstraction. S50-PA and S70-PA were found to be soluble in THF and chloroform, allowing ^{1}H nuclear magnetic resonance (NMR) spectroscopy to be used to further characterise the products. Structure elucidation of inverse vulcanised polymers, which are composed of sulfur as the main component remain a challenge throughout the reported literature.[27] The most abundant isotope of sulfur, ^{32}S has no nuclear spin, and is thus inactive in NMR spectroscopy. ^{33}S nuclei are indeed active in NMR spectroscopy (spin

I=3/2). However, ^{33}S NMR spectroscopy is not a feasible method for elucidating the structures of inverse vulcanised polymers for several reasons. The difficulty in conducting ^{33}S NMR spectroscopy is due to low natural abundance (0.76%) of ^{33}S nuclei, low gyromagnetic ratio resulting in poor signal to noise ratios in spectra, along with anisotropic broadening in spectra arising from quadrupolar interactions.[28] For this reason, the characterisation of inverse vulcanised polymers by NMR spectroscopy is often limited to ^{1}H and ^{13}C nuclei, permitting that the polymer has some solubility in NMR solvents such as deutrated chloroform. The limitation of using ^{1}H and ^{13}C NMR spectroscopy means that structure elucidation of sulfur species that are not in proximity to carbon or hydrogen atoms i.e polysulfide segments, cannot be achieved. However, ^{1}H and ^{13}C NMR spectroscopy can be used to assess any structural changes in the monomers such as loss of signals corresponding to alkene units, or the presence of new peaks that may arise from bonding to sulfur. Consistent with FT-IR spectroscopy, resonances in the NMR spectra of S50-PA and S70-PA (Figure 2.8) corresponding to alkene units of perillyl alcohol are diminshed, confirming consumption of the C=C double bonds during inverse vulcanisation. Furthermore, resonances in the region of 3.5-4 ppm are indicative of S-C-H protons which suggest the formation of crosslinks between sulfur and the alkenes of perillyl alcohol.[18]

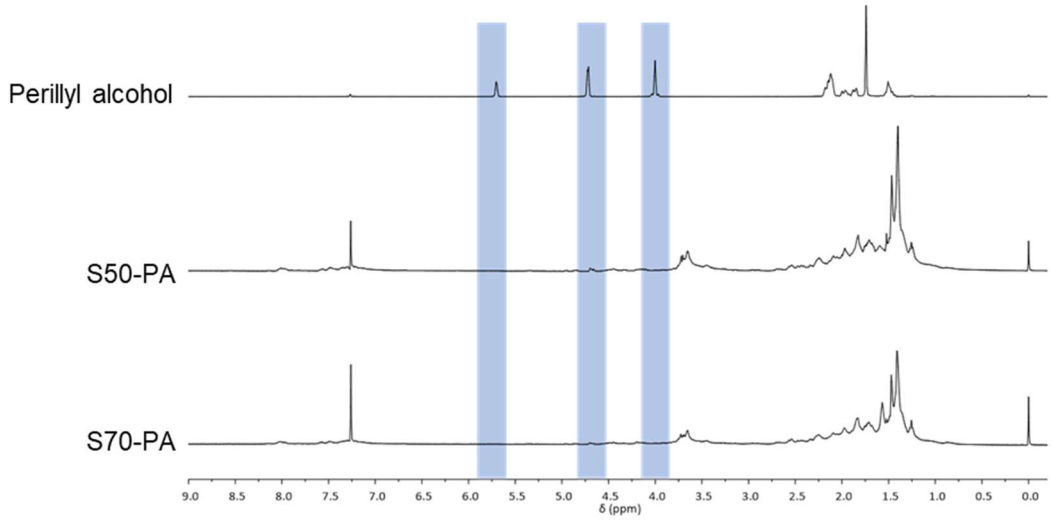

Figure 2.8: ^{1}H NMR spectra of perillyl alcohol, S50-PA and S70-PA. Highlighted are chemical shifts consistent with those of vinylic and allylic protons which are present in the spectrum for perillyl alcohol but not in the spectra of the respective polymers suggesting consumption of alkene units during reaction.

The solubility of S-PA in THF and chloroform suggests that the product is not a fully crosslinked polymer. Given that the FT-IR and ^{1}H NMR spectra of S50-PA and S70-PA suggest full cosumption of the alkene units, the products should theoretically be crosslinked, according to the proposed mechanism of inverse vulcanisation (Figure 1.7). It is therefore likely that the reaction of sulfur and perillyl alcohol can also proceed by another route. It is possible that perillyl alcohol can undergo hydrogen abstraction during inverse vulcanisation which could lead to aromatisation, and therefore fewer available alkene units to form crosslinks with sulfur.[29] This has been seen for limonene, a structurally similar cyclic terpene, which has been shown to undergo 1,3-hydrogen shifts with loss of hydrogen leading to aromatisation to give *p*-cymene, with further dehydrogenation leading to the production 1-methyl-4-(2-propenyl)benzene (Figure 2.9). [16, 30, 31] It is thought that loss of H_2 from limonene takes place by hydrogen abstraction to form H_2S during inverse vulcanisation.[32]

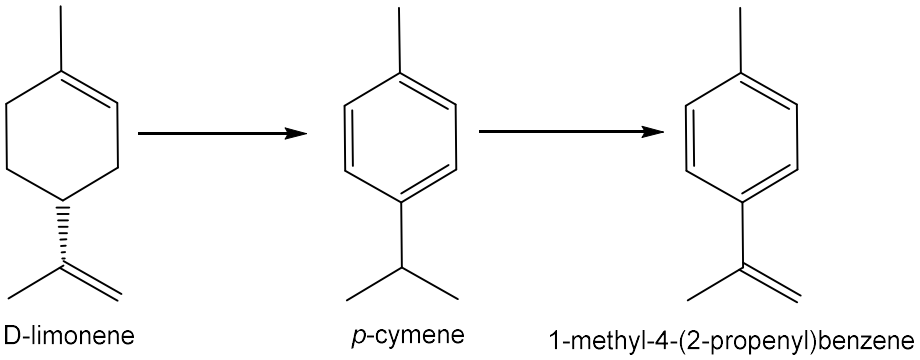

Figure 2.9: Limonene can undergo 1,3-hydrogen shifts with loss of hydrogen leading to aromatisation to give *p*-cymene, with further dehydrogenation leading to the production 1-methyl-4-(2-propenyl)benzene.

Weak resonances in the aromatic region of the spectra of S50-PA and S70-PA at around 8 ppm suggest that perillyl alcohol does indeed form aromatic structures, which would explain the lower than expected crosslinking density of the polymer. It is therefore possible that the polymer structure of S-PA consists of both linear and branching character (Figure 2.10). Parker *et al.* also noted the presence of aromatic resonances in the ^{1}H NMR spectra of polymers synthesised from perillyl alcohol and sulfur.[29]

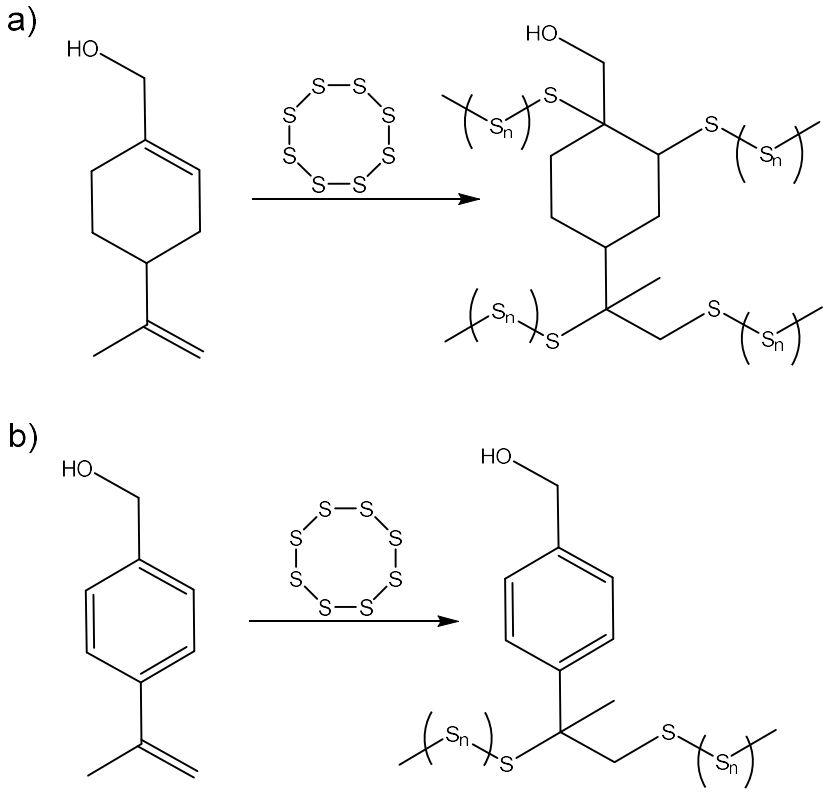

Figure 2.10: Proposed structures of the products of inverse vulcanisation of perillyl alcohol to give a) branched and b) linear structures derived from the aromatisation of perillyl alcohol by 1,3-hydrogen shifts with loss of hydrogen.

Polymers synthesised from the copolymerisation of sulfur and DIB resulted in similar products to those of the copolymerisation of sulfur and perillyl alcohol as described above as red glassy materials. S50-DIB and S70-DIB have T_g's of 27 °C and 10 °C respectively, similar to those of S-PA at the same sulfur:comonomer ratio (Table 2.1, Appendix 2.6 and 2.7). Consumption of the alkene units of DIB was confirmed by FT-IR spectroscopy (Appendix 2.8). Similarly to S-PA, new peaks present at around 750 cm^{-1} may be attributed to the C-S stretching vibration. The sulfur content of the polymers was determined by combustion analysis, where both S50-DIB and S70-DIB were found to have similar sulfur contents to the theoretical values (Table 2.3). S50-DIB and S70-DIB also show solubility in THF and chloroform, which suggests that the polymers formed from the synthesis of sulfur and DIB at these sulfur:comonomer ratios are not true crosslinked polymers. The lower than expected crosslink

density observed for S-PA could be attributed to aromatisation of perillyl alcohol during inverse vulcanization, however, this cannot be the case for DIB which already consists of an aromatic ring. It is thought that thiyl radicals produced during the inverse vulcanisation of sulur and DIB can recombine intramolecularly to form sulfur loops (Figure 2.11) and this may be the reason for the lower than expected crosslinking density of S-DIB.[15,33]

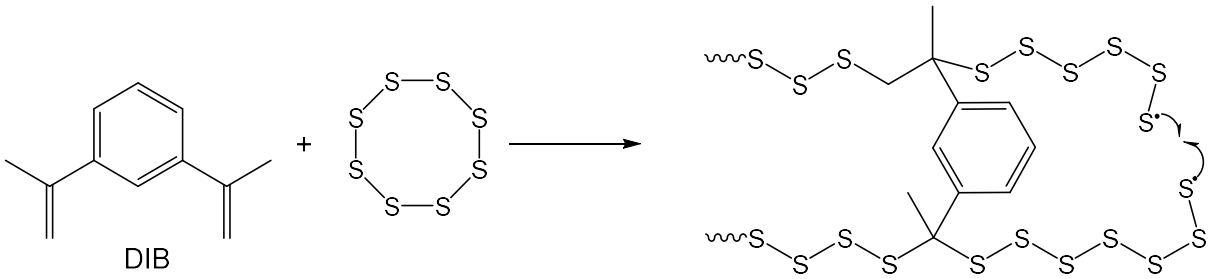

Figure 2.11: Depiction of intramolecular thiyl radical combination to give S-S loop structures.

The third set of polymers were synthesised from vegetable oils, namely linseed oil and rapeseed oil which consist of triglycerides and fatty acids such as linolenic acid and oleic acid (Figure 2.12). Inverse vulcanised polymers synthesised with vegetable oils have lower T_g (<0 °C) due to the flexibility of long carbon chains present in triglycerides. Polymers synthesised from sulfur and linseed and rapeseed oil, denoted S-LO and S-RO respectively were synthesised at 30 (S30-LO and S30-RO) and 50 wt% sulfur (S50-LO and S50-RO). Triglycerides are known for only being able to stabilise around 30 wt% of sulfur during inverse vulcanisation.[29] When synthesised at higher wt% of sulfur, the materials formed are composites of polymeric material and crystalline sulfur. DSC analysis of S30-LO indicates the formation of a polymeric material with a T_g of -12 °C (Figure 2.13, Table 2.1), as expected due to its rubbery and flexible properties. S50-LO also had a T_g of -12 °C (Appendix 2.10, Table 2.1), despite having a different sulfur:comonomer ratio to that of S30-LO. Generally, the higher the sulfur content of inverse vulcanised polymers, the lower the T_g of the resultant material.[15] It is proposed that higher sulfur content results in longer sulfur chains which are expected to be flexible and thus would give the polymer structure more flexibility. The reason that the T_g's of

both S30-LO and S50-LO are similar could be due to the formation of similar polymer structures. The DSC of S30-LO shows no melting transitions corresponding to crystalline sulfur, indicating that all crystalline sulfur has reacted. However, the thermogram of S50-LO shows that some elemental sulfur has not been stabilised within the polymer, as evidenced by small endothermic transitions at temperatures of approximately 104 °C and 119 °C, which are consistent with the melting of orthorhombic α-sulfur and monoclinic β-sulfur.[34] As not all of the sulfur has been incorporated into the polymer, it is likely that the chains of sulfur within S50-LO are shorter than expected, and may be similar to that of S30-LO, which would result in materials with similar T_g's.

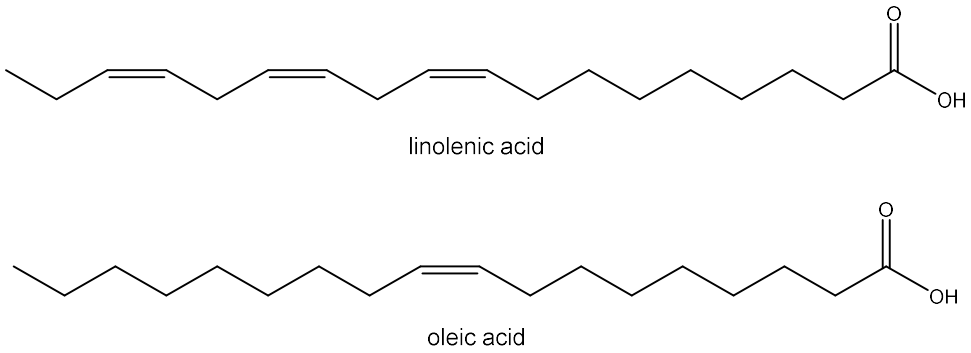

Figure 2.12: Chemical structures of linolenic acid and oleic acid, examples of fatty acids that are present in vegetable oils such as linseed and rapeseed oil.

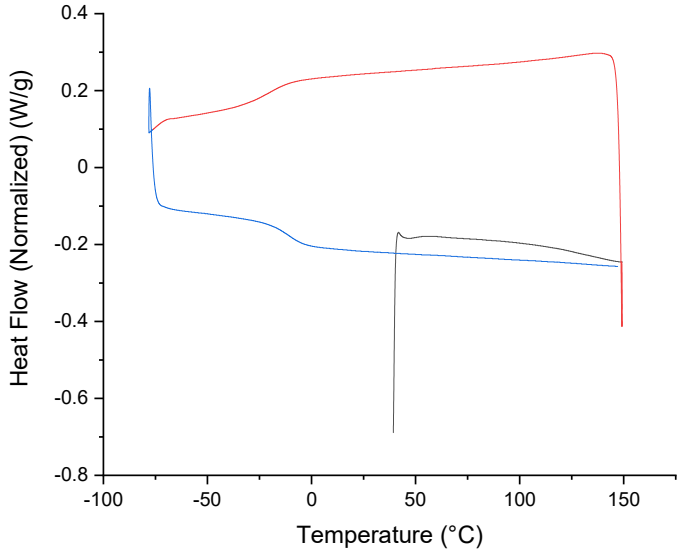

Figure 2.13: DSC traces of S30-LO showing the first heating cycle to 150 °C (black), cooling to -80 °C (red), and the second heating cycle to 150 °C (blue).

Consumption of the alkene units of linseed oil after polymerisation with sulfur was assessed by FT-IR spectroscopy (Figure 2.14), where loss of signals corresponding to =C-H and C=C stretching vibrations was observed. New signals at around 750 cm^{-1} were present in the spectra of S30-LO and S50-LO which may be attributed to C-S stretching vibrations.

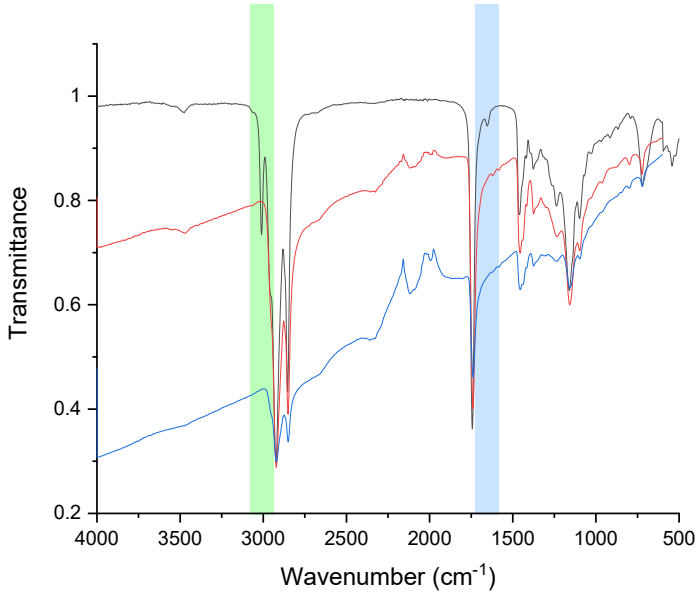

Figure 2.14: FT-IR spectra of linseed oil (black), S30-LO (red) and S50-LO (blue). Highlighted in green at ca. 3100 cm^{-1} is the signal corresponding to =C-H stretch, and highlighted in blue at ca. 1640 cm^{-1} is the signal corresponding to an alkene C=C stretch. Both signal intensities are reduced in the polymer spectra compared to the monomer suggesting alkene consumption during the reaction.

Similarly to S-PA and S-DIB, S30-LO and S50-LO were found to be soluble in THF and chloroform. ^{1}H NMR spectroscopy was used to compare the obtained products of the polymerisation of sulfur and linseed oil to that of unreacted linseed oil. Loss of signals corresponding to vinylic and allylic protons was observed after reaction (Figure 2.15). Broadening of the peaks of the resultant materials was also observed, consistent with other inverse vulcanised polymers that give rise to line broadening in NMR.[35]

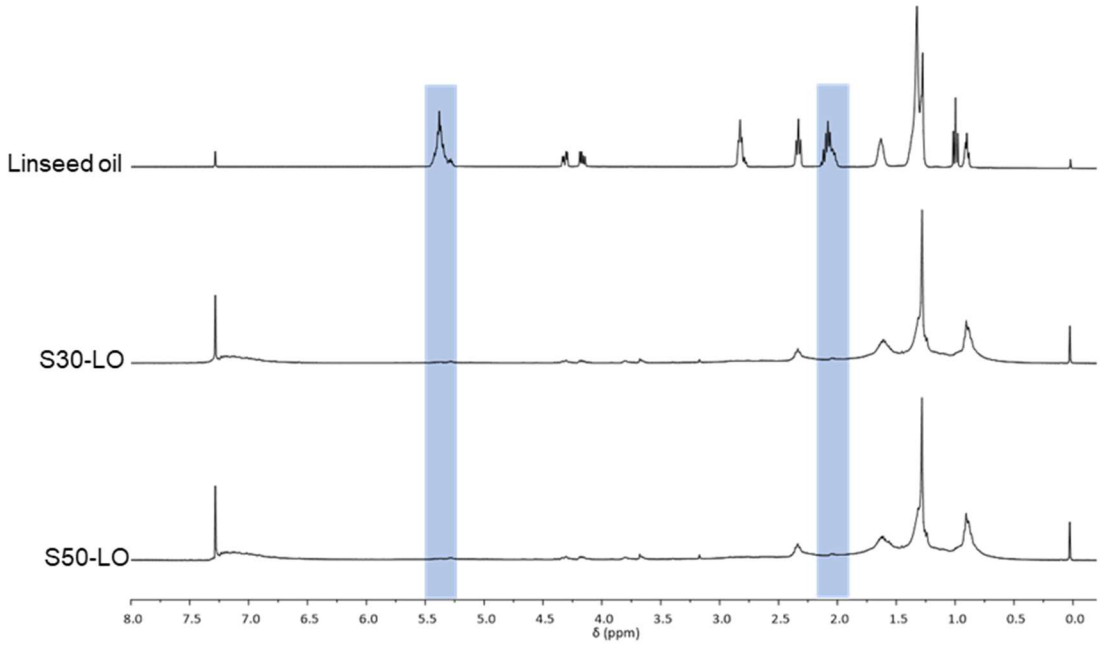

Figure 2.15: ^{1}H NMR spectra of linseed oil, S30-LO 30 and S50-LO. Highlighted are chemical shifts consistent with those of vinylic protons (at ca. 5-5.5 ppm) and allylic protons (at ca. 1.9 ppm) which are present in the spectrum for linseed oil but not in the spectra of the respective polymers suggesting consumption of alkene units during reaction.

Similarly to S-LO, sulfur was polymerised with rapeseed oil at 30 ad 50 wt% sulfur to produce S30-RO and S50-RO. The resultant materials were also found to have low T_g values of -30 °C and -31 °C for S30-RO and S50-RO, respectively (Table 2.1, Appendix 2.11 and Appendix 2.12). As for S50-LO, S50-RO also contained crystalline sulfur as presented by melting transitions in its thermogram (Appendix 2.12), whereas such transitions were not present in the thermogram for S30-RO. The similarity of the T_g values for S30-RO and S50-RO could be for the same reasons as discussed for S-LO, where a similar amount of sulfur has been incorporated into the polymer at both 30 and 50 wt% sulfur loadings. The consumption of the alkene units of rapeseed oil were confirmed by both FT-IR and ^{1}H NMR spectroscopy (Appendix 2.13-Appendix 2.14), confirming reaction at the C=C double bonds as expected for inverse vulcanisation.

The sulfur rank, i.e the length of polysulfide segments R-$S_{(n)}$-R, of inverse vulcanised polymers is expected to be dependent on both the comonomer type and the sulfur:comonomer ratio employed in the reaction feedstock. Increasing the amount of sulfur in the feedstock is expected to give higher sulfur ranks, but this also depends on the ability of the comonomer to stabilise large amounts of sulfur. However, there is a limit to the maximum sulfur rank that can be achievable. Increasing the sulfur content beyond the limit at which it can be stabilised by the comonomer will no longer give a higher sulfur rank, and instead the material becomes a composite that consists of polymer and elemental sulfur.[14] Determination of the sulfur rank of inverse vulcanised polymers by analytical methods remains challenging. However, unreacted crystalline S_8 which is not incorporated into the polymer chains and therefore cannot contribute to the sulfur rank can be detected by methods such as DSC. The average sulfur rank in the polymers can be calculated providing that all S_8 was consumed during reaction (often determined by a lack of a sulfur melting transition in the DSC trace) and by calculating the molar ratio of alkene units to sulfur atoms.[15] The average sulfur rank for the polymers synthesised for this study is shown in Table 2.1. The polymers are likely to have various sulfur ranks within the chains, however, the calculated average sulfur rank provides a useful comparative value. The average sulfur rank for S-LO and S-RO could not be calculated as the molar ratio of alkene units is unknown due to the oils being composed of various triglycerides.

2.4.2 Antibacterial Properties

Antibacterial testing of all polymers against methicillin-resistant *S. aureus* (USA300) and *P. aeruginosa* (PAO1) was carried out by submerging the polymer cubes (1 cm^3) in bacterial culture, followed by incubation. Polypropylene cut to 1 cm^3 cubes was used as a negative control for all tests, and each sample was tested in triplicate. Three incubation temperatures were used with the aim of testing the samples at their glassy state ($T < T_g$) and at their rubbery state ($T > T_g$). The T_g of polymers has been found to be particularly important for polymers with potential biological applications, such as for drug delivery systems. The T_g of a polymer can act as a thermal switch triggering drug release from the polymer when the temperature exceeds the T_g.[36] The three temperatures chosen were (3 ± 1) °C, (21 ± 1) °C and (37 ± 0.3) °C. Temperatures below the selected range were not investigated as low temperatures would result in freezing of the culture medium, and higher temperatures may result in cell death. A similar method reported by Smith *et al*. was used to assess the antibacterial activity of the polymers, which followed the ISO 22196:2011 method.[8] The reduction in viable cells in solution and viable cells extracted from the surface of the materials was investigated (Figure 2.16). To enumerate the viable cells in solution, after incubation, the bacterial solution surrounding each sample was removed and the viable cells were enumerated after serial dilution of the solution in phosphate buffered saline (PBS) onto Luria-Bertani (LB) agar, using the Miles and Misra method (Figure 2.16 and Figure 2.17).[38] The Miles and Misra method is used to enumerate bacterial suspensions by counting the number of colony forming units (CFU) after inoculation on solid medium i.e agar. This method can only be used to calculate viable cells, as inoculation of dead cells on agar will not result in the growth of a colony forming unit. To enumerate the viable cells extracted from the surface of the materials, the cubic polymers were gently rinsed with PBS to remove any planktonic cells and were vortexed in LB broth to remove any adhered cells. The vortexed solution was serially diluted in PBS and the viable

cells associated with the sample surface were enumerated using the Miles and Misra method (Figure 2.16 and Figure 2.17).

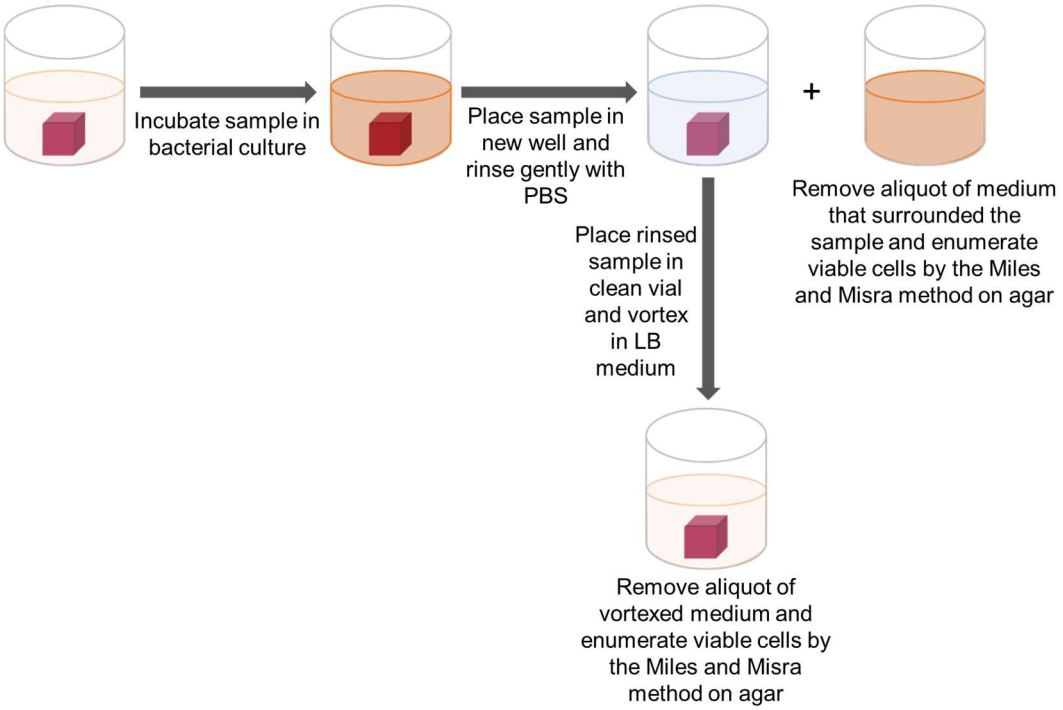

Figure 2.16: Simplified scheme depicting the antibacterial testing of 1 cm^3 samples to enumerate the number of viable cells on the same surface, and the number of viable cells in the solution surround the samples.

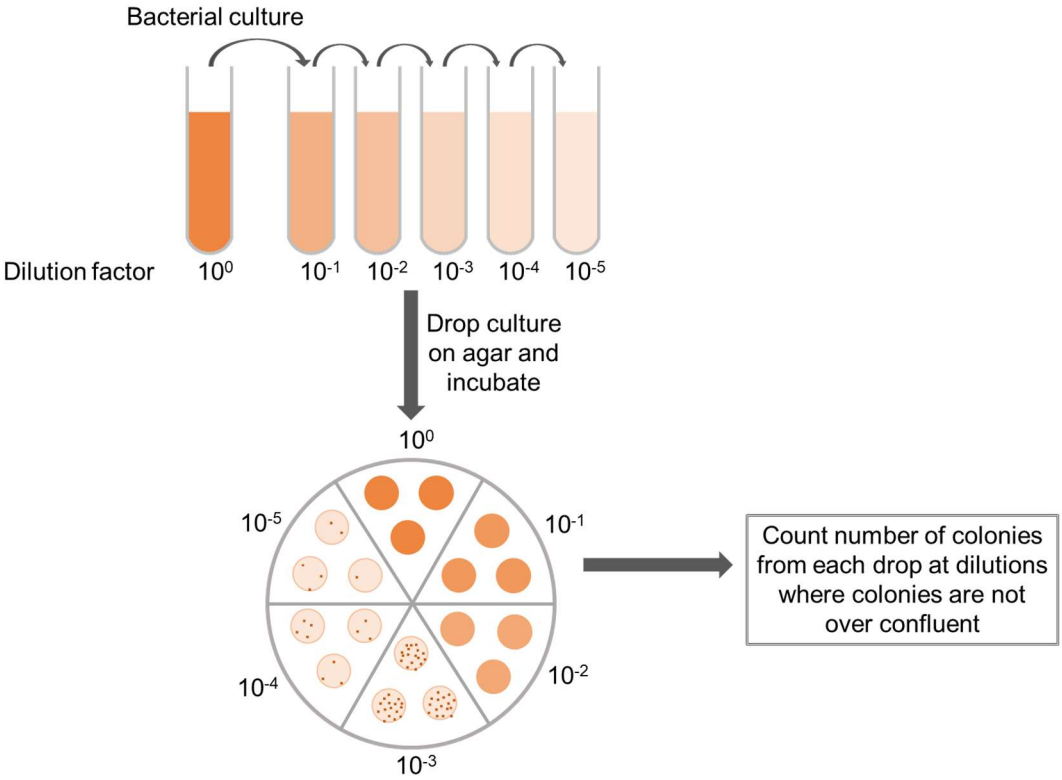

Figure 2.17: Schematic describing the Miles and Misra method for enumerating viable cells on agar.

S50-PA and S70-PA were found to have T_g's of (34 ± 3) °C and (14 ± 4) °C respectively (Table 2.1). S50-PA and S70-PA were tested against a methicillin-resistant *S. aureus* strain (USA300) at (3 ± 1) °C, (21 ± 1) °C and (37 ± 0.3) °C. The polymers behaved differently at each temperature (Figure 2.18). At 3 °C, neither of the polymers showed a reduction in viable cells in solution compared to polypropylene, and only S70-PA showed a reduction in surface associated cells (74 % reduction). At this temperature, both polymers are in their glassy state ($T < T_g$). It is possible that S70-PA has greater antibacterial activity at this temperature compared to S50-PA due to higher sulfur content and thus a higher sulfur rank (length of polysulfide segments R-$S_{(n)}$-R) and more labile S-S bond that could react with thiol containing proteins of the bacteria.[32,33] By increasing the test temperature to 21 °C, S50-PA showed a moderate reduction in surface associated viable cells (44 % reduction relative to polypropylene control, p=0.06), where at lower test temperature no effect was seen, however, no reduction in viable cells in solution was observed. For S70-PA at 21 °C, the reduction in surface associated

cells appears similar to the result at 3 °C, however, there is a reduction in the viable cells in solution (83 % reduction). At 21°C, S50-PA is in its glassy state (T < T_g), whereas S70-PA is in its rubbery state (T > T_g). When the test temperature was increased further to 37 °C both S50-PA and S70-PA show a reduction in the viable cells extracted from the surface (89% for S-50PA and 92% for S70-PA) and from solution (77% for S50-PA and 98% for S70-PA). It is worth noting that S70-PA had lost its shape and yellow precipitates were present on the materials surface after incubation at 37 °C. The results show that both S50-PA and S70-PA show an antibacterial effect against *S. aureus*, however, this effect is dependent on the test temperature and could therefore be related to the physical state of the polymer. Little antibacterial effect is seen when the test temperature is well below the T_g of the polymers, however, when the temperature approaches the T_g of the polymers, there is a reduction in surface associated viable cells. A reduction in the viable cells in solution is seen when the test temperature is above the T_g of the polymers. It is important to note that the test temperature effects bacterial growth. During the study, the bacterial cultures in the absence of polymers were found to grow faster at 37 °C compared to 21 and 3 °C. To ensure that the differences in antibacterial activity is due to the physical state of the polymer, rather than the temperature conditions themselves, the final cell density of the control samples was kept constant at each temperature. To allow the samples to reach the same final cell density, the incubation times were varied. Tests at 37 °C were conducted with 5 hr incubation time, 21 °C at 24 h and 3 °C at 48 h.

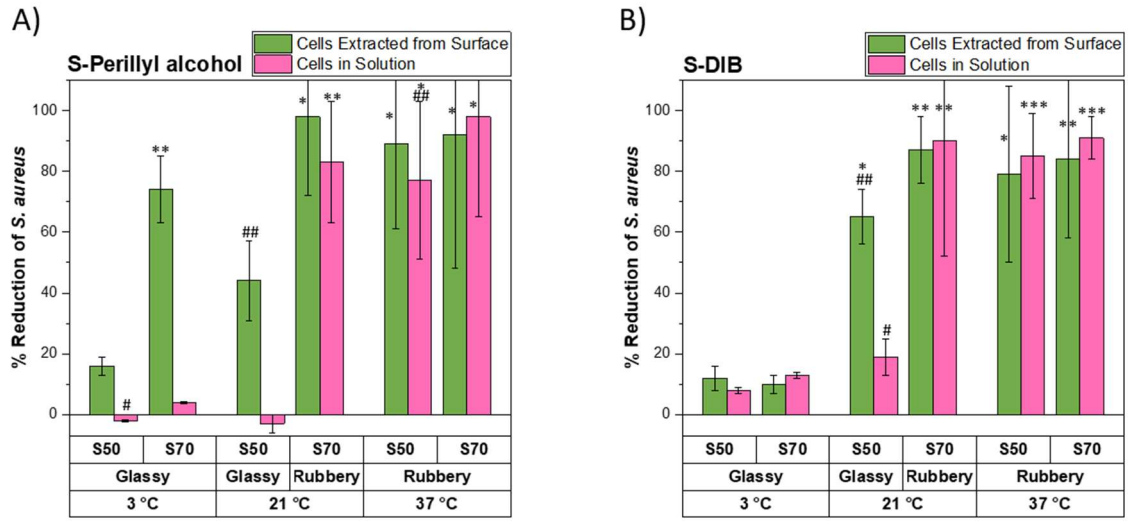

Figure 2.18: A summary of the % reduction in viable *S. aureus* cells extracted from the surface and from solution compared to polypropylene for A) S-PA and B) S-DIB at varying test temperature and sulfur:comonomer ratio. * $p<0.05$ relative to polypropylene, ** $p<0.01$ relative to polypropylene, *** $p<0.001$ relative to polypropylene, $^{\#}$ $p<0.05$ for S50 compared to S70, $^{\#\#}$ $p<0.01$ for S50 compared to S70 at the same test conditions.

To assess if the observation that the antimicrobial effect is dependent on the physical state of the polymer (i.e rubbery or glassy) is limited to individual comonomers, or, if it is seen for other polymers with similar T_g's synthesized with different comonomers, S-DIB was also studied. The antibacterial activity of S50-DIB has been investigated by Smith *et al.*, however no other sulfur:comonomer ratio was investigated. Therefore the antibacterial activity of S50-DIB was reassessed for this study, to compare the antibacterial properties of S50-DIB and S70-DIB.[10] S50-DIB and S70-DIB gave T_g's of (27 ± 1) °C and (10 ± 4) °C, therefore at each test temperature the state of each sample should be the same as for the perillyl alcohol equivalents (at 3 °C both samples are glassy, at 21 °C 50 wt% sulfur is glassy and 70 wt% sulfur is rubbery, at 37 °C both samples are rubbery). The results of the percentage reduction in viable surface associated cells and the viable cells in solution for S-DIB are shown in (Figure 2.18). The results show a similar trend to that of the perillyl alcohol equivalents, whereby when the polymers are in their glassy state at a test temperature of 3 °C, no significant antibacterial effect is seen against *S. aureus* for either cells in solution or surface associated cells. At 21 °C both polymers show a reduction in surface associated viable cells, but only S70-DIB shows a

significant reduction in the viable cells in solution, and at 37 °C both polymers show a reduction in both the surface associated cells (79% for S50-DIB and 84% for S70-DIB) and the cells in solution (85% for S50-DIB and 91% for S70-DIB).

Table 2.4: A summary of the % reduction in viable *S. aureus* cells extracted from the surface and from solution compared to polypropylene for various S-polymers. The T_g and test temperature are also summarised for each polymer.

Polymer	T_g (°C)	Test Temperature (°C)	Test temperature > T_g ?	Surface Reduction (%)	Solution Reduction (%)
S50-DCPD	88	37	N	-24 ± 5	9 ± 3
S70-DCPD	45	37	N	74 ± 15	4 ± 0.1
S50-DVB	72	37	N	20 ± 5	15 ± 3
S70-DVB	52	37	N	53 ± 16	23 ± 0.1
S30-RO	-31	3	Y	75 ± 12	29 ± 2
S50-RO	-30	3	Y	90 ± 35	40 ± 5
S30-LO	-12	3	Y	55 ± 1	31 ± 7
S50-LO	-12	3	Y	51 ± 1	33 ± 9

The tests against *S. aureus* were also repeated for the other two sets of polymers, the high T_g set synthesised from DCPD and DVB, and the low T_g set synthesised from linseed oil and rapeseed oil (Table 2.4). Due to their high T_g (45-88 °C) (Table 2.4), the polymers synthesised from DCPD and DVB were tested only at 37 °C, as the polymers will be in the glassy state at all test temperatures. The results show that S50-DCPD and S50-DVB show no, or very little reduction in the viable surface associated cells and viable cells in solution compared to polypropylene. S70-DCPD and S70-DVB show a greater reduction in viable surface associated cells compared to the 50 wt.% sulfur equivalents, suggesting that the sulfur content of the polymers is influencing their antibacterial properties. These results are also consistent with the observations made by Smith *et al.* whereby S-DCPD synthesised at 50 wt.% sulfur did not show an antibacterial effect against *S. aureus* whereas S-DIB did show an inhibitory effect.[10] It was suggested that these differences could be due to the higher sulfur rank expected for S-DIB compared to S-DCPD, which could explain why S70-DCPD in this study does show a

moderate reduction in the viable surface associated cells compared to polypropylene whereas S50-DCPD does not show an inhibitory effect. S-polymers using rapeseed and linseed oil as comonomers were synthesised at 30 and 50 wt.% sulfur, due to such vegetable oils only being able to stabilise lower amounts of sulfur.[14] Both polymers show signs of inhomogeneity, especially at 50 wt.% sulfur feeds whereby crystalline sulfur was visible on the sample surface. The polymers formed from rapeseed and linseed oil at 30 and 50 wt.% sulfur have T_gs below 0 °C (Table 2.4), and therefore these samples were tested against *S. aureus* at 3 °C, a temperature at which the polymers exhibit their rubbery state. S30-RO, S50-RO, S30-LO and S50-LO sulfur show a reduction in viable surface associated cells and viable cells in solution.

The polymers from all six of the comonomers tested against *S. aureus* showed a correlation between the % reduction in viable cells in solution and whether the sample was in the rubbery or glassy state at the testing temperature. All samples tested above their T_g showed a greater than 25% reduction, whereas all samples tested below their T_g showed a less than 25% reduction (Appendix 2.15). A possible reason for an enhanced % reduction in viable cells in solution when the polymers are tested above their T_g could be the leaching of antimicrobial species from the polymer. Above the T_g, when the polymer is in its rubbery state, polymer chains have increased mobility and could allow for the diffusion of any potential antimicrobial species from the polymer to the surface that could leach into solution. It is possible that low molecular weight species such as oligomers are present in the final material, which may be susceptible to leaching out of the polymer.

High sulfur content terpolymers using perillyl alcohol and DCPD were synthesised and tested against *S. aureus* to investigate the antibacterial activity with increasing wt.% of DCPD. The terpolymers, denoted S-PA-DCPD, were synthesised at 50 wt.% sulfur and varying the PA:DCPD ratio (Table 2.5) by increasing the DCPD content in 5 wt.% increments. DSC analysis of all terpolymers consisted of only one T_g, showing that the materials formed are one

terpolymer rather than a blend of two copolymers (Appendix 2.16-Appendix 2.21). If a blend of two copolymers were formed, two T_g's should be present in the DSC spectrum of the material, one representing the T_g of S-PA, and the other representing S-DCPD.

Table 2.5: Table summarizing the ratios of S:PA:DCPD used to synthesise terpolymers and their calculated average sulfur rank.

Polymer	wt.% Sulfur	wt.% Perillyl alcohol	wt.% DCPD	Average sulfur rank
S50-PA	50	50	0	2.375
50:45:05	50	45	5	2.339
50:40:10	50	40	10	2.305
50:35:15	50	35	15	2.272
50:30:20	50	30	20	2.239
50:25:25	50	25	25	2.208
50:20:30	50	20	30	2.177
S50-DCPD	50	0	50	2.031

The T_g of the resultant materials increased whilst the soluble fraction of the materials decreased with increasing wt.% DCPD (Figure 2.19). The increase in T_g and decrease in soluble fraction of the terpolymers with increasing wt.% DCPD can be attributed to higher crosslink density provided by DCPD.

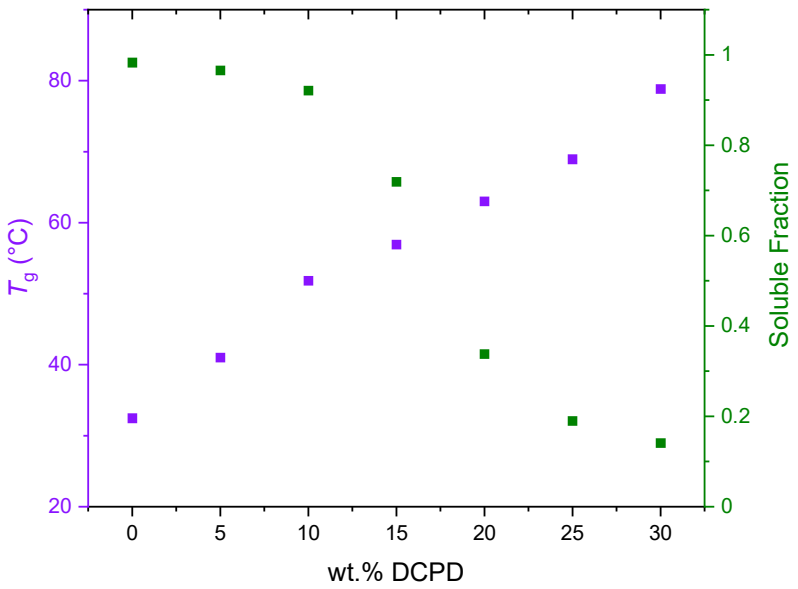

Figure 2.19: A plot of the T_g (°C) and soluble fraction of S-PA-DCPD terpolymers with increasing wt.% DCPD.

Terpolymers synthesised with S:PA:DCPD ratios of 50:45:5, 50:35:15 and 50:25:25 were tested against *S. aureus* and compared to S50-PA and S50-DCPD copolymers (Figure 2.20). The results show that the terpolymers have different antibacterial properties depending on the ratio of PA:DCPD employed. The S-PA-DCPD terpolymer with a ratio of 50:45:5 showed a similar reduction in the viable cells on the surface relative to polypropylene to that of S50-PA, however, the solution effect of the 50:45:5 terpolymer is diminished compared to S50-PA. The T_g of S50-PA is 34 °C, however, doping the polymer with 5 wt.% DCPD increased the T_g to 41 °C. At the test temperature of 37 °C, S50-PA is rubbery whereas the 50:45:5 terpolymer is glassy. It is possible that the solution effect is decreased due to the increase in T_g resulting in lower mobility of the polymer chains for the 50:45:5 terpolymer that could prevent any potential antimicrobial species from leaching out into solution. As the DCPD content is increased further to 15 and 25 wt.%, there is a decrease in the reduction of viable cells on the surface compared to S50-PA and the 50:45:5 terpolymer. The decrease in surface effect could be attributed to a decrease in the average sulfur rank with increasing DCPD content (Table 2.5).

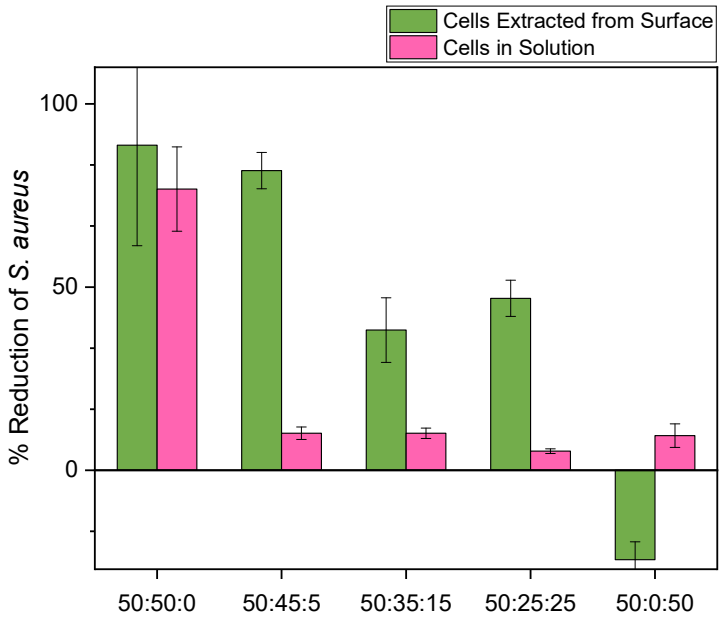

Figure 2.20: A summary of the % reduction in viable *S. aureus* cells extracted from the surface and from solution for S-PA-DCPD terpolymers at varying ratios.

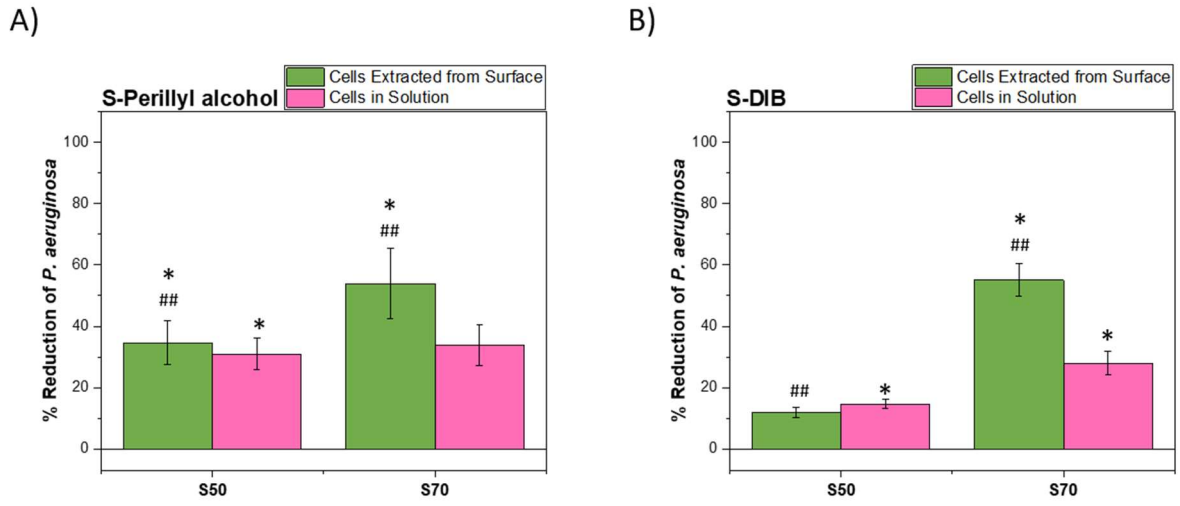

Figure 2.21: A summary of the % reduction in viable *P. aeruginosa* cells extracted from the surface and from solution compared to polypropylene for A) S50-PA and S70-PA and B) S50-DIB and S70-DIB. *p<0.05 relative to polypropylene $^{\#\#}p$<0.01 for S50-PA compared to S70-PA.

P. aeruginosa is a Gram-negative, rod-shaped pathogen that is a leading cause of persistent nosocomial infections.[38] S50-PA, S70-PA, S50-DIB and S70-DIB were tested against *P. aeruginosa* at 37 °C. The polymers drove a reduction in the viable cells both in solution and on the polymer surface (Figure 2.21). Statistical analysis conducted by one-way analysis of

variance (ANOVA) demonstrates that S50-PA and S70-PA show a similar reduction in the viable cells in the solution that surrounded the samples during incubation, however, S70-PA shows a greater reduction in the viable cells associated with the surface (p<0.01 vs S50-PA). For the S-DIB equivalents against *P. aeruginosa*, S70-DIB results in a greater reduction in both the viable cells in solution and on the surface compared to S50-DIB, and the results are comparable to that of S70-PA. Therefore, the polymers show an inhibitory effect against both Gram-positive and Gram-negative pathogens.

Pathogens that can form biofilms are less sensitive to antibiotic treatment than planktonic cells.[39] *S. aureus* and *P. aeruginosa* can both form biofilms, both on environmental surfaces and during infection.[40] Therefore the development of antibacterial surfaces that can prevent bacterial adhesion and reduce the ability of pathogens to form biofilms are of particular interest.[41] A methicillin-resistant *S. aureus* strain (USA300) was used to investigate the ability of high sulfur content polymers to inhibit biofilm formation on their surfaces. Briefly, cubic polymers were incubated statically with *S. aureus* at 37 °C for 2, 24 and 48 h to allow for biofilm growth (Figure 2.22). After incubation, the samples were rinsed with PBS to remove any planktonic cells or loosely adhered cells and stained with 0.25 % crystal violet stain. Excess stain was washed off thoroughly with water. The thorough washing step ensures that any cells that are not strongly adhered to the surface i.e not likely to be part of a biofilm, are removed. After washing (Figure 2.23), the stain was solubilised with 1.2 ml ethanol and the absorbance of the solution was measured at 600 nm (Figure 2.22 and Figure 2.24). The absorbance at 600 nm is related to the amount of biofilm on the sample surface, which becomes stained with crystal violet during the staining process. Therefore, the higher the absorbance at 600 nm, the higher the amount of biofilm on the sample surface.

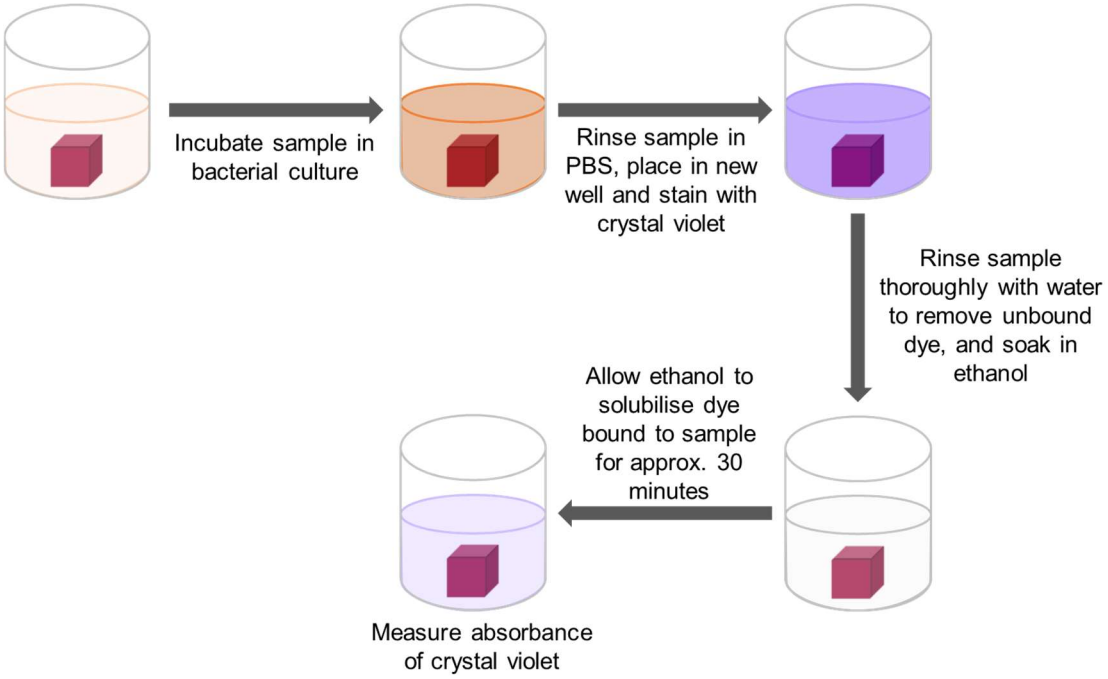

Figure 2.22: A scheme summarising the method used to assess the formation of biofilms on the surfaces of 1 cm^3 samples suing crystal violet.

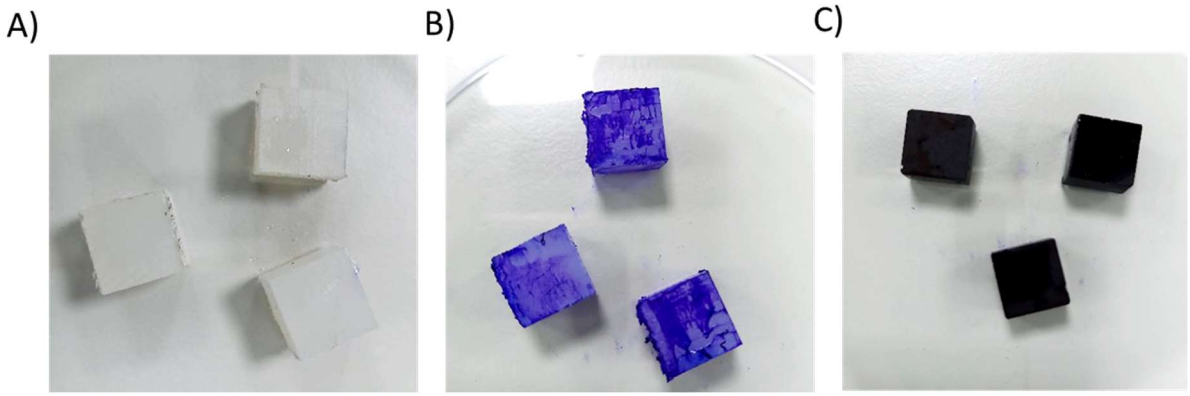

Figure 2.23: Photograph of A) clean polypropylene B) polypropylene stained with crystal violet after 48 h incubation at 37 °C with *P. aeruginosa* and C) S50-DCPD stained with crystal violet after 48 h incubation at 37 °C with *P. aeruginosa*.

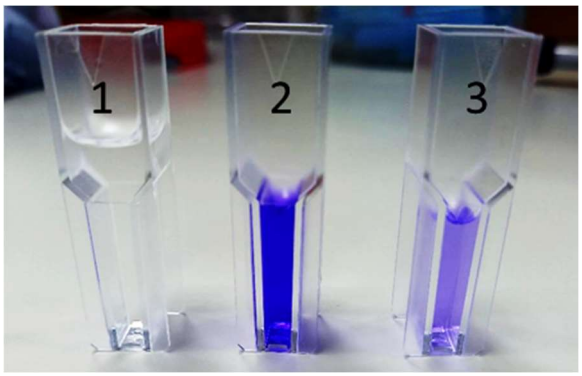

Figure 2.24: Photograph of 1) ethanol as blank solution for absorbance measurements 2) solubilised crystal violet dye from the surface of polypropylene and 3) solubilised crystal violet dye from the surface of S50-DCPD after 48 h incubation at 37 °C with *P. aeruginosa*.

At 2, 24 and 48 h incubation periods at 37 °C, S50-PA and S70-PA have lower absorbance values at 600 nm compared to polypropylene (Figure 2.25), which suggests that biofilms form less readily on the surfaces of S-PA compared to polypropylene. The study was also repeated at 3 and 21 °C to cover all temperatures at which S-PA was tested for its antibacterial activity (Appendix 2.22 and Appendix 2.23). The absorbance at 600 nm after 24 h at 3 °C was similar for polypropylene, S50-PA and S70-PA. After 48 h incubation, the absorbance at 600 nm was higher for polypropylene compared to both S-PA samples, suggestive of lower biofilm prevalence on S50-PA and S70-PA compared to polypropylene. The absorbance at 600 nm after 24 and 48 h incubation for polypropylene at 3 °C was lower than that at 37 °C, as expected due to slower biofilm formation at lower temperatures. At incubation temperatures of 21 °C, at both 24 and 48 h (Appendix 2.23) the absorbance at 600 nm was highest for polypropylene and lowest for S70-PA. The absorbance values are also consistent with the results shown in Figure 2.18 whereby less viable cells were extracted from the surface of S70-PA relative to S50-PA. *P. aeruginosa* biofilm formation was also studied on the surfaces of S-PA (Appendix 2.24) and it was found that the absorbance at 600 nm for S50-PA and S70-PA was more than half the absorbance for polypropylene. The absorbance at 600 nm for polypropylene after incubation with *P. aeruginosa* is higher than that after incubation with *S. aureus*, suggesting that *P. aeruginosa* forms biofilms more readily than *S. aureus*. S50-DCPD and S70-DCPD were also

tested against *S. aureus*. After 2 h incubation, the absorbance value for S50-DCPD and S70-DCPD are similar to that of polypropylene (Figure 2.25), which suggests that there is a similar amount of biofilms on the surfaces of the samples. However, after 24 and 48 h incubation periods, the absorbance values for both S50-DCPD and S70-DCPD are lower than that of polypropylene, suggestive of lower biofilm prevalence on the S-DCPD samples compared to polypropylene. It is likely that *S. aureus* biofilm formation is negligible at 2 h incubation, whereas after prolonged incubation more biofilms have formed on the surface of polypropylene compared to S-DCPD. This coincides with the observation that the absorbance at 600 nm for polypropylene after incubation with *P. aeruginosa* was higher than with *S. aureus*, suggestive of slower *S. aureus* biofilm formation compared to *P. aeruginosa*. *P. aeruginosa* biofilm formation was also inhibited by S-DCPD relative to polypropylene whereby the absorbance at 600 nm was reduced by more than half for S50-DCPD and S70-DCPD in comparison to polypropylene (Appendix 2.25). Biofilm formation on the surfaces of S-DVB was also investigated, and it was found that the absorbance at 600 nm after 24 and 48 h incubation with *S. aureus* at 37 °C was lower for S50-DVB and S70-DVB compared to polypropylene (Appendix 2.26). These results suggest that high sulfur content polymers can inhibit biofilm formation on their surfaces. *S. aureus* biofilm formation on the surfaces of S30-LO and S50-LO was investigated at incubation temperatures of 37 °C (Appendix 2.27). After 24 and 48 h incubation the absorbance values for polypropylene were higher than S30-LO and S50-LO. The antibacterial activity for both S30-LO and S50-LO was tested at 3 °C (Table 2.4), at this temperature both polymers show similar activity relative to polypropylene, however, the biofilm staining results at 37 °C suggest that *S. aureus* biofilm growth is inhibited on the surface of S50-LO to a greater extent than for S30-LO. *S. aureus* biofilm formation on the surfaces of S-RO was studied at incubation times of 24 and 48 h at 37 °C (Appendix 2.28). After 24 h and 48 h it was found that the absorbance values at 600 nm were greater for polypropylene

compared to S30-RO and S50-RO. After 48 h incubation with *S. aureus*, the absorbance values at 600 nm were similar for S30-RO and S50-RO, consistent with the results in Table 2.4 whereby the % reduction in viable *S. aureus* cells extracted from the surfaces was also similar for both samples.

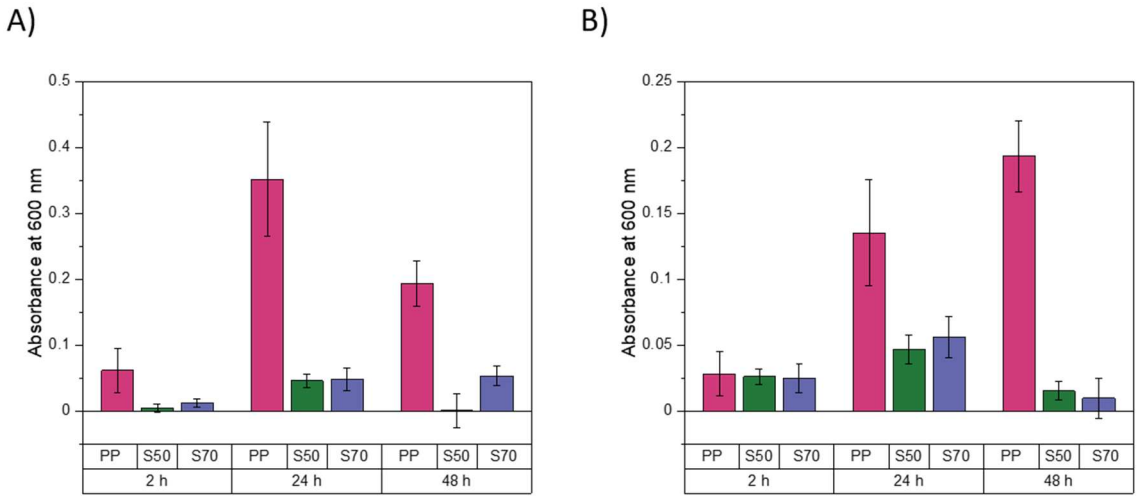

Figure 2.25: Absorbance at 600 nm for A) S-PA and B) S-DCPD, after staining with crystal violet at 2, 24 and 48 h incubation times with *S. aureus*. Where PP: polypropylene, S50: 50 wt.% sulfur polymer and S70: 70 wt.% sulfur polymer.

2.4.3 Surface Wettability and Topography

Several factors are expected to influence bacterial adhesion on surfaces, such as surface charge, hydrophilicity/hydrophobicity and the roughness of the surface.[37] To investigate if the variation in antibacterial activity with different comonomers is due to differences in the sample surfaces, the wettability and surface morphologies were assessed. The wettability of the surfaces was measured by dropping 5 μL droplets of water onto the surfaces and measuring the contact angle formed using the Young-Laplace fitting method. All polymers tested have water contact angles >90 ° and are therefore hydrophobic (Figure 2.26), however, no correlation was found between the antibacterial activity of the polymers and their hydrophobicity/hydrophilicity.

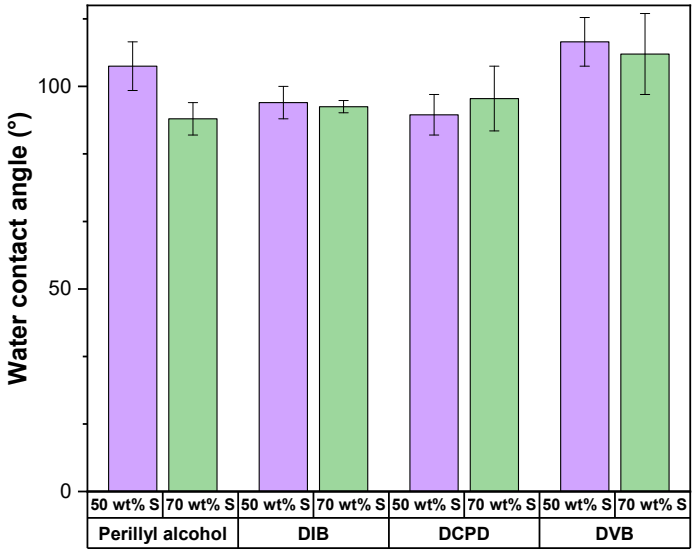

Figure 2.26: The water contact angle (°) of several polymers synthesised at 50 and 70 wt% sulfur measured using the sessile drop mode and Young-Laplace fitting method.

The morphology of the surfaces was visualised by scanning electron microscopy (SEM) to probe whether any differences in the roughness of the sample surface might be playing a role in the antibacterial activity. Neither S50-PA, nor S50-DCPD, have a completely smooth surface (Appendix 2.29) and consist of some 'rough' areas with the presence of particles which may be attributed to contamination, or, S_8 crystals due to depolymerisation. Samples were also imaged after incubation with *S. aureus* to visualise the cells on the surface (Figure 2.27).

Spherical species with diameters of approximately 0.5-1 μm were frequently observed on the surface of polypropylene, which were not visible on the surface of clean polypropylene (Appendix 2.30). The size and shape of these species are consistent with the appearance of *S. aureus* cells, which appear to be growing within a biofilm, with visible extracellular matrix structures.[42] *S. aureus* cells were also found on the surface of S50-DCPD, although at reduced abundance relative to the polypropylene sample, however, no biofilms were seen. No biofilms or cells were found on the surface of S50-PA (Figure 2.27), as suggested from the biofilm staining assay using crystal violet (Figure 2.25). The non-spherical species visible on the surface of S50-PA after incubation with *S. aureus* (Figure 2.27) are also visible on the images of clean S50-PA (Appendix 2.29). These non-spherical species could be crystalline sulfur. The absence of cells on the surfaces of S50-PA does not mean that no cells were adhered to the surface, as only small areas of the sample are scanned during electron microscopy. Sample preparation for SEM imaging required rinsing the samples of non-adhered cells, submerging in glutaraldehyde to fixate the cells, followed by soaking the cells in increasing concentrations of ethanol (Section 2.6.6). Each step of the sample preparation could result in loss of cells from the surface, however, the images are consistent with the results discussed in section 2.4.2 where S50-PA was shown to have an inhibitory effect against surface associated *S. aureus* cells compared to polypropylene (Figure 2.18).

Deng *et al.* found that the composition of S-DIB on the sample surface differed to that of the bulk, where the carbon to sulfur ratio was increased at the surface.[8] Differences in homogeneity of the sample composition may influence the antibacterial activity of the polymers, especially as it is hypothesised that sulfide segments are important for the antimicrobial activity of sulfur polymers. The chemical composition of the surfaces of S50-PA and S50-DCPD were compared by Energy-dispersive X-ray spectroscopy (EDS) (Appendix 2.29) to investigate if the polymers had a similar distribution of sulfur and carbon. Both polymers were synthesised with the same

amount of sulfur, however, that does not necessarily mean that the homogeneity of the materials are the same. EDS analysis shows a similar distribution of both sulfur and carbon on the surfaces of both S50-PA and S50-DCPD. This shows that potential homogeneity differences between the samples can be disregarded as resulting in different antibacterial properties between the polymers. Oxygen was detected in the EDS spectrum of S50-PA, which could be due to the alcohol group on perillyl alcohol.

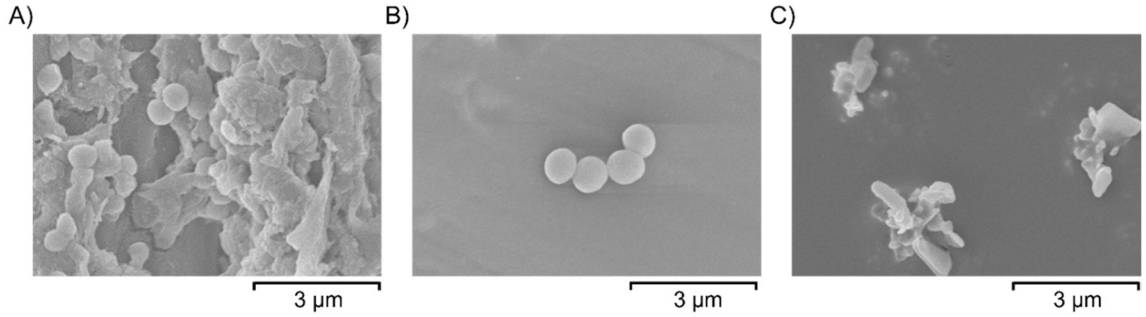

Figure 2.27: SEM images of A) polypropylene B) S50-DCPD and C) S50-PA after incubation with *S. aureus*.

2.4.4 Polymer Leaching Study

To further understand what is causing the reduction in viable cells in solution, a leaching study was conducted. The observation that some of the samples result in a reduction in viable cells in the solution that surrounds the samples suggests that active antibacterial species may be leaching out of the polymers.[43] The reduction in *S. aureus cells* in the presence of S50-PA and S70-PA in solution showed time-dependency when tested at 21 °C (Figure 2.28). No significant reduction in *S. aureus* cells in solution was observed after 5 h for both polymers relative to polypropylene, and, after 24 h only S70-PA showed a reduction relative to polypropylene. However, after 48 h, S50-PA and S70-PA show a reduction in viable *S. aureus* cells in solution compared to polypropylene. At 21 ˚C the S50-PA is glassy whereas the S70-PA is rubbery. It is expected that antibacterial species that may be leaching out of the polymers should do so at a faster rate for a rubbery polymer, where the mobility of the polymer chains aids the migration of active species to the surface of the sample.[44]

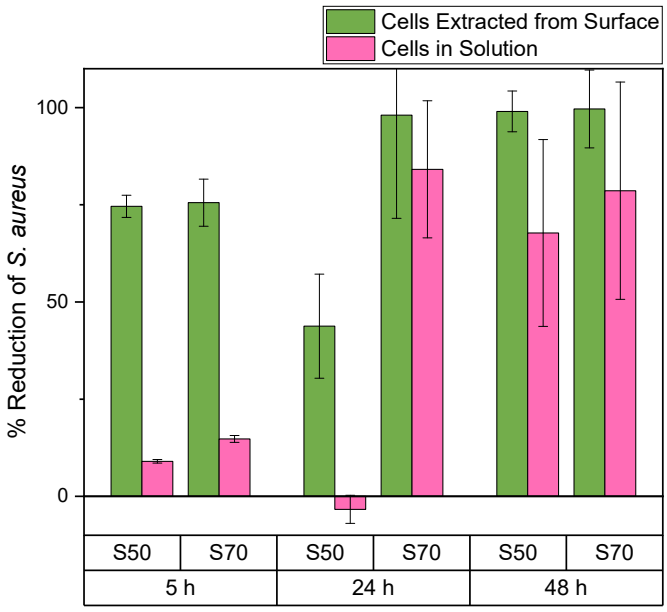

Figure 2.28: A summary of the % reduction in viable *S. aureus* cells extracted from the surface and from solution for S50-PA and S70-PA compared to polypropylene at 5, 24 and 48 h at room temperature.

To investigate what species may be leaching out of the sulfur polymers, S70-PA was studied. Briefly, 1 cm^3 cubic samples of S70-PA were incubated at 37 °C in 1.2 mL deionised water (or D_2O for NMR analysis) for 24 h. After incubation, the samples had lost their shape and yellow precipitates were present on the surface (Figure 2.29).

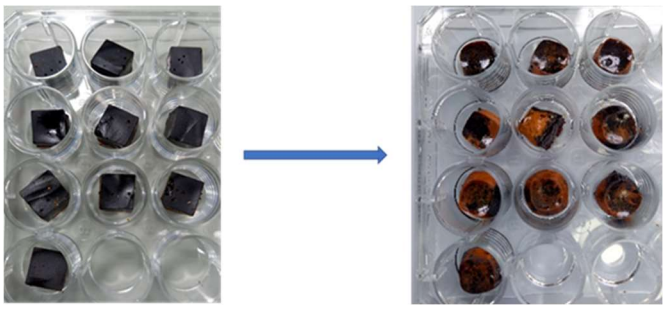

Figure 2.29: A photograph of S70-PA before (left) and after 24 h incubation in water at 35 °C (right) for the leaching study.

DSC analysis was conducted on the samples before and after incubation, which suggests that the yellow precipitate is elemental sulfur due to the presence of a sulfur melting peak in the thermogram after incubation where it was not present in the thermogram prior to incubation (Figure 2.30).

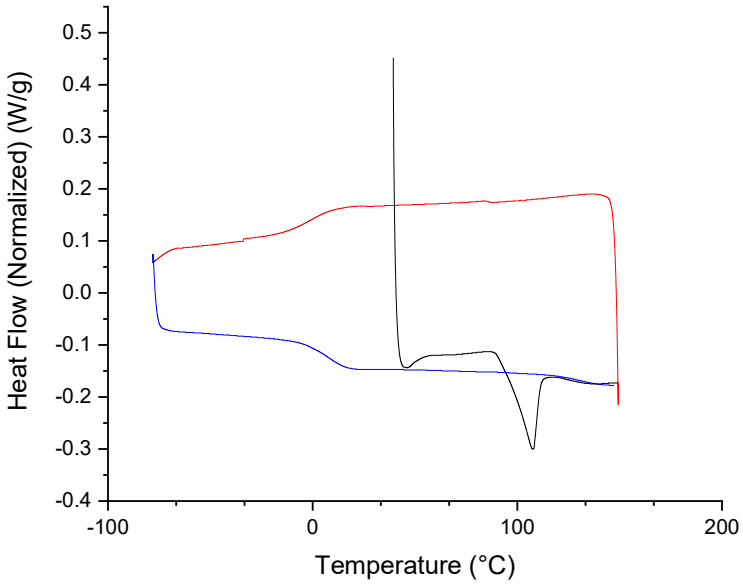

Figure 2.30: Differential scanning calorimetry (DSC) traces for S70-PA after 24 h incubation at 37 ºC, showing the first heating cycle to 150 °C (black), cooling to -80 °C (red), and the second heating cycle to 150 °C (blue).

The D_2O solution which surrounded the samples was subjected to ^1H NMR analysis to detect any unreacted perillyl alcohol or any oligomers that were potentially leaching out of the samples, no peaks were present in the spectra, which suggests that no species containing hydrogen were detectable in the leachate. The solution in water was also submitted for Inductively Coupled Plasma Optical Emission Spectroscopy (ICP-OES) analysis to determine if any sulfur species were leaching out into solution, and it was found that sulfur was detectable in the leachate at a concentration of 2 ppm. As yellow precipitates were visible on the sample surfaces after incubation, and as sulfur was detected in the leachate by ICP-OES, it is possible that unreacted sulfur migrates to the surface when the polymer is held at a temperature above its T_g and could therefore leach out of the sample into the surrounding medium. It is also worth noting that although no crystalline elemental sulfur was detected by DSC prior to incubation, thin-layer chromatography analysis of the sample suggested the presence of elemental sulfur (Figure 2.31). Analysis of S50-PA and S70-PA by thin-layer chromatography shows the presence of two components, one with a retention factor similar to that of elemental sulfur, and one that interacts strongly with the stationary phase. The second components' retention factor was different to that of perillyl alcohol, indicating that no unreacted perillyl alcohol remains in the polymer (Figure 2.31)

Figure 2.31: Thin-layer chromatography plate for S-PA analysis in order to detect any unreacted perillyl alcohol and/or elemental sulfur where 1: elemental sulfur, 2: perillyl alcohol, 3: S50-PA 4: S70-PA using 1:1 hexane:ethyl acetate as the eluent.

There are several possible antibacterial species that could be leaching out of the polymers such as elemental sulfur, unreacted comonomers, and hydrogen sulfide. Further studies will be required to investigate what species can leach out of the polymers and if such species are antibacterial. Antibacterial materials that rely on the leaching of bactericidal species are known to have finite antibacterial activity, therefore the longevity of the solution effect will also require further investigation.[45] The mode of action of inverse vulcanised polymers against bacteria is still unclear, however, this study shows that the polymers have an inhibitory effect against Gram-positive and Gram-negative bacterial cells both on the surface and in solution, and that the effect is related to the T_g of the materials. Potential mechanisms include sulfur−sulfur bond interactions with thiol groups present in bacterial cell wall/outer membrane proteins or release of superoxide radical anions interfering with bacterial metalloproteins.[38] Polysulfides are redox active, and H_2S_x species can reduce dioxygen to $O_2^{\bullet-}$ and other reactive oxygen species that result in oxidative stress.[38,39] Whether this action takes place by a direct interaction of the bacteria with the surface of the polymer or by the release of a sulfide species from within the polymer, it is rational that the glass transition temperature and, therefore, physical state of the polymer would influence these processes. Below the T_g, the polymer chains are held in a rigid, glassy state. This would be expected to hinder not only the mobility of the chains themselves, but also the diffusion of any species into or out of the polymer structure. Above the T_g, in the rubbery state the polymer chains would be free to move and, therefore, with more chance of collisions of S−S bonds or radical chain ends with bacterial outer membrane or cell wall components. There would also be much more rapid diffusion out of the polymer of any low molecular weight polysulfide species (e.g., RS_xH) generated by the redox behavior of the bacteria.

2.5 Conclusions

In summary, high sulfur content polymers synthesised by inverse vulcanisation show an inhibitory effect against Gram-positive methicillin-resistant *S. aureus* and Gram-negative *P. aeruginosa*. The antibacterial activity of the polymers was found to be dependent on the comonomer employed and the sulfur/comonomer ratio. Furthermore, biofilm formation is inhibited on the surfaces of sulfur polymers relative to polypropylene. The antibacterial activity of the polymers was found to vary with the temperature at which they are tested, which suggests that the T_g of the polymers is an important parameter for antibacterial applications. The mechanism of action of sulfur polymers against bacteria remains unclear, particularly for the surface activity.

2.6 Experimental Details

2.6.1 Materials and Equipment

Ground sulfur sublimed powder reagent grade ≥99.5 % was obtained from Brenntag UK & Ireland. Dicyclopentadiene (stabilised with BHT) >97%, and 1,3-Diisopropenylbenzene (stabilized with TBC) >97% were obtained from Tokyo Chemicals Industry. Divinylbenzene technical grade 80 %, (S)-(−)-Perillyl alcohol food grade ≥95%, Linseed oil, Luria–Bertani broth (Miller), LB agar, phosphate buffered saline (PBS) and glutardialdehyde were purchased from Sigma-Aldrich. Rapeseed Oil (Crisp 'n Dry®) was purchased from Tesco. Methicillin-resistant *S. aureus* strain USA300 and *P. aeruginosa* PAO1 were cultured from frozen stocks stored at the University of Liverpool.

DSC was performed using a TA Instruments Q200 DSC, programmed using a heat/cool/heat method for three cycles by heating to 150 °C, cooling to −80 °C, and reramping to 150 °C. The heating/cooling rate was set to 10 °C/min. The second heating curve was analysed and used to determine the glass transition temperature.

^{1}H NMR spectroscopy was conducted using a Bruker Advance DRX (400 MHz) spectrometer using deuterated chloroform as the solvent, all experiments were carried out at room temperature.

FT-IR spectroscopy was conducted with a Bruker Vertex V70 FT-IR spectrometer, with a germanium ATR crystal.

Absorbance measurements were obtained using a BMG Labtech FLUOstar® Omega microplate reader using 96-well plates.

Static contact angle measurements were obtained using a DSA100 Expert Drop Shape Analyser (Kruss GmbH) operating with Young-Laplace fitting and using 5 μL water droplets.

2.6.2 Polymer Synthesis

Polymerisations were carried out in 40 mL glass vials placed in aluminium heating blocks. Sulfur:crosslinker weight ratios were varied between 30-70 wt% sulfur, with the total reaction scale maintained at 10 g. All reactions were begun by allowing the sulfur to melt at 135 °C, before adding the organic crosslinker under stirring. The reaction temperature was increased to 175 °C for perillyl alcohol, DIB, rapeseed oil and linseed oil, 160 °C for DCPD and maintained at 135 °C for DVB. Molded objects were prepared by transferring the reaction into a silicone mould (1 cm^3 cubes) and curing overnight in an oven at 140 °C. The mixture was transferred from the stirred vial to the mould when the reaction mixture had become homogeneous and viscous (an aliquot of the reaction mixture, when removed on a spatula and allowed to cool to room temperature, would no longer visibly separate to clear organic monomer, and precipitated yellow sulfur powder).

2.6.3 Bacteria Preparation, Storage and Enumeration

Glycerol stocks of *Staphylococcus aureus* (*S. aureus*) strain USA300 and *Pseudomonas aeruginosa* (*P. aeruginosa*) strain PAO1 were stored at -80 °C for long term storage. For experimental use, frozen glycerol stocks of *S. aureus* and *P. aeruginosa* were defrosted and spread onto LB agar plates which were incubated overnight at 37 °C. Bacterial cultures were prepared by swabbing one colony into 10 ml LB broth followed by overnight incubation at 37 °C. Colony forming units (CFU) were enumerated by serially diluting the cultures in PBS onto LB agar, using the Miles and Misra method. CFU/cm^2 and CFU/ml were calculated using the following equation:

CFU = (no. of colonies x dilution factor) / volume of culture plate

2.6.4 Viable Cell Enumeration Assay

S. aureus USA300 and *P. aeruginosa* PAO1 were used to evaluate the antibacterial efficiency of the sulfur polymers molded into 1 cm^3 cubes using polypropylene cubes as a control. 1 cm^3

cubic samples were soaked in ethanol, allowed to air dry and placed in separate wells of a 24-well plate. Overnight cultured bacteria prepared in LB broth were diluted to 10^5 CFU/mL (OD600 = 0.001). 1.2 mL of diluted bacterial solution was added to each sample in the 24-well plate and allowed to incubate statically. For *S. aureus*, incubation times were 5 h at 37 °C and 24 h at room temperature, and 48 h at 3 °C. For *P. aeruginosa*, the incubation time was 3 h at 37 °C. After incubation, the bacterial solution surrounding each sample was removed and the viable cells were enumerated after serial dilution of the solution in PBS onto LB agar, using the Miles and Misra method. The cubic samples were gently rinsed with 1 mL of PBS to remove any planktonic cells and were vortexed at high speed in 1 mL of LB broth for 10 s to remove any adhered cells. The vortexed solution was serially diluted in PBS and the viable cells associated with the sample surface were enumerated using the Miles and Misra method on LB agar, as above. All samples were tested in technical triplicate.

Statistical analysis: Statistical analysis was conducted using one-way analysis of variance (ANOVA) on the calculated CFU/cm^2 values for the sample surface and the calculated CFU/ml in solution. Differences were deemed as statistically significant if a value of $p < 0.05$ was obtained.

2.6.5 Biofilm Staining Assay

1 cm^3 samples (high sulfur content polymers and polypropylene) were placed in separate wells of a 24-well plate. Overnight cultured bacteria prepared in LB broth was diluted to 10^5 CFU/mL (OD600 = 0.001). 1.2 mL of diluted bacterial solution was added to each sample well and allowed to incubate statically for 5, 24 and 48 h at 37 ºC. After static incubation the samples were washed with 1.2 mL PBS and allowed to dry in a new 24-well plate. Once dried, 1.2 mL of 0.25% crystal violet stain was added to each well containing samples and was kept for a minimum of 30 minutes at room temperature. The samples were washed thoroughly with water to remove excess stain and were allowed to dry. 1.2 mL of ethanol was used to solubilise the

remaining dye on each sample. The absorbance of the solubilised dye was measured at 600 nm using ethanol as a blank.

2.6.6 SEM Imaging

Scanning electron microscopy (SEM) was performed using a Hitachi S-4800 cold-field emission scanning electron microscope. The 1 cm^3 samples were mounted onto SEM stubs using conductive silver paint. Prior to imaging, samples were coated with gold using a current of 120 mA for 15 s to give approximately 15 nm gold coatings using a Quorum S1505 ES sputter coater. To image samples after incubation with *S. aureus*, samples were rinsed with PBS after incubation, and soaked overnight in glutardialdehyde. The samples were rinsed with PBS and soaked in series of ethanol dilutions (50, 70, 90, 95 and 100 % v/v) for a minimum of 5 minutes in each dilution. The samples were mounted onto SEM stubs using conductive silver paint and sputter coated with gold prior to imaging.

2.6.7 Leaching Study

1 cm^3 cubic samples were placed in separate wells of a 24-well plate. To each sample, 1.2 mL of distilled water was added. The well plate was incubated at 37 °C for 24 h. The solution surrounding the samples was removed and analysed by inductively coupled plasma optical emission spectrometry (ICP-OES).

2.7 References

1 S.-M. Tsao and M. –. Yin, *J. Antimicrob. Chemother.*, 2001, **47**, 665–670.

2 S. Saedi, M. Shokri and J.-W. Rhim, *Arab. J. Chem.*, 2020, **13**, 6580–6588.

3 M. Nakamoto, K. Kunimura, J.-I. Suzuki and Y. Kodera, *Exp. Ther. Med.*, 2020, **19**, 1550–1553.

4 R. Leontiev, N. Hohaus, C. Jacob, M. C. H. Gruhlke and A. J. Slusarenko, *Sci. Rep.*, 2018, **8**, 6763.

5 S. Ankri and D. Mirelman, *Microbes Infect.*, 1999, **1**, 125–129.

6 P. RATTANACHAIKUNSOPON and P. PHUMKHACHORN, *Biosci. Biotechnol. Biochem.*, 2008, **72**, 2987–2991.

7 I. S. Shchelik and K. Gademann, *ACS Med. Chem. Lett.*, 2021, **12**, 1898–1904.

8 Z. Deng, A. Hoefling, P. Théato and K. Lienkamp, *Macromol. Chem. Phys.*, 2018, **219**, 1700497.

9 V. S. Wadi, K. K. Jena, K. Halique and S. M. Alhassan, *ACS Appl. Polym. Mater.*, 2020, **2**, 198–208.

10 J. A. Smith, R. Mulhall, S. Goodman, G. Fleming, H. Allison, R. Raval and T. Hasell, *ACS Omega*, 2020, **5**, 5229–5234.

11 C. R. Westerman and C. L. Jenkins, *Macromolecules*, 2018, **51**, 7233–7238.

12 J. Cubero-Cardoso, P. Gómez-Villegas, M. Santos-Martín, A. Sayago, Á. Fernández-Recamales, R. Fernández de Villarán, A. A. Cuadri, J. E. Martín-Alfonso, R. Borja, F. G. Fermoso, R. León and J. Urbano, *Polym. Test.*, 2022, **109**, 107546.

13 H. Shen, H. Qiao and H. Zhang, *Chem. Eng. J.*, 2022, **450**, 137905.

14 J. A. Smith, S. J. Green, S. Petcher, D. J. Parker, B. Zhang, M. J. H. Worthington, X. Wu, C. A. Kelly, T. Baker, C. T. Gibson, J. A. Campbell, D. A. Lewis, M. J. Jenkins, H. Willcock, J. M. Chalker and T. Hasell, *Chem. – A Eur. J.*, 2019, **25**, 10433–10440.

15 W. J. Chung, J. J. Griebel, E. T. Kim, H. Yoon, A. G. Simmonds, H. J. Ji, P. T. Dirlam, R. S. Glass, J. J. Wie, N. A. Nguyen, B. W. Guralnick, J. Park, Á. Somogyi, P. Theato, M. E. Mackay, Y.-E. Sung, K. Char and J. Pyun, *Nat. Chem.*, 2013, **5**, 518–524.

16 M. P. Crockett, A. M. Evans, M. J. H. Worthington, I. S. Albuquerque, A. D. Slattery, C. T. Gibson, J. A. Campbell, D. A. Lewis, G. J. L. Bernardes and J. M. Chalker, *Angew. Chem. Int. Ed. Engl.*, 2016, **55**, 1714–1718.

17 F. Stojcevski, M. K. Stanfield, D. J. Hayne, M. Mann, N. A. Lundquist, J. M. Chalker and L. C. Henderson, *Sustain. Mater. Technol.*, 2022, **32**, e00400.

18 D. J. Parker, H. A. Jones, S. Petcher, L. Cervini, J. M. Griffin, R. Akhtar and T. Hasell, *J. Mater. Chem. A*, 2017, **5**, 11682–11692.

19 M. J. H. Worthington, R. L. Kucera, I. S. Albuquerque, C. T. Gibson, A. Sibley, A. D. Slattery, J. A. Campbell, S. F. K. Alboaiji, K. A. Muller, J. Young, N. Adamson, J. R. Gascooke, D. Jampaiah, Y. M. Sabri, S. K. Bhargava, S. J. Ippolito, D. A. Lewis, J. S.

Quinton, A. V Ellis, A. Johs, G. J. L. Bernardes and J. M. Chalker, *Chem. – A Eur. J.*, 2017, **23**, 16219–16230.

20 R. Xie, A. R. Weisen, Y. Lee, M. A. Aplan, A. M. Fenton, A. E. Masucci, F. Kempe, M. Sommer, C. W. Pester, R. H. Colby and E. D. Gomez, *Nat. Commun.*, 2020, **11**, 893.

21 G. Kutney, ed. G. B. T.-S. Second E. Kutney, ChemTec Publishing, Oxford, 2013.

22 T. T. P. Cheung, *Kirk-Othmer Encycl. Chem. Technol.*, 2001.

23 L. J. Dodd, Ö. Omar, X. Wu and T. Hasell, *ACS Catal.*, 2021, **11**, 4441–4455.

24 B. L. Rivas, B. F. Urbano and J. Sánchez, *Front. Chem.*, 2018, **6**, 320.

25 T. C. Chen, C. O. Da Fonseca and A. H. Schönthal, *Am. J. Cancer Res.*, 2015, **5**, 1580–1593.

26 L. J. Dodd, C. Lima, D. Costa-Milan, A. R. Neale, B. Saunders, B. Zhang, A. Sarua, R. Goodacre, L. J. Hardwick, M. Kuball and T. Hasell, *Polym. Chem.*, 2023, **14**, 1369–1386.

27 Y. Zhang, R. S. Glass, K. Char and J. Pyun, *Polym. Chem.*, 2019, **10**, 4078–4105.

28 A. Sasaki, L. B. Ibarra and S. Wimperis, *Phys. Chem. Chem. Phys.*, 2017, **19**, 24082–24089.

29 D. J. Parker, S. T. Chong and T. Hasell, *RSC Adv.*, 2018, **8**, 27892–27899.

30 J. A. Smith, X. Wu, N. G. Berry and T. Hasell, *J. Polym. Sci. Part A Polym. Chem.*, 2018, **56**, 1777–1781.

31 M. Martin-Luengo, M. Yates, E. Rojo, D. Arribas, D. Aguilar and E. Ruiz-Hitzky, *Appl. Catal. A-general - APPL CATAL A-GEN*, 2010, **387**, 141–146.

32 J. A. Smith, X. Wu, N. G. Berry and T. Hasell, *J. Polym. Sci. Part A Polym. Chem.*, 2018, **56**, 1777–1781.

33 M. J. H. Worthington, R. L. Kucera and J. M. Chalker, *Green Chem.*, 2017, **19**, 2748–2761.

34 L. Zhang, Y. Ren, X. Liu, F. Han, K. Evans-Lutterodt, H. Wang, Y. He, J. Wang, Y. Zhao and W. Yang, *Sci. Rep.*, 2018, **8**, 4558.

35 V. K. Shankarayya Wadi, K. K. Jena, S. Z. Khawaja, K. Yannakopoulou, M. Fardis, G. Mitrikas, M. Karagianni, G. Papavassiliou and S. M. Alhassan, *ACS Omega*, 2018, **3**, 3330–3339.

36 F. Pan, A. Amarjargal, S. Altenried, M. Liu, F. Zuber, Z. Zeng, R. M. Rossi, K. Maniura-Weber and Q. Ren, *ACS Appl. Bio Mater.*, 2021, **4**, 4271–4279.

37 J. K. Oh, Y. Yegin, F. Yang, M. Zhang, J. Li, S. Huang, S. V Verkhoturov, E. A. Schweikert, K. Perez-Lewis, E. A. Scholar, T. M. Taylor, A. Castillo, L. Cisneros-Zevallos, Y. Min and M. Akbulut, *Sci. Rep.*, 2018, **8**, 17247.

38 T. Schneider, A. Baldauf, L. Ba, V. Jamier, K. Khairan, M.-B. Sarakbi, N. Reum, M. Schneider, A. Röseler, K. Becker, T. Burkholz, P. Winyard, M. Kelkel, M. Diederich and C. Jacob, *J. Biomed. Nanotechnol.*, 2011, **7**, 395–405.

39 U. Münchberg, A. Anwar, S. Mecklenburg and C. Jacob, *Org. Biomol. Chem.*, 2007, **5**, 1505–1518.

2.8 Appendix

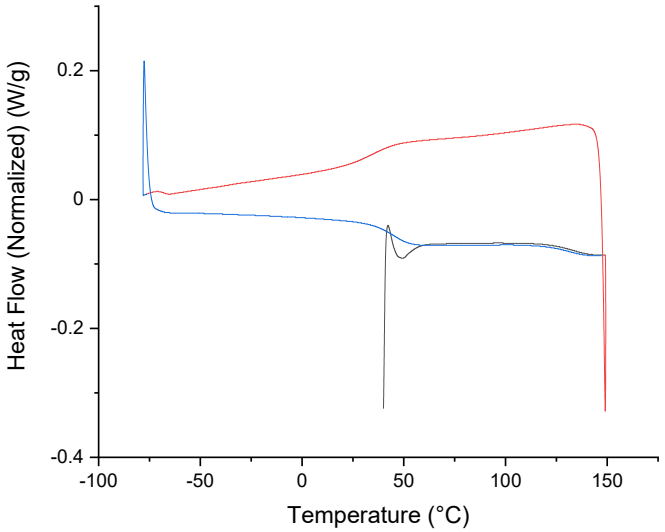

Appendix 2.1: DSC traces of S70-DCPD showing the first heating cycle to 150 °C (black), cooling to -80 °C (red), and the second heating cycle to 150 °C (blue).

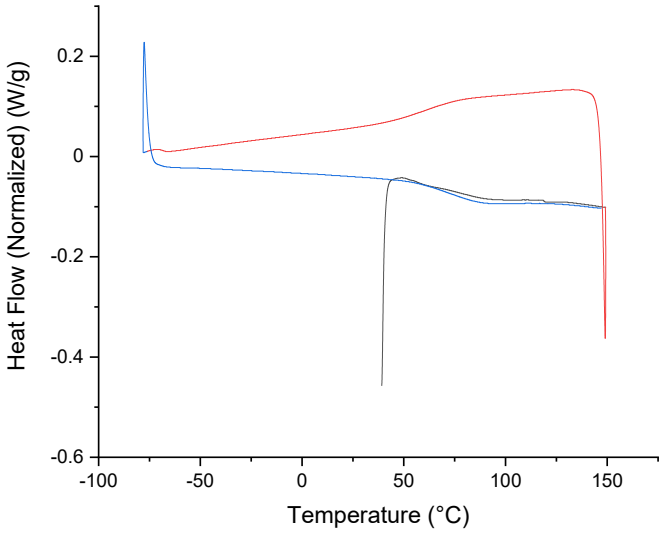

Appendix 2.2: DSC traces of S50-DVB showing the first heating cycle to 150 °C (black), cooling to -80 °C (red), and the second heating cycle to 150 °C (blue).

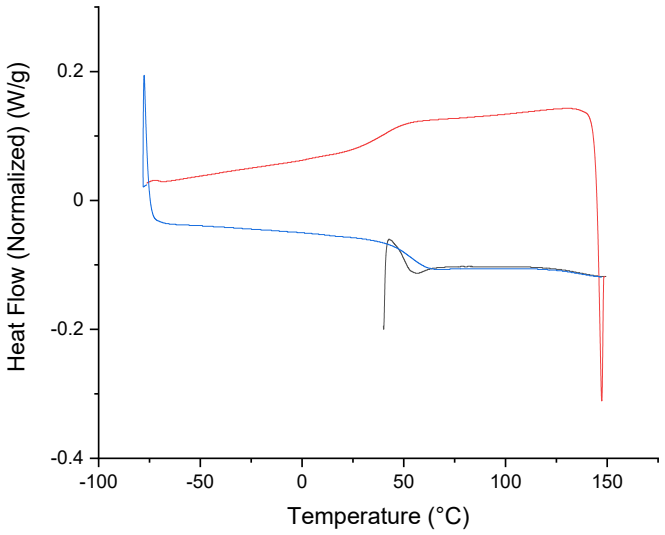

Appendix 2.3: DSC traces of S70-DVB showing the first heating cycle to 150 °C (black), cooling to -80 °C (red), and the second heating cycle to 150 °C (blue).

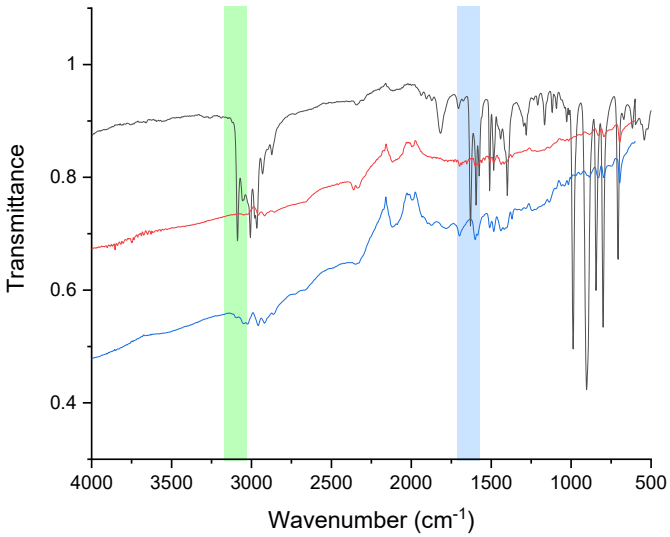

Appendix 2.4: FT-IR spectra of DVB (black), S50-DVB (red) and S70-DVB (blue). Highlighted in green at ca. 3100 cm^{-1} is the signal corresponding to =C-H stretch, and highlighted in blue at ca. 1640 cm^{-1} is the signal corresponding to an alkene C=C stretch. Both signal intensities are reduced in the polymer spectra compared to the monomer suggesting alkene consumption during the reaction.

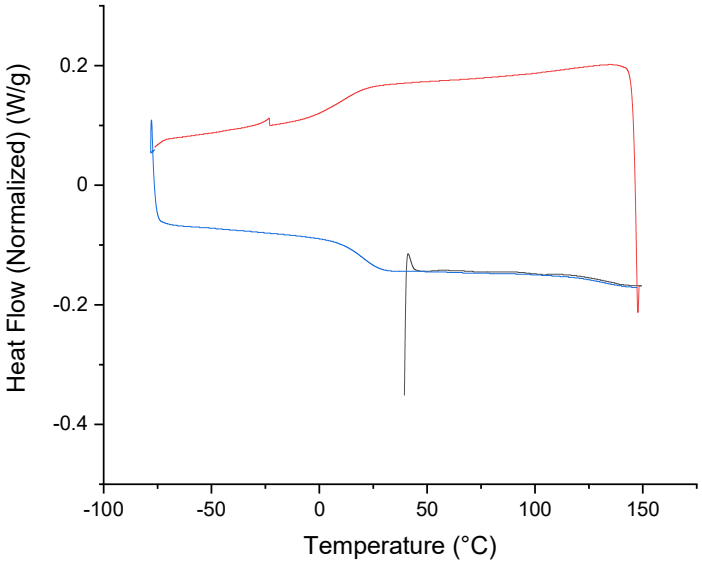

Appendix 2.5: DSC traces of S70-PA showing the first heating cycle to 150 °C (black), cooling to -80 °C (red), and the second heating cycle to 150 °C (blue).

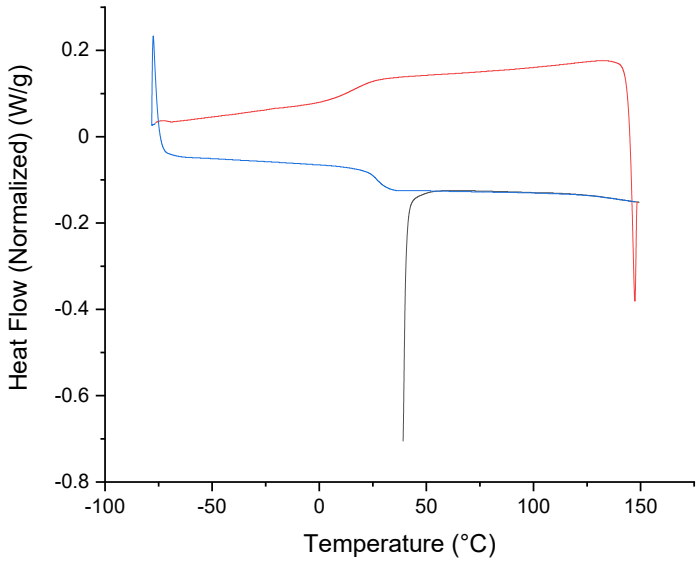

Appendix 2.6: DSC traces of S50-DIB showing the first heating cycle to 150 °C (black), cooling to -80 °C (red), and the second heating cycle to 150 °C (blue).

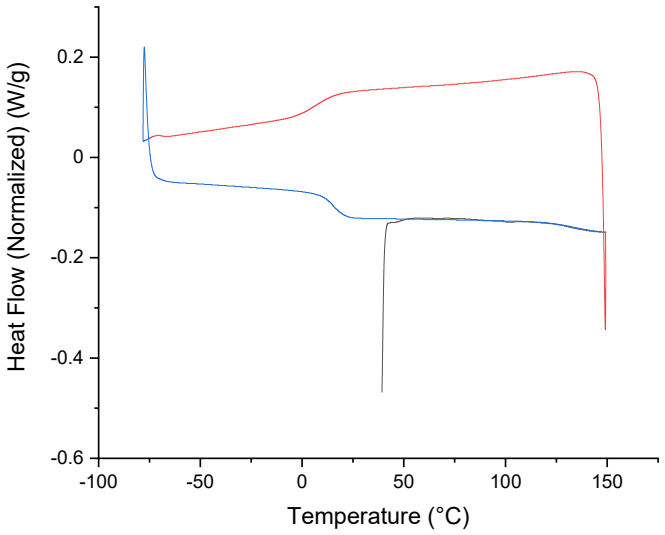

Appendix 2.7: DSC traces of S70-DIB showing the first heating cycle to 150 °C (black), cooling to -80 °C (red), and the second heating cycle to 150 °C (blue).

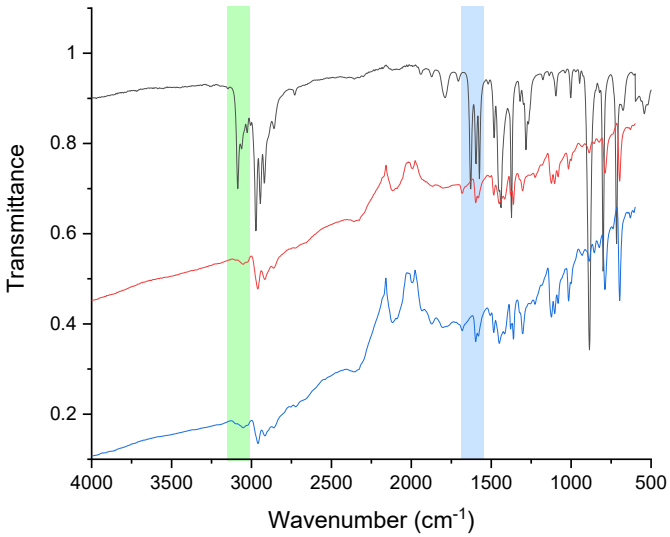

Appendix 2.8: FT-IR spectra of DIB (black), S50-DIB (red) and S70-DIB (blue). Highlighted in green at ca. 3100 cm^{-1} is the signal corresponding to =C-H stretch, and highlighted in blue at ca. 1640 cm^{-1} is the signal corresponding to an alkene C=C stretch. Both signal intensities are reduced in the polymer spectra compared to the monomer suggesting alkene consumption during the reaction.

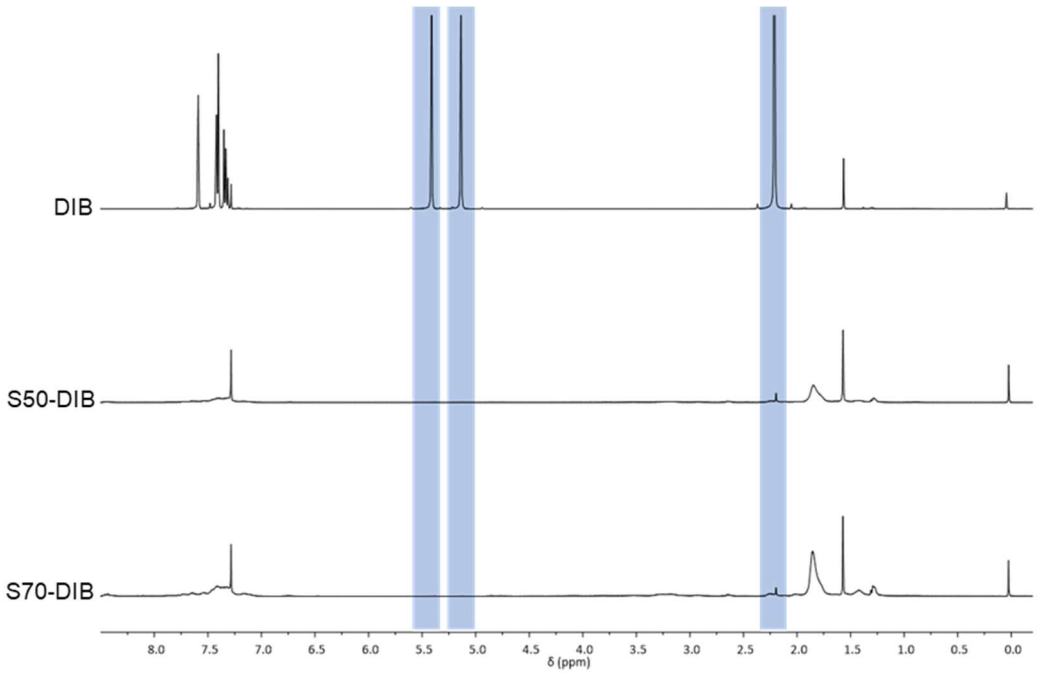

Appendix 2.9: ^{1}H NMR spectra of DIB, S50-DIB and S70-DIB. Highlighted are chemical shifts consistent with those of vinylic (ca 5-5.5 ppm) and allylic protons (ca. 2.25 ppm) which are present in the spectrum for DIB but not in the spectra of the respective polymers suggesting consumption of alkene units during reaction.

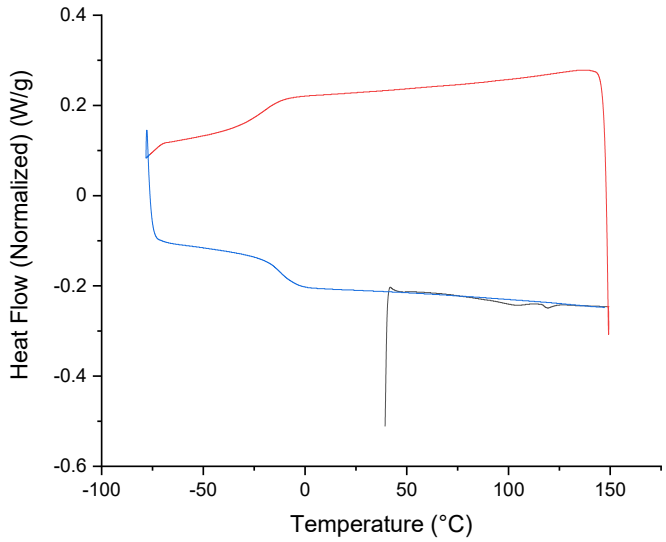

Appendix 2.10: DSC traces of S50-LO showing the first heating cycle to 150 °C (black), cooling to -80 °C (red), and the second heating cycle to 150 °C (blue).

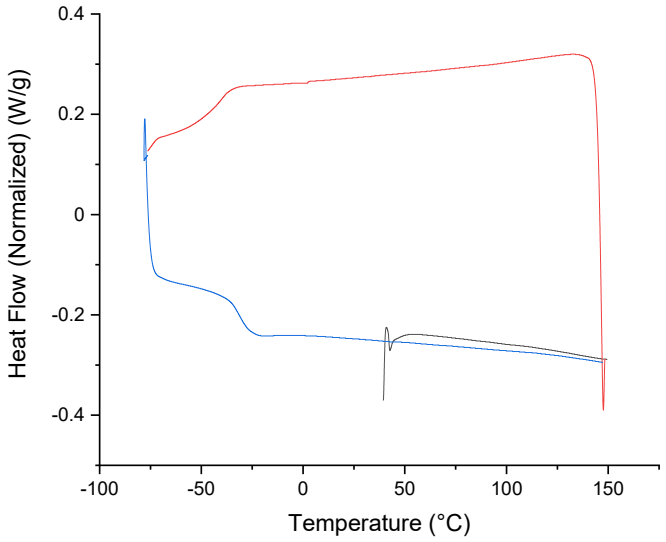

Appendix 2.11: DSC traces of S30-RO showing the first heating cycle to 150 °C (black), cooling to -80 °C (red), and the second heating cycle to 150 °C (blue).

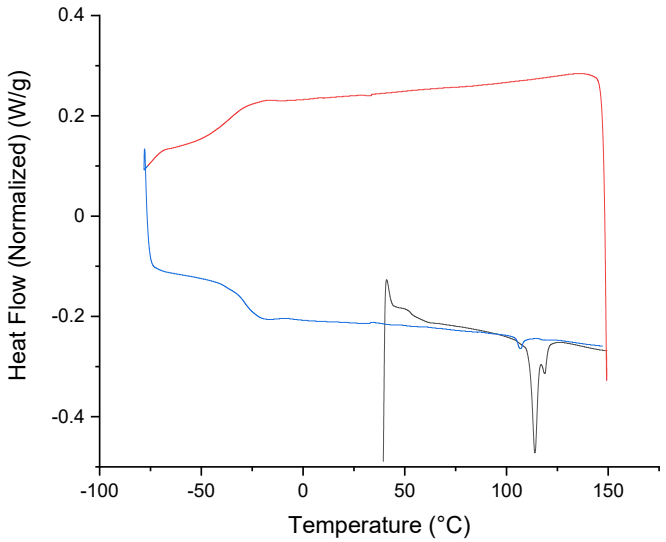

Appendix 2.12: DSC traces of S50-RO showing the first heating cycle to 150 °C (black), cooling to -80 °C (red), and the second heating cycle to 150 °C (blue).

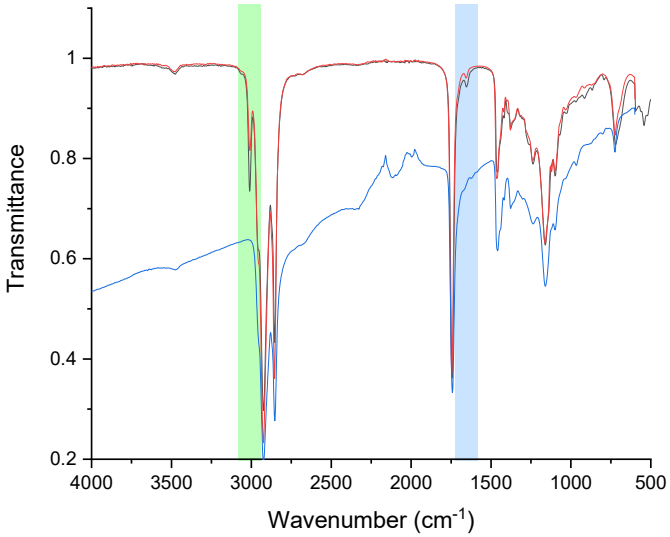

Appendix 2.13: FT-IR spectra of rapeseed oil (black), S30-RO (red) and S50-RO (blue). Highlighted in green at ca. 3100 cm^{-1} is the signal corresponding to =C-H stretch, and highlighted in blue at ca. 1640 cm^{-1} is the signal corresponding to an alkene C=C stretch. Both signal intensities are reduced in the polymer spectra compared to the monomer suggesting alkene consumption during the reaction.

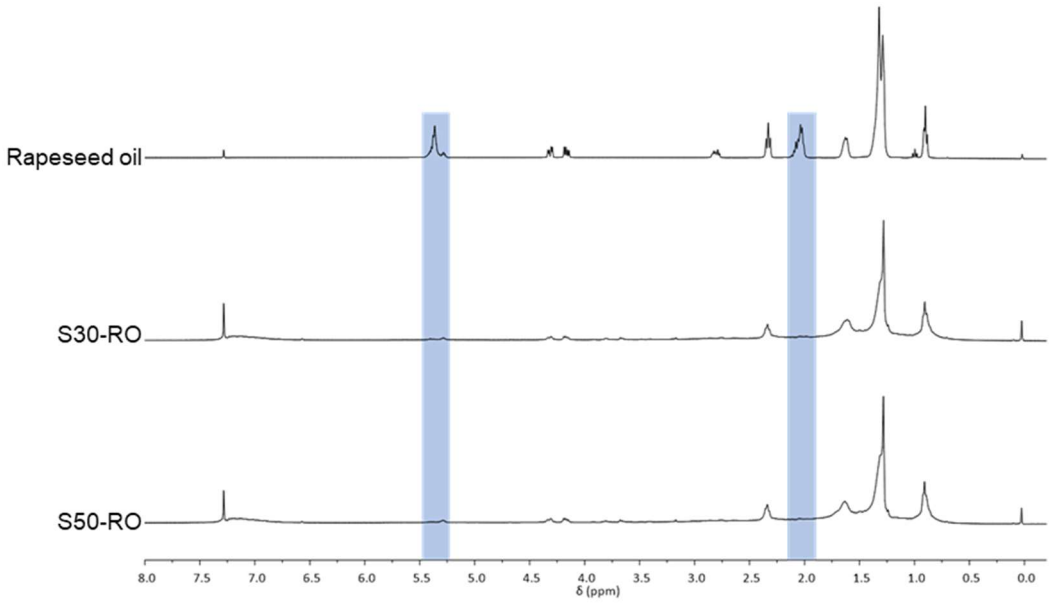

Appendix 2.14: ^{1}H NMR spectra of rapeseed oil, S30-RO and S50-RO. Highlighted are chemical shifts consistent with those of vinylic protons (at ca. 5-5.5 ppm) and allylic protons (at ca. 1.9 ppm) which are present in the spectrum for rapeseed oil but not in the spectra of the respective polymers suggesting consumption of alkene units during reaction.

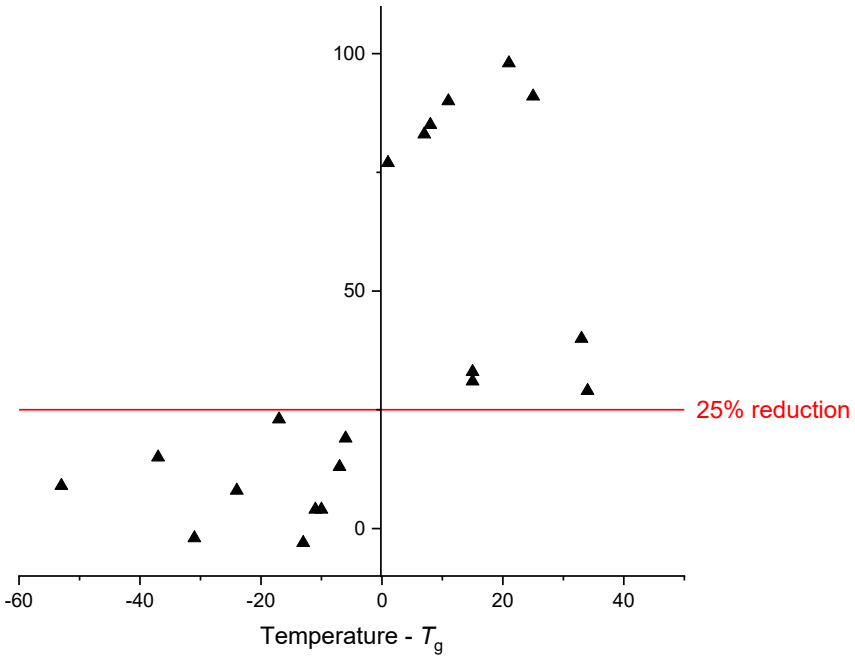

Appendix 2.15: A plot of the % reduction in *S. aureus* cells in solution against (Temperature – T_g), where negative x axis values correspond to polymers in their glassy state and positive values correspond to polymers in the rubbery state. A greater than 25% reduction in viable cells in solution is observed for all polymers in their rubbery state.

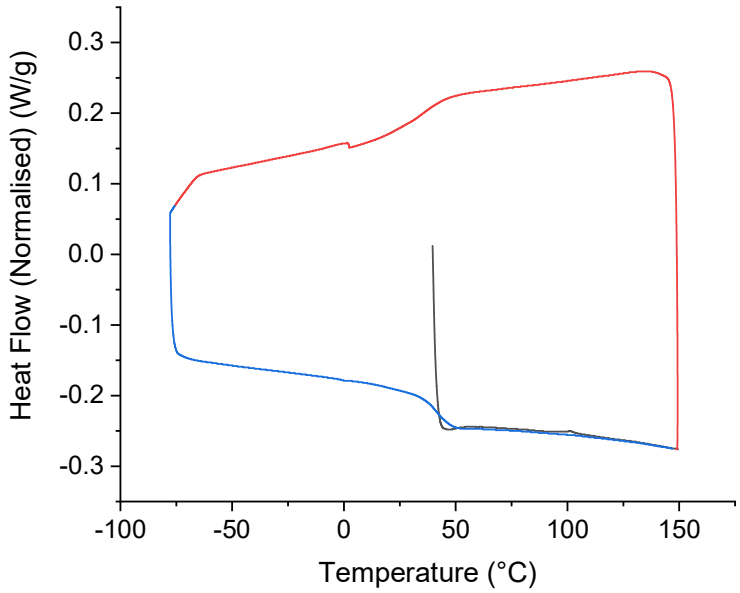

Appendix 2.16: DSC traces of S-PA-DCPD terpolymer at a ratio of 50:45:5 showing the first heating cycle to 150 °C (black), cooling to -80 °C (red), and the second heating cycle to 150 °C (blue).

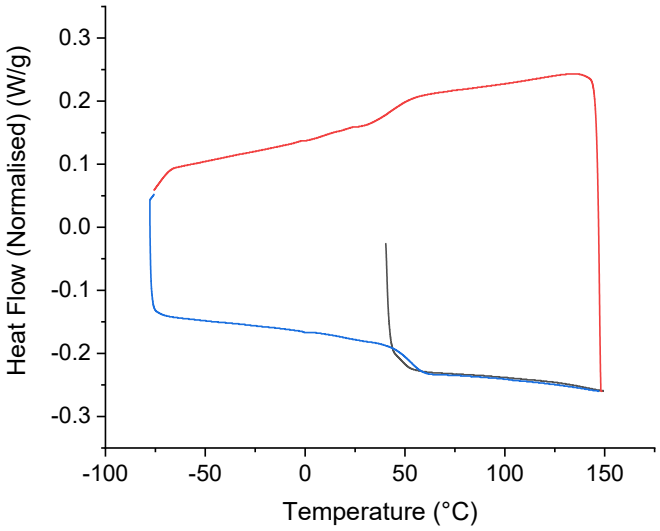

Appendix 2.17: DSC traces of S-PA-DCPD terpolymer at a ratio of 50:40:10 showing the first heating cycle to 150 °C (black), cooling to -80 °C (red), and the second heating cycle to 150 °C (blue).

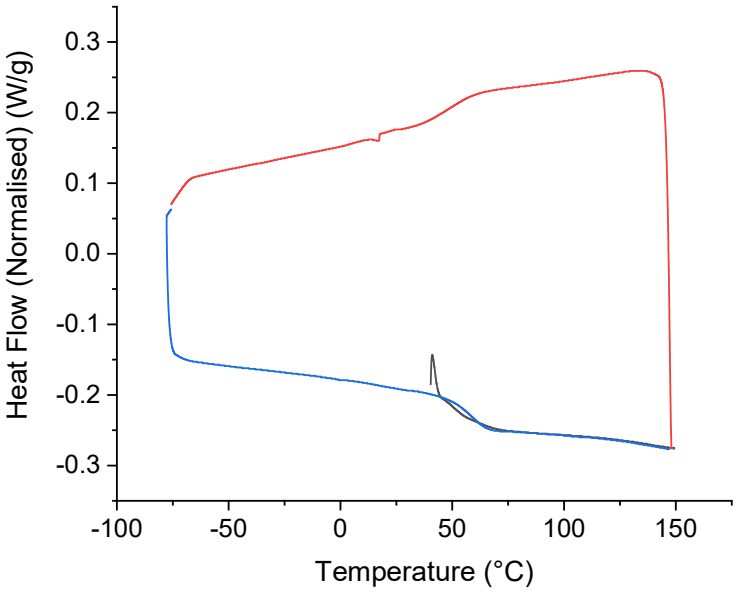

Appendix 2.18: DSC traces of S-PA-DCPD terpolymer at a ratio of 50:35:15 showing the first heating cycle to 150 °C (black), cooling to -80 °C (red), and the second heating cycle to 150 °C (blue).

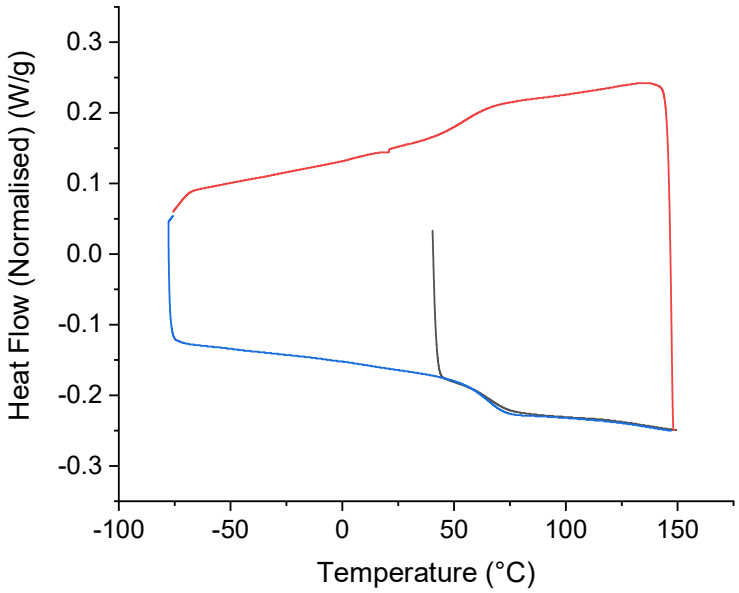

Appendix 2.19: DSC traces of S-PA-DCPD terpolymer at a ratio of 50:30:20 showing the first heating cycle to 150 °C (black), cooling to -80 °C (red), and the second heating cycle to 150 °C (blue).

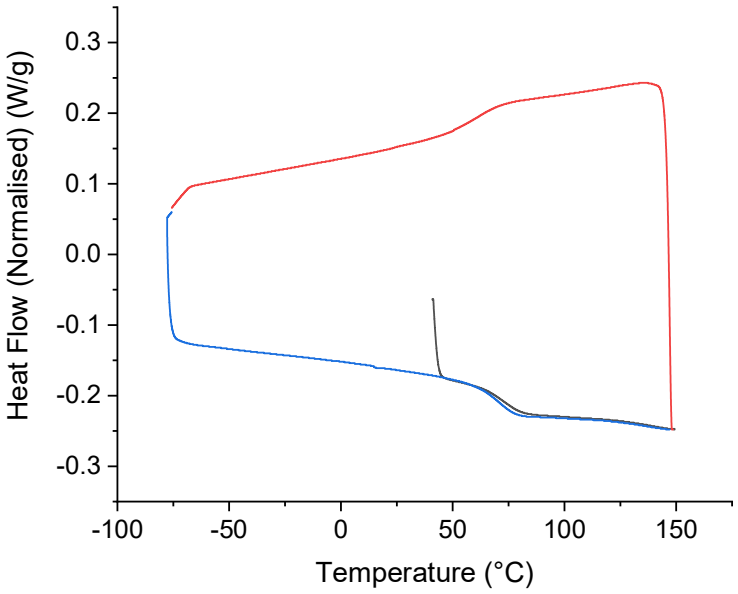

Appendix 2.20: DSC traces of S-PA-DCPD terpolymer at a ratio of 50:25:25 showing the first heating cycle to 150 °C (black), cooling to -80 °C (red), and the second heating cycle to 150 °C (blue).

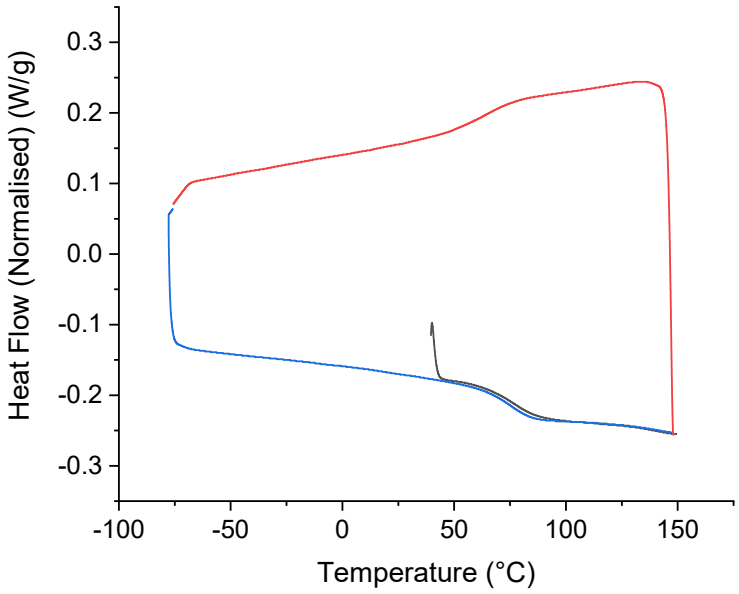

Appendix 2.21: DSC traces of S-PA-DCPD terpolymer at a ratio of 50:20:30 showing the first heating cycle to 150 °C (black), cooling to -80 °C (red), and the second heating cycle to 150 °C (blue).

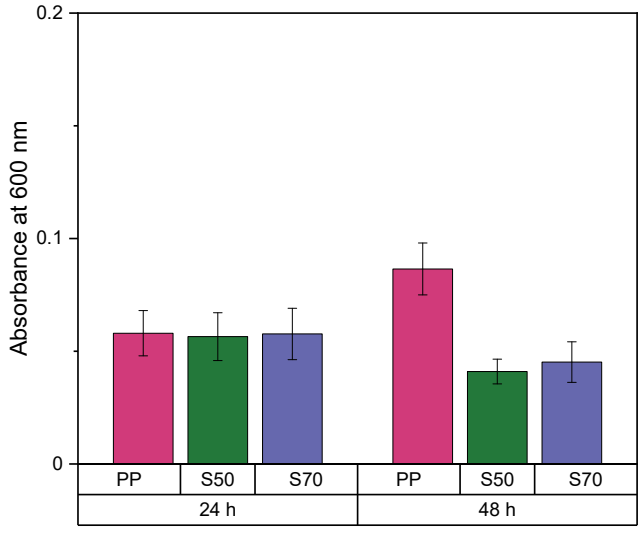

Appendix 2.22: Absorbance at 600 nm for S-PA after staining with crystal violet after 24 and 48 h incubation at 3 °C with *S. aureus*. Where PP: Polypropylene, S50: S50-PA and S70: S70-PA.

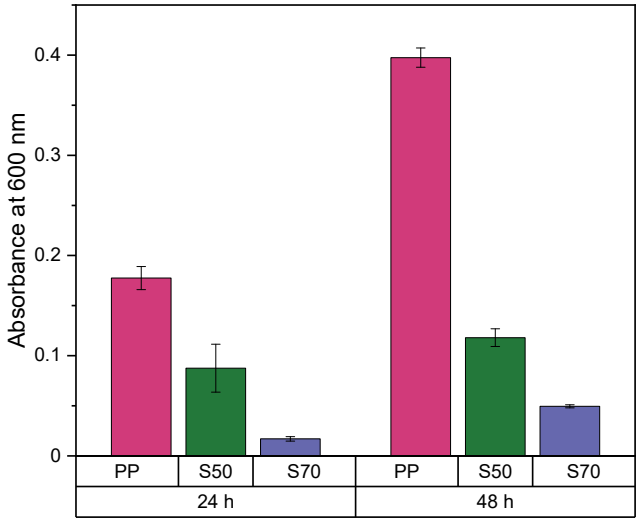

Appendix 2.23: Absorbance at 600 nm for S-PA after staining with crystal violet after 24 and 48 h incubation at 21 °C with *S. aureus*. Where PP: Polypropylene, S50: S50-PA and S70: S70-PA.

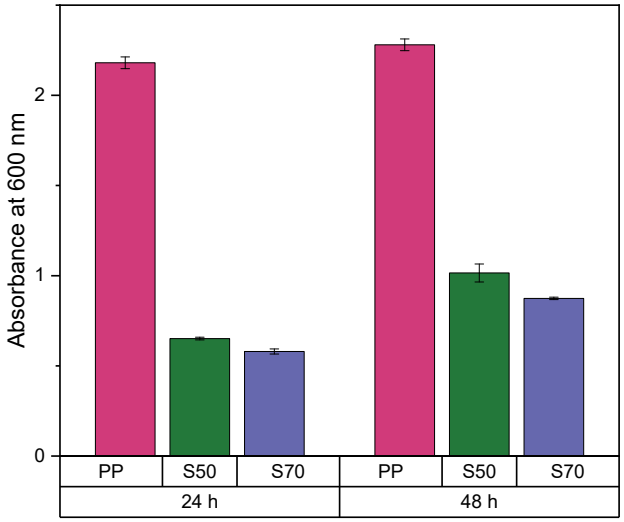

Appendix 2.24: Absorbance at 600 nm for S-PA after staining with crystal violet after 24 and 48 h incubation at 37 °C with *P. aeruginosa*. Where PP: Polypropylene, S50: S50-PA and S70: S70-PA.

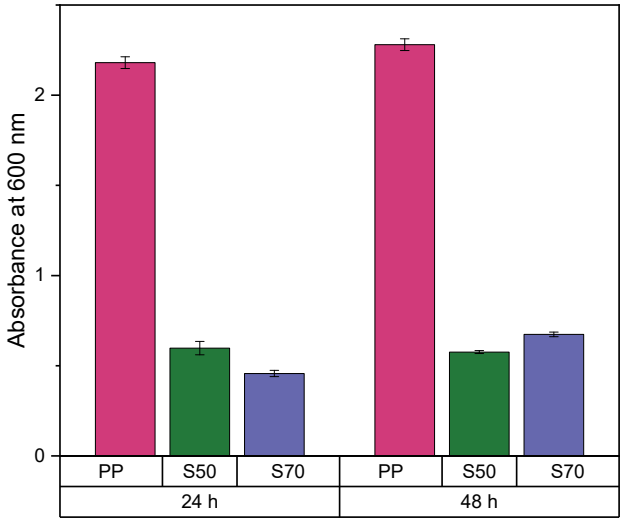

Appendix 2.25: Absorbance at 600 nm for S-DCPD after staining with crystal violet after 24 and 48 h incubation at 37 °C with *P. aeruginosa*. Where PP: Polypropylene, S50: S50-DCPD and S70: S70-DCPD

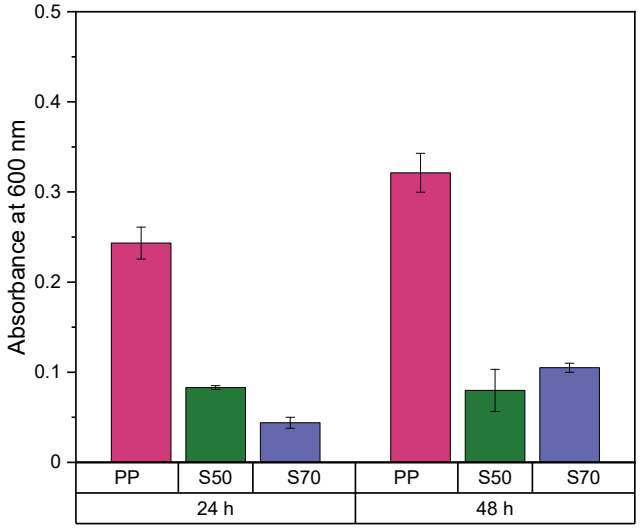

Appendix 2.26: Absorbance at 600 nm for S-DVB after staining with crystal violet after 24 and 48 h incubation at 37 °C with *S. aureus*. Where PP: Polypropylene, S50: S50-DVB and S70: S70-DVB.

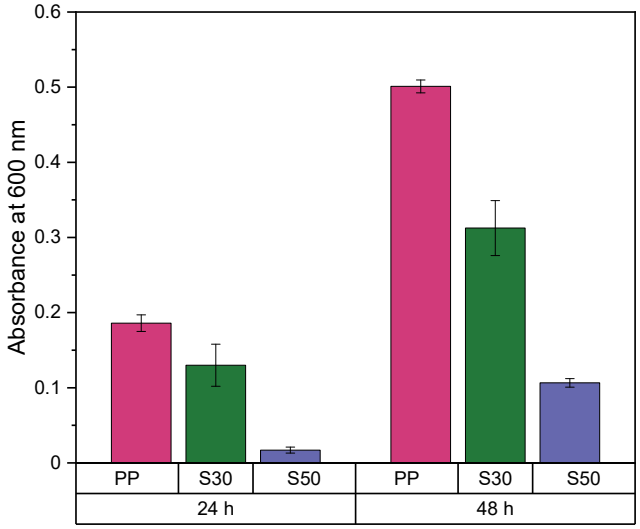

Appendix 2.27: Absorbance at 600 nm for S-LO after staining with crystal violet after 24 and 48 h incubation at 37 °C with *S. aureus*. Where PP: Polypropylene, S30: S30-LO and S50: S50-LO.

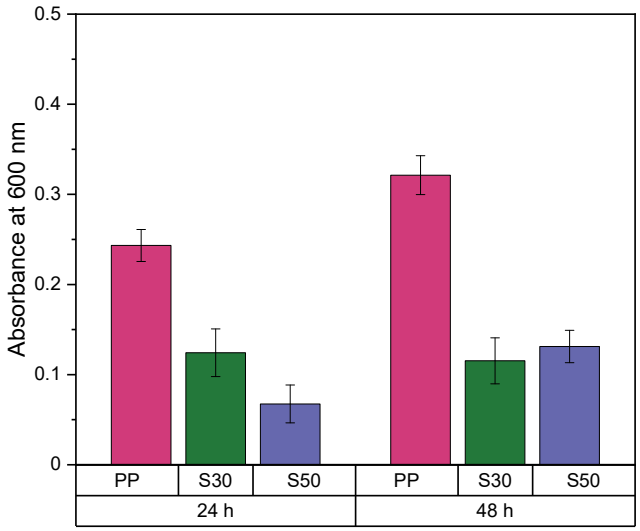

Appendix 2.28: Absorbance at 600 nm for S-RO after staining with crystal violet after 24 and 48 h incubation at 37 °C with *S. aureus*. Where PP: Polypropylene, S30: S30-RO and S50: S50-RO.

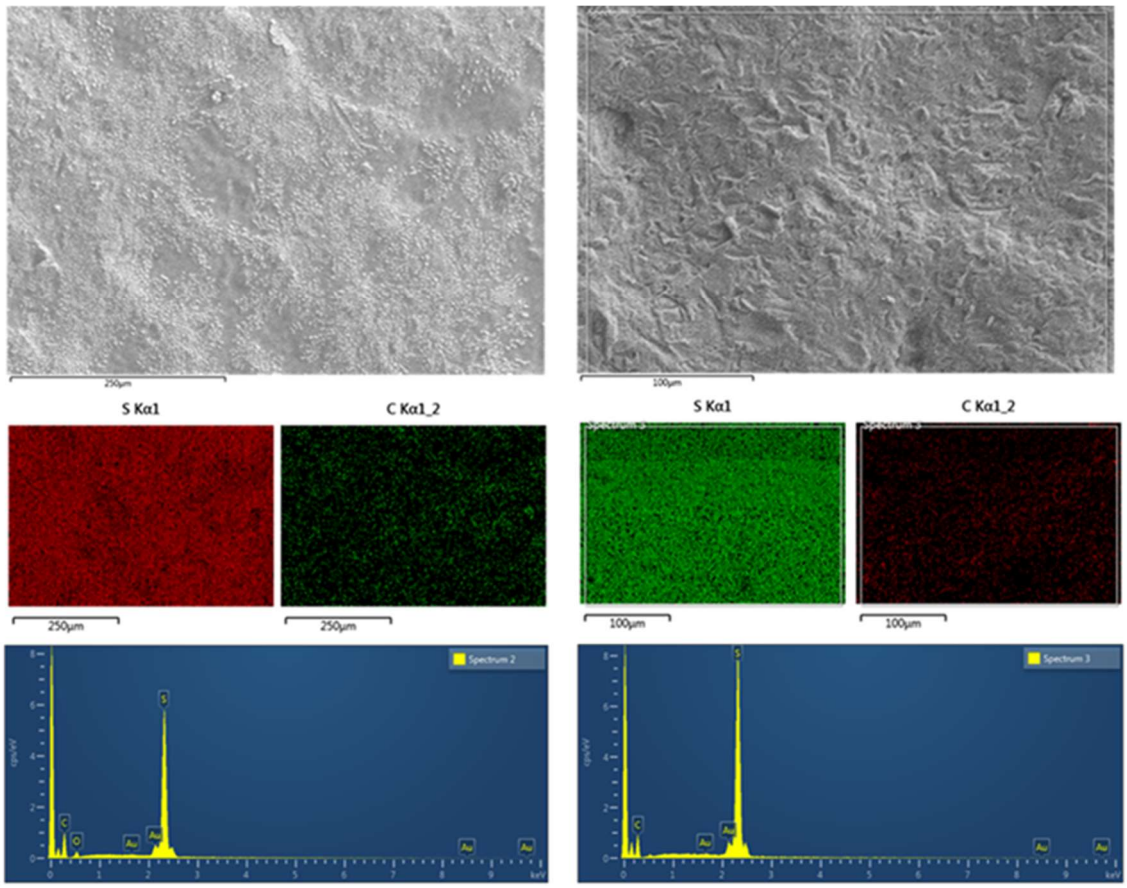

Appendix 2.29: Scanning electron microscopy (SEM) and Energy-dispersive X-ray spectroscopy (EDS) of S50-PA (left) and S50-DCPD (right).

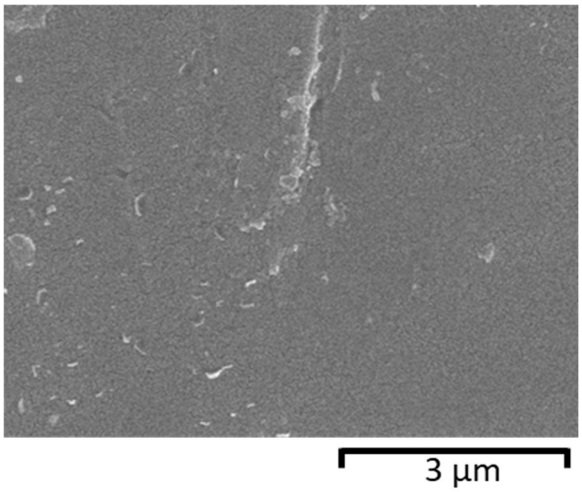

Appendix 2.30: SEM image of clean polypropylene.

Chapter 3

Preparation and Antibacterial Properties of Sulfur-Polymer Nanoparticles

3.1 Abstract

Formulating high sulfur content polymers into nanoparticles has several potential outcomes. High sulfur content polymers are often hydrophobic and have low water solubility and dispersibility, formulating polymeric nanoparticles could allow for the polymers to be dispersed in aqeuous media. In addition to this, some high sulfur content polymers have poor physical properties and do not form solid materials, instead they are sticky and tacky materials that are difficult to use. Post-polymerisation processing of these sticky materials into nanoparticles could be a more convenient way of using such polymers. Furthermore, the high surface areas of nanoparticles compared to the bulk could provide improved properties where high surface area is beneficial. All of these potential outcomes could open up new applications for high sulfur content polymers, or, improve existing applications. In this chapter we discuss the synthesis of high sulfur content polymeric nanoparticles and their antibacterial activity and cytotoxicity.

3.2 Introduction

Polymeric nanoparticles are widely reported, often for use as novel therapeutics and drug delivery systems. Nanoparticles are described by the International Union of Pure and Applied Chemistry (IUPAC) as particles of any shape with dimensions in the range of 1-100 nm. The lower limit in distinguishing micro and nanoparticles remains a matter of debate and in the field of nanomedicine, particles with dimensions up to 1000 nm are often defined as nanoparticles.[1,2] Polymer nanoparticles can be prepared by several techniques, and depending on the preparation method two types of structures can be formed which are known as nanospheres and nanocapsules (Figure 3.1). Nanospheres have solid-core structures whereas nanocapsules have hollow-core structures which are normally a liquid core of either oil or water used to entrap substances into the nanoparticles. Both types of polymeric nanoparticle can be used to encapsulate drug molecules for applications in drug delivery.[3–5]

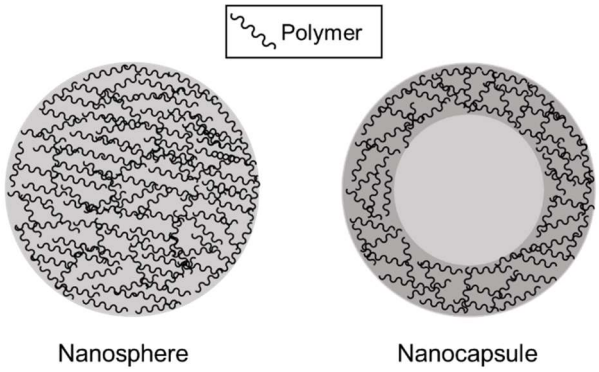

Figure 3.1: A diagram depicting the simplified structures of nanospheres and nanocapsules.[6]

The preparation methods for polymer nanoparticles can be divided into two general categories, namely, methods that consist of the polymerisation of monomers and methods that require preformed polymers. Polymerisation methods for the preparation of polymer nanoparticles include interfacial polymerisation and emulsion polymerisation techniques. Interfacial polymerisation is a type of condensation polymerisation that occurs at the interface of two immiscible phases, whereas emulsion polymerisation employs a surfactant to emulsify

the two immiscible phases. Such polymerisation methods have some limitations such as requiring extensive purification steps to remove unreacted monomers and initiators and poor control of the polymer nanoparticle properties such as size.[5] Preparation methods that require preformed polymers can be sub-divided into two categories: two-step methods that require emulsification and one-step methods that do not require an emulsification step.[7] One of the most commonly used two-step methods is the emulsion-solvent evaporation technique (Figure 3.2). The emulsion-solvent evaporation method consists of dissolving the preformed polymer in a volatile organic solvent such as dichloromethane and chloroform. The polymer solution is then emulsified with an aqueous solution that is immiscible with the organic phase and is a poor solvent for the polymer. High energy methods such as high-speed homogenisation and ultrasonication are required to form emulsions consisting of nanodroplets, and surfactants are commonly dissolved in the aqueous phase to aid emulsification.[8] An aqueous dispersion of polymer nanoparticles is then formed upon evaporation of the volatile organic solvent. Other two-step methods exist that are very similar to the emulsion-solvent evaporation method, but differ in the removal of the volatile organic solvent. Other removal methods include salting-out and fast diffusion. [7,9]

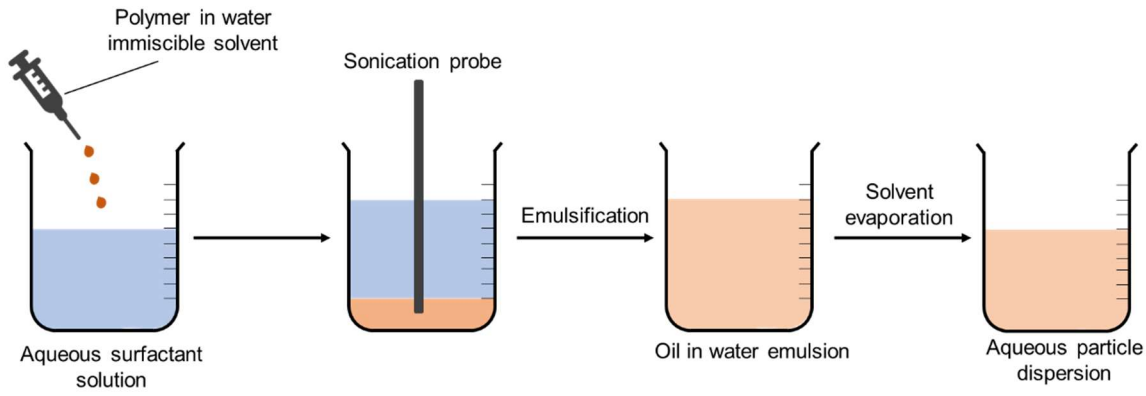

Figure 3.2: A summary of the emulsion-solvent evaporation method for the preparation of polymeric nanoparticles.[10]

Unlike two-step methods such as the emulsion-solvent evaporation technique, one-step methods do not require an emulsification step. The nanoprecipitation method, also known as the antisolvent precipitation method or solvent displacement method is one of the most widely reported one-step polymer nanoparticle preparation techniques (Figure 3.3). This method requires two miscible solvents, most systems reported use water as the aqueous phase and acetone as the water-miscible organic phase. The polymer must be fully dissolved in the organic phase but must not be soluble in the aqueous phase.[11] The polymer dissolved in the water-miscible organic phase is added into a stirred aqueous solution either dropwise, at a controlled rate or in one addition. Nanoparticles form as soon as the polymer solution is dropped into the aqueous phase as they precipitate in the presence of the aqueous anti-solvent. The solution is then allowed to stir until the volatile organic solvent has evaporated to give an aqueous dispersion of polymer nanoparticles. Surfactants are not needed for the nanoprecipitation method, however, surfactants are often dissolved in the aqueous solution to enhance the stability of the dispersion formed.[8] The method has many variables such as the concentration of the polymer in the organic solvent, the ratio of solvent to antisolvent, the rate of stirring amongst several others. Studies have been conducted in order to gain an understanding of the effect of changing some of the variables on the properties of the polymeric nanoparticles formed, of most interest is the effect on the size of the particles.[12]

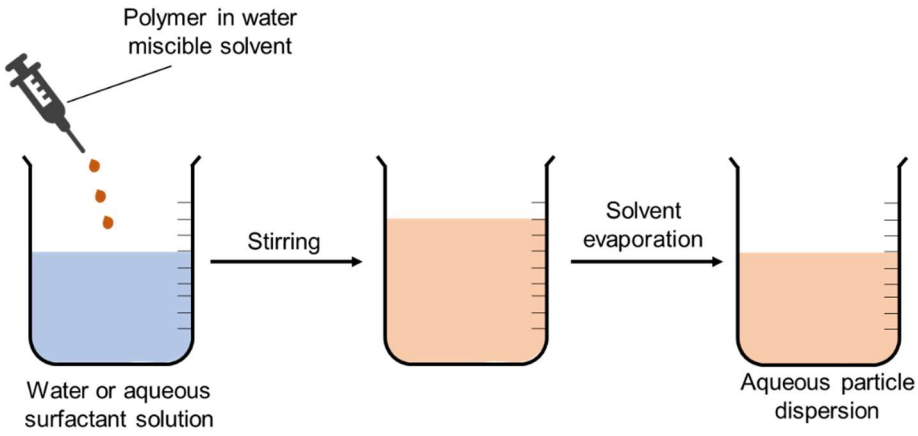

Figure 3.3: A summary of the nanoprecipitation method for the preparation of polymeric nanoparticles.[13]

Polymeric nanoparticles have potential applications in bioimaging[14], drug delivery[15] and as novel antimicrobial therapies amongst many others.[16] Although not polymeric nanoparticles, sulfur nanoparticles have been reported to have antimicrobial activity. Due to the insolubility of elemental sulfur in water, S_8 is inaccessible for biological applications, however, sulfur nanoparticles have been reported to have water dispersibility. In 2011, Schneider *et al.* investigated the antimicrobial properties of water dispersible sulfur nanoparticles synthesised by redox comproportionation of Na_2SO_3 and $Na_2S{\cdot}9H_2O$.[17] The study found that the particles exerted an inhibitory effect against the protozoa *Plasmodium falciparum*, which can cause malaria, but exerted low toxicity against mammalian cells.[17] In 2018, Shankar *et al.* reported the synthesis of chitosan-capped sulfur nanoparticles that showed antibacterial activity against *E. coli* and *S. aureus*. In addition to this, they reported that the sulfur nanoparticles inhibited the proliferation of cancer cells with minimal toxic effects against normal cells.[18] More recently, Shivalkar *et al.* reported the light-mediated antibacterial activity of sulfur quantum dots.[19] The synthesised sulfur quantum dots were found to have bactericidal activity against ampicillin-resistant *E. coli* in the presence of sunlight. It was proposed that the mechanism of action of the sulfur quantum dots involves the photogeneration of electrons

which are able to transfer to cellular oxygen species forming reactive oxygen species (ROS) which lead to oxidative stress of the bacterial cells.[19] Similarly, Wang *et al.* demonstrated that negatively charged sulfur quantum dots can be prepared using poly(sodium 4-styrenesulfonate) as a capping agent.[20] Negatively charged particles were found to have an inhibitory effect against methicillin-resistant *S. aureus* and *P. aeruginosa*. The membrane integrity of both *S. aureus* and *P. aeruginosa* was assessed after treatment with the sulfur quantum dots by SEM, and it was found that the membrane integrity of the cells were destroyed, more so for *P. aeruginosa*. It was also found that the metabolic activity of both bacterial species were reduced after treatment with sulfur quantum dots. The quantum dots were found to be hemocompatible with no evidence of cytotoxicity against human umbilical vein endothelial cells.[20] ROSwere generated during incubation with bacteria, where hydroxyl radicals (•OH) and singlet oxygen ($^1O_2$) were detected by electron paramagnetic resonance spectroscopy, and further confirmed by trapping with a radical scavenger. It is thought that ROS can damage membrane proteins and enzymes and can block respiratory and electronic transport systems of bacteria, leading to cell death.[20]

Lim and co-workers reported the *in situ* synthesis of water dispersible high sulfur content nanoparticles by the interfacial polymerisation of sodium polysulfide and 1,2,3-trichloropropane in water. Dynamic light scattering (DLS) measurements showed nanoparticles with an average hydrodynamic diameter of 172.8 ± 33.1 nm.[21] Composites of inverse vulcanised polymers with nanoparticles such as lead sulfide (PbS) have been reported whereby PbS nanoparticles were incorporated into the inverse vulcanised polymer with demonstrated tuneable optical properties.[22] At the start of this project, high sulfur content polymeric nanoparticles prepared by a nanoprecipitation method had not been reported. In 2022, Zhang *et al.* reported the preparation of high sulfur content polymer nanoparticles by a nanoprecipitation method.[23] Terpolymers were synthesised from sulfur, perillyl alcohol and

DCPD *via* inverse vulcanisation. The polymers were formulated into nanoparticles by a nanoprecipitation method using ethanol as an anti-solvent. The high sulfur content polymer nanoparticles were found to selectively remove mercury from a mixed-ion solution. Furthermore, mercury filter membranes were fabricated using the polymeric nanoparticles, demonstrating that high sulfur content polymer nanoparticles have potential applications in environmental remediation by means of heavy metal uptake.[23]

3.3 Aims of Chapter

In Chapter 2, we demonstrate that high sulfur content polymers show antibacterial activity against *S. aureus* and *P. aeruginosa*. Some of the polymers discussed, such as S-PA and S-DIB are soluble in THF and chloroform. The solubility of these polymers in such organic solvents makes them suitable candidates for the preparation of polymeric nanoparticles by the nanoprecipitation and emulsion-solvent evaporation methods. The work discussed in this chapter will focus on the preparation of high sulfur content polymeric nanoparticles by both nanoprecipitation and emulsion-solvent evaporation methods to investigate their antibacterial properties and cytotoxicity. At the start of this study, polymeric nanoparticles of inverse vulcanised polymers prepared by post-processing methods had not been reported. Furthermore, the antibacterial properties of inverse vulcanised polymer nanoparticles have not been previously investigated. This is the first study to investigate the antibacterial properties of water dispersible inverse vulcanised polymer nanoparticles prepared by post-polymerisation methods.

Aims in summary:-

- Preparation of suitable polymers for nanoparticle preparation
- Optimisation of nanoparticle formulation by post-polymerisation methods
- Investigate the stability of nanoparticle dispersions
- Assess the antibacterial activity of polymeric nanoparticles against methicillin-resistant *S. aureus* and *P. aeruginosa*
- Investigate the interactions between nanoparticles and bacterial cells
- Evaluate the antibiofilm activity of the polymeric nanoparticles
- Assess the cytotoxicity of sulfur polymer nanoparticles against mammalian cells

- Investigate the interaction of sulfur polymer nanoparticles with cellular thiols as a potential mechanism of action
- Investigate the potential of sulfur polymer nanoparticles as combination therapies

3.4 Results and Discussion

The experimental details related to the results of this chapter are detailed in section 3.6.

3.4.1 Synthesis of S-Ger

Two polymers were chosen to prepare high sulfur content polymeric nanoparticles; the product of the copolymerisation of sulfur and perillyl alcohol (S-PA) which was discussed in Chapter 2, and, the product of the copolymerisation of sulfur and geraniol (S-Ger). Geraniol (Figure 3.4) is a naturally occurring monoterpene alcohol found in the essential oils of many aromatic plants such as lavender, lemongrass and citronella amongst others. It is amongst many industrially important fragrance terpenes used because of its flowery aroma. The properties of geraniol and geraniol containing essential oils have been investigated for many years and have been found to exhibit insecticidal, antimicrobial and anticancer activities.[24] Geraniol is an attractive monomer for inverse vulcanisation as it contains unsaturation allowing for cross-linking and is relatively cheap compared to other expensive monomers such as DIB currently used in inverse vulcanisation. Other terpenes have been investigated as monomers for inverse vulcanisation, of which include myrcene and farnesene.[25] Successful reaction between elemental sulfur and terpenes demonstrates that inverse vulcanised polymer can be prepared from bio-derived renewables.[25]

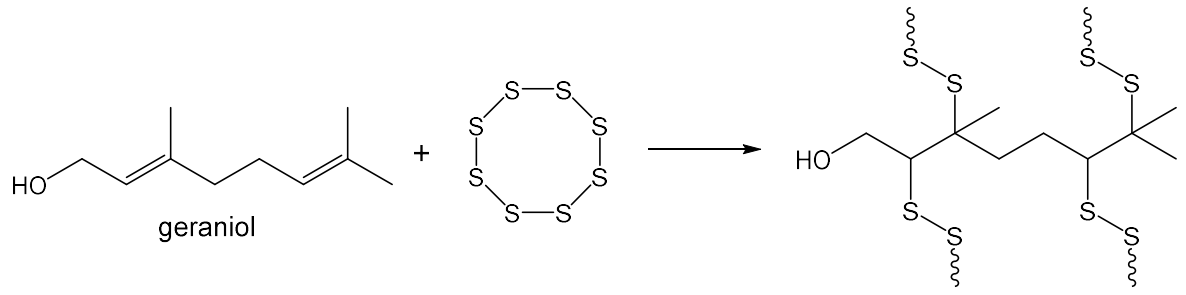

Figure 3.4: Simplified scheme of the reaction of geraniol with elemental sulfur.

The reactions of sulfur and geraniol were carried out with 50 wt% and 70 wt% sulfur feedstocks, both reactions yielded black pliable materials that become brittle after refrigeration

(97% yield). DSC analysis of both materials formed showed a T_g of 5.8 °C for the 50 wt% material (S50-Ger) (Figure 3.5) and 3.1 °C for the 70 wt% material (S70-Ger) (Figure 3.6), indicating the successful formation of polymers (Figure 3.4). The T_g of the polymers synthesised with geraniol are relatively low compared to inverse vulcanised polymers synthesised using crosslinkers such as DIB and DCPD, however they are comparable to other sulfur-terpene polymers which have T_g's below 10 °C.[25] The T_g of inverse vulcanised polymers have been found to be effected by the type and amount of crosslinker used. Crosslinkers with rigid functional groups such as aromatic rings, have been shown to yield high T_g polymers for example S-DCPD, whereas more flexible crosslinkers such as vegetable oils give very low T_g polymers. In addition, higher ratios of sulfur:crosslinker tend to give lower T_g's, as the sulfur chains are expected to be more flexible compared to rigid crosslinkers.[26]

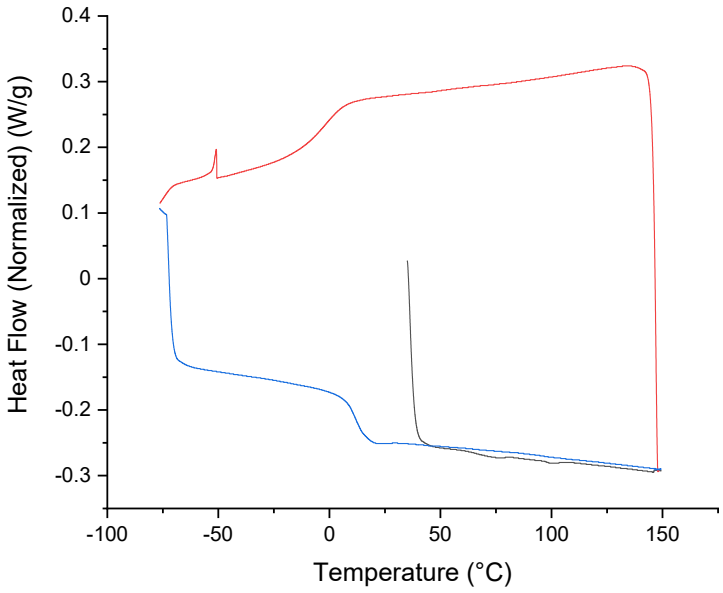

Figure 3.5: DSC trace obtained for S50-Ger (Black: First heating ramp to 150 °C. Red: Cooling to -80 °C. Blue: Second heating ramp to 150 °C).

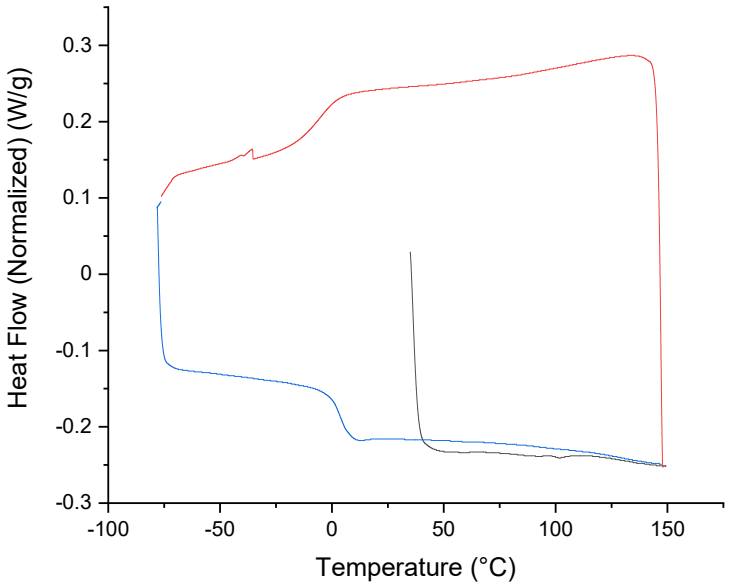

Figure 3.6: DSC trace obtained for S70-Ger (Black: First heating ramp to 150 °C. Red: Cooling to -80 °C. Blue: Second heating ramp to 150 °C).

Both polymers have good solubility in chloroform, tetrahydrofuran (THF) and toluene and are sparingly soluble in acetone and acetonitrile (Figure 3.7). Polysulfides that are insoluble in most common solvents, such as S-DCPD are known to have high-molecular weights, whereas polysulfides that are soluble in some common solvents such as S-limonene and sulfur-terpene polymers have low molecular weights. The solubility of S-Ger in solvents such as THF suggests that the polymers formed are of low molecular weights.

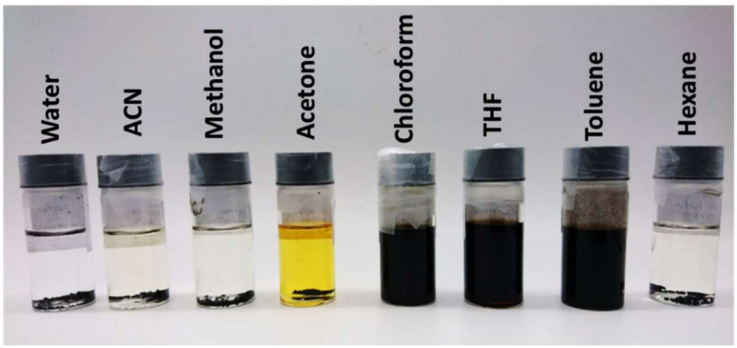

Figure 3.7: Photograph of S50-Ger in a range of solvents.

Maladeniya *et al.* identified the formation of cyclic microstructures during the inverse vulcanisation of sulfur and geraniol.[27] It was found that S-Ger had a lower than expected crosslink density, and compressive strengths similar to that of the product obtained from the inverse vulcanisation of sulfur and the monoalkene, citronellol. A mechanistic study was conducted with the aims of understanding these observations, and was postulated that geraniol may undergo intramolecular cyclisation during inverse vulcanisation to form cyclohexane derivatives which would result in a lower crosslink density (Figure 3.8).[27] Geraniol is known to form such cyclic derivatives by methods other than inverse vulcanisation, such as enzymatic catalysis, acid catalysis, and by the use of zeolites.[28–30] The cyclisation of geraniol during inverse vulcanisation has been proposed to occur by hydrogen abstraction of allylic protons, and could also occur by direct radical addition across the alkene (Figure 3.8).[27]

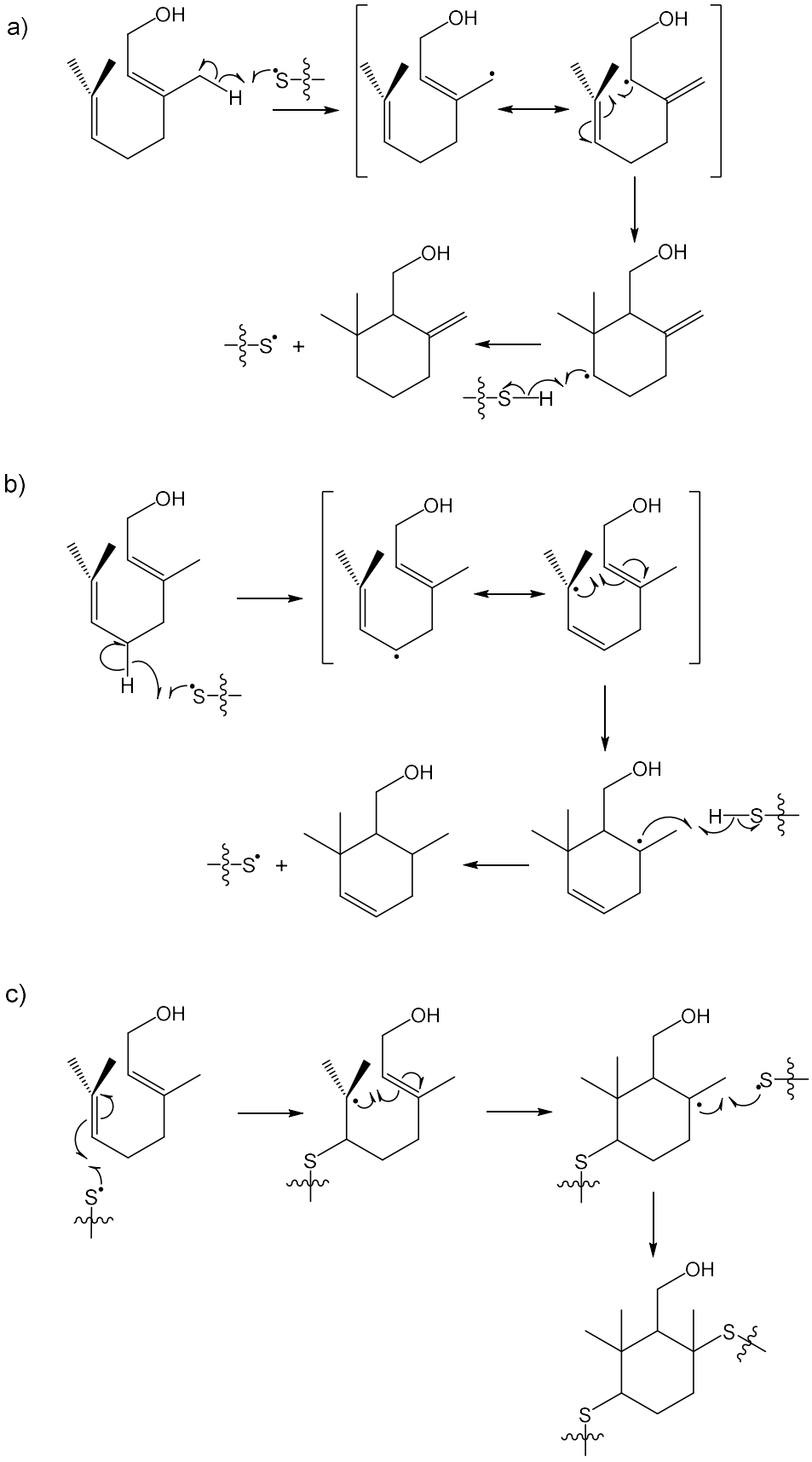

Figure 3.8: Proposed mechanisms of sulfur-radical induced geraniol cyclisation *via* initial hydrogen abstraction (a) and (b), and addition across C=C (c). Adapted from Maladeniya *et al.*[27]

The FTIR spectra of the materials synthesised also suggests successful reaction of sulfur and geraniol. Comparison of the spectrum of S70-Ger and geraniol shows that the alkene C-H bending peak at 1000 cm^{-1} for geraniol is no longer visible in the spectrum of S50-Ger and S70-Ger (Figure 3.9). The absence of this peak is indicative of complete or almost complete consumption of the alkene units in S-Ger after reaction with sulfur. This is further confirmed by the absence of a C=C stretching peak visible at 1670 cm^{-1} in the spectrum of geraniol. The O-H stretching peak at 3300 cm^{-1} is present in the spectrum of S-Ger, indicating that the alcohol functional group remains intact after the reaction of geraniol and sulfur. ^{1}H NMR analysis of the materials formed compared against geraniol also confirms consumption of the alkene units of the monomer (Figure 3.10). The alkene proton resonances between 5-5.5 ppm are not present in the spectrum of S50-Ger further indicating the formation of a polymeric material. Resonances in the region of 3.5-4 ppm are indicative of S-C-H protons which suggest the formation of crosslinks between sulfur and the alkenes of geraniol.[25]

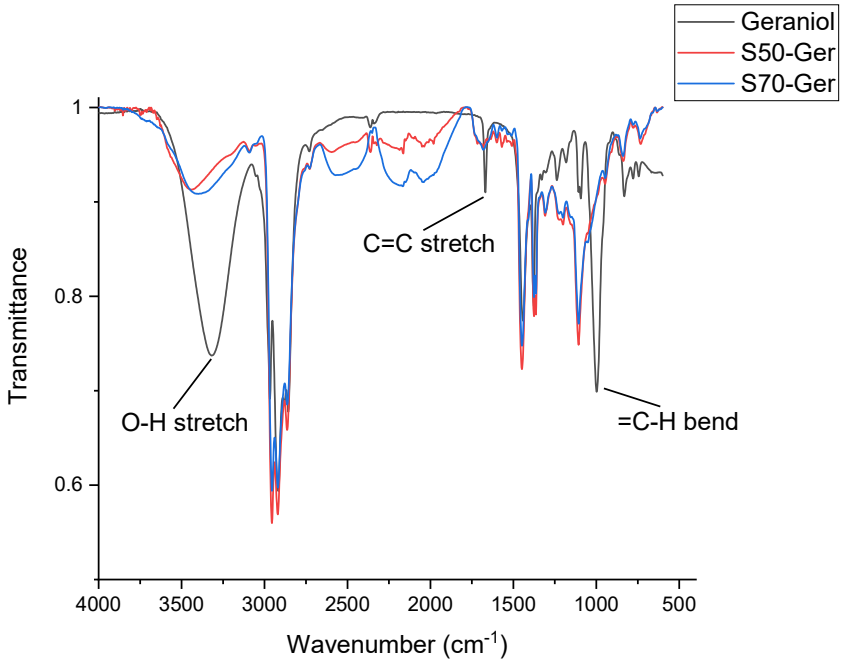

Figure 3.9: A comparison of the FTIR spectra of geraniol, S50-Ger and S70-Ger.

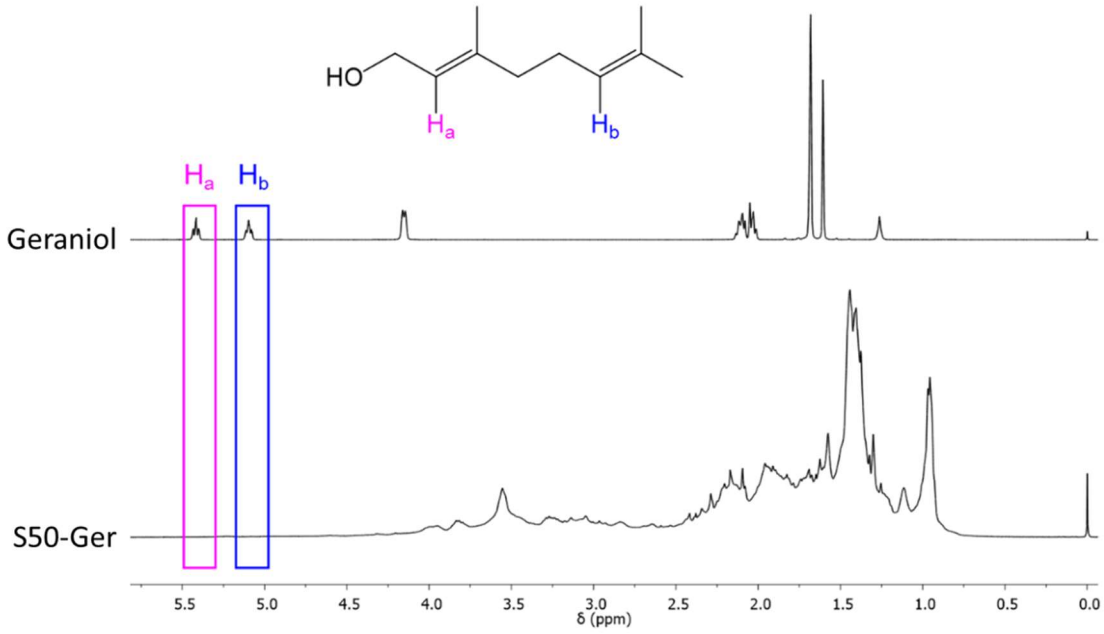

Figure 3.10: A comparison of the ^{1}H NMR spectra of geraniol and S50-Ger, highlighting the alkene proton resonances.

The alkene proton resonances between 5 and 5.5 ppm are neither present in the ^{1}H NMR spectrum of S70-Ger (Appendix 3.1). Elemental analysis of both materials show comparable percentage values for carbon, hydrogen and sulfur to theoretical calculated values (Table 3.1).

Table 3.1: *Calculated and obtained elemental analysis of sulfur-geraniol polysulfides.*

Sample	Calc. % carbon	Calc. % hydrogen	Calc. % sulfur	**C/H ratio**	Actual % carbon	Actual % hydrogen	Actual % sulfur	**C/H ratio**
S50-Ger	38.94	5.88	50	**6.62**	42.76	5.65	49.28	**7.57**
S70-Ger	23.36	3.53	70	**6.62**	23.08	3.2	72.97	**7.22**

The percentages of carbon remain almost the same or are slightly higher compared to calculated values which suggests that it is unlikely that geraniol has evaporated in any significant amount during the reaction, which is expected as the reaction was conducted at 175 °C whereas the boiling temperature of geraniol is 230 °C.[31] A possible reason for the increase in carbon percentage seen for S50-Ger could be sublimation of sulfur, which is also supported by a lower than expected sulfur percentage. Calculation of the C/H ratios from the theoretical percentages and the obtained percentages from elemental analysis shows that the C/H ratio is higher than

expected for both polymers. A possible explanation for the increase in C/H ratio is the generation of hydrogen sulfide. In addition to the potential of forming cyclic microstructures during inverse vulcanisation (Figure 3.8) as proposed by Maladeniya *et al.*,[27] geraniol is susceptible to autoxidation upon exposure to air forming allergenic hydroperoxides and other secondary oxidation products (Figure 3.11).[32,33]

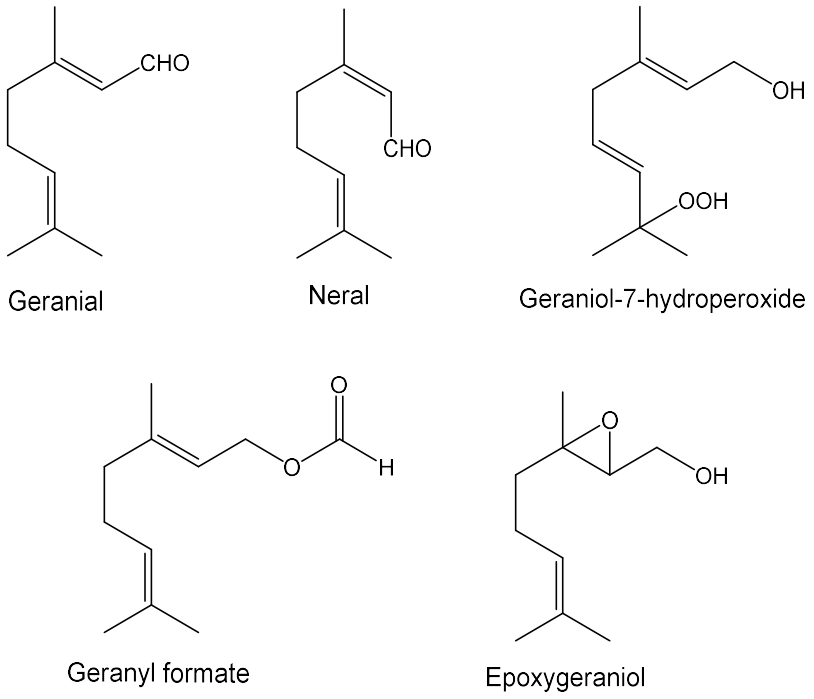

Figure 3.11: The chemical structures of some of the possible products of geraniol oxidation[32,33]

The oxidation of geraniol is initiated by hydrogen abstraction resulting in the formation of an allylic radical. It has been suggested that the most likely site for hydrogen abstraction of geraniol is the allylic hydrogen α to the alcohol group, however, other radicals may also be formed (Figure 3.12).[32,33]

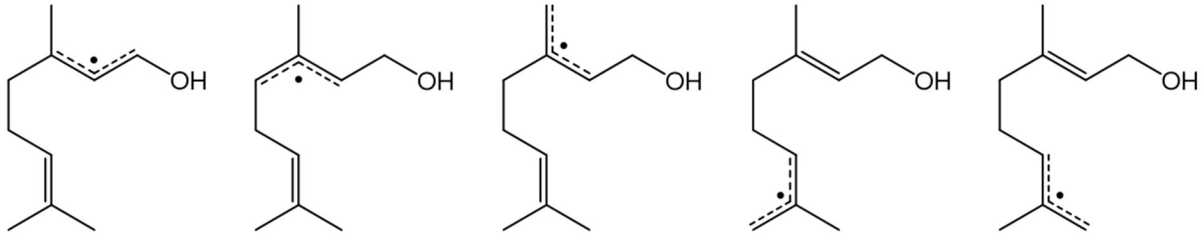

Figure 3.12: The possible structures after hydrogen abstraction of geraniol.[32]

There is no evidence of autoxidation of geraniol from both the FT-IR and ^{1}H NMR spectrum of the starting material, however, it is possible that during the reaction with sulfur, hydrogen abstraction may have occurred. Hydrogen abstraction could also lead to the generation of hydrogen sulfide, which has been reported for some inverse vulcanised reactions.[34] The generation of hydrogen sulfide is a possible explanation to the higher than expected C/H ratios in both of the products, as the percentages of carbon should remain the same providing no geraniol has evaporated during the reaction, however the percentages of hydrogen would reduce when forming hydrogen sulfide. The obtained C/H ratio is slightly higher for S50-Ger compared to S70-Ger. Several reports have shown that some inverse vulcanised polymers, especially those with higher sulfur loadings, can be unstable whereby polymer chains can revert back to crystalline elemental sulfur. Thin layer chromatography analysis of S50-Ger and S70-Ger (Appendix 3.2) suggest the presence of elemental sulfur, however no crystalline sulfur melting peaks are present in the DSC traces.

3.4.2 Formulation of High Sulfur Content Polymeric Nanoparticles

The solubility of S-PA and S-Ger in chloroform and THF is ideal for the formulation of nanoparticles by techniques that require preformed polymers. The solubility of both solvents in these solvents also allowed for two methods for nanoparticle formulation to be investigated, namely the nanoprecipitation method and the emulsion-solvent evaporation method. S50-Ger was used to formulate nanoparticles by both methods. Water-based coatings are more desirable than solvent-based coatings due to the potential harmful effects of toxic solvents upon the

environment, therefore water was chosen as the antisolvent for both methods. Although chloroform and THF were used as the solvents for the polymers synthesised, the volumes used are much lower than the volume of anti-solvent required, and evaporation of the volatile solvent means there should only be trace amount of organic solvent, if any, present in the final dispersions of polymer nanoparticles. The dispersions were analysed by Dynamic Light Scattering (DLS) where the main parameters measured were the z-average diameter and the polydispersity index (PDI). The correlogram was analysed to ensure a smooth decay with no fluctuations in the baseline, which would indicate the presence of large aggregates. Each dispersion was measured at a range of concentrations to establish suitable concentrations at which the z-average diameter does not vary with concentration. The effect of various parameters such as the concentration of polymer in the solvent and the type and concentration of surfactant on the z-average diameter and PDI of the resulting dispersions were studied.

An emulsion-solvent evaporation method for the preparation of polymeric nanoparticles was investigated for S-Ger. For this method, an oil-in-water (chloroform/water) emulsion was formed whereby the polymer was dissolved in the oil phase and a suitable surfactant was dissolved in the water phase. The formation of an oil-in-water emulsion allows the preparation of an aqueous dispersion of polymeric nanoparticles rather than a dispersion in oil. Various emulsifiers were trialled, of which included Tween 80, polyvinyl alcohol (PVA), Brij S20 and sodium dodecyl sulfate (SDS) (Figure 3.13). Tween 80 and Brij S20 are both non-ionic surfactants with a hydrophile-lipophile balance of 15, PVA is a non-ionic polymer that is often used as an emulsifier whereas SDS in an anionic surfactant.

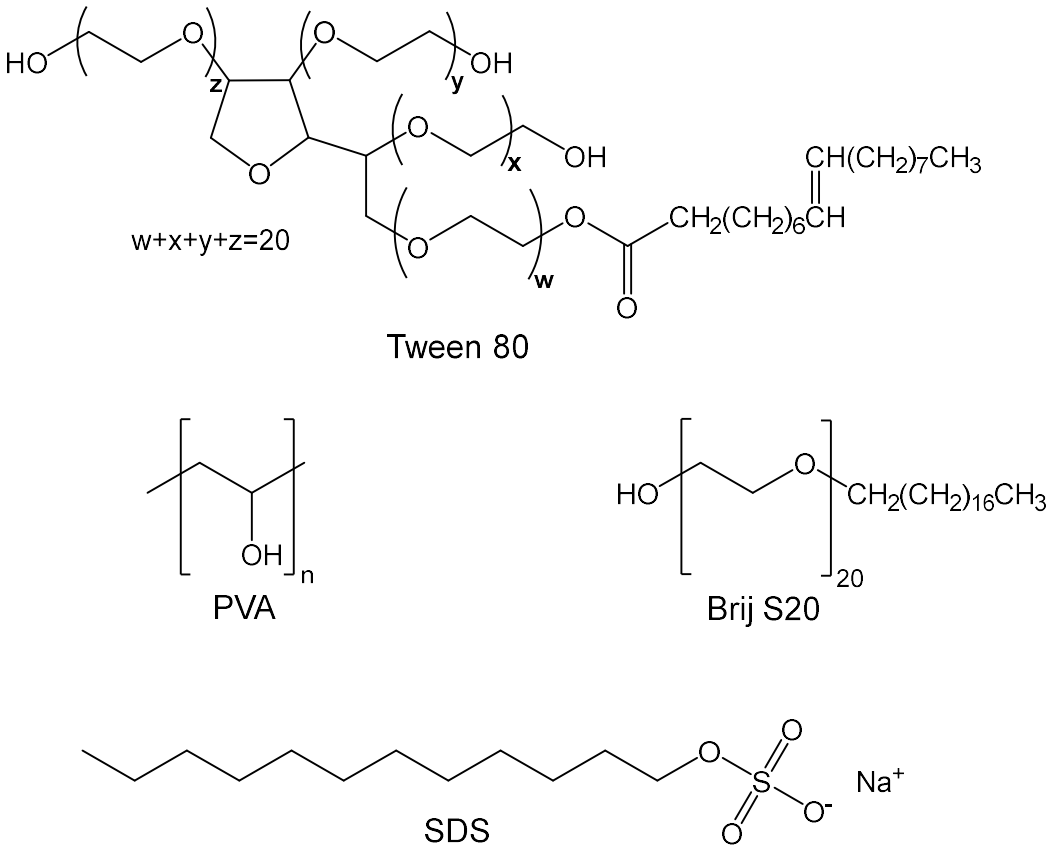

Figure 3.13: The chemical structures of the surfactants investigated for the preparation of polymer nanoparticles.

The trial formulation for the preparation of S50-Ger dispersions consisted of a concentration of 5 mg/ml of polymer in chloroform and 10 mg/ml of surfactant in water, with an oil to water ratio of 1:9. A formulation without the addition of a surfactant was also trialled, upon ultrasonication of this mixture a cream coloured emulsion was formed which phase-separated immediately as expected, for this reason a formulation without surfactant was deemed unsuitable for the preparation of polymeric nanoparticles. Stable emulsions were formed with all surfactants trialled which were then allowed to stir at room temperature to allow for the evaporation of chloroform. The resulting dispersions were cream coloured with no visible aggregates (Appendix 3.3). DLS analysis of the dispersions formed with both Brij S20 and SDS were multimodal with poor quality results (Appendix 3.4 and Appendix 3.5), thus Brij S20 and SDS were deemed unsuitable as surfactants for the preparation of S50-Ger nanoparticles. DLS of the nanodispersions of S-geraniol prepared with PVA as an emulsifier

gave monomodal distributions at various dilutions with a z-average diameter of 367.7 nm and a PDI of 0.173 (Appendix 3.6). A preliminary stability study of this dispersion was conducted whereby the dispersion was left to stand without agitation and was re-analysed by DLS after 7 and 14 days. Prior to re-analysis by DLS the dispersions were shaken briefly but were not subjected to ultrasonication. The results of the short stability study are summarised in Figure 3.14. After 7 days there is little change in both the z-average diameter and PDI of the particles which implies that the dispersions are relatively stable for 7 days. A relatively small increase in both the particle size and PDI was observed after 14 days which suggests that the particles in the dispersion may have aggregated and may not be stable for prolonged periods of time.

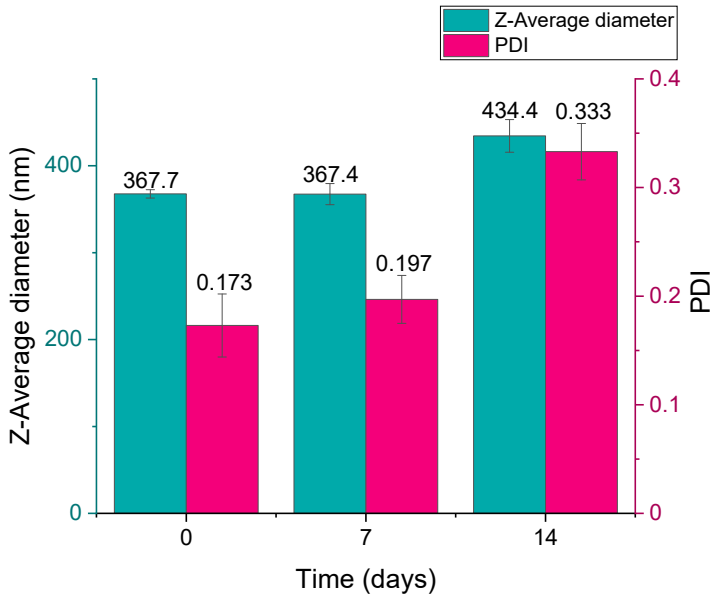

Figure 3.14: A summary of the z-average diameter and PDI obtained for dispersions of S50-Ger formed by an emulsion-solvent evaporation method with PVA after 0, 7 and 14 days.

Analysis of the dispersions formulated using Tween 80 gave smaller particle sizes compared to formulations with PVA, a stability test comparing data after 7 days was also obtained and is summarised in Figure 3.15. Similarly to the formulations employing PVA, the dispersions seem to be stable after 7 days with no significant increase in the size and PDI of the particles. The difference in the nanoparticle size when formulated with PVA and Tween80 could be due to the

ability of the surfactants to stabilise the emulsion in the first step before solvent evaporation. Optical microscopy was used to look at the emulsions formed in the first step of the emulsion-solvent evaporation method, it was found that smaller oil droplets were formed when employing Tween80 as a surfactant compared to PVA (Figure 3.16).

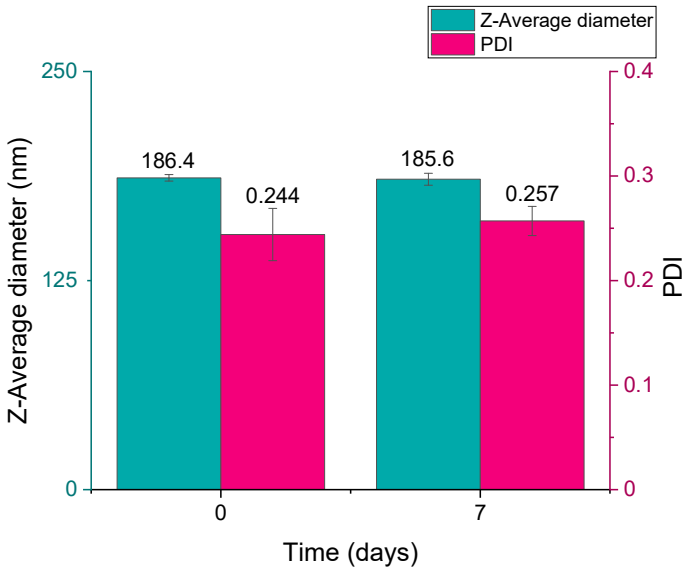

Figure 3.15: A summary of the z-average diameter and PDI values obtained for dispersions of S50-Ger formed by an emulsion-solvent evaporation method with Tween 80 after 0 and 7 days.

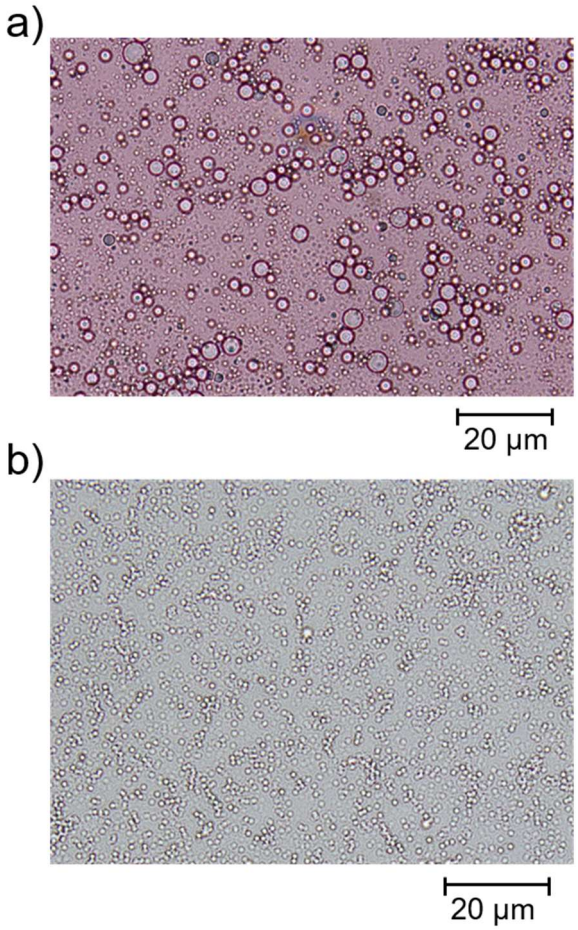

Figure 3.16: Optical microscope images of the chloroform in water emulsions with a) PVA and b) Tween80 as surfactants.

The formulations contain a large excess of surfactant at a concentration of 10 mg/ml, therefore reducing the concentration of surfactant in the aqueous phase was investigated. The critical micelle concentration (CMC) of Tween 80 is 0.015 mg/ml, therefore concentrations that were closer to the CMC were chosen to be investigated. Dispersions of S-geraniol with Tween 80 at concentrations of 0.05 and 0.1 mg/ml were trialled, the presence of large aggregates was visible in both dispersions formed and DLS analysis confirmed that both concentrations were unsuitable for S-Ger nanoparticle preparation (Appendix 3.7 and Appendix 3.8). Purification of the nanoparticles by centrifugation was investigated as it seems that an excess of surfactant is necessary for the preparation of the nanoparticles. The

dispersions were centrifuged at 6000 rpm for 30 minutes, the supernatant was removed and the particles were redispersed in water. This was repeated a total of three times. The supernatant and redispersed particles after 3 cycles of centrifugation and washing were analysed by DLS and compared to the sample prior to centrifugation, the results of which are summarised in Figure 3.17. The z-average diameter of a repeated dispersion of S-Ger with Tween 80 is comparable to that of the previous dispersion with diameters of 197.5 nm (Figure 3.17) and 186.4 nm (Figure 3.15) respectively which shows that the dispersions are reproducible. After 3 cycles of centrifugation the sediment was redispersed and analysed by DLS giving a higher z-average diameter compared to the dispersion prior to centrifugation. This could be explained by the possible occurrence of aggregation during centrifugation, however, it is more likely that particles of different sizes have been separated during centrifugation whereby the larger particles have sedimented and the smaller particles remain in the supernatant. This is also supported by the data obtained from the supernatant after 3 cycles where the z-average diameter is lower than that of the original dispersion. Comparison of the PDI values of the original suggests that the particles have been separated as the PDI values for the redispersed sediment and the supernatant are lower than that of the original dispersion. This suggests that the original dispersion contains a wider range of particle sizes whereas the redispersed sediment and supernatant contain a narrower range of particle sizes within the samples, which is expected for the separation of particles based on their size. The aim of the centrifugation process was not to separate the particles by their size, but to separate the particles from a solution of excess surfactant, however this does provide a useful way to obtain samples with smaller z-average diameters but also means that the yield of nanoparticles is compromised. Centrifugation at higher rpm of 20,000 was attempted, however, smaller particles remained in the supernatant.

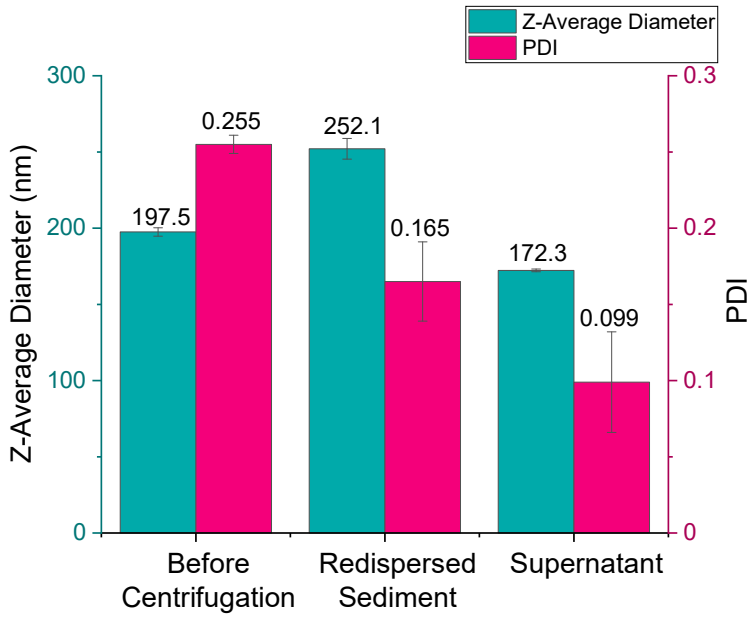

Figure 3.17: A summary of the z-average diameter and PDI values obtained for a dispersion of S50-Ger formed by an emulsion-solvent evaporation method with Tween80 before and after centrifugation.

A nanoprecipitation method was also investigated for inverse vulcanised polymer nanoparticles, THF was chosen as the solvent for the polymer and water as the anti-solvent. The nanoprecipitation method does not require the use of a surfactant; therefore, a surfactant-free dispersion was formulated to establish whether S50-Ger polymer nanoparticles can be formed. The trial formulation consisted of 5 mg/ml polymer dissolved in THF, with a THF to water ratio of 1:9. After evaporation of THF a cream coloured cloudy solution remained with no visible aggregates. The size distribution by intensity obtained by DLS indicates the successful synthesis of polymeric nanoparticles with monomodal distributions (Appendix 3.9). The particles obtained have a z-average diameter of 138 nm and a relatively low PDI of 0.165. The effect of the concentration of polymer dissolved in THF was studied by employing concentrations of 5, 10 and 20 mg/ml (Figure 3.18). The smallest particles were obtained with the lowest concentrations of polymer and increasing the concentration results in an increase in both the nanoparticle z-average diameter and the PDI.

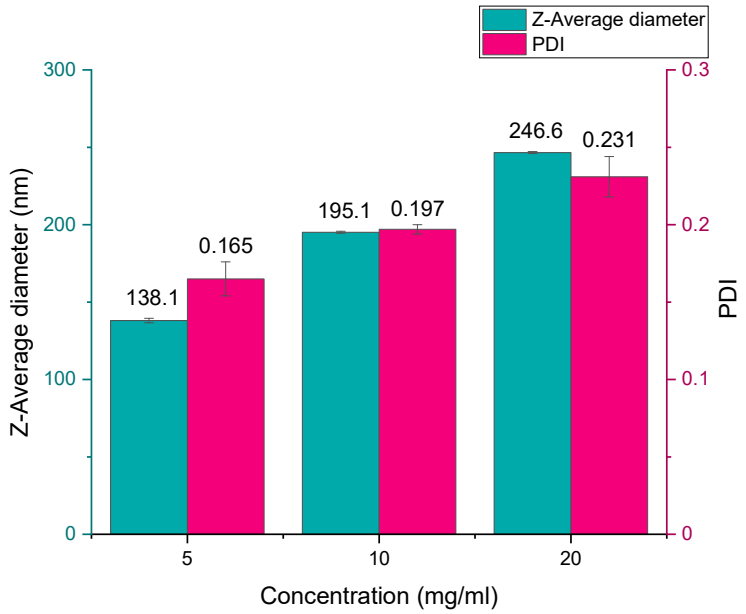

Figure 3.18: A summary of the z-average diameter and PDI values obtained for a dispersion of S50-Ger formed by a nanoprecipitation method without surfactant at varying polymer concentrations.

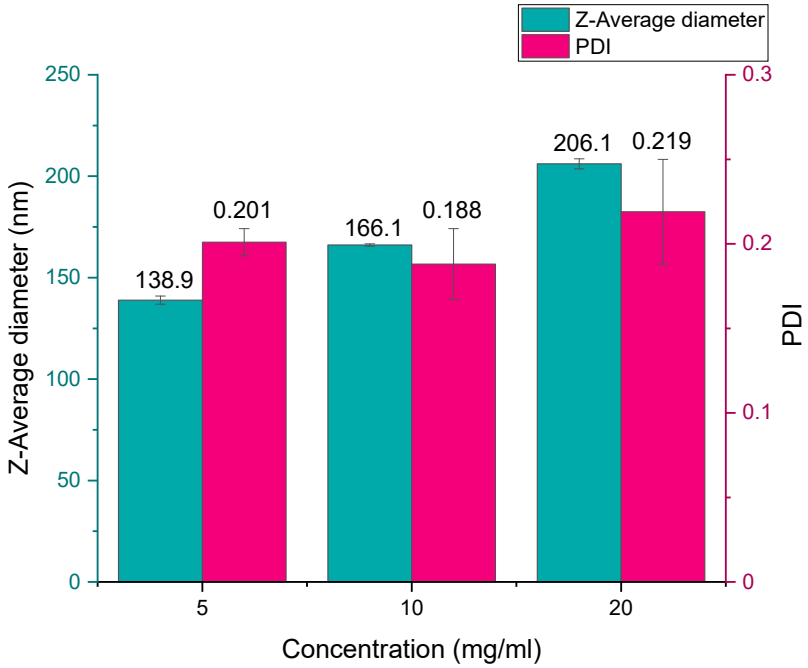

Figure 3.19: A summary of the z-average diameter and PDI values obtained for a dispersion of S50-Ger formed by a nanoprecipitation method with Tween 80 at varying polymer concentrations.

Although the nanoprecipitation method does not require the use of a surfactant, it has been reported that employing a surfactant can often result in enhanced stability of the dispersion and smaller nanoparticles.[35] Dispersions of S50-Ger by the nanoprecipitation methods were

repeated using aqueous solutions of Tween 80 at a concentration of 10 mg/ml as the anti-solvent. The obtained sizes and PDI values for the dispersions formed in the presence of Tween 80 are summarised in Figure 3.19. The z-average diameter of the particles formed using Tween 80 are the same as the particles formed in the absence of a surfactant when employing a polymer concentration of 5 mg/ml. Similarly to the surfactant-free dispersions, the z-average diameter and PDI tend to increase with increasing the polymer concentration in THF. However, at higher concentrations the dispersions formed using Tween 80 have z-average diameters that are lower than those of the surfactant-free dispersions at the same polymer concentration. It is thought that the addition of a surfactant increases the viscosity of the dispersant and can cover the polymeric nanoparticles providing steric stabilisation to prevent coalescence and aggregation of particles resulting in smaller average sizes.[36] In order to establish if the nanoprecipitation method can be used to formulate dispersions of other inverse vulcanised polymers, the method was repeated for S50-PA. DLS analysis of the dispersions formed in the absence of a surfactant using S50-PA at a concentration of 5 mg/ml in THF in gave particles with monomodal distribution, a z-average diameter of 142.5 nm and a PDI of 0.148 (Figure 3.20). SEM images of the nanoparticles (Figure 3.21) show that the particles are spherical and uniformly sized, consistent with the DLS data.

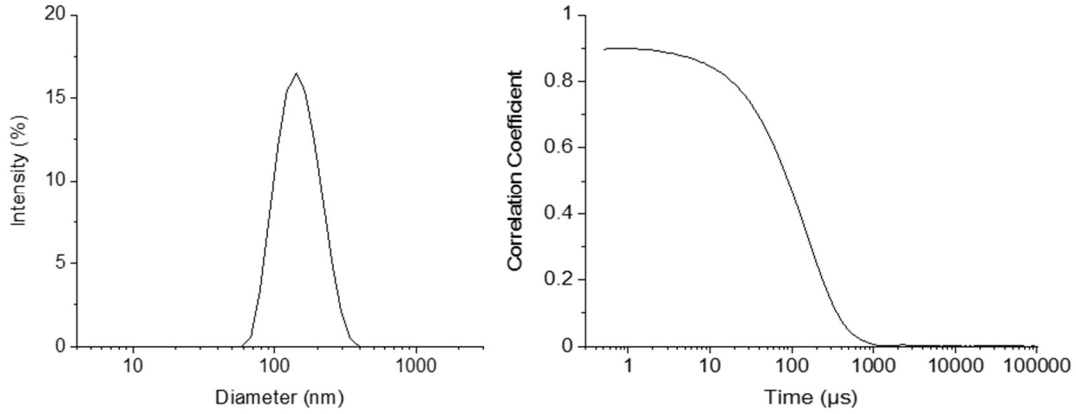

Figure 3.20: The size distribution by intensity and correlogram traces obtained for dispersions of S50-PA formed by a nanoprecipitation method without a surfactant.

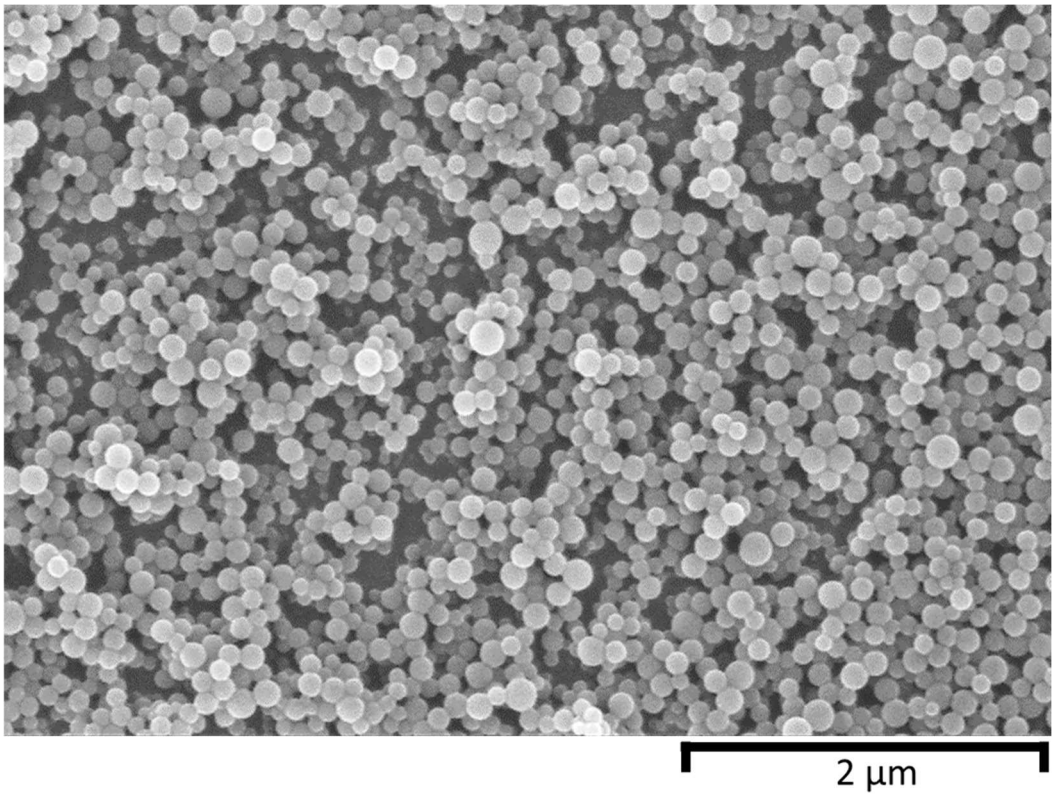

Figure 3.21: SEM image of S50-PA polymeric nanoparticles formulated in water as the antisolvent phase.

The obtained sizes of the particles are very similar to those obtained with S50-Ger formulated at the same concentration of polymer in THF. This suggests that the nanoprecipitation method

could be suitable to formulate nanoparticles of a range of inverse vulcanised polymers provided the polymer has good solubility in a water miscible solvent such as THF. It also shows that surfactant-free formulations are possible which are particularly desirable as additional purification steps can be avoided.

The preparation of polymeric nanoparticles was investigated in different anti-solvents to probe if there was any relation between the solvent properties such as polarity or viscosity on the size of the prepared nanoparticles. S50-PA nanoparticles were prepared in ethanol as the antisolvent, upon precipitation large aggregates were visible. SEM imaging of the obtained dispersions show aggregated particles (Figure 3.22), unlike the spherical particles obtained when using water as the antisolvent.

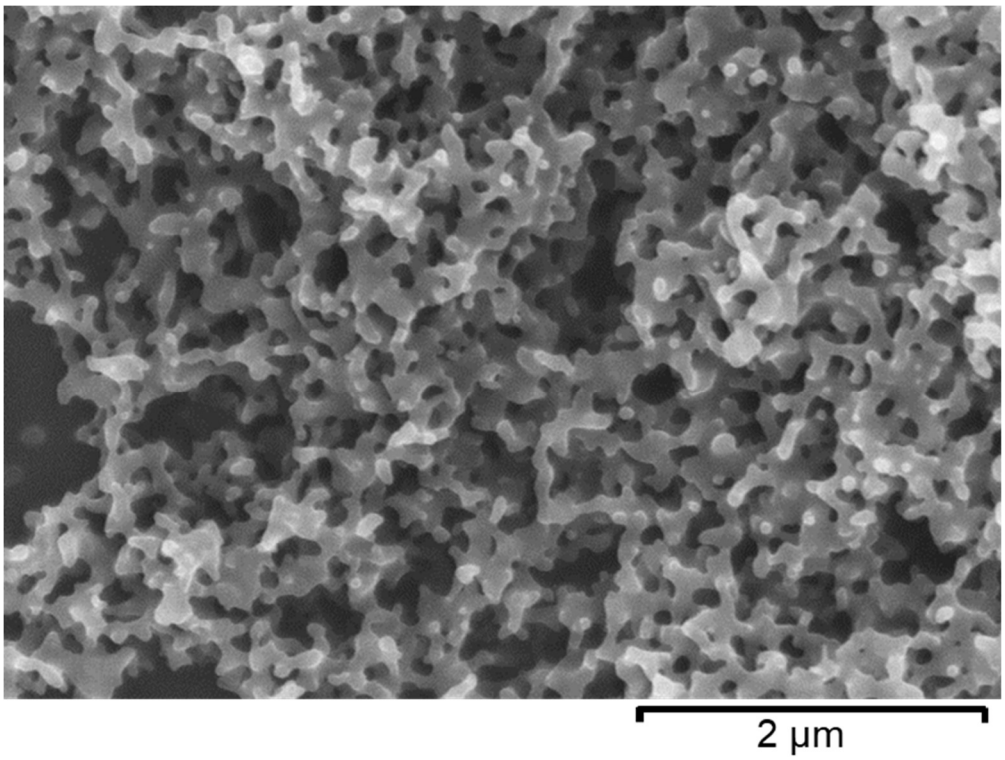

Figure 3.22: SEM image of S50-PA polymeric nanoparticles formulated in ethanol as the antisolvent phase

The size of the nanoparticles formed in increasing concentrations of ethanol in a water/ethanol mixed antisolvent phase was investigated (Figure 3.23). At 25% v/v ethanol in water, the

obtained dispersions have similar size distributions to that in water, however with a slight shift in the distrubution to larger diameters. Increasing the ethanol content further causes multimodal distrubtions in the DLS traces, especially for 75% v/v ethanol antisolvent which has new distribution peaks at much higher diameters compared to the dispersions obtained in water alone (Figure 3.23). This demonstrates that increasing the ethanol content of the anti-solvent phase results in aggregation of the resultant nanoparticles.

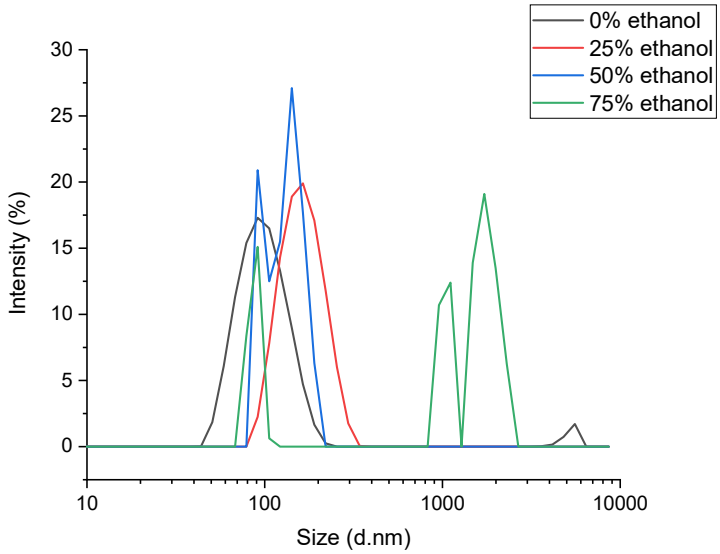

Figure 3.23: The size distribution by intensity traces obtained for dispersions of S50-PA formed by a nanoprecipitation method in mixed water/ethanol antisolvent phase, varying from 0-75 % v/v ethanol.

Other antisolvents were also trialled in the formulation of S50-PA nanoparticles. Water, methanol, ethanol and ethylene glycol were compared, as they have varying polarties and viscosities, in addition to having boiling points higher than that of THF, allowing THF to be removed from the solvent/antisolvent mixture. Dispersions of S50-PA obtained by using methanol as the antisolvent gave similar z-average diameters to those obtained in water, whereas the traces obtained from using ethylene glycol are similar to that obtained in ethanol, resulting in a multimodal distribution of particle sizes (Figure 3.24). The z-average diameter of the obtained dispersions increased in the order: methanol < water < ethanol < ethylene glycol, which may be related to the viscosities of the solvents, rather than their polarities. It is

possible that higher viscosities of the antisolvent phase reduce the ability of the solvent phase to mix, resulting in less homogeneous distribution of the solvent phase in the antisolvent phase, resulting in larger nanoparticles.

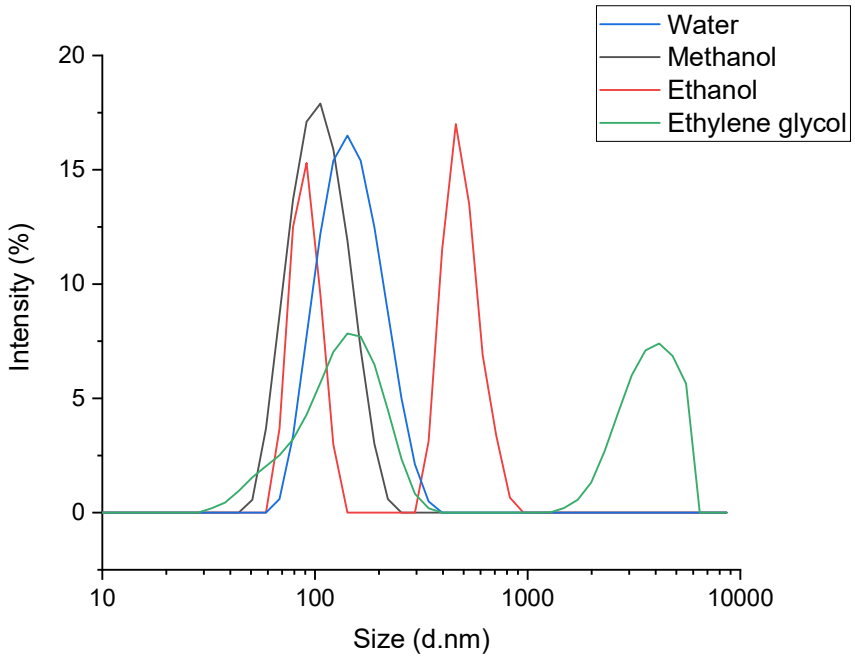

Figure 3.24: The size distribution by intensity traces obtained for dispersions of S50-PA formed in different antisolvents; water, methanol, ethanol and ethylene glycol.

3.4.3 Antibacterial Activity of High Sulfur Content Polymeric Nanoparticles

The antibacterial activity of S-polymer nanoparticles dispersed in water was assessed against Gram-positive methicillin-resistant *S. aureus* (strain USA300) and Gram-negative *P. aeruginosa* (strain PAO1). Nanoparticles were incubated in media containing bacteria, the viable cells were enumerated to assess whether the nanoparticles induce an antibacterial effect against the cells compared to a blank solution. The blank was prepared by dropping THF into water and allowing the solution to stir overnight at room temperature. The preparation of the blank followed the same procedure for the preparation of the polymer nanoparticles, however, with no polymer dissolved in the solvent phase. Polymer nanoparticles were tested at various concentrations to investigate the effect of concentration on the cells. S50-PA nanoparticles at concentrations of 14, 27, 55, 220 and 440 μg/ml were tested over a period of 5 h (Figure 3.25) against *S. aureus* in nutrient-rich LB medium at 37 °C. During the first 90 minutes of incubation, all samples including the blank have viable cell densities similar to the initial concentration of bacteria at t=0. After 90 minutes, it was found that the higher the concentration of nanoparticles, the lower the viable cell density of the culture. After 5 h, a 1.07 (>90 %) and 3.2 log (>99.9 %) reduction in the number of viable cells compared to the blank was achiebed for 14 μg/ml and 440 μg/ml of nanoparticles respectively. The higher concentrations of 220 and 440 μg/ml were further tested after 24 h, and were found to have reduced the number of viable cells by 1.09 log (>90%) compared to the blank.

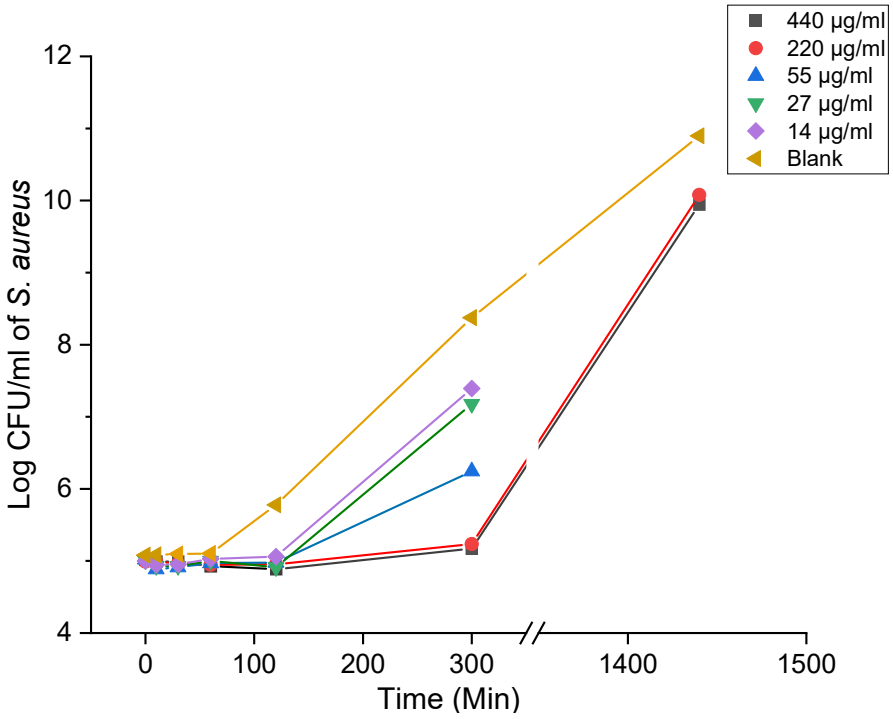

Figure 3.25: *S. aureus* growth curve in the presence of S50-PA nanoparticles over 24 h in nutrient-rich LB medium. Log CFU/ml values were determined from one sample and do not represent an average across replicates.

The minimum inhibitory concentration (MIC) of S50-PA nanoparticles was evaluated during a 24 h incubation period according to the European Committee on Antimicrobial Susceptibility Testing (EUCAST) standards. The MIC of an antimicrobial is defined as the lowest concentration of the antimicrobial that will inhibit the visible growth of a bacterial culture.[37] The antimicrobial susceptibility of bacterial species is commonly expressed in terms of MIC_{50} and MIC_{90} values, which are defined as the lowest concentration of the antimicrobial at which 50 and 90% of the isolates were inhibited, respectively.[38] The MIC of S50-PA nanoparticles was assessed with methicillin-resistant *S. aureus* at various nanoparticle concentrations (Figure 3.26). A 50% growth inhibition (MIC_{50}) in *S. aureus* compared to untreated samples was found at a nanoparticle concentration of 64 µg/ml, and an approximately 90% inhibition (MIC_{90}) was achieved at 512 µg/ml.

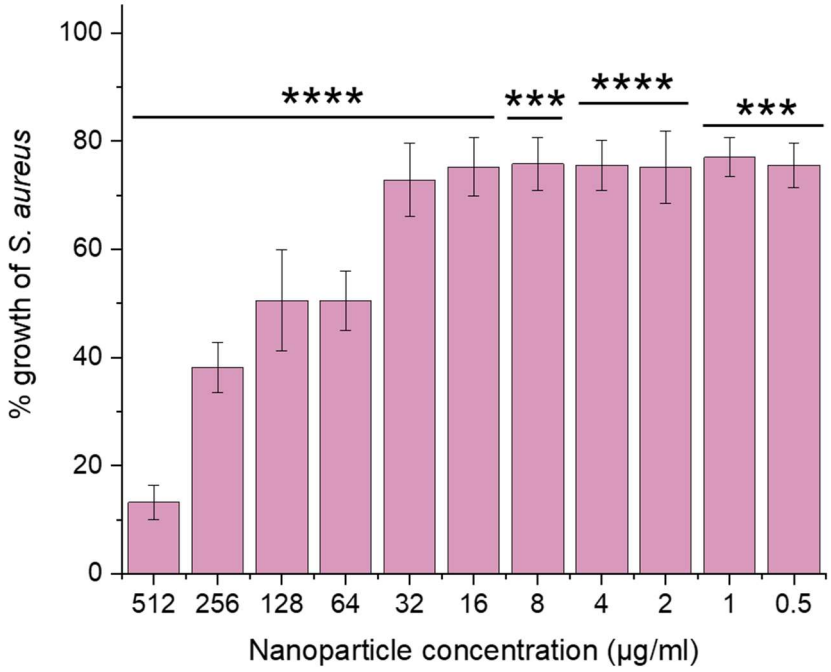

Figure 3.26: Graph summarising the % growth of *S. aureus* relative to a positive control, in the presence of S50-PA nanoparticles at various concentrations during a 24 h incubation period. ***$p < 0.001$, ****$p < 0.0001$ compared to control.

S70-PA nanoparticles were also tested during an incubation period of 5 h against *S. aureus* in LB growth medium to give final nanoparticle concentrations of 14, 27 and 55 µg/ml (Figure 3.27). After 5 h incubation, the same trend was observed whereby the higher the concentration of nanoparticles, the higher the log reduction in viable cells compared to the blank. At 14, 27 and 55 µg/ml of nanoparticles, a log reduction in viable cells of 3.31, 3.42 and 3.48 was achieved respectively (>99.9 % reduction in all cases). The log reduction for S50-PA nanoparticles at the same concentrations after 5 h were lower than those of S70-PA, whereby S50-PA nanoparticles at 14, 27 and 55 µg/ml achieved log reductions of 1.07, 1.28 and 2.22 respecitvely. This suggests that the S70-PA nanoparticles have an increased antibacterial effect compared to S50-PA nanoparticles against *S. aureus*.

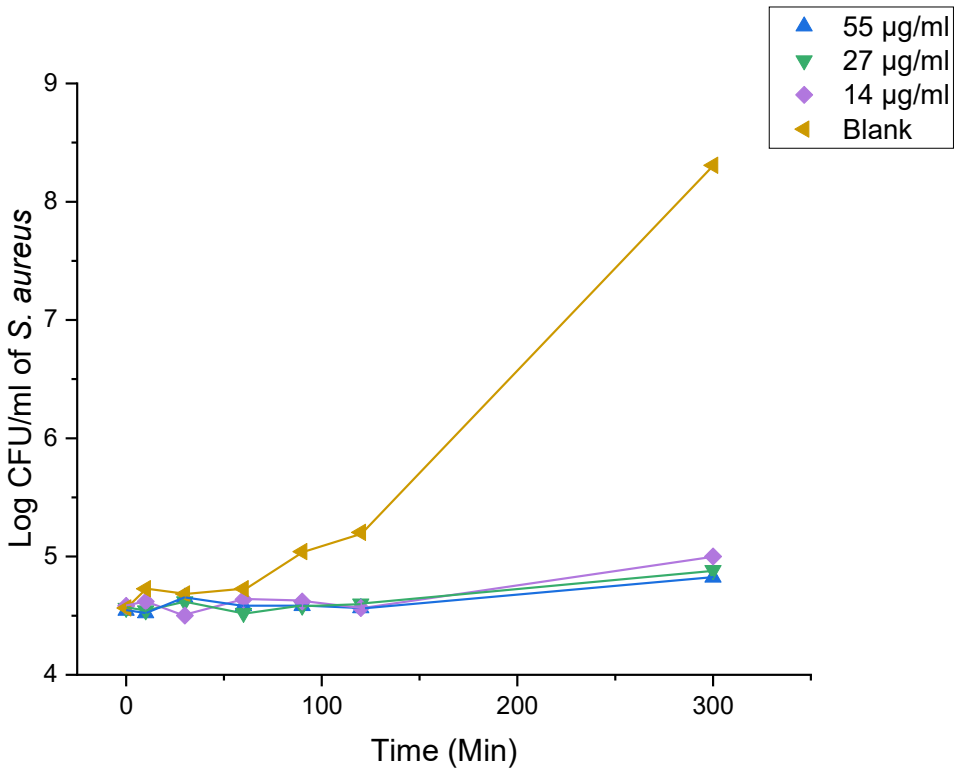

Figure 3.27: *S. aureus* growth curve in the presence of S70-PA nanoparticles after 5 h incubation in nutrient-rich LB medium. Log CFU/ml values were determined from one sample and do not represent an average across replicates.

S50-Ger nanoparticles formulated in the same way as S50-PA were also found to have an inhibitory effect against *S. aureus* after a 5 h incubation period (Figure 3.28), demonstrating that the antibacterial activity is not limited to only one type of comonomer.

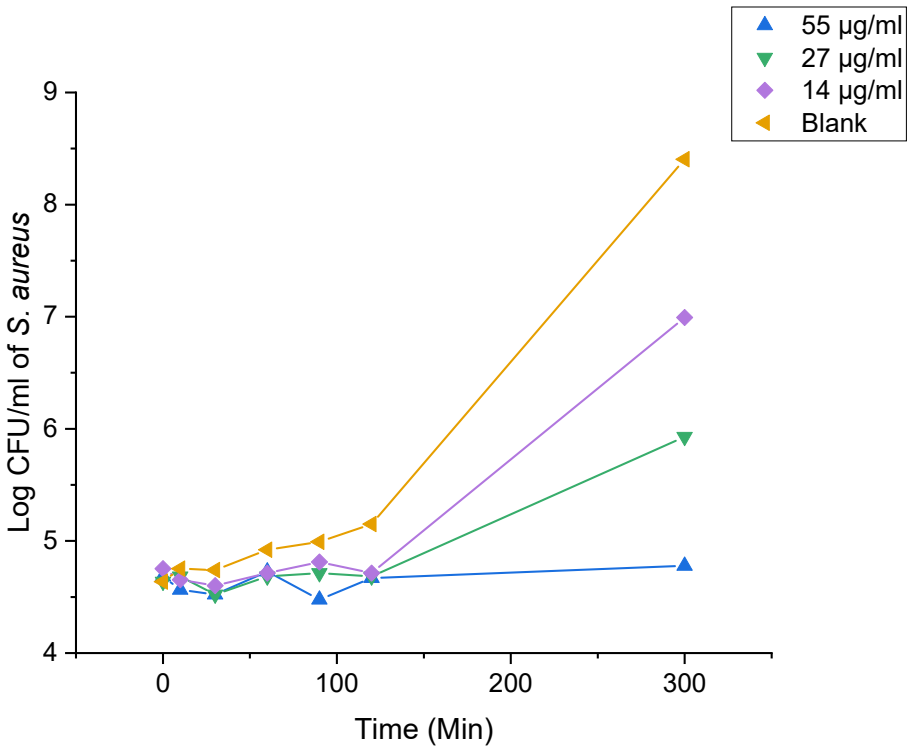

Figure 3.28: *S. aureus* growth curve in the presence of S50-Ger nanoparticles after 5 h incubation in nutrient-rich LB medium. Log CFU/ml values were determined from one sample and do not represent an average across replicates.

The data presented in Figure 3.25-Figure 3.28, show that compared to the blank solutions, the number of viable *S. aureus* cells have decreased. However, for S50-Ger there is some evidence that the presence of the nanoparticles result in the number of viable cells decreasing compared to the initial number of viable cells present at t=0 min (Figure 3.28). This suggests that S50-Ger may be exerting a bactericidal effect, that is, the particles kill bacterial cells, rather than merely suppressing cell growth. The initial *S. aureus* concentration was lowered from approximately 100,000 CFU/ml (5 log CFU/ml) (Figure 3.25-Figure 3.28) to 100 CFU/ml (2 log CFU/ml) (Figure 3.29) in an effort to see if a bactericidal effect is present for S50-PA nanoparticles. A decline in the number of viable cells compared to the intial culture would be more prominent, as the nature of the logarithmic growth of bacteria can often obscure these effects. After 5 h incubation time, the number of viable cells has indeed decreased for cultures containing nanoparticles, whereas the culture containing the blank solution showed an increase

in the number of viable cells (Figure 3.29). The effect of additional dosing of nanoparticles was also investigated (Figure 3.29), where the cultures were spiked with an additional 100 µl dose of particles or control after 2 h of incubation, the effect was enumearted after 5 h and it was found that the additional dose reduced the number of viable cells further.

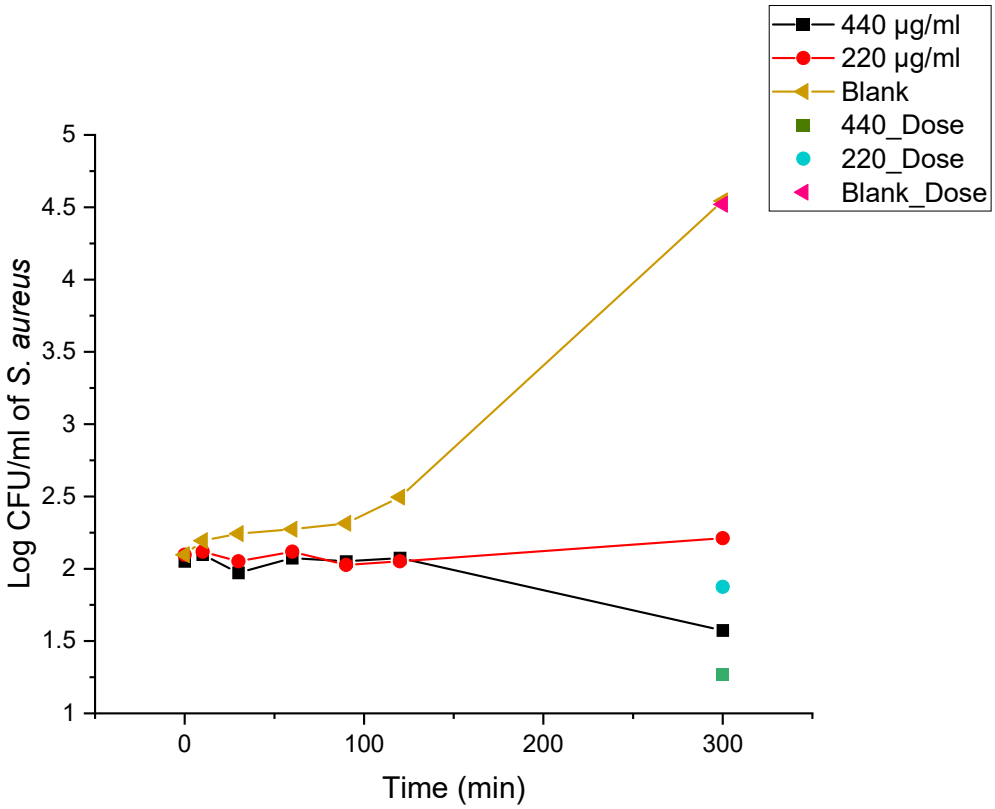

Figure 3.29: *S. aureus* growth curve at a lower intial cell concentration in the presence of S50-PA nanoparticles during 5 h incubation at 37 °C. Points labelled X_Dose represent time-points that were given an additional 100 µl dose of nanoparticles or blank at 120 min. Log CFU/ml values were determined from one sample and do not represent an average across replicates.

P. aeruginosa is a Gram-negative, rod shaped opportunistic pathogen that is a common cause of nosocomial infections and often shows innate resistance to a wide range of antibiotics.[39] S50-PA polymeric nanoparticles were tested against *P. aeruginosa* strain PAO1 in nutrient-rich LB broth for a period of 5 h (Figure 3.30) at final concentrations of 220 and 440 µg/ml. After 5 h incubation it was found that both concentrations of nanoparticles achieved a 2.9 log (>99 %) reduction in viable *P. aeruginosa* cells compared to the control sample. This shows that S50-PA polymeric nanoparticles behave similarly to the bulk material, which have

been shown to exhibit an antibacterial effect against both *S. aureus* and *P. aeruginosa*.[40] The MIC values of S50-PA nanoparticles was assessed in the presence of *P. aeruginosa* (Appendix 3.10), and was found to have an MIC_{50} of 128 µg/ml. S50-Ger nanoparticles were also found to have an inhibitory effect on *P. aeruginosa* during a 5 h incubation period, showing that the antibacterial activity of high sulfur content nanoparticles against *P. aeruginosa* is not limited to only one comonomer type (Appendix 3.11).

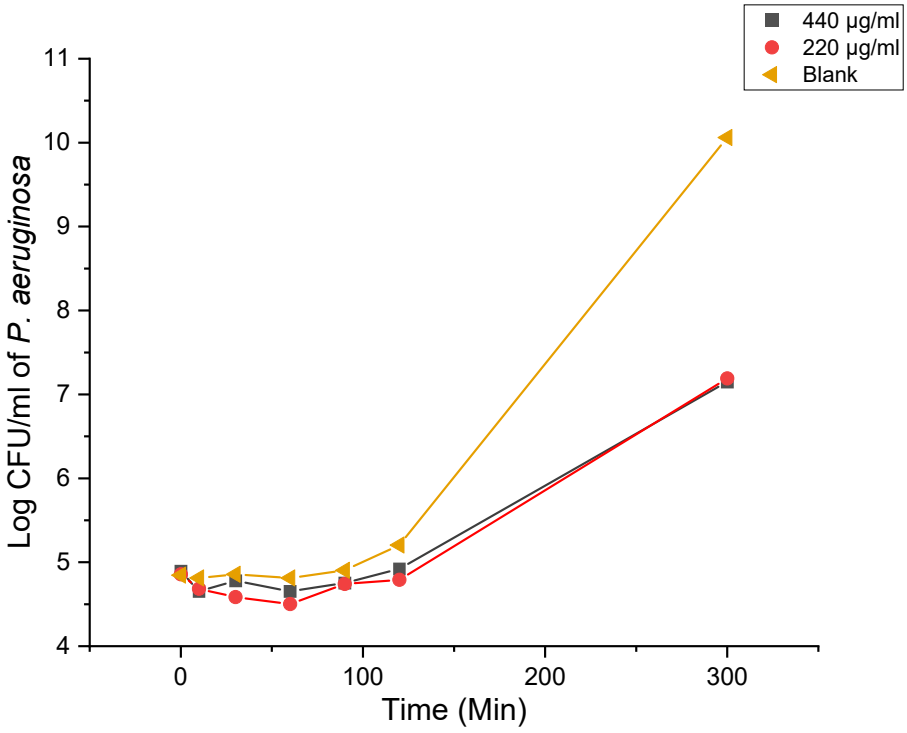

Figure 3.30: *P. aeruginosa* growth curve in the presence of S50-PA nanoparticles after 5 h incubation in nutrient-rich LB medium. Log CFU/ml values were determined from one sample and do not represent an average across replicates.

It is possible that upon addition of the dissolved polymer into the antisolvent phase during the nanoprecipitation process, that low molecular weight species could remain soluble in the antisolvent i.e water-soluble. To establish whether it is the nanoparticles that are having an antibacterial effect, or if it is due to potential water-soluble species, a disc diffusion (Kirby-Bauer test) assay was conducted (Figure 3.31).[41] In brief, empty antimicrobial susceptibility

test discs were soaked with nanoparticles, or water as the control. The loaded discs were placed on agar plates streaked with bacteria (*S. aureus* USA300 and *P. aeruginosa* PAO1) and incubated for 24 h. The disc diffusion method (Figure 3.31) is used to assess the antimicrobial actvity of species that are able to diffuse through the disc and agar. Species that are antimicrobial will leave a clear zone/halo around the disc, where bacteria was unable to grow.

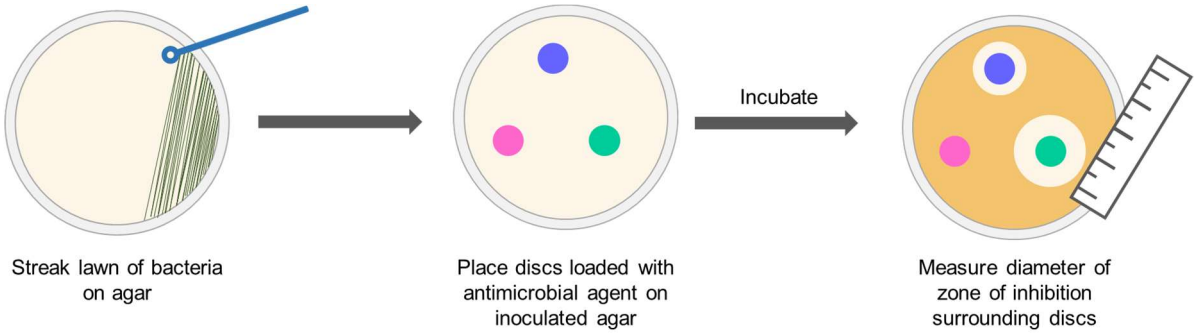

Figure 3.31: Summary of the disc diffusion (Kirby-Bauer) assay to assess the antimicrobial activity of antiobiotics.

S50-PA nanoparticles were found to not have an antibacterial effect against *S. aureus* USA300 and *P. aeruginosa* PAO1 when tested using the disc diffusion assay (Figure 3.32). The results of this assay contradict the results of the broth-based methods discussed above, and suggest that the disc containing particles has no antibacterial effect against *S. aureus* and *P. aeruginosa*. The reason that S50-PA nanoparticles show different antibacterial activities depending on the method used to test them, could be due to the size of the particles which will limit or prohibit the diffusion of the nanoparticles through agar. Kourmoli *et al.* investigated the effect of particle size on the outcome of the disc diffusion assay.[41] It was found that gold nanoparticles with diamaters of 10-40 nm had negligible diffusibility through the agar, and therefore did not exert an antimicrobial effect during the disc diffusion assay. S50-PA nanoparticles have been found to have z-average diameters of approximately 150 nm, determined by DLS (Figure 3.20) and SEM (Figure 3.21), and are therefore larger than the Au nanoparticles investigated by Kourmoli *et al.*[41] It is therefore plausible to suggest that S50-PA nanoparticles are too large to

diffuse through the agar, and therefore are not able to exert an antibacterial effect during the disc diffusion method. The results of the disc diffusion assay also suggest that if there are any low molecular weight, water-soluble species present, that they are not responsible for the antibacterial activity observed.

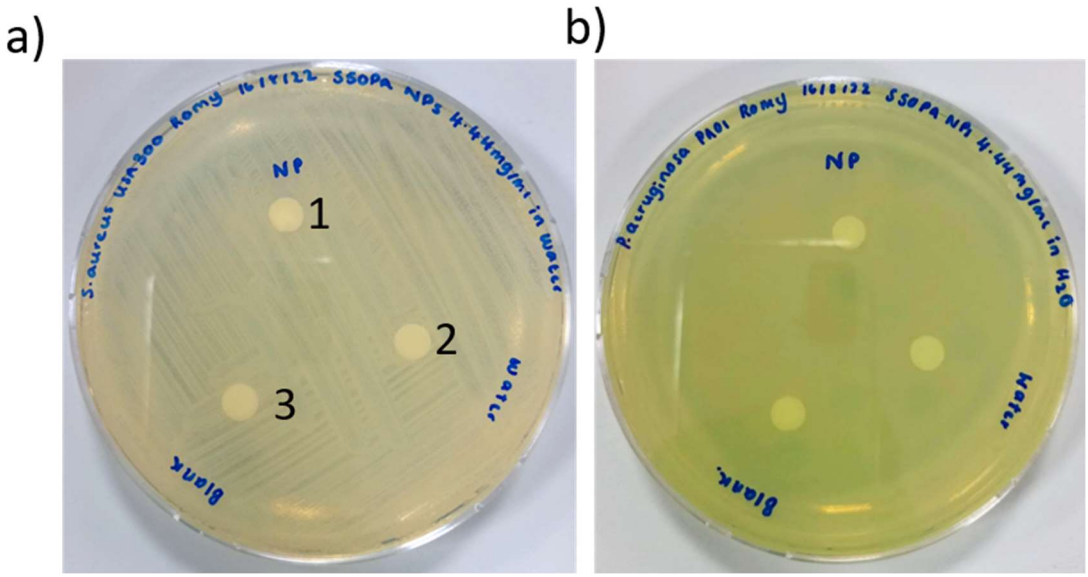

Figure 3.32:Photograph of agar plate streaked with a) *S. aureus* USA300, and b) *P. aeruginosa* PAO1 loaded with antimicrobial susceptibility test discs containing 1) S50-PA nanoparticles 2) water and 3) empty disc.

To probe the antibacterial activity of the nanoparticles in different bacterial culture conditions, a nutrient-restricted medium was chosen to represent systems that do not have optimal growth conditions for bacteria. Using a nutrient-restricted medium to culture bacteria also provides a method to slow down the growth of cells, allowing longer incubation periods to be studied before the cell density becomes too high. M9 Minimal Medium was selected as the nutrient-restricted medium to compare the antibacterial activity of the nanoparticles in nutrient-restricted and nutrient-rich media (LB medium). M9 supplemented with 20 % glucose was not a suitable medium for *S. aureus* USA300 growth, as the cell viability of the control sample containing only *S. aureus* cells and M9 decreased during an incubation period of 24 h.

S. aureus has been found to show amino acid auxotrophies, inlcuding arginine auxotrophy. Auxotrophic bacterial strains are unable to synthesise certain components that are required for their growth.[42] Therefore minimal media such as M9 may need to be supplemented with arginine or other essential amino acids for the medium to sustain cell viabilty for prolonged periods of time.[43,44] *P. aeruginosa* PAO1 was found to be able to grow in M9 medium, with no additional supplements apart from glucose. The growth of *P. aeruginosa* in M9 was much slower than in nutrient-rich LB medium, whereby cells reached a cell density of 6.7 log CFU/ml after 24 h at 37 °C (Figure 3.33) compared to 10 log CFU/ml after 5 h in LB medium (Figure 3.30). It was hypothesised, that the antibacterial activity of S50-PA nanoparticles would be enhanced in nutrient-restricted media compared to nutrient-rich media, as the growth conditions of PAO1 would not be optimal and thus should be easier for the nanoparticles to inhibit their proliferation. At final nanoparticle concentrations of 220 and 440 μg/ml, a log reduction in viable cells of 0.3 and 0.2 was achieved respectively after 5 h in nutrient-restricted M9 medium (Figure 3.33), compared to a 2.9 log reduction in nutrient-rich LB (Figure 3.30). This result is not consistent with the hypothesis that the antibacterial effect of the nanoparticles should be enhanced in nutrient-restricted medium. One possible reason for the reduced antibacterial activity in M9 medium is that the nanoparticles were found to aggregate in M9, forming visible aggregates that sedimented to the bottom of the culture vials. It is expected that aggregation of the nanoparticles into large visible aggregates will reduce the surface area of the particles, which could therefore reduce their antibacterial activity.

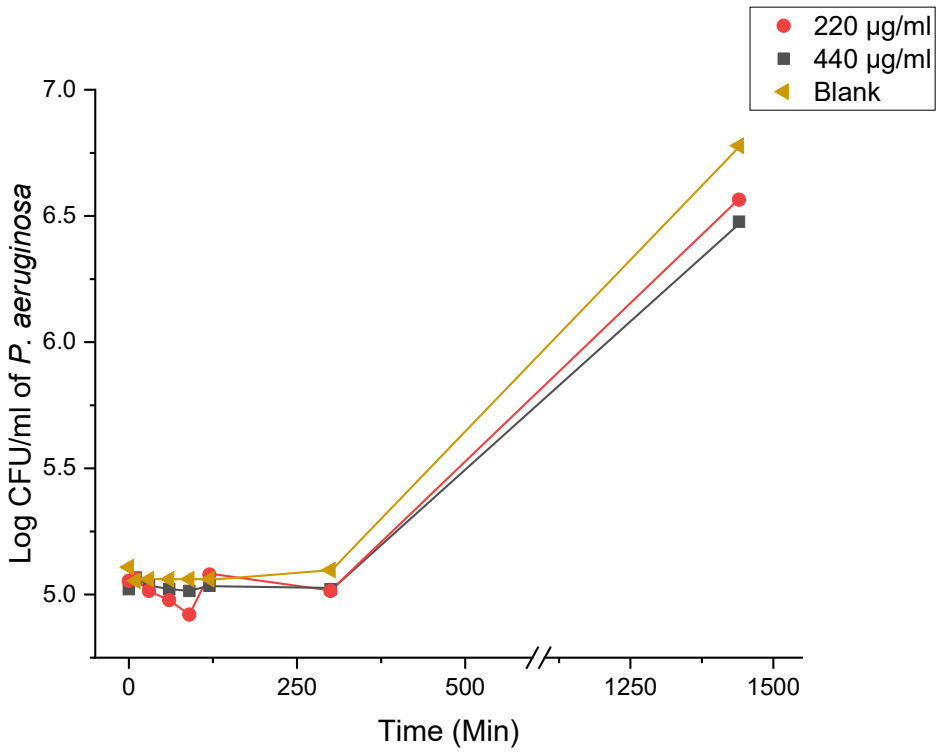

Figure 3.33: *P. aeruginosa* growth curve in the presence of S50-PA nanoparticles after 24 h incubation in nutrient-restriced M9 medium. Log CFU/ml values were determined from one sample and do not represent an average across replicates.

S50-PA nanoparticles were analysed by DLS when dispersed in LB and M9 media to investigate the differences in the nanoparticle size and surface charge. When dispersed in water, S50-PA nanoparticles have z-average diameters of around 150 nm, and a zeta potential of (-47.5 ± 1.5) mV. Upon dispersion of the nanoparticles in LB broth, the z-average diameter was found to remain at 150 nm (Appendix 3.12), however, the magnitude of the negative zeta potential is decreased compared to the particles in water, having a zeta potential of (-13.6 ± 1.2) mV. Dispersion of S50-PA nanoparticles in M9 caused immediate aggregation. The aggregates formed in M9 medium were too large to be analysed by DLS, whereby large fluctuations in the correlogram were seen (Appendix 3.13). Therefore z-average diameters and

zeta potential of S50-PA nanoparticles in M9 were unable to be obtained. A possible explanation for the rapid aggregation of particles in M9 compared to in LB and water, could be due to the presence of salts in the medium. Polymeric nanoparticles can be stabilised sterically or electrostatically (Figure 3.34). Steric stabilisation involves the use of bulky ligands that are anchored to the surface of the nanoparticle. The ligand chains form a protective barrier around the nanoparticle which inhibits particle-particle interactions due to the repulsive interactions that would occur by overlapping ligand shells.[45] Electrostatic stabilisation of nanoparticles arises when nanoparticles have a surface charge. Electrostatic repulsive forces between two like-charged particles can provide a sufficient energy barrier to inhibit the interaction and aggregation of particles.[46] Charge stability of nanoparticles are often assessed by measuring the zeta potential of colloids.[45] The fluid surrounding particles exists as two layers: 1) an inner layer of ions that are strongly bound to the particle surface, termed the Stern layer, and 2) an outer layer where ions are less strongly bound to the particle surface, termed the diffuse layer (Figure 3.35).[47] Under an electric field, the ions that interact with the particle surface will migrate with the particle, whereas other ions will move with the rest of the dispersive medium. The zeta potential is the electrostatic potential at the interface of the stationary ion layer surrounding the particle and the dispersive medium.[47] Therefore, the zeta potential is used as a measure of the charge of colloidal nanoparticles, where dispersions with a zeta potential > ±30 mV are considered electrostatically stable.[45] However, charge stabilised nanoparticles are often unstable in the presence of salts, which can screen the charges of the nanoparticles leading to particle-particle interactions and thus aggregation.[48]

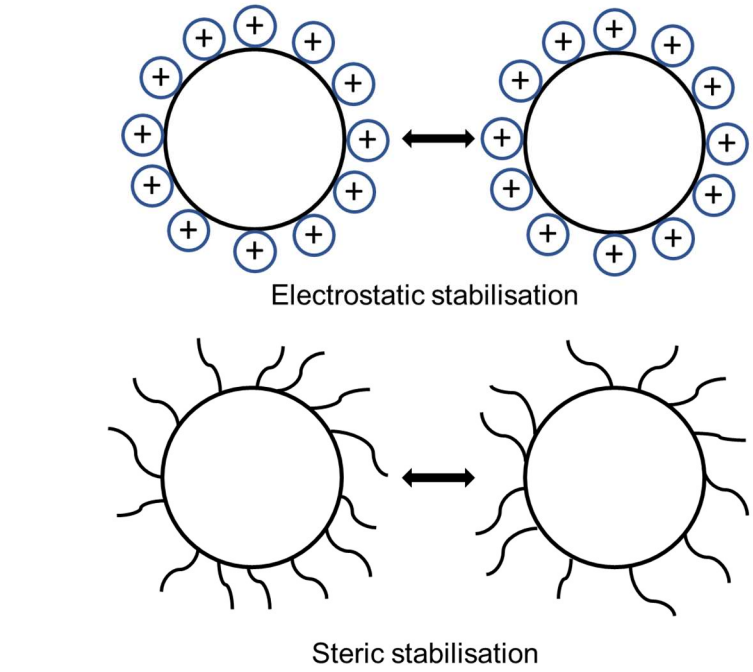

Figure 3.34: Simplified diagram depicting electrostatic and steric stabilisation of polymeric nanoparticles, adapted from Ramesh *et al*. [49]

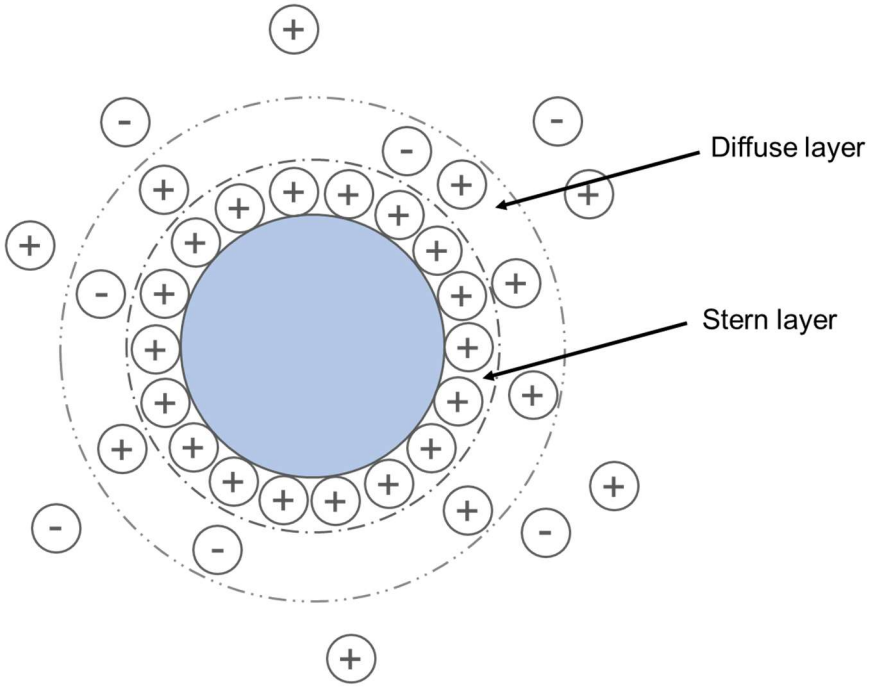

Figure 3.35: Diagram depicting a negatively charged particle with associated positively charged ions present in the stern layer and more loosely bound ions in the diffuse layer. Adapted from Lowry *et al*.[47]

M9 medium contains various salts; KH_2PO_4 (15 g/L), NaCl (2.5 g/L), Na_2HPO_4 (33.9 g/L) and NH_4Cl (5 g/L), whereas the salt content of LB medium consists of NaCl (10 g/L). Therefore the salt content and therefore the ionic strength of M9 medium is higher than that of LB. To probe the effect of salt concentration on the stability of S50-PA nanoparticles, the average hydrodynamic diameter and zeta potential of the particles was measured in various NaCl solutions. NaCl solutions at concentrations of 1, 5, 25, 50 and 100 g/L were prepared, to which the nanoparticles were dispersed. The average hydrodynamic diameter and zeta potential of the nanoparticles were measured at 0, 1 and 7 days (Figure 3.36). Particles in the presence of >5 g/L NaCl were found to have immediately aggregated and were deemed unsuitable for DLS measurements, whereas particles in the presence of 5 g/L NaCl showed signs of aggregation due to the presence of a peak at higher particle diameters. At day 0, S50-PA particles in the presence of 1 g/L NaCl were found to be stable, and had DLS traces that overlapped with particles in water. After 24 h, the aggregation of the particles in 5 g/L NaCl had progressed and thus the particles were unsuitable for DLS measurements. Particles in 1 g/L NaCl were stable during the 7 day testing period, in which the DLS traces were similar to those of the particles with no salt present. These results suggest that the instability of S50-PA nanoparticles in M9 medium could be due to the high concentration of salts present.

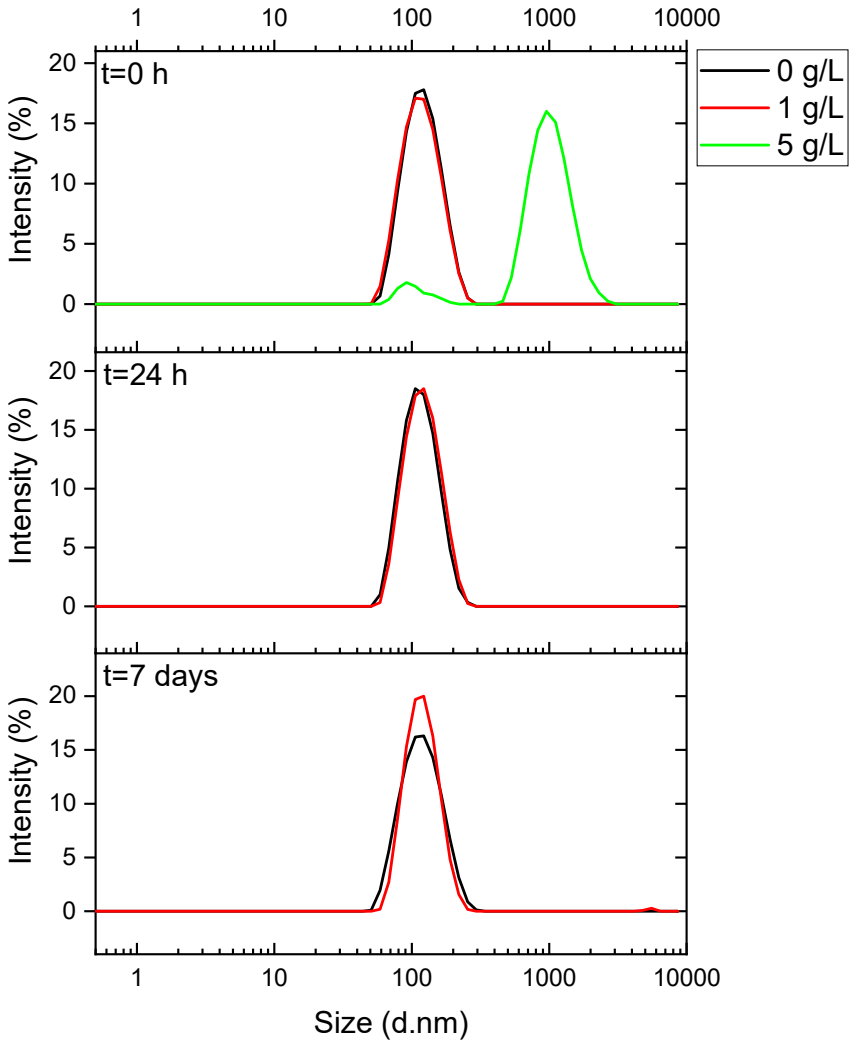

Figure 3.36: DLS traces of S50-PA nanoparticles in water in the presence of NaCl at various concentrations (0,1, 5, 25, 50 and 100 g/L) after 0, 1 and 7 days.

S50-PA polymeric nanoparticles formulated with Tween80 were prepared to investigate if the inclusion of a non-ionic surfactant could provide stability to the nanoparticles against salts, by providing steric stabilisation instead of relying on electrostatic stabilisation (Figure 3.34). S50-PA was dissolved to 5 mg/mL in THF and injected into aqueous Tween 80 at a concentration of 10 mg/ml (THF:water ratio of 1:9) under stirring. The solution was allowed to stir overnight at room temperature to allow THF to evaporate. The resulting dispersion was analysed by DLS, which gave z-average diameters of (110 ± 2) nm, similar to S50-PA

nanoparticles formulated without Tween80. As previously done for S50-PA nanoparticles in water, NaCl solutions at concentrations of 1, 5, 25, 50 and 100 g/L were prepared, to which the nanoparticles in Tween80 were dispersed. The resulting dispersions were analysed by DLS after 0, 1 and 7 days (Figure 3.37). S50-PA particles in Tween80 were found to be stable to all NaCl solutions for the 7 day period.

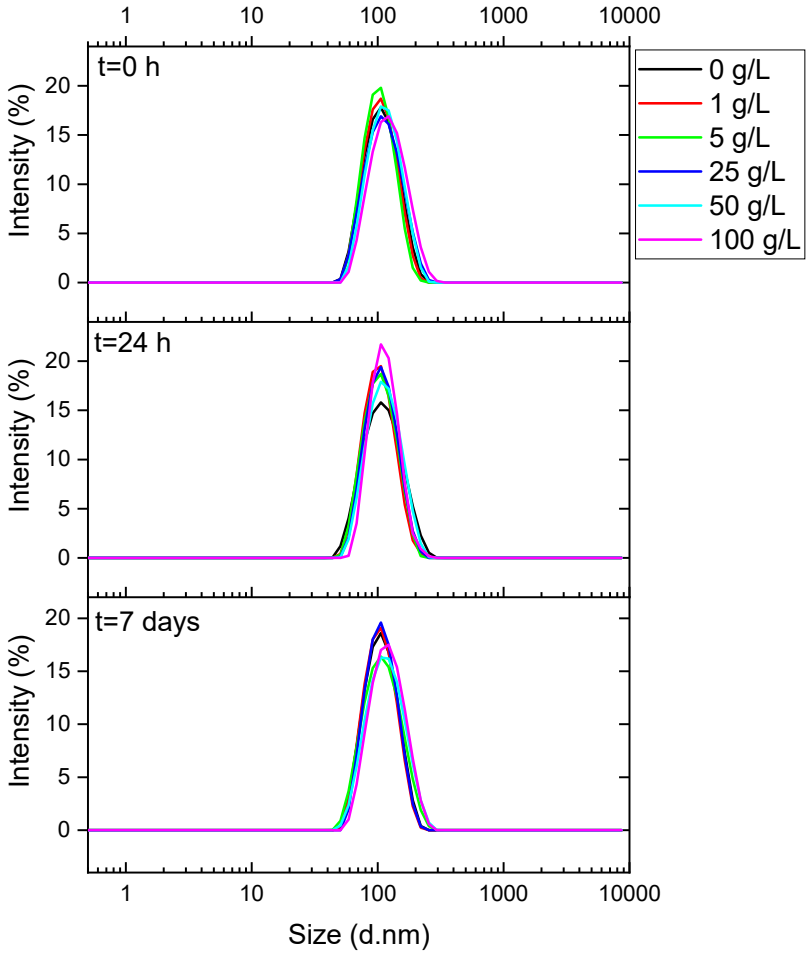

Figure 3.37: DLS traces of S50-PA nanoparticles in Tween80 in the presence of NaCl at various concentrations (0,1, 5, 25, 50 and 100 g/L) after 0, 1 and 7 days.

The zeta potential of S50-PA nanoparticles with and without Tween80 in NaCl solutions were analysed. In the absence of NaCl, S50-PA nanoparticles forumlated without Tween80 have zeta potentials of (-56 ± 1) mV (Figure 3.38). It is possible that S50-PA nanoparticles are charge-

stabilised due to having a large negative zeta potential.[50] The addition of Tween80 in the formulation of the nanoparticles results in a less negative zeta potential of (-31 ± 2) mV. Tween80 is a non-ionic surfactant, and thus if adsorbed onto the surface of S50-PA nanoparticles is expected to reduce the magnitude of the zeta potential of the nanoparticles.[51] When diluted in salt solutions containing NaCl at 1 and 5 g/L, the zeta potential of the nanoparticles with and without Tween80 are reduced further in magnitude. The higher concentration of NaCl results in higher ionic strength of the dispersive medium, which can screen the charges of the nanoparticles and thus reduce the electrostatic repulsion forces between particles.[52]

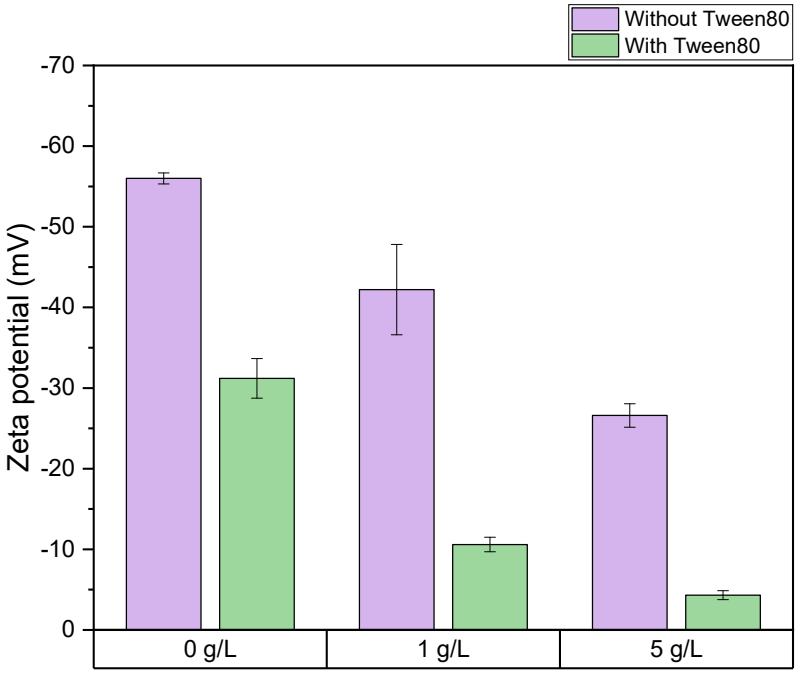

Figure 3.38:The zeta potential of S50-PA nanoparticles forumlated with and without Tween80 in the presence of NaCL at 0, 1 and 5 g/L.

These results suggest that high-sulfur content polymeric nanoparticles that are stable to high ionic strengths can be prepared by employing a non-ionic surfactant in the nanoprecipitation method. However, the presence of a non-ionic surfactant could effect the antibacterial activity of S50-PA nanoparticles, therefore Tween80-stabilised S50-PA particles were tested for their

antibacterial activity. The Tween80-stabilised particles were tested against *S. aureus* USA300 for a period of 5 h at 37 °C (Figure 3.39), a stock solution of Tween80 at a concentration of 10 mg/ml was used as a control to investigate if the surfactant alone had any effect on USA300 growth.

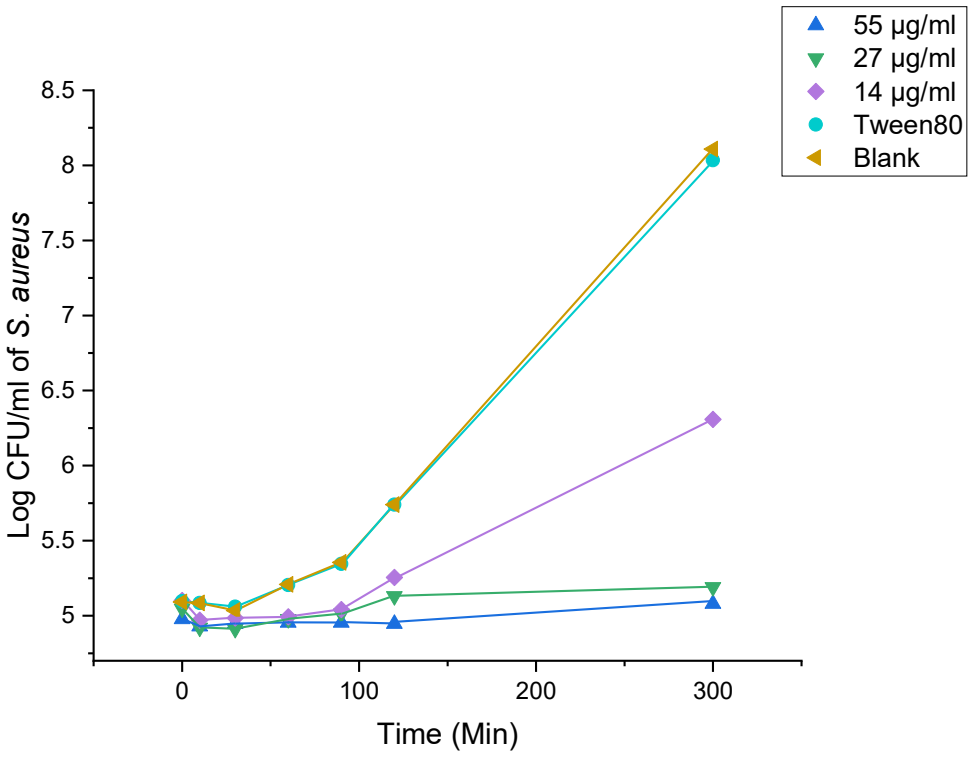

Figure 3.39: *S. aureus* growth curve in the presence of S50-PA nanoparticles stabilised with Tween80 over 5 h in nutrient-rich LB medium. Log CFU/ml values were determined from one sample and do not represent an average across replicates.

After 5 h incubation at 37 °C the cell density of the blank and Tween80 solutions reached 8.1 and 8 log CFU/ml respectively. This suggests that Tween80 at 10 mg/ml does not have an antibacterial effect against USA300. For bacterial cultures containing Tween80-stabilised S50-PA nanoparticles at final concentrations of 14, 27 and 55 µg/ml of nanoparticles, log reductions of 1.8, 2.92 and 3.03 were achieved compared to the blank after 5 h. The results show that stabilising S50-PA nanoparticles with Tween80 does not inhibit their antibacterial activity. Furthermore the antibacterial activity is enhanced compared to S50-PA naoparticles formulated

without Tween80 (Figure 3.25), where those particles achieved log reductions of 1.07, 1.28 and 2.22 compared to the blank after 5 h. Similarly, the antibacterial activity of Tween80-stabilised particles were evaluated against *P. aeruginosa* (Figure 3.40) and were found to have similar activity to particles formulated without Tween80 (Figure 3.30). The Tween80-stabilised particles were redispersed in M9 medium and were analysed by DLS to determine their stability. Particles formed in the presence of Tween80 were found to be stable in M9 medium (Appendix 3.14), suggesting that the surfactant-free nanoparticle instability (Appendix 3.13) is likely due to charge-shielding by high ionic strengths.

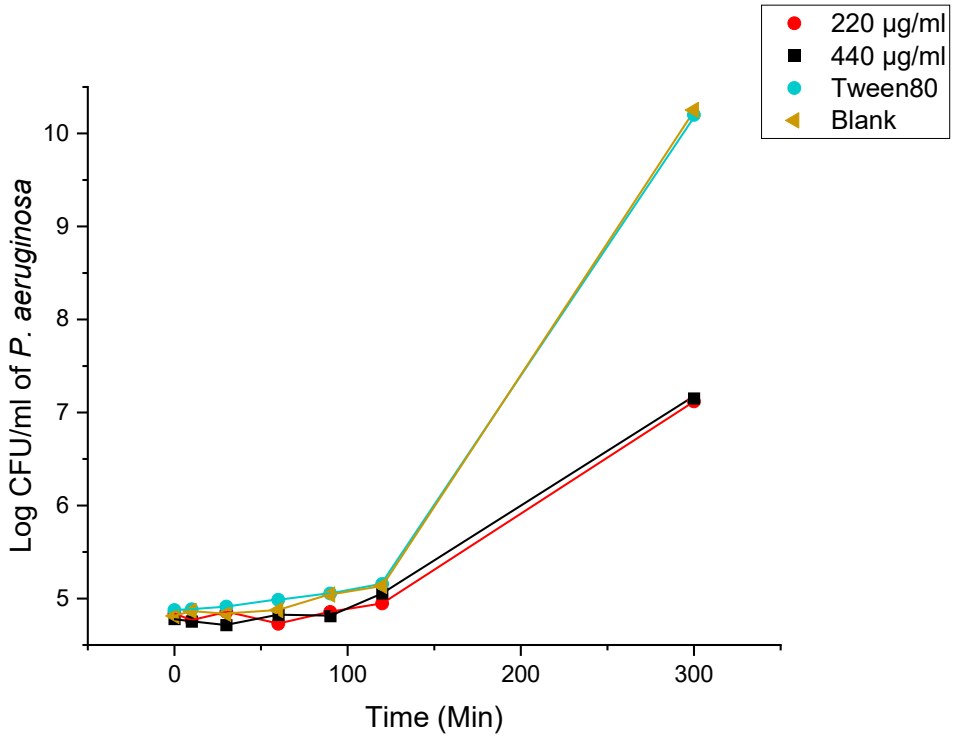

Figure 3.40: *P. aeruginosa* growth curve in the presence of S50-PA nanoparticles stabilised with Tween80 after 5 h incubation in nutrient-rich LB medium. Log CFU/ml values were determined from one sample and do not represent an average across replicates.

The stability of the Tween80-stabilised S50-PA nanoparticles in M9, and the persistance of their antibacterial activity allowed for re-testing the particles against *P. aeruginosa* in M9

without any competing effects due to aggregation and loss of surface area (Figure 3.41). During the 5 hr incubation period, bacteria of the blank solution remained in stasis whereby no bacterial growth was observed. Bacteria in the presence of S50-PA nanoparticles were also found to remain in stasis, with the log CFU/ml of bacteria after 5 h being similar to that of the initial culture before incubation. The viable cell density for PAO1 in the presence of particles is similar to that of the blank solution, suggesting that the particles have no inhibitory effect after 5 h in M9 medium with PAO1. However, an inhibitory effect was seen against PAO1 in the presence of particles after 5 h in LB. In LB medium, the blank samples show growth within the 5 h incubation period, whereas in M9 there is no growth of the control. It has been reported that nutrient conditions can effect the susceptibility of bacteria to antibiotics. *E. coli* grown in nutrient rich conditions, that is, fast-growing *E. coli*, has been found to be more susceptible to antibiotics than slow-growing *E. coli*.[53] In addition, Ciprofloxacin, a fluoroquinone antibiotic, is known to have an increased inhibitory effect against growing, compared to non-growing planktonic *P. aeruginosa* cells, as its main mode of action is the inhibition of DNA replication.[54,55] It is therefore possible that *P. aeruginosa* PAO1 becomes more susceptible to the antibacterial effect of the sulfur polymer nanoparticles when they are actively growing, compared to when they are in stasis.

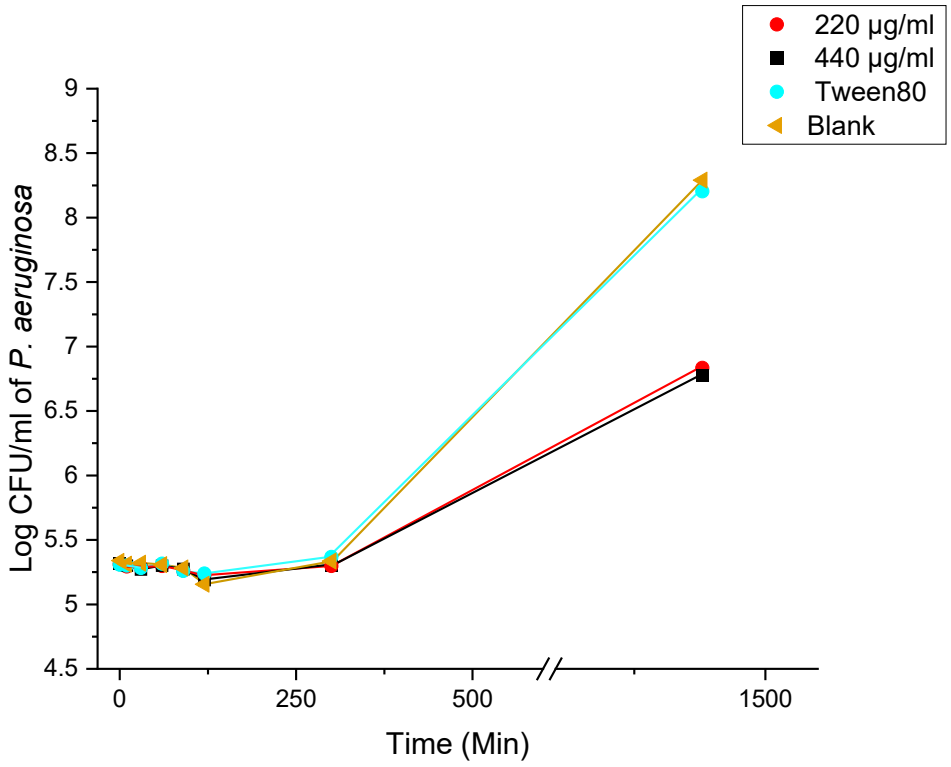

Figure 3.41: *P. aeruginosa* growth curve in the presence of S50-PA nanoparticles stabilised with Tween80 after 24 h incubation in nutrient-restricted M9 medium. Log CFU/ml values were determined from one sample and do not represent an average across replicates.

3.4.4 Nanoparticle-Bacteria Charge Interactions

The charge of the polymer nanoparticles is expected to have an impact on the interaction with bacterial cells, for example, the lipopolysaccharide (LPS) component of Gram-negative outer membranes is negatively charged due to the presence of negatively charged phosphate groups.[56] Teichoic acids, which are polyol phosphate polymers, that are bound to the peptidoglycan layer of Gram-positive bacterial cells also carry a negative charge.[57] The zeta potential of S50-PA nanoparticles was found to be (-13.6 ± 1.2) mV when dispersed in LB medium, compared to (-47.5 ± 1.5) mV in water. Capping the nanoparticles with Tween80 was found to lower the magnitude of the negative zeta potential further (Figure 3.38). This may be the reason for the higher inhibitory effect of Tween80-capped particles against *S. aureus* compared to S50-PA particles without Tween80, due to a reduction in repulsive interactions

between the negatively charged particles and the negatively charged cell wall of Gram-positive bacteria. We hypothesise that the antibacterial activity of the polymer nanoparticles can be tuned depending on the type of surfactant used. However, determining whether an increase or decrease in antibacterial activity with different surfactants is due to the charge differences alone, or, if the surfactant itself is having an effect would be difficult to determine. Therefore, instead of changing the charge of the nanoparticles, we conducted a study to modulate the charge of the bacterial surface, to probe the effect of charge interaction between nanoparticles and bacteria. For this study we looked at the inhibition of two *P. aeruginosa* strains: LESB65 and LESB65Δ*pmrB* (Figure 3.43). The deletion of the *pmrB* gene in LESB65Δ*pmrB* results in a greater negative charge on the LPS of the outer membrane of the bacterial cell, as the absence of PmrB signalling restricts the activation of LPS modification pathways that add positively charged aminoarabinose to the lipid A component of LPS.[58] Here, the nanoparticles showed an increased antibacterial effect against LESB65 compared to LESB65Δ*pmrB*, which may be due to increased repulsive charge interactions between LESB65Δ*pmrB* and the negatively charged nanoparticles. To further test this hypothesis, both bacterial strains were pre-incubated with the cationic polyamine spermidine (Figure 3.42). Pre-incubation with spermidine results in a less negatively charged outer membrane, as the polyamine coats the surface and negates the charge.[58]

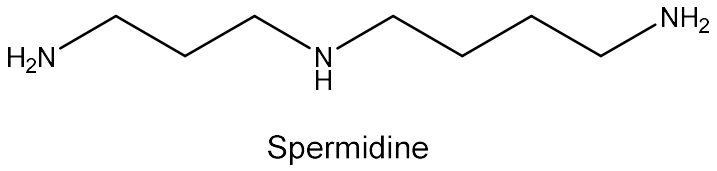

Spermidine

Figure 3.42: Chemical struture of spermidine.

The antibacterial activity of the nanoparticles against LESB65Δ*pmrB* was increased following preincubation with spermidine, as compared to in the absence of spermidine. This suggests that the charge interactions between the bacterial cells and nanoparticles is important to consider for future applications.

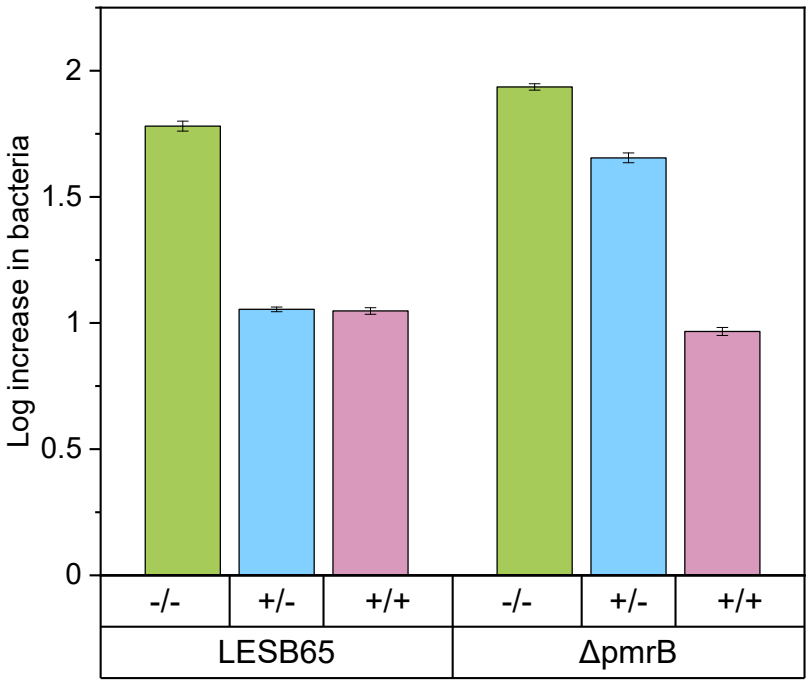

Figure 3.43: Log increase in LESB65 and LESB65ΔpmrB compared to initial culture for, -/- : culture only, no particles and no preincubation with spermidine, +/-: culture + nanoparticles, +/+: culture + nanoparticles + preincubation with spermidine.

3.4.5 Anti-biofilm Activity of High Sulfur Content Polymeric Nanoparticles

Biofilms provide favourable conditions for bacteria as they offer protection from the immune system of the host, exhibit phenotypic resistance to antimicrobial agents, and ensure efficient distribution of resources throughout the microbial population. These factors make biofilm bacteria more challenging than planktonic cells.[59]

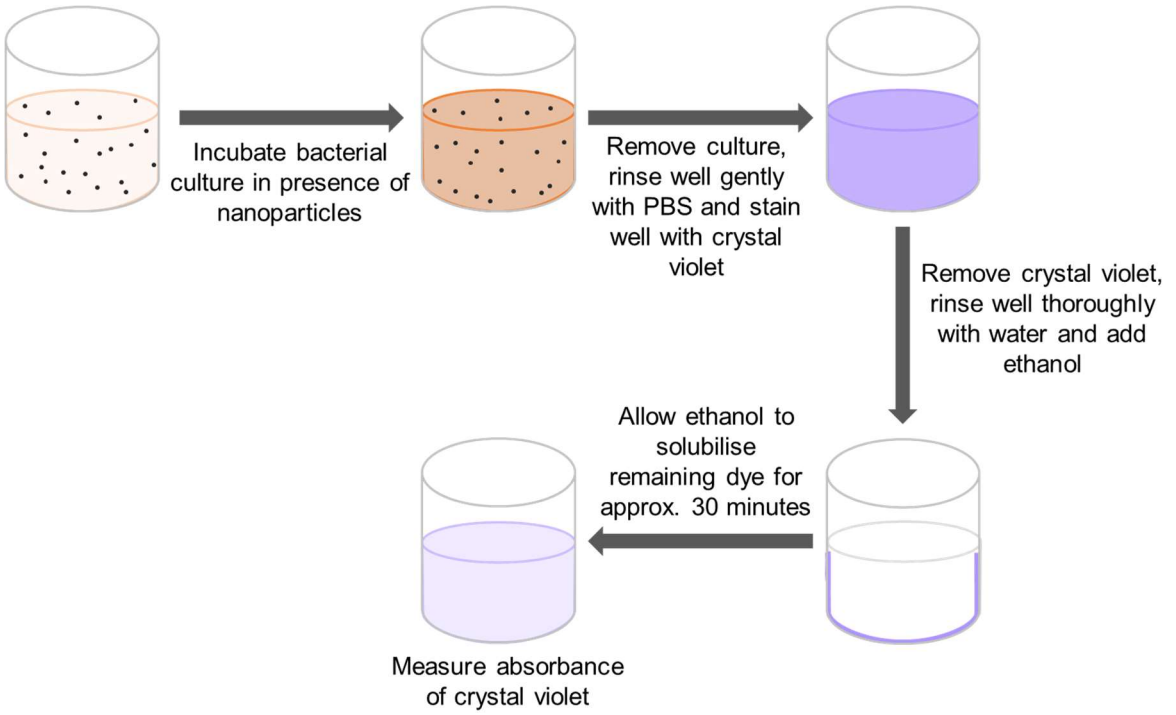

Figure 3.44: Schematic depicting the method use for assessing biofilm formation on the surfaces of wells containing nanoparticles.

The antibiofilm activity of bulk S50-PA was assessed and discussed in Chapter 2, however this activity corresponded to the inhibition of biofilm on the surface of the material. S50-PA polymer nanoparticles have approximate diameters of 100-200 nm, and therefore it is not expected that biofilms will form on the particle 'surface'. Furthermore, the nanoparticle sizes are smaller than those of *S. aureus* cells. However, the addition of particles to a container of bacterial culture, may be able to inhibit biofilm formation on the containers surface. The ability of S50-PA nanoparticles to inhibit biofilm formation on the surface of a container was evaluated against *S. aureus* USA300 and *P. aeruginosa* PAO1. Wells of polypropylene well-plates were used as 'containers' used for biofilm formation. Polypropylene well-plates are commonly used

to grow biofilms of bacterial isolates.[60] Nanoparticles were added to vials containing bacterial culture and were statically incubated for 24 and 48 h, a control sample was prepared by adding water to the culture instead of nanoparticles (Figure 3.44). Biofilm growth was visible on the surfaces of the well-plates of the control samples after staining with crystal violet. S50-PA nanoparticles were found to inhibit *S. aureus* biofilm formation over 48 h, however, the nanoparticles did not inhibit *P. aeruginosa* biofilm formation (Figure 3.45). Sulfide containing molecules such as allicin, have been reported to have much higher minimal inhibitory concentrations for *P. aeruginosa* in comparison to other organisms[61], therefore the tested concentrations of nanoparticles in this instance may not have been high enough to achieve an inhibitory effect against *P. aeruginosa* over prolonged periods of time.

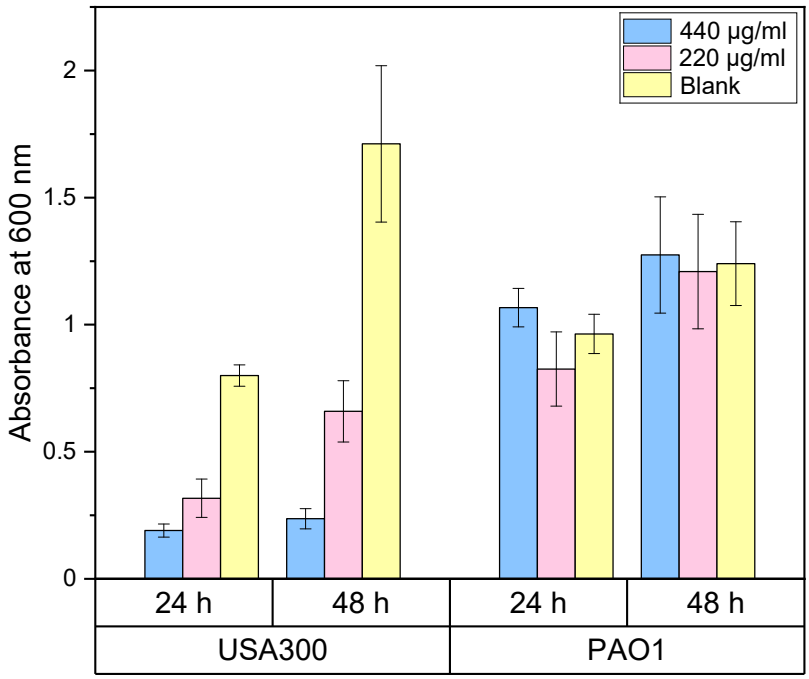

Figure 3.45: Absorbance at 600 nm for wells containing USA300 and PAO1 in the presence of S50-PA nanoparticles at final concentrations of 440 and 220 µg/ml, after 24 and 48 h.

3.4.6 Cysteine-Mediated H_2S Release Study

The mechanism of action of high-sulfur content polymers against bacteria is poorly understood. Many studies have been conducted into the antimicrobial activity of allyl sulfides such as DAS, DADS and DATS (Chapter 1) and several possible mechanisms of action have been postulated, one of which is the interaction of polysulfides with thiol-containing enzymes and membranes of bacterial cells.[62–65] Two examples of cellular thiols are those in glutathione, an important antioxidant, and, cysteine, an amino acid which is used in enzymatic reactions and protein synthesis.[66] Kim *et al.* investigated the antimicrobial activity of alkenyl sulfides derived from garlic and onions and found that monosulfides were not antimicrobial, but higher order tri- and tetra-sulfides were highly inhibitory against the yeast *Candida utilis* and *S. aureus*.[63] The study found that the antimicrobial activity of the synthesised alkenyl sulfides decreased with increasing concentration of added cysteine, suggesting that the sulfides react with cysteine. The observation suggests that the mechanism of action of the alkenyl sulfides could be due to reaction of the sulfide moieties with cellular thiols, such as cysteine.[63] Similarly, Liang *et al.* found that DATS reacts rapidly with glutathione to release H_2S during an exchange reaction (Figure 3.46).[67] In 2017, Ercole *et al.* investigated the incorporation of trisulfide linkers to poly(ethylene glycol)–cholesterol conjugates for use as therapeutic H_2S delivery systems.[68] The investigation found that the trisulfide linked conjugate can react with cysteine to produce H_2S as a product of the exchange reaction between the polysulfide and thiol.

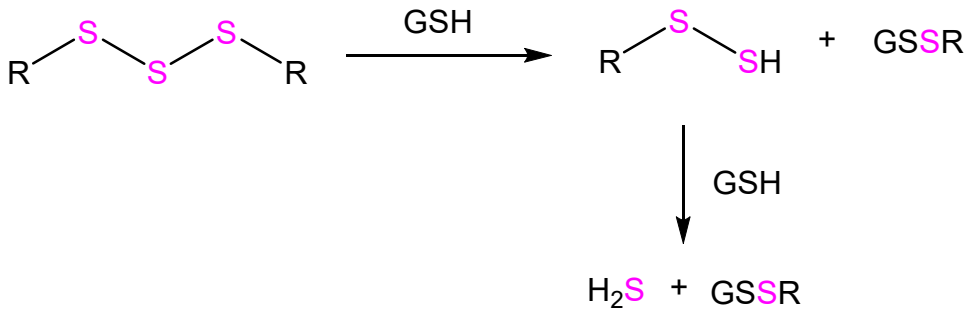

Figure 3.46: Schematic depicting the exchange reaction between trisulfide and glutathione (GHS) to form H_2S, adapted from Liang *et al.*[67]

The products of the copolymerisation of elemental sulfur and diene monomers in this study are expected to have high sulfur content, and therefore expected to contain some higher order polysulfide segments within the polymer chains. Similarly to the studies conducted by Kim *et al.* and Ercole *et al.*, the interaction of S50-PA polymer nanoparticles and cysteine was investigated. In brief, cysteine was added to S50-PA nanoparticles diluted in water under stirring. The generation of H_2S was assessed qualitatively using lead (II) acetate test strips (lower detection limit of 4 ppm H_2S) adhered to the inside of the cap of the vial (Figure 3.47). Two controls were prepared, one consisted of cysteine in the absence of S50-PA nanoparticles, and the other contained S50-PA nanoparticles in the absence of cysteine. After 5 minutes of stirring at room temperature, a colour change in the lead (II) acetate test strip was observed for the vial containing S50-PA nanoparticles and cysteine. The brown colour is consistent with that of lead sulfide, suggesting that H_2S was generated in this vial during the first 5 minutes of stirring. After 5 hours, the colour of the strip darkened further. No colour change was observed during the 5 hour period for both of the control samples. The results show that S50-PA nanoparticles are able to form H_2S in the presence of cysteine (Figure 3.47), which suggests that the particles are able to undergo exchange reactions with thiols and could therefore react with cellular thiols such as glutathione.

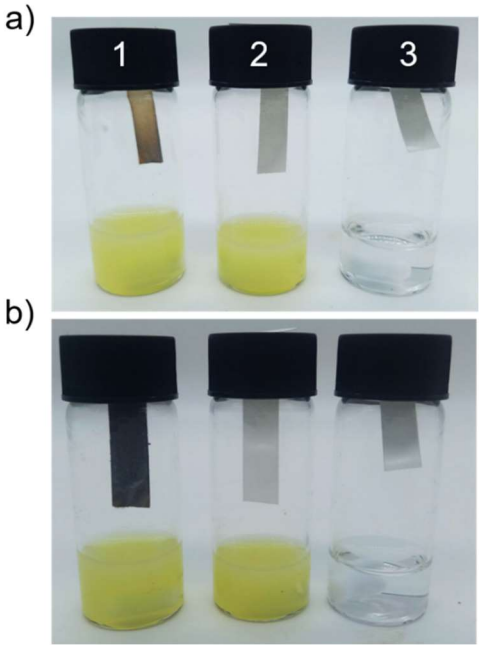

Figure 3.47: Photograph of vials containing a) Lead acetate paper after 5 minutes exposure and b) 5 hr exposure to 1: S50-PA nanoparticles and cysteine, 2: S50-PA nanoparticles and 3: cysteine.

H_2S generation during the incubation of *S. aureus* with S50-PA nanoparticles was investigated during a 24 hour period (Figure 3.48). During the 24 hour incubation period it was found that H_2S was generated in the vial containing nanoparticles and *S. aureus*, no H_2S was detected in the controls. The results show that S50-PA nanoparticles are able to form H_2S in the presence of cysteine and *S. aureus* cells, which suggests that the particles are able to undergo exchange reactions with cellular thiols.

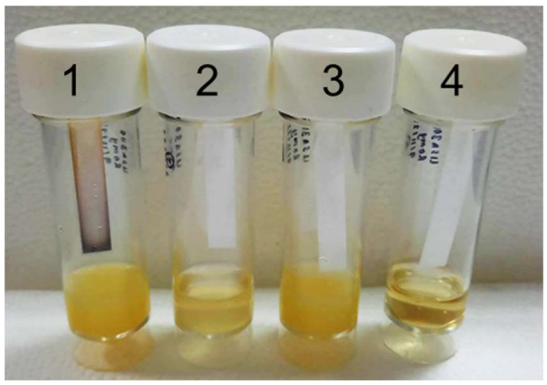

Figure 3.48: Photographs of lead acetate paper after 24 h exposure to 1: S50-PA nanoparticles and *S. aureus* in LB medium, 2: *S. aureus* in LB medium, 3: S50-PA nanoparticles in LB medium and 4: LB medium.

SEM imaging of *S. aureus* cells before and after treatment with S50-PA nanoparticles (Figure 3.49) shows the presence of smaller particles, consistent with the morphologies observed in the SEM images of the nanoparticles, on the surface of the bacterial cells. The bacterial cells have lost uniformity of size and shape, following nanoparticle treatment. It is therefore possible that the particles are exerting an effect by directly interacting with the surface of the cells.

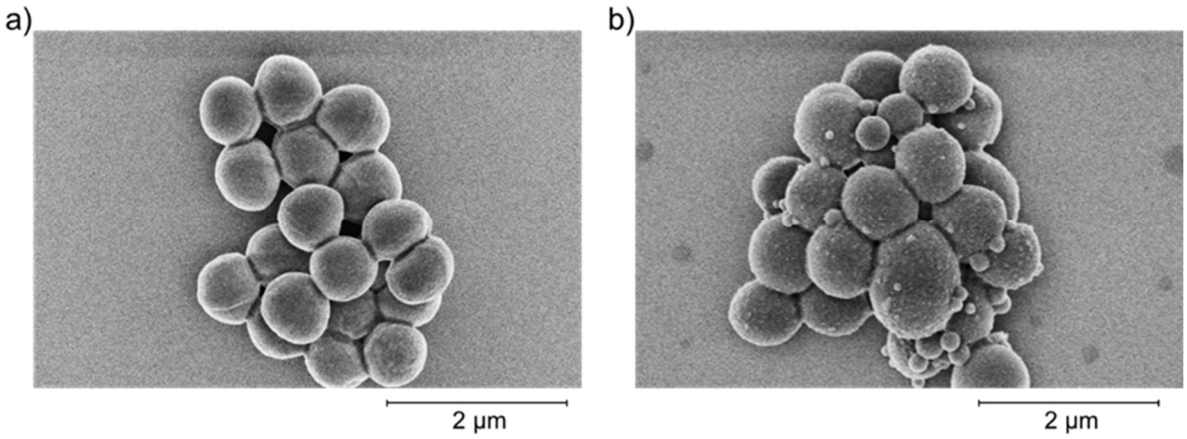

Figure 3.49: SEM images of *S. aureus* a) before and b) after treatment with S50-PA nanoparticles.

3.4.7 Sulfur Polymer Nanoparticles as Combination Therapies

The potential of using high sulfur content nanoparticles as combination therapies with antibiotics was investigated. Nanoparticles were tested against an extensively drug-resistant *P. aeruginosa* strain (B9) that carries a megaplasmid harbouring several important antimicrobial resistance genes, in combination with tobramycin, an aminoglycoside antibiotic that is used to treat complicated infections such as septicaemia and urinary tract infections and to manage *P. aeruginosa* infections in people with cystic fibrosis.[69,70] The effect of varying the tobramycin concentration (1-512 μg/ml) whilst maintaining a nanoparticle concentration of 128 μg/ml was investigated (Figure 3.50). In the absence of antibiotics, 512 ug/ml of nanoparticles were required to inhibit >50% of the growth ($p < 0.0001$) of the highly drug-resistant *P. aeruginosa* B9 strain. With treatment of tobramycin alone, B9 growth was completely inhibited only at the top concentration of 512 μg/ml ($p < 0.0001$), however, with the addition of nanoparticles the growth was completely inhibited at a concentration of 256 μg/ml ($p < 0.0001$). Furthermore, reductions in growth with dual nanoparticle plus tobramycin treatment, relative to treatment with tobramycin alone, were observed at all tobramycin concentrations between 16 and 128 μg/ml. This demonstrates the potential of using the polymer nanoparticles in combination with other drugs. This may enable use of lower antibiotic concentrations, for antimicrobial stewardship, or help alleviate the side effects of long term, high dose, antimicrobial therapy.

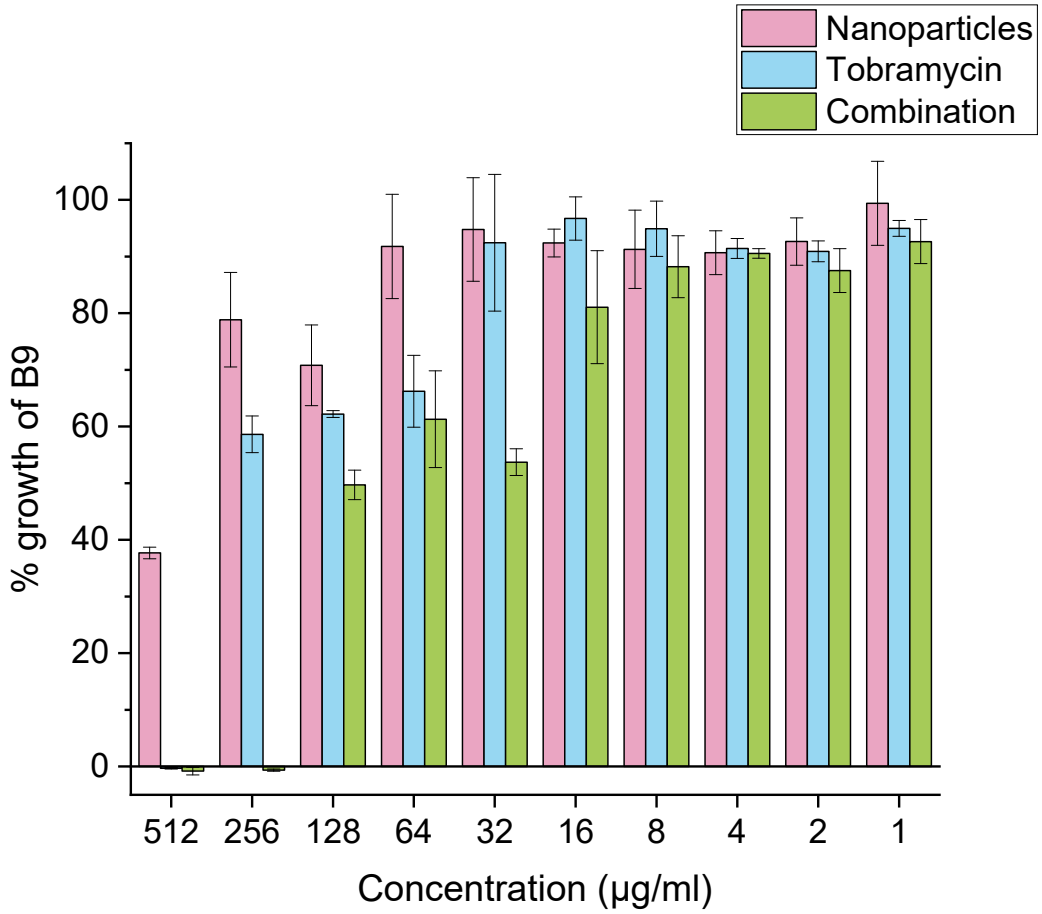

Figure 3.50: % growth of *P. aeruginosa* strain B9 compared to untreated culture in the presence of S50-PA nanoparticles (512-1 µg/ml), tobramycin (512-1 µg/ml) and a combination of nanoparticles and tobramycin where the nanoparticle concentration was set to 128 µg/ml and the tobramycin concentration was varied between 512-1 µg/ml.

3.4.8 Cytotoxicity of High Sulfur Content Polymeric Nanoparticles

The cytotoxicity of high sulfur content polymers are not widely reported and thus their safety for uses in potential applications such as environmental remediation, IR optics and novel antimicrobials is poorly understood. In 2016, Crockett *et al.* investigated the cytotoxicity of the product of the copolymerisaton of sulfur and limonene. [71] The polymer was allowed to soak in water for 24 h, allowing any potential species to leach into solution. The solution was then introduced to HepG2 and Huh7 cells to evaluate if the polymer was able to leach any cytotoxic species into water. HepG2 and Huh7 are immortalised cell lines that are commonly used to evaluate the hepatotoxicity and general cytotoxicity of drugs and nanomaterials.[72,73] The study found that water that has been exposed to the polysulfide is not cytotoxic during the 24 hr contact time with the cells. The results are a promising start to investigating the safety of high sulfur content polymers.[71] It is expected that the comonomers used during the copolymerisation of elemental sulfur will result in materials with different cytotoxicity. Furthermore, the properties of a nanomaterial can often differ from the bulk due to an increase in surface area. Similarly to the study conducted by Crockett *et al.*, the cytotoxicity of S50-PA nanoparticles in this study were evaluated against HepG2 human liver cells. The cytotoxicity of high sulfur content polymeric nanoparticles was investigated using the MTT assay.[74] The MTT assay is a colorimetric assay, that measures the reduction of the tetrazolium MTT dye to the insoluble, purple formazan (Figure 3.51) by NADPH-dependent cellular oxidoreductase enzymes. The assay can therefore be used to measure cell viability by probing enzymatic activity of viable cells.[75]

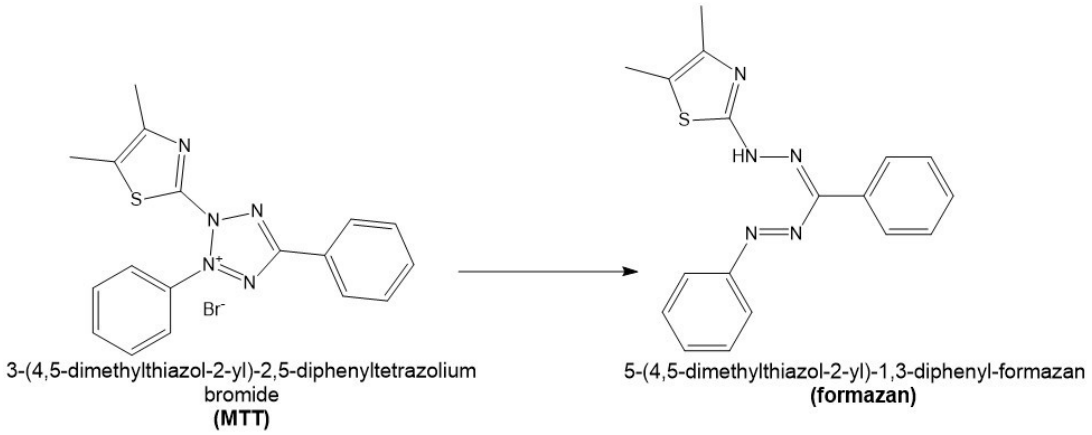

Figure 3.51: Chemical structures of MTT which is reduced to formazan by NADPH-dependent cellular oxidoreductase enzymes.

In brief, the nanoparticles were added to approximately 80% confluent HepG2 cells and were incubated for 24 h. Several controls were prepared, of which included nanoparticles in the absence of cells, growth medium only and growth medium in the presence of cells. Growth medium in the presence of cells was used as the negative control i.e untreated cells. Ater incubation the solutions were removed and replaced with fresh medium containing MTT labelling agent. The solutions were incubated for 4 h, before the solubilising agent was added. The absorbance at 595 nm was measured after leaving the solutions in the presence of the solubilising agent to incubate overnight (Figure 3.52).

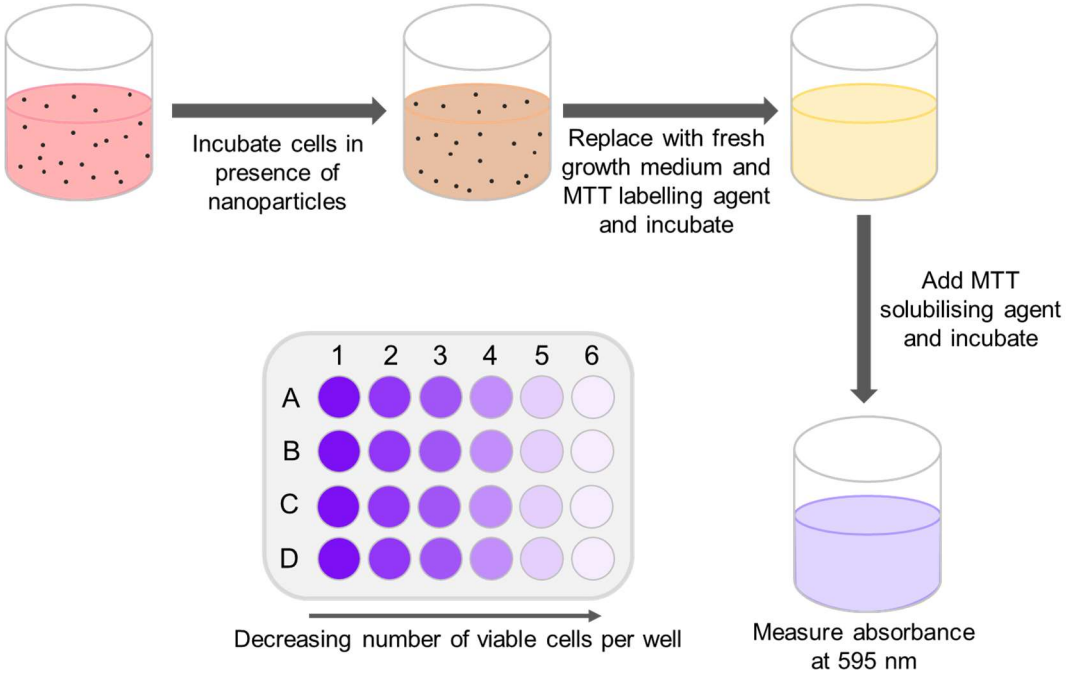

Figure 3.52: General scheme depicting the MTT colorimetric assay to evaluate the cytotoxicity of polymeric nanoparticles.

S50-PA nanoparticles at final concentrations of 14, 27, 55, 220 and 440 µg/ml were evaluated for their cytotoxicity against HepG2. The cytotoxicity of the nanoparticles was expressed as % cell viability compared to the blank i.e HepG2 cells in the absence of nanoparticles (Figure 3.53). It was found that all nanoparticle concentrations gave >80 – 100 % cell viability by considering the extremities of the error bars. No trend was observed between the cell viability and the nanoparticle concentration.

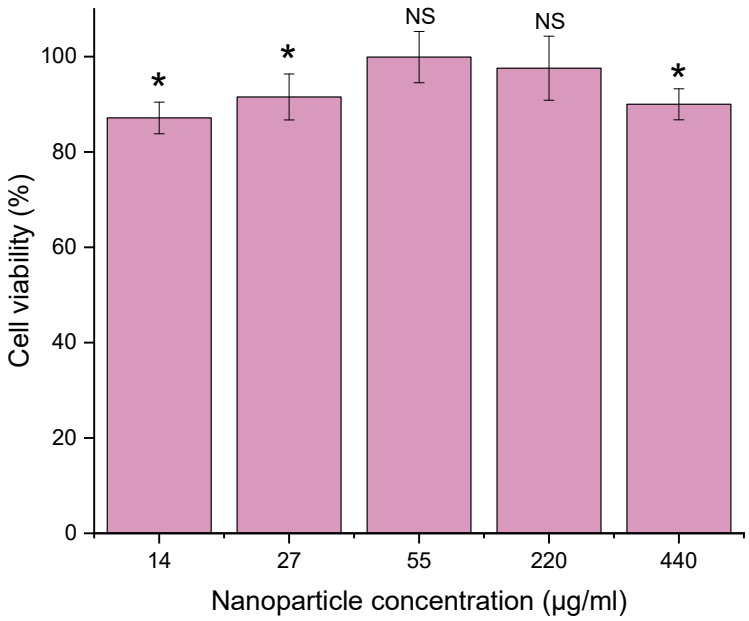

Figure 3.53: The cell viability (%, calculated against untreated cells) of HepG2 mammalian liver cells after treatment with different concentrations of S50-PA nanoparticles.

3.5 Conclusions

In summary we have shown that high sulfur content polymeric nanoparticles can be prepared by both nanoprecipitation and emulsion-templated methods. The nanoparticles are water-dispersible, with average hydrodynamic radii of approximately 100-200 nm and were found to be stable during a 2 week stability study. High sulfur content polymeric nanoparticles show antibacterial activity against both Gram-positive methicillin-resistant *S. aureus* and Gram-negative *P. aeruginosa,* and were shown to inhibit *S. aureus* biofilm formation over 48 h. To our knowledge, this was the first study of the antibacterial properties of high sulfur content polymeric nanoparticles prepared by inverse vulcanisation. Nanoparticles of elemental sulfur have been reported in the literature, the presence of an organic comonomer could allow for further functionalisation of the nanoparticles that may improve the biological properties of the polymers and nanoparticles. We demonstrate that formulating high sulfur content polymers into nanoparticles does not result in the loss of antibacterial activity of the materials compared to the bulk polymers. One possible mechanism of action of the polymeric nanoparticles could be interaction with cellular thiols, as demonstrated by the interaction of the nanoparticles with cysteine. The possible mechanism of action by interaction with cellular thiols suggests that the particles are non-selective and could therefore be toxic to mammalian cells. S50-PA polymeric nanoparticles show little cytotoxicity against the mammalian HepG2 cell line at various concentrations spanning 14-440 μg/ml.

3.6 Experimental Details

3.6.1 Materials and Equipment

Materials: Ground sulfur sublimed powder reagent grade ≥99.5% was obtained from Brenntag U.K. and Ireland. (S)-(−)-perillyl alcohol food grade ≥95%, geraniol food grade ≥97%, Luria−Bertani broth (Miller), LB agar and phosphate buffered saline (PBS), M9 minimal salts X5, glucose, magnesium sulfate suitable for cell culture, crystal violet, cell proliferation kit I (MTT) and lead (II) acetate test strips were purchased from Sigma-Aldrich. Eagle's Minimum Essential Medium (EMEM) was purchased from ATCC. Methicillin-resistant *S. aureus* strain USA300 and *P. aeruginosa* strains PAO1, LESB65, LESB65Δ*pmrB* and B9 were cultured from frozen stocks stored at the University of Liverpool.

^{1}H NMR spectroscopy was conducted using a Bruker Advance DRX (400 MHz) spectrometer using deuterated chloroform as the solvent, all experiments were carried out at room temperature.

FT-IR spectroscopy was conducted with a Bruker Vertex V70 FT-IR spectrometer, with a germanium ATR crystal.

Dynamic Light Scattering (DLS) and zeta potential measurements were obtained at 25 °C on a Malvern Instruments Ltd. Zetasizer Nano Series Nano-ZS spectrometer using the automatic attenuator and measurement position settings. The z-average diameter was measured using 1 cm path length disposable cuvettes. Nanoparticles were dispersed at a range of concentrations to determine a size independent of the concentration.

Scanning electron microscopy (SEM) was performed using a Hitachi S-4800 cold-field emission scanning electron microscope. The nanoparticle dispersions were dropped onto silicon wafer chips which were subsequently mounted onto SEM stubs using conductive silver paint. For imaging cells after treatment with nanoparticles, diluted *S. aureus* cultures

supplemented with nanoparticles, or water as a control, were incubated for 5 h. The cultures were pelleted by centrifugation and washed with PBS. The pellets were incubated overnight in glutardialdehyde and then dispersed and spun down in a series of ethanol dilutions (50, 70, 90, 95 and 100 % v/v). The pellets were redispersed in ethanol, and the resulting dispersions were dropped onto silicon wafers. Prior to imaging, samples were coated with gold using a current of 120 mA for 15 s to give approximately 15 nm gold coatings using a Quorum S1505 ES sputter coater.

Absorbance measurements were obtained using a BMG Labtech FLUOstar® Omega microplate reader using 96-well plates.

3.6.2 Synthesis of High Sulfur Content Polymers

Polymerization were carried out in 40 mL glass vials placed in aluminum heating blocks. Sulfur/crosslinker weight ratios of 50 and 70 wt % sluufer were used, with the total reaction scale maintained at 10 g. All reactions were begun by allowing the sulfur to melt at 135 °C before adding the organic cross-linker under stirring. The reaction temperature was increased to 175 °C for perillyl alcohol and geraniol. Molten pre-polymer was poured into silicone moulds followed by curing overnight in an oven at 140 °C. The mixture was transferred from the stirred vial to the mold when the reaction mixture had become homogeneous and viscous (an aliquot of the reaction mixture, when removed on a spatula and allowed to cool to room temperature, would no longer visibly separate to clear organic monomer, and precipitated yellow sulfur powder). The cured polymers were allowed to cool and were ground into powders using a pestle and mortar.

3.6.3 Preparation of Polymeric Nanoparticles

Emulsion-solvent evaporation method: 9 ml of aqueous surfactant solution (varying concentrations) was added to a 14 ml glass vial. 1 ml of S50-Ger in chloroform (5 mg/ml, 50 wt% S) was added to the vial and immediately sonicated for 40 s. The vial was equipped with

a 15 x 6 mm magnetic stirrer bar and the resulting cream coloured emulsion was allowed to stir at 600 rpm and at room temperature overnight or until the chloroform had evaporated.

Nanoprecipitation method: 9 ml of aqueous surfactant solution (10 mg/ml) or distilled water was added to a 14 ml glass vial and allowed to stir at room temperature at 600 rpm. 1 ml of S-Ger or S-PA in THF (varying concentrations, 50 and 70 wt% S) was added to the aqueous solution dropwise with continued stirring at 600 rpm. Once 1 ml of the polymer dissolved in THF was added to the vial, the solution was continued to stir at room temperature at 600 rpm overnight or until THF had evaporated fully.

3.6.4 Bacteria Preparation, Storage, and Enumeration

Glycerol stocks of *S. aureus* strain USA300 and *P. aeruginosa* strain PAO1 were stored at −80 °C for long-term storage. For experimental use, frozen glycerol stocks of *S. aureus* and *P. aeruginosa* were defrosted and spread onto LB agar plates which were incubated overnight at 37 °C. Bacterial cultures were prepared by swabbing one colony into 10 mL of LB broth, followed by overnight incubation at 37 °C. Colony forming units (CFU) were enumerated by serially diluting the cultures in PBS onto LB agar, using the Miles and Misra method. CFU/cm^2 and CFU/mL were calculated using the following equation:

$$\text{CFU} = (\text{No. of colonies} \times \text{dilution factor})/\text{vol of culture plate}$$

3.6.5 Viable Bacterial Cell Enumeration Assay

S. aureus USA300 and *P. aeruginosa* PAO1 were used to evaluate the antibacterial efficiency of the high sulfur content polymeric nanoparticles. Blank samples were prepared by dropping 1 ml of THF into 9 ml water followed by overnight stirring (600 rpm) at room temperature overnight to allow for the THF to evaporate. Overnight cultured bacteria prepared in LB broth were diluted to 10^5 CFU/mL (OD600 = 0.1) in LB or M9 media. 900 µL of diluted bacterial solution was added to 2 mL vials along with 100 µL of nanoparticles dispersed in water (final concentration of nanoparticles: 14, 27, 55, 220 and 440 µg/mL) or blank. The samples were

incubated for 5 h at 37 °C on a roller. viable cells were enumerated after serial dilution of the solution in PBS onto LB agar, using the Miles and Misra method at 0, 10, 30, 60, 90, 120 and 300 minutes.

3.6.6 Minimum Inhibitory Concentration Assay

Minimum inhibitory concentrations of sulfur nanoparticles were assessed according to the European Committee on Antimicrobial Susceptibility Testing (EUCAST) guidelines[76], for an incubation period of 24 h against *S. aureus* strain USA300 and *P. aeruginosa* strain PAO1, in LB medium. An initial OD600 of 0.1 (~5 x 10^5 CFU/ml) was used for the cell cultures prior to incubation. Nanoparticles were tested at 2-fold dilutions spanning a concentration range of 0.5-512 μg/ml. The OD600 was measured using a FLUOstar® Omega microplate reader. The same method was used to investigate the antibacterial activity of the nanoparticles, combined with tobramycin, against the extensively drug resistant *P. aeruginosa* strain B9, isolated from an acute respiratory infection in Thailand.[69]

3.6.7 Disc Diffusion Assay

S. aureus USA300 and *P. aeruginosa* PAO1 were used to evaluate the antibacterial efficiency of the high sulfur content polymeric nanoparticles using the disc diffusion assay. Overnight cultures bacteria prepared in LB broth was streaked onto LB agar discs. Blank antimicrobial susceptibility testing discs were soaked with 50 μL of nanoparticles. A control sample was prepared by soaking the empty discs with 50 μL of water. The discs were placed on top of the lawn of bacteria, and the plates were incubated for 24 h at 37 °C.

3.6.8 Nanoparticle-Bacteria Charge Interaction Study

Nanoparticle-bacteria charge interactions were investigated using *P aeruginosa* strain LESB65 and a mutant derived from this strain, LESB65Δ*pmrB*.[58] Overnight cultures of both strains were diluted in LB medium to an approximate cell density of 10^5 CFU/ml. Aliquots of both diluted strains were pre-incubated for 30 minutes with spermidine (2 mM), and were washed

with PBS after centrifugation. The cell pellets after incubation with spermidine were redispersed in LB medium to an approximate cell densitry of 10^5 CFU/ml. 100 µl of S50-PA nanoparticles were dispersed in 900 µl of the diluted cultures of both strains and the cultures pre-incubated with spermidine. The samples were incubated on a roller for 5 h at 37 °C.

3.6.9 Biofilm Staining Assay

S. aureus USA300 and *P. aeruginosa* PAO1 were used to evaluate biofilm formation in the presence of high sulfur content polymeric nanoparticles. Blank solutions were prepared by dropping 1 ml of THF into 9 ml water followed by overnight stirring (600 rpm) at room temperature overnight to allow for the THF to evaporate. Overnight cultured bacteria prepared in LB broth was diluted to 10^5 CFU/mL (OD600 = 0.1). 900 µL of diluted culture and 100 µL of nanoparticles dispersed in water (final concentrations of 220 and 440 µg/ml) or blank solution were added to seaparate wells of a 24-well plate. The well plate was incubated statically at 37 °C for 24 and 48 hr. After incubation the solutions from the well plate were discarded and rinsed with 1 ml PBS, which was then discarded and the plate was allowed to dry. The dried wells were stained with 1 ml 0.25% crystal violet for 30 minutes. The dye was discarded, the well plate was thoroughly rinsed with water and allowed to dry. 1 ml of ethanol was added to each well in order to solubilise any remaining dye. The absorbance at 600 nm was measured using ethanol as a blank.

3.6.10 Cell Culture

HepG2 cells were maintained in Eagle's Minimum Essential Medium (EMEM) cell culture medium (ATCC) supplemented with 10% Fetal Bovine Serum (FBS). Cells were maintained in a 5% CO_2 incubator at 37 °C.

3.6.11 Cell Viability Assay

Cell viabiliy was evaluated using the MTT assay. HepG2 cells were seeded at a concentration of 5×10^4 cells/well in 100 µl culture medium and incubated (5% CO_2, 37 °C) for 48 hours or until approximately 80% confluent. Culture media was removed and replaced with 90 µL culture medium and 10 µL of nanoparticles (final concentration of nanoparticles: 14, 27, 55, 220 and 440 µg/mL) or blank solution. The cells in the presence of nanoparticles/blank were incubated for 24 h (5% CO_2, 37 °C). After 24 h incubation the media containing nanoparticles/blank was removed and replaced with 100 µL culture medium and 10 µL of the MTT labeling reagent (final concentration of 0.5 mg/ml). The microplate was incubated for a further 4 hr (5% CO_2, 37 °C). 100 µl of the solubilizing buffer was added to each well, and the microplae was allowed to stand overnight in the incubator. The solubilization of the purple formazan crystals was measured at an absorbance wavelength of 595 nm.

3.6.12 Cysteine-Mediated H_2S Release

L-cysteine (5 mg/mL) in PBS was added to an equal volume of S50-PA nanoparticles (5 mg/mL) in water in a 14 mL glass vial. Control solutions were prepared by adding L-cysteine to water, and adding water to S50-PA nanoparticles. Stirrer beads were added to the vials, and approximately 1 cm of lead (II) acetate test paper was attached to the inside of the lid of the vial. The vials were allowed to stir over a period of 5 h at room temperature.

To assess H_2S generation during the incubation of S50-PA nanoparticles with *S. aureus* USA300, approximately 1 cm of lead (II) acetate test paper was attached to the inside of the lid of a 30 mL universal vial. 4.5 ml of diluted *S. aureus* culture in LB medium with an approximate cell density of 10^5 CFU/ml was added to the vial, along with 0.5 mL of S50-PA nanoparticles. The lid was screwed onto the vial, ensuring that the lead paper was not submerged in the culture. The samples were statically incubated for 24 hr at 37 °C.

3.6.13 Statistical Analysis

Statistical analysis was conducted using one-way analysis of variance (ANOVA) followed by Tukeys post hoc test. Differences were deemed as statistically significant if a value of $p < 0.05$ was obtained.

3.7 References

1 M. Vert, Y. Doi, K.-H. Hellwich, M. Hess, P. Hodge, P. Kubisa, M. Rinaudo and F. Schué, *Pure Appl. Chem.*, 2012, **84**, 2, 377-410.

2 J. Jeevanandam, A. Barhoum, Y. S. Chan, A. Dufresne and M. K. Danquah, *Beilstein J. Nanotechnol.*, 2018, **9**, 1050–1074.

3 J. Escobar-Chávez, I. Rodríguez Cruz, C. Domínguez-Delgado, R. Díaz-Torres, A. Revilla Vazquez and N. Aléncaster, 2012, p. 50.

4 M. Sharma, in *Applications of Targeted Nano Drugs and Delivery Systems*, eds. S. S. Mohapatra, S. Ranjan, N. Dasgupta, R. K. Mishra and S. Thomas, Elsevier, 2019, pp. 499–550.

5 J. P. Rao and K. E. Geckeler, *Prog. Polym. Sci.*, 2011, **36**, 887–913.

6 Satyajeet Sahoo, Anitha Gopalan, S. Ramesh, P. Nirmala, G. Ramkumar, S. Agnes Shifani, Ram Subbiah, J. Isaac JoshuaRamesh Lalvani, *Adv. Mater. Sci. Eng.* , 2021, 1-9.

7 C. I. C. Crucho and M. T. Barros, *Mater. Sci. Eng. C*, 2017, **80**, 771–784.

8 J.-Y. Zhang, Z.-G. Shen, J. Zhong, T.-T. Hu, J.-F. Chen, Z.-Q. Ma and J. Yun, *Int. J. Pharm.*, 2006, **323**, 153–160.

9 Y. Wang, P. Li, T. Truong-Dinh Tran, J. Zhang and L. Kong, *Nanomater.*, 2016, **6**, 2, 26.

10 R. H. Staff, K. Landfester and D. Crespy, ed. V. Percec, Springer International Publishing, Cham, 2013, pp. 329–344.

11 S. Salatin, J. Barar, M. Barzegar-Jalali, K. Adibkia, F. Kiafar and M. Jelvehgari, *Res. Pharm. Sci.*, 2017, **12**, 1–14.

12 W. Huang and C. Zhang, *Biotechnol. J.*, 2018, **13**, 1700203.

13 Y. Liu, G. Yang, D. Zou, Y. Hui, K. Nigam, A. P. J. Middelberg and C.-X. Zhao, *Ind. Eng. Chem. Res.*, 2020, **59**, 4134–4149.

14 Y. Braeken, S. Cheruku, A. Ethirajan and W. Maes, *Mater.*, 2017, **10**, 12, 1420.

15 B. Begines, T. Ortiz, M. Pérez-Aranda, G. Martínez, M. Merinero, F. Argüelles-Arias and A. Alcudia, *Nanomaterials*, 2020, 10.

16 V. A. Spirescu, C. Chircov, A. M. Grumezescu and E. Andronescu, *Polymers*, 2021, **13**, 5, 724.

17 T. Schneider, A. Baldauf, L. Ba, V. Jamier, K. Khairan, M.-B. Sarakbi, N. Reum, M. Schneider, A. Röseler, K. Becker, T. Burkholz, P. Winyard, M. Kelkel, M. Diederich and C. Jacob, *J. Biomed. Nanotechnol.*, 2011, **7**, 395–405.

18 S. Shankar, R. Pangeni, J. W. Park and J.-W. Rhim, *Mater. Sci. Eng. C*, 2018, **92**, 508–517.

19 S. Shivalkar, F. Arshad, A. K. Sahoo and M. P. Sk, *ACS omega*, 2022, **7**, 33358–33364.

20 Y. Wang, Y. Zhao, J. Wu, M. Li, J. Tan, W. Fu, H. Tang and P. Zhang, *Nano Lett.*, 2021,

21, 9433–9441.

21 J. Lim, U. Jung, W. T. Joe, E. T. Kim, J. Pyun and K. Char, *Macromol. Rapid Commun.*, 2015, **36**, 1103–1107.

22 J. C. Bear, W. J. Peveler, P. D. McNaughter, I. P. Parkin, P. O'Brien and C. W. Dunnill, *Chem. Commun.*, 2015, **51**, 10467–10470.

23 B. Zhang, S. Petcher, R. A. Dop, P. Yan, W. Zhao, H. Wang, L. J. Dodd, T. O. McDonald and T. Hasell, *J. Mater. Chem. A*, 2022, **10**, 13704–13710.

24 W. Chen and A. Viljoen, *South African J. Bot. - S AFR J BOT*, 2010, **76**, 643–651.

25 D. J. Parker, H. A. Jones, S. Petcher, L. Cervini, J. M. Griffin, R. Akhtar and T. Hasell, *J. Mater. Chem. A*, 2017, **5**, 11682–11692.

26 J. A. Smith, S. J. Green, S. Petcher, D. J. Parker, B. Zhang, M. J. H. Worthington, X. Wu, C. A. Kelly, T. Baker, C. T. Gibson, J. A. Campbell, D. A. Lewis, M. J. Jenkins, H. Willcock, J. M. Chalker and T. Hasell, *Chem. – A Eur. J.*, 2019, **25**, 10433–10440.

27 C. Maladeniya, M. Karunarathna, M. Lauer, C. Lopez, T. Thiounn and R. Smith, *Mater. Adv.*, 2020, **1**, 1665-1674.

28 S. C. Hammer, A. Marjanovic, J. M. Dominicus, B. M. Nestl and B. Hauer, *Nat. Chem. Biol.*, 2015, **11**, 121–126.

29 G. Carr, C. Dean and D. Whittaker, *J. Chem. Soc. Perkin Trans. 2*, 1989, 71–76.

30 W. Yu, F. Bian, Y. Gao, L. Yang and Z.-L. Liu, *Adv. Synth. Catal.*, 2006, **348**, 59–62.

31 Geraniol, https://pubchem.ncbi.nlm.nih.gov/compound/geraniol, (accessed 17 June 2020).

32 L. Hagvall, C. Backtorp, S. Svensson, G. Nyman, A. Borje and A.-T. Karlberg, *Chem. Res. Toxicol.*, 2007, **20**, 807–814.

33 C. Backtorp, L. Hagvall, A. Borje, A.-T. Karlberg, P.-O. Norrby and G. Nyman, *J. Chem. Theory Comput.*, 2008, **4**, 101–106.

34 V. K. Shankarayya Wadi, K. K. Jena, S. Z. Khawaja, K. Yannakopoulou, M. Fardis, G. Mitrikas, M. Karagianni, G. Papavassiliou and S. M. Alhassan, *ACS Omega*, 2018, **3**, 3330–3339.

35 T. Quérette, C. Bordes and N. Sintes-Zydowicz, *Colloids Surfaces A Physicochem. Eng. Asp.*, 2020, **589**, 124371.

36 S. Guhagarkar, V. Malshe and P. Devarajan, *AAPS PharmSciTech*, 2009, **10**, 935–942.

37 J. M. Andrews, *J. Antimicrob. Chemother.*, 2001, **48**, 1, 5–16.

38 T. Yamazhan, S. Aydemir, A. Tünger, D. Serter and D. Gökengin, *Med. Princ. Pract. Int. J. Kuwait Univ. Heal. Sci. Cent.*, 2005, **14**, 413–416.

39 H. Fazeli, R. Akbari, S. Moghim, T. Narimani, M. R. Arabestani and A. R. Ghoddousi, *J. Res. Med. Sci. Off. J. Isfahan Univ. Med. Sci.*, 2012, **17**, 332–337.

40 R. A. Dop, D. R. Neill and T. Hasell, *Biomacromolecules*, 2021, **22**, 5223–5233.

41 A. Kourmouli, M. Valenti, E. van Rijn, H. J. E. Beaumont, O.-I. Kalantzi, A. Schmidt-

Ott and G. Biskos, *J. Nanoparticle Res.*, 2018, **20**, 62.

42 J. Lv, S. Wang, Y. Wang, Y. Huang and X. Chen, *Archaea*, 2015, **2015**, 483194.

43 H. Machado, L. L. Weng, N. Dillon, Y. Seif, M. Holland, J. E. Pekar, J. M. Monk, V. Nizet, B. O. Palsson and A. M. Feist, *Appl. Environ. Microbiol.*, 2019, **85**, 21, 01773-19.

44 A. S. Nuxoll, S. M. Halouska, M. R. Sadykov, M. L. Hanke, K. W. Bayles, T. Kielian, R. Powers and P. D. Fey, *PLOS Pathog.*, 2012, **8**, e1003033.

45 F. Matter, A. Luna Barron and M. Niederberger, *Nano Today*, 2020, **30**, 100827.

46 S. Mo, X. Shao, Y. Chen and Z. Cheng, *Sci. Rep.*, 2016, **6**, 36836.

47 G. V Lowry, R. J. Hill, S. Harper, A. F. Rawle, C. O. Hendren, F. Klaessig, U. Nobbmann, P. Sayre and J. Rumble, *Environ. Sci. Nano*, 2016, **3**, 953–965.

48 X. Zhang, M. R. Servos and J. Liu, *J. Am. Chem. Soc.*, 2012, **134**, 9910–9913.

49 D. Ramesh, G. Prasad and A. Raaj, *Int. J. Mech. Eng.*, 2015, **3**, 5, 124-127.

50 H. Cortés, H. Hernández-Parra, S. A. Bernal-Chávez, M. L. Del Prado-Audelo, I. H. Caballero-Florán, F. V Borbolla-Jiménez, M. González-Torres, J. J. Magaña and G. Leyva-Gómez, *Materials (Basel).*, 2021, **14**.

51 L. Felicia, J. Johnson and J. Philip, *J. Nanofluids*, 2014, **3**, 4, 328-335(8).

52 W. Choi, U. Mahajan, S.-M. Lee, J. Abiade and R. K. Singh, *J. Electrochem. Soc.*, 2004, **151**, G185.

53 P. Sinclair, M. Carballo-Pacheco and R. J. Allen, *Phys. Biol.*, 2019, **16**, 46001.

54 S. J. Pamp, M. Gjermansen, H. K. Johansen and T. Tolker-Nielsen, *Mol. Microbiol.*, 2008, **68**, 223–240.

55 A. Shariati, M. Arshadi, M. A. Khosrojerdi, M. Abedinzadeh, M. Ganjalishahi, A. Maleki, M. Heidary and S. Khoshnood, *Front. Public Heal.*, 2022, **10**, 10:1025633.

56 B. Bertani and N. Ruiz, *EcoSal Plus*, 2018, **8**, 1.

57 S. Brown, J. P. J. Santa Maria and S. Walker, *Annu. Rev. Microbiol.*, 2013, **67**, 313–336.

58 C. M. Hasan, S. Pottenger, A. E. Green, A. A. Cox, J. S. White, T. Jones, C. Winstanley, A. Kadioglu, M. H. Wright, D. R. Neill and J. L. Fothergill, *JCI insight*, 2022 , **7**, 22, e158879.

59 J. Tasse, S. Trouillet-Assant, J. Josse, P. Martins-Simões, F. Valour, C. Langlois-Jacques, S. Badel-Berchoux, C. Provot, T. Bernardi, T. Ferry and F. Laurent, *PLoS One*, 2018, **13**, e0200064.

60 G. Lotfi, H. Hassaine, N. Klouche, A. Khadir, N. Aissaoui, F. Nas Ep Rabehi and W. Zingg, *J. Bacteriol. Res.*, 2014, **6**, 1–6.

61 A. Müller, J. Eller, F. Albrecht, P. Prochnow, K. Kuhlmann, J. E. Bandow, A. J. Slusarenko and L. I. O. Leichert, *J. Biol. Chem.*, 2016, **291**, 11477–11490.

62 W.-R. Li, Y.-K. Ma, X.-B. Xie, Q.-S. Shi, X. Wen, T.-L. Sun and H. Peng, *Front. Microbiol.*, 2019, **9**, 9:3222.

63 J. Kim, J. Huh, S. Kyung and K. Kyung, *Food Sci. Biotechnol*, 2004, **13**, 235–239.

64 Z. M. Ross, E. A. O'Gara, D. J. Hill, H. V Sleightholme and D. J. Maslin, *Appl. Environ. Microbiol.*, 2001, **67**, 475–480.

65 U. Münchberg, A. Anwar, S. Mecklenburg and C. Jacob, *Org. Biomol. Chem.*, 2007, **5**, 1505–1518.

66 J. E. Biaglow, M. E. Varnes, E. P. Clark and E. R. Epp, *Radiat. Res.*, 1983, **95**, 437–455.

67 D. Liang, H. Wu, M. W. Wong and D. Huang, *Org. Lett.*, 2015, **17**, 4196–4199.

68 F. Ercole, M. R. Whittaker, M. L. Halls, B. J. Boyd, T. P. Davis and J. F. Quinn, *Chem. Commun.*, 2017, **53**, 8030–8033.

69 A. Cazares, M. P. Moore, J. P. J. Hall, L. L. Wright, M. Grimes, J.-G. Emond-Rhéault, P. Pongchaikul, P. Santanirand, R. C. Levesque, J. L. Fothergill and C. Winstanley, *Nat. Commun.*, 2020, **11**, 1370.

70 M. Rosalia, E. Chiesa, E. M. Tottoli, R. Dorati, I. Genta, B. Conti and S. Pisani, *Int. J. Mol. Sci.*, 2022, **23**, 22, 14080.

71 M. P. Crockett, A. M. Evans, M. J. H. Worthington, I. S. Albuquerque, A. D. Slattery, C. T. Gibson, J. A. Campbell, D. A. Lewis, G. J. L. Bernardes and J. M. Chalker, *Angew. Chem. Int. Ed. Engl.*, 2016, **55**, 1714–1718.

72 S. A. Snopov, N. P. Teryukova, E. I. Sakhenberg, V. V Teplyashina and R. F. Nasyrova, *Cell tissue biol.*, 2017, **11**, 405–415.

73 I. Greco, N. Molchanova, E. Holmedal, H. Jenssen, B. Hummel, J. Watts, J. Håkansson, P. Hansen and J. Svenson, *Sci. Rep.*, 2020, **10**, 13206.

74 M. Ghasemi, T. Turnbull, S. Sebastian and I. Kempson, *Int. J. Mol. Sci.*, 2021, **22**, 23, 12827.

75 V. Kuete, O. Karaosmanoğlu and H. Sivas, ed. V. B. T.-M. S. and V. from A. Kuete, Academic Press, 2017, pp. 271–297.

76 The European Committee on Antimicrobial Susceptibility Testing, EUCAST reading guide for broth microdilution, version 4.0, 2022.

3.8 Appendix

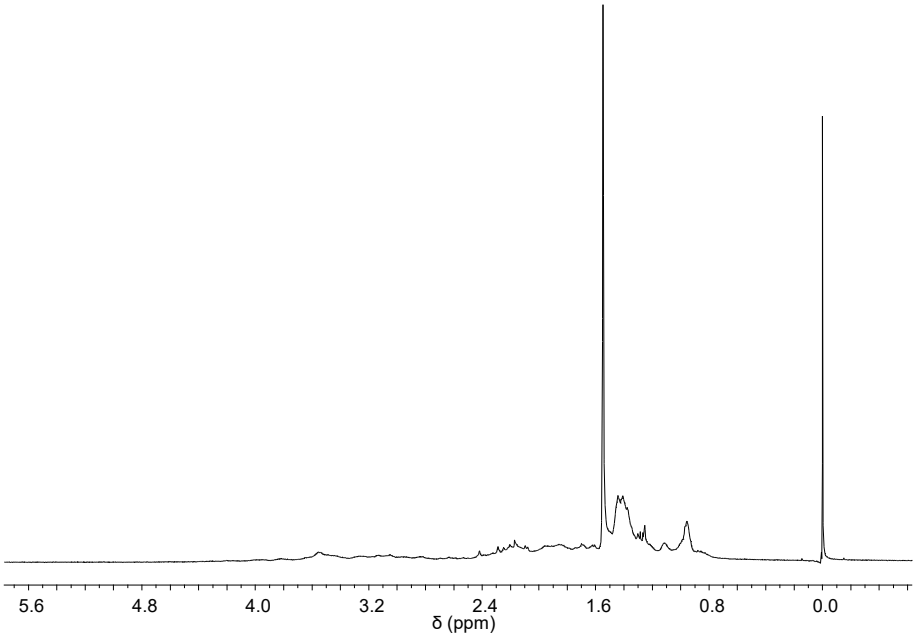

Appendix 3.1: ^{1}H NMR spectrum of S70-Ger.

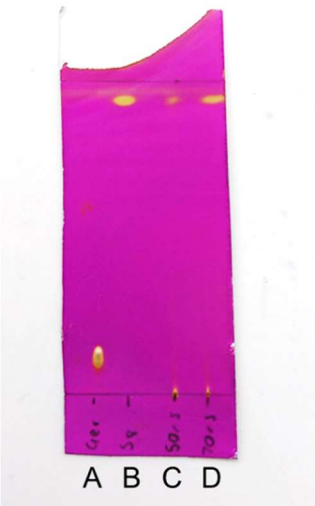

Appendix 3.2: Thin-layer chromatography plate for S-Ger analysis to detect any unreacted geraniol and/or elemental sulfur where A: geraniol, B: elemental sulfur, C: S50-Ger D: S70-Ger using 1:1 hexane:ethyl acetate as the eluent.

Appendix 3.3: Photograph of the dispersion formed from S50-Ger.

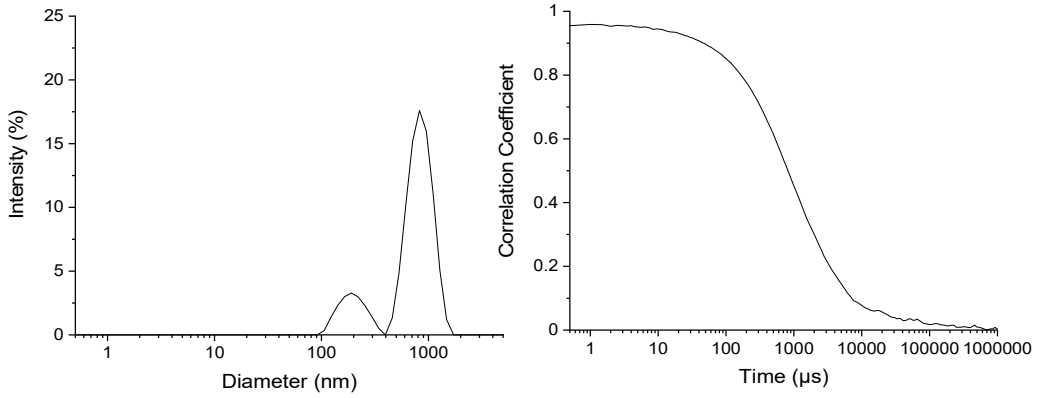

Appendix 3.4: The size distribution by intensity and correlogram traces obtained for dispersions of S50-Ger formed by an emulsion-solvent evaporation method employing Brij S20 as a surfactant

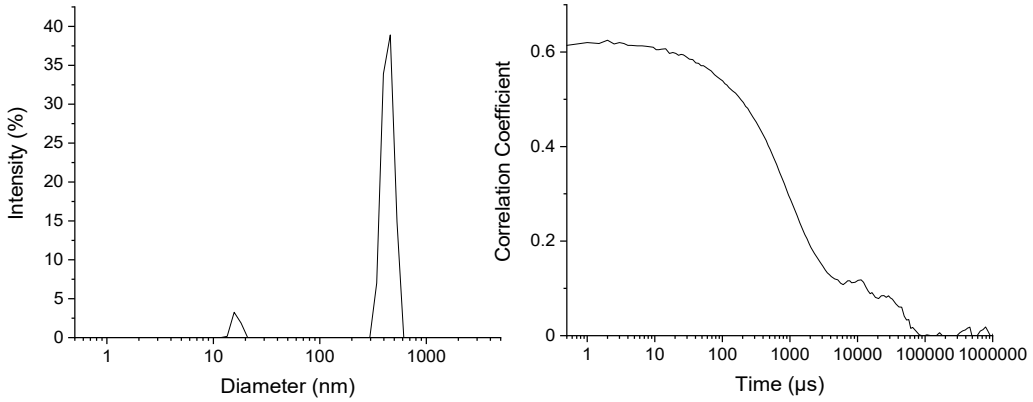

Appendix 3.5: The size distribution by intensity and correlogram traces obtained for dispersions of S50-Ger formed by an emulsion-solvent evaporation method employing SDS as a surfactant.

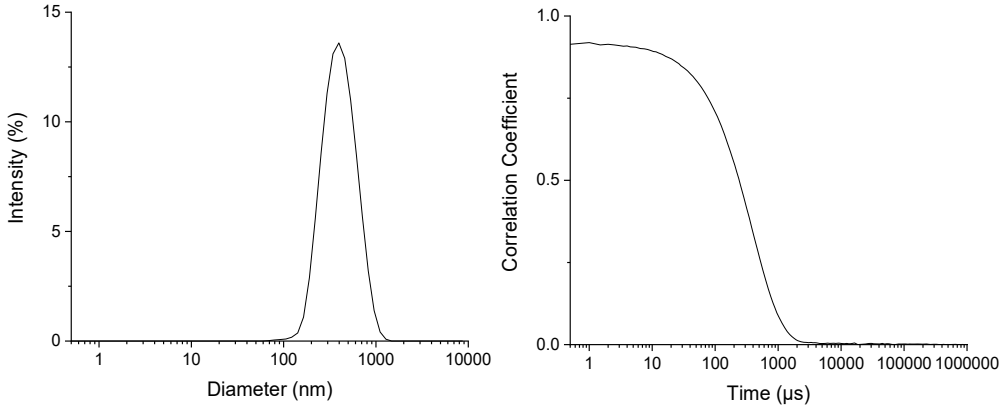

Appendix 3.6: The size distribution by intensity and correlogram traces obtained for dispersions of S50-Ger polysulfide formed by an emulsion-solvent evaporation method employing PVA as a surfactant.

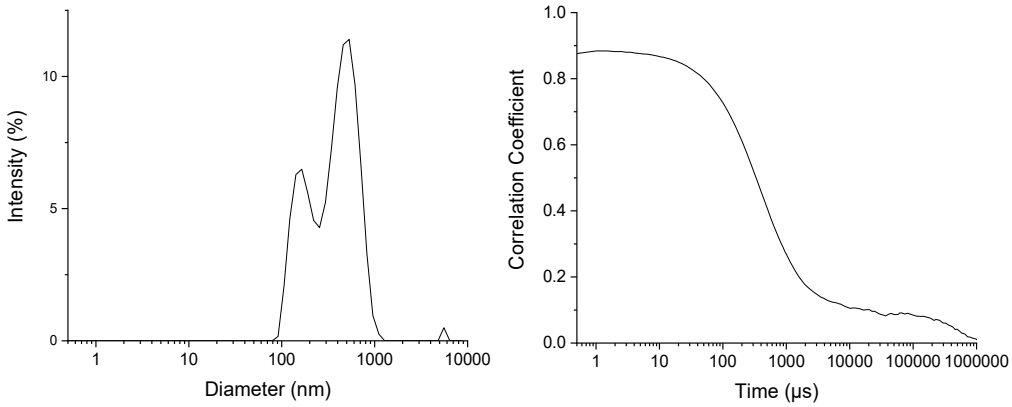

Appendix 3.7: The size distribution by intensity and correlogram traces obtained for dispersions of S50-Ger by an emulsion-solvent evaporation method employing Tween 80 at a concentration of 0.05 mg/ml.

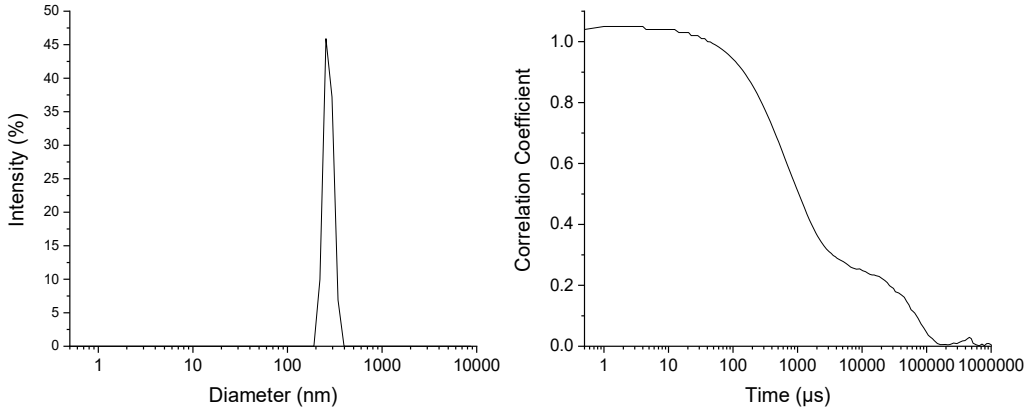

Appendix 3.8: The size distribution by intensity and correlogram traces obtained for dispersions of S50-Ger formed by an emulsion-solvent evaporation method employing Tween 80 at a concentration of 0.1 mg/ml.

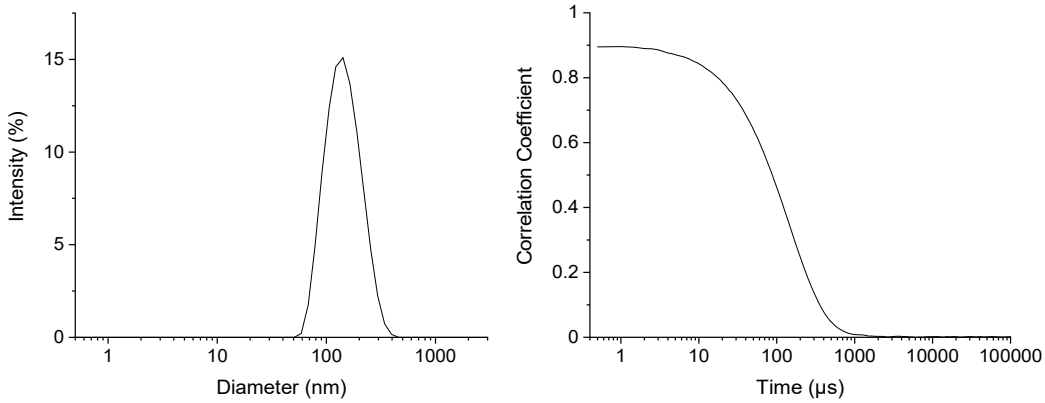

Appendix 3.9: The size distribution by intensity and correlogram traces obtained for dispersions of S50-Ger formed by a nanoprecipitation method without a surfactant.

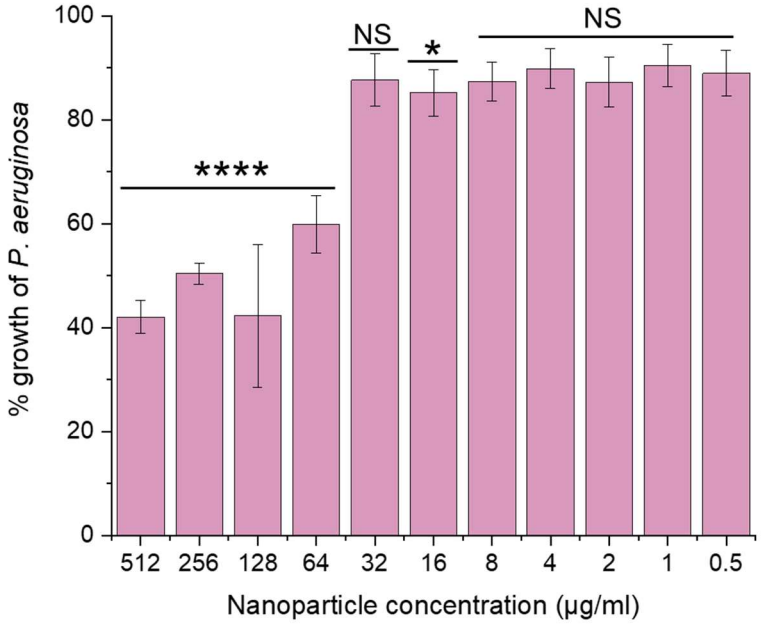

Appendix 3.10: Graph summarising the % growth of *P. aeruginosa* relative to a positive control, in the presence of S50-PA nanoparticles at various concentrations during a 24 h incubation period. *p < 0.05, ****p < 0.0001, NS denotes a value that is not statistically significant compared to the control.

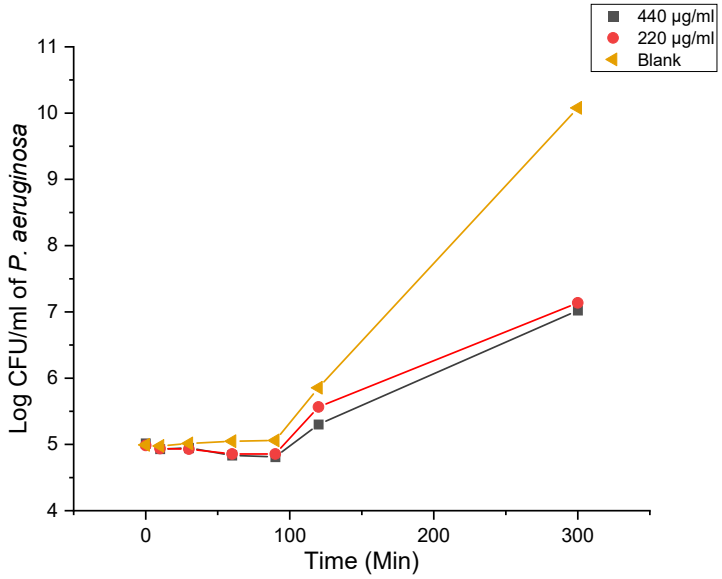

Appendix 3.11: *P. aeruginosa* growth curve in the presence of S50-Ger nanoparticles after 5 h incubation in nutrient-rich LB medium.

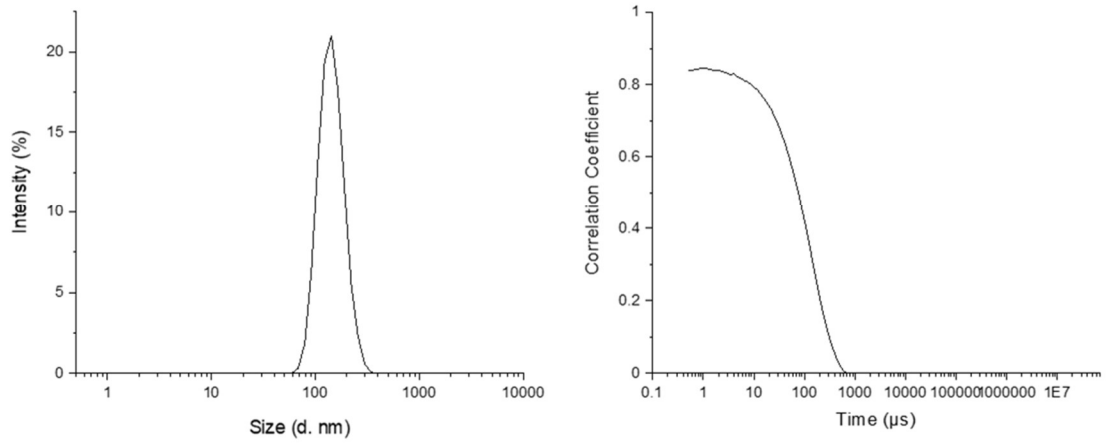

Appendix 3.12: The size distribution by intensity and correlogram traces obtained for dispersions of S50-PA formed by a nanoprecipitation method without a surfactant dispersed in LB medium.

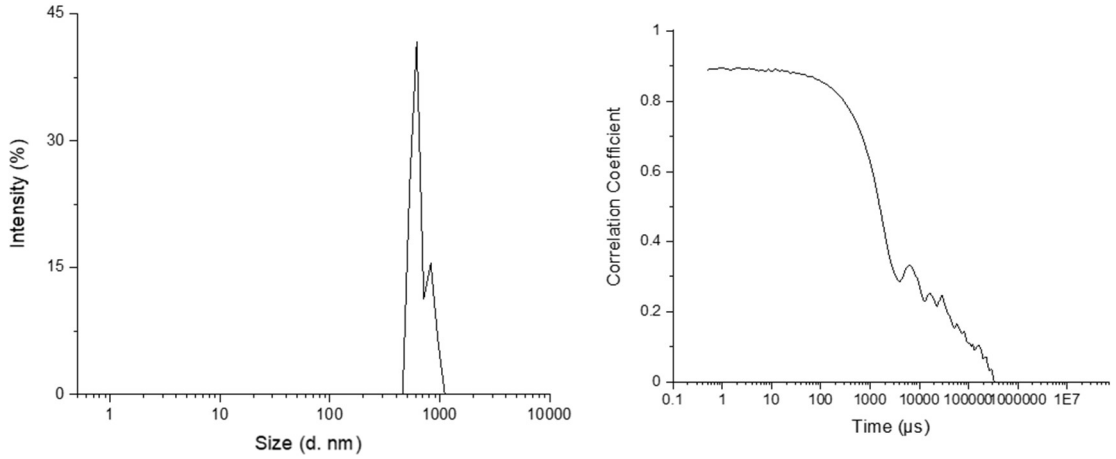

Appendix 3.13: The size distribution by intensity and correlogram traces obtained for dispersions of S50-PA formed by a nanoprecipitation method without a surfactant dispersed in M9 medium.

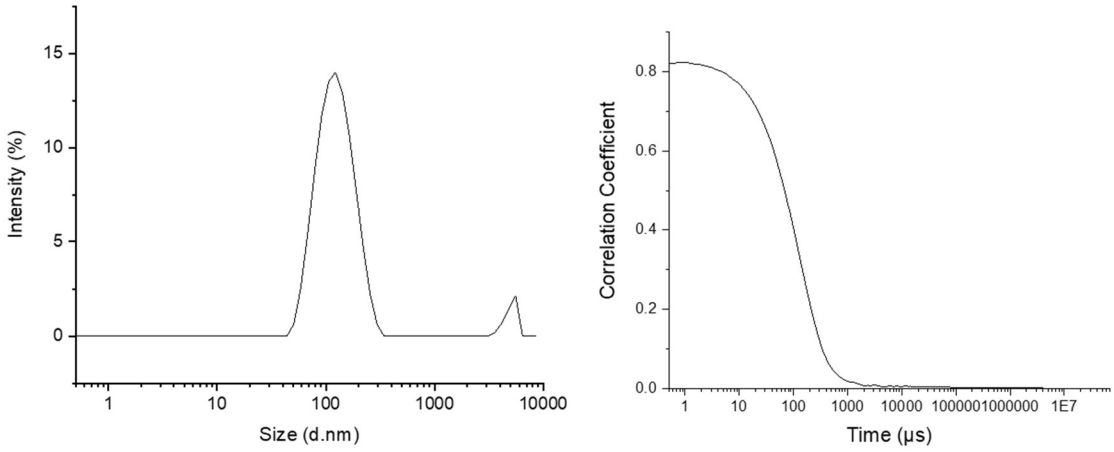

Appendix 3.14: The size distribution by intensity and correlogram traces obtained for dispersions of S50-PA formed by a nanoprecipitation method with Tween80 dispersed in M9 medium.

Chapter 4

Fabrication of Sulfur Polymer Surface Coatings

4.1 Abstract

High-sulfur content polymers have been shown to have antibacterial activity against both Gram-positive and Gram-negative bacteria. In this chapter we discuss the fabrication of surface coatings of high sulfur content polymers for potential applications as antibiofouling and antibacterial surfaces. Surface coatings were prepared by spray deposition of high sulfur content polymeric nanoparticles, which were found to have poor adhesion to glass and low thermal stability. Coatings were also prepared by spray deposition of silica-polymer composites, where silica was coated with high sulfur content polymers followed by dispersion in ethanol. Coatings of the silica-polymer composites were found to have water contact angles > 170° and sliding angles of ~ 6° and can be characterised as superhydrophobic surfaces. The superhydrophobic surfaces were found to have antibacterial and antibiofilm activity.

4.2 Introduction

4.2.1 Bacterial Adhesion and Biofilm Formation

The prevention of bacterial adhesion and biofilm formation on surfaces is a subject of medical importance. A biofilm is an assembly of surface-associated microbes that are often embedded within a self-produced polymeric matrix.[1,2] Biofilm formation is an important virulence factor that is often responsible for treatment failure due to device-associated infections caused by *S. aureus*. The formation of biofilms takes places in four stages (Figure 4.1): 1) reversible attachment of planktonic cells 2) proliferation of the cells and irreversible attachment to the surface forming microcolonies 3) maturation of the biofilm whereby the biofilm continues to expand and the clusters of multi-layered cells begin to synthesise extracellular polymeric substances (EPS) that comprise the matrix surrounding the bacteria 4) dispersal of planktonic cells from the biofilm that can go on to establish biofilms elsewhere.[3,4] Biofilms provide favourable conditions for bacteria as they are often protected from the immune system of the host and can exhibit phenotypic resistance to antimicrobial agents, making them more difficult to eradicate compared to planktonic bacteria.[5] Of particular concern are infections caused by *P. aeruginosa* due to a continuously high rate of antibiotic failure against such infections. The pathogenesis of many infections caused by *P. aeruginosa* are dependent on its biofilm formation ability and thus the development of novel therapies aimed at specifically targeting biofilms is needed.[6]

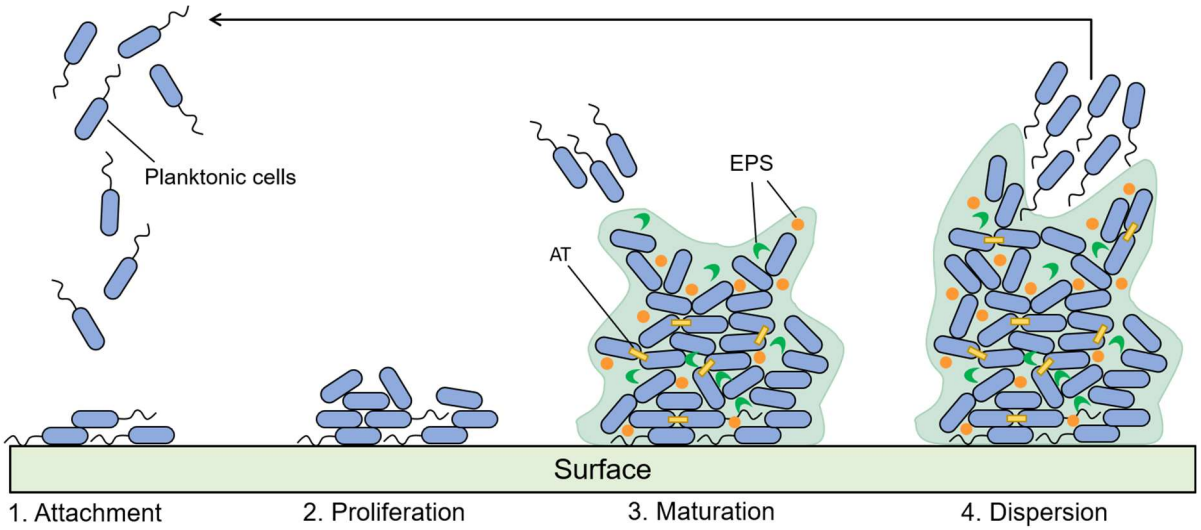

Figure 4.1: Schematic diagram summarising the four stages of biofilm formation. Autotransporters (ATs) are a group of proteins important for virulence and adhesion. Extracellular polymeric substances (EPS) include lipids, nucleic acids and polysaccharides. Figure adapted from "Role of bacterial efflux pumps in biofilm formation" by Rahman *et al.*[4]

4.2.2 Antifouling Surface Coatings

Recent studies in the field of antifouling materials have focussed on the development of surface coatings to inhibit the formation of biofilms.[7] The so-called superhydrophobic, also known as ultrahydrophobic, surface coatings are one of the widely reported types of antibiofouling surface coatings. Materials with high water contact angles (WCA) (> 150°) and low sliding angles (< 5°) are often classified as superhydrophobic.[8]

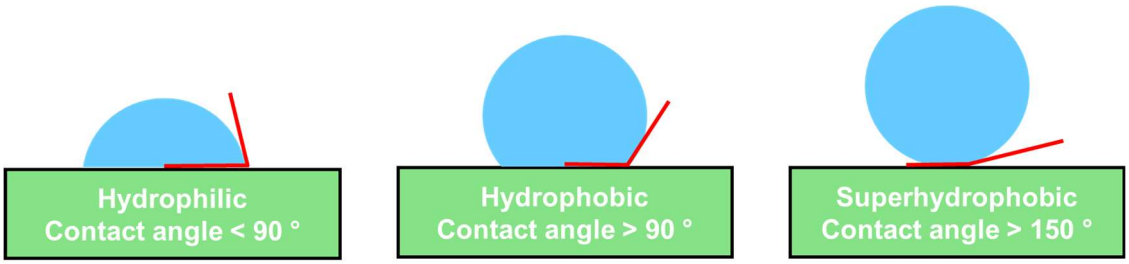

Figure 4.2: Schematic of the water contact angles associated with hydrophilic, hydrophobic and superhydrophobic surfaces.

Superhydrophobic surfaces are often self-cleaning, such as the surface of the lotus leaf whereby contaminants are trapped in water droplets that fall onto the leaf and are subsequently removed from the surface by the rolling of the droplet off the surface.[9] Non-wetting surfaces can be explained by the Cassie-Baxter and Wenzel states of wetting. Both Cassie-Baxter and Wenzel

found that the wettability of surface depends on the topography of the surface, not just on the free energy of the surface.[10,11] The models describe the wetting of surfaces that consist of nanotopographies, or simply 'rough' surfaces. The Wenzel model (Figure 4.3) describes the scenario where a water droplet on a rough surface can penetrate the topographies of the surface, thus allowing high-adhesive forces between the surface and the droplet.[10,12] To describe superhydrophobicity, which exhibits low-adhesive forces between liquid and the surface, the Wenzel model is replaced with the Cassie-Baxter state of wetting (Figure 4.3). In the Cassie-Baxter model, water droplets placed onto a rough surface do not penetrate the topographies. This leads to the trapping of air in the voids between the grooves of the rough surface. The water droplet is in contact with a lower surface area of the surface, and thus will have low-adhesion to the surface.[11,12]

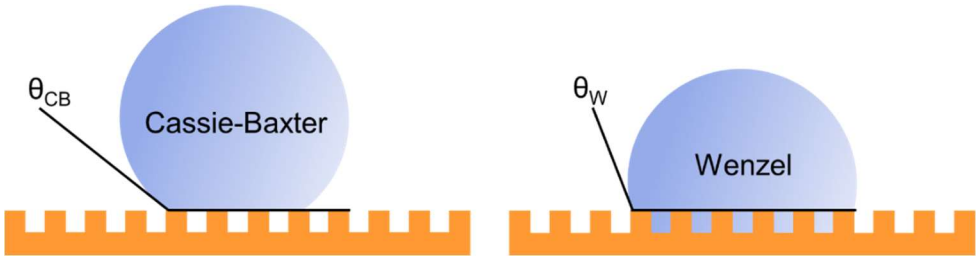

Figure 4.3: A schematic showing the Cassie-Baxter and Wenzel wetting states on a nanostructured surface.[13]

Superhydrophobic surfaces have many potential applications, such as for self-cleaning surfaces[14], anti-icing coatings [15,16], oil-water separation devices [17], coatings for stain-resistant fabrics [18] and corrosion-protective coatings amongst others.[19] Superhydrophobic surfaces also have the potential to be used for biomedical applications, particularly as surfaces to inhibit bacterial adhesion and protein adsorption.[20] The inhibition of bacterial adhesion is particularly important to prevent the formation of biofilms on implanted medical devices such as catheters and orthopedic implants.[21] Superhydrophobic materials have also been reported to have applications as novel wound dressings that have been found to prevent blood loss due to limiting blood wetting and reducing bacterial attachment.[22]

The development of low-cost methods suitable for large-scale preparation are of particular interest when investigating novel antibiofouling surfaces. Among many of the methods investigated for such surface coatings, it is thought that one of the most promising methods is spray coatings of hydrophobic nanoparticles.[23] Fluorinated hydrophobic coatings have been shown to be particularly successful in decreasing bacterial attachment to surfaces and to inhibit protein adhesion which is often problematic in the development of novel nanomedicines, however perfluorinated compounds often found in such coatings can be toxic and can bioaccumulate. The need for more environmentally friendly coatings which are low-cost and scalable are therefore highly desirable for antibiofouling surface coatings.[24,25] Inverse vulcanised polymers can be made purely from otherwise waste materials or from a combination of waste materials and bio-derived compounds in high yields, at low-cost without the use of solvents. The porous polysulfide of sulfur and canola oil reported by Worthington *et al.* was shown to have a WCA of 130° ± 10° averaged over 15 measurements, with a maximum individual measurement of 156°. These results suggest that inverse vulcanised polymers could indeed be hydrophobic with the possibility of being superhydrophobic with sufficient nano-roughness at the surface.[26]

4.2.3 Sulfur Polymers as Surface Coatings

With the expansion of the research regarding inverse vulcanised polymers, in recent years the fabrication of surface coatings of inverse vulcanised polymers has increased in interest. As mentioned in both Chapter 1 and Chapter 2, Deng *et al.* investigated the use of sulfur polymers for biomedical applications.[27] The study involved investigating the antibacterial activity of thin films of S-DIB, which were prepared by spin coating solutions of S-DIB onto silicon wafers. The coatings were analysed by X-ray photoelectron spectroscopy (XPS) to determine the composition at the surface, and the film thickness was measured using atomic force microscopy. XPS analysis showed that the sulfur content at the air-polymer

interface was lower than expected, and it was proposed that the carbon rich segments of the polymeric material moved to the surface to minimise the surface energy of the film. The films were found to be hydrophobic in nature, with larger water contact angles upon increasing the DIB content of the material.[27]

Mann *et al.* aimed to fabricate surface coatings of S-DCPD, a polymer that is normally insoluble in common organic solvents due to its high crosslinking density and thus prevents post-polymerisation processing of the polymer by solution based methods.[28] To prepare coatings of S-DCPD by circumventing the issue of insolubility, sulfur was first reacted with the more reactive norbornene alkene of DCPD to form a linear polymer. The linear polymer was shown to be soluble in chloroform, which was then used to coat several surfaces including silica, aluminium, polyvinyl chloride and concrete.The coated substrates were subjected to thermal curing to form the crosslinked coating, by reaction of the pentene alkene unit of DCPD. S-DCPD coatings were able to capture toxic metals such as mercury, in addition to providing the coated surfaces with protection against corrosion, solvents and acids, demonstrating that the coating has the potential to be used for multiple applications.[28]

Combining inverse vulcanisation with silane chemistry has been shown to have potential in fabricating surface coatings of sulfur polymers.[29,30] Scheiger *et al.* reported the synthesis of high sulfur content polymers combined with silane functionality to give polymers with mild post-polymerisation processing conditions.[29] The polymer was synthesised by inverse vulcanisation of sulfur with styrylethyltrimethoxysilane (styTMS) (Figure 4.4). It was shown that the alkoxy functionality of styTMS was maintained after inverse vulcanisation, which enabled a polycondensation reaction triggered by mild acidic conditions to take place (Figure 4.4). Coating on several substrates including gold, silicon and glass by spin coating, dip coating and solution casting methods was achieved. The study showed that the film thickness of the resulting coatings could be controlled, down to a thickness of 15 nm. It was

proposed that such coatings could expand the use of sulfur polymers for optical applications, as the film thickness was found to affect the colour of the films, which could be used to alter the red/black colouration of sulfur polymers. Filter materials for mercury remediation were prepared by coating the polymer onto silica microparticles, and was found that the coated particles improved mercury uptake in comparison to pristine silica.[29] Although not demonstrated in the study, it was suggested that silane functional sulfur polymers could have potential applications in the fabrication of antibacterial surfaces.[29] The combination of inverse vulcanisation and silane chemistry was further expanded by Grimm *et al.* which demonstrated that inverse vulcanisation of vinylated silica particles results in high surface area materials that can be used for heavy metal remediation.[30]

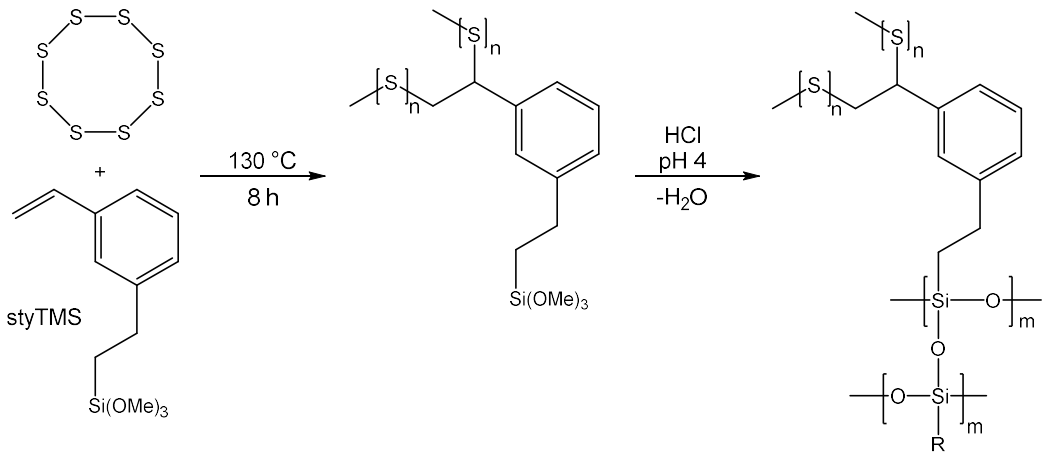

Figure 4.4: Reaction scheme of the inverse vulcanisation of sulfur with styryltrimethoxysilane (styTMS), followed by hydrolysis and polycondensation of the alkoxy functionality. From Scheiger *et al.*[29]

More recently, superhydrophobic coatings have been prepared from coating silica with S-DIB and 1H,1H,2H-perfluoro-1-octene (PFO).[31] To prepare surface coatings, glass and magnesium alloy surfaces were sprayed with an adhesive, before spray coating with the silica/S-DIB/PFO composite termed SiO_2@PSDP. The role of SiO_2 was to implement surface roughness to the coated surfaces, whereas PFO was chosen as a coating additive due to its low surface energy to aid achievement of a superhydrophobic surface. The WCA of the surface was

assessed, and it was found that SiO_2@PSDP indeed exhibited superhydrophobicity, with a maximum achieved WCA of 154.8°.[31] The self-cleaning ability of the surface was assessed by contaminating the sprayed surfaces with sand. The addition of water droplets to the contaminated surfaces returned the surface to its clean state, where the droplet was able to roll off the surface, picking up traces of sand as it rolled off. The anticorrosive properties of the coating were assessed by comparing pristine magnesium alloy to magnesium alloy coated with SiO_2@PSDP. It was found that the presence of SiO_2@PSDP coating reduced the corrosion of the surface when subjected to submersion in seawater. The antibacterial activity of dispersed SiO_2@PSDP particles was assessed against *E. coli* and *S. aureus*, which were shown to reduce the prevalence of both species by 75% and 81% respectively.[31] Miao *et al.* have expanded on the fabrication of superhydrophobic coatings using sulfur polymers.[32] Titanium nitride (TiN) nanoparticles were chosen due to their greater hydrophobicity compared to SiO_2, and the method allowed the preparation of fluorine-free coatings. The coating polymer was prepared by inverse vulcanisation of sulfur with 3,3'-(butane-1,4-diyl)bis(1-vinyl1H-imidazol-3-ium) bromide (VIMBr), an ionic liquid. Copolymerisation of sulfur and an ionic liquid was chosen due to the large anionic and cationic dipole moments of ionic liquids, which allows the coating of polar nanoparticles. In addition to this, ionic liquids have been reported to have antibacterial activity and good biocompatibility.[32]

4.3 Aims of Chapter

In Chapter 2, we demonstrate that high sulfur content polymers have antibacterial activity against both Gram-positive methicillin-resistant *S. aureus* and Gram-negative *P. aeruginosa*. High sulfur content polymers often are difficult to process after polymerisation due to their insolubility in most common solvents. Fabricating surface coatings of high sulfur content polymers may provide further scope for developing new applications such as for biomedical applications and environmental remediation by means of heavy metal uptake. In Chapter 3 we show that high sulfur content polymers can be formed into polymeric nanoparticles that exhibit antibacterial activity. Formulating polymeric nanoparticles of the bulk materials could enhance the applicability of the polymers due to their water dispersibility and could therefore be used to develop surface coatings. This chapter will discuss the fabrication of superhydrophobic coatings using inverse vulcanised polymers and their antibacterial activity, which at the start of this study had not been previously investigated.

Aims in summary:-

- Develop surface coatings of polymeric nanoparticles formulated and discussed in Chapter 3
- Fabricate surface coatings of silica-polymer composites
- Assess the antibacterial properties of coated surfaces
- Assess the antibiofilm properties of coated surfaces

4.4 Results and Discussion

The experimental details related to the results of this chapter are detailed in section 4.6.

4.4.1 Coatings of High-Sulfur Content Polymeric Nanoparticles

To achieve superhydrophobicity, many surfaces require morphologies that give the surface roughness.[33] Surface roughness can be achieved through various nanomorphologies such as nanorods, nanoflakes, nanofibres and nanoparticles.[8] High sulfur content polymers are commonly hydrophobic due to the hydrophobicity of sulfur. Nanoparticles of high sulfur content polymers can be fabricated to give monomodal size distributions, with z-average diameters of around 100-200 nm, as discussed in Chapter 3. The hydrophobicity of the polymers and the ability to form nanoparticles makes the materials suitable candidates to fabricate superhydrophobic surfaces of the polymeric nanoparticles. As discussed in section 4.2.2 Antifouling Surface Coatings, surface coatings are commonly fabrictaed by methods such as dip-coating, spin-coating and spray coating amongst others. Due to the <500 nm size of the high sulfur content polymeric nanoparticles formed in Chapter 3, and their dispersibility in water, a spray coating method was investigated to prepare surface coatings on glass. Spray coating was carried out using an airbrush gun attached to a compression pump. Spraying using an airbrush under compression results in the deposition of small water droplets on the surface, allowing the surface to dry quicker than simply depositing dispersions on the surface in larger volumes. The dispersions were sprayed onto glass slides layer by layer, allowing each layer to dry before spraying on the next layer. To assess the wettability of the surface, a crude test was conducted where drops of water were added to the coated surface and visually assessed. The surfaces were deemed suitable for determination of the water contact angle using a DSA100 Expert Drop Shape Analyser (Kruss GmbH), if the droplets did not smear and wet the surface. Glass coated with 1, 4 and 10 layers of dispersions of S50-PA (T_g of 34 °C) nanoparticles in water were found to be hydrophilic, similar to that of uncoated glass. This result was not

expected due to the hydrophobicity of bulk S50-PA (T_g of 34 °C) (Chapter 2). It was hypothesised that the nanoparticles become mobilised upon the addition of the water droplet, resulting in the water droplet coming in contact with the uncoated, hydrophilic glass surface. Adhesion of the particles to the surface could circumvent the issue of particle mobilisation when in contact with water. To encourage particle adherence to glass, the coated surfaces were heated in an oven at 140 °C for 30 minutes. The resulting surfaces had greater hydrophobicity (Figure 4.5) than the surfaces that had not undergone heat treatment.

Figure 4.5: Photograph of glass spray coated with S50-PA nanoparticles after heating at 140 °C.

The surfaces formed from spray deposition of S50-PA nanoparticles on glass were compared to those of the bulk polymer, which is expected to have a relatively smooth surface in comparison to the surface deposited with nanoparticles. The bulk polymer coating was prepared by pouring the molten pre-polymer on glass, followed by overnight curing at 140 °C to complete the polymerisation process. It was hypothesised that the surface coated with nanoparticles would have a higher water contact angle to that of the bulk polymer due to the expected increase in surface roughness. Both surfaces were found to have similar water contact angles in the region of 90-100°. The topography of the surfaces formed from spray deposition of S50-PA nanoparticles with and without heat treatment at 140 °C were investigated by SEM. Spray deposition of particles in the absence of thermal treatment showed that the shape and size of particles was unaltered by the spraying process (Figure 4.6), when compared to the dispersions formed in Chapter 3 (Figure 3.21). SEM imaging of the heat treated surfaces shows

a different topography to that of the particles that were not heat treated (Figure 4.7). Large aggregates that do not represent particles were seen throughout imaging of the heat treated surface. The topography is more consistent to that of bulk material than nanoparticles. It is likely that the thermal treatment was conducted at too high of a temperature and for too long, thus transforming the nanoparticles into bulk material. This transition from nanoparticle to bulk may explain why the water contact angles of the heat treated surfaces are similar to that of the bulk material.

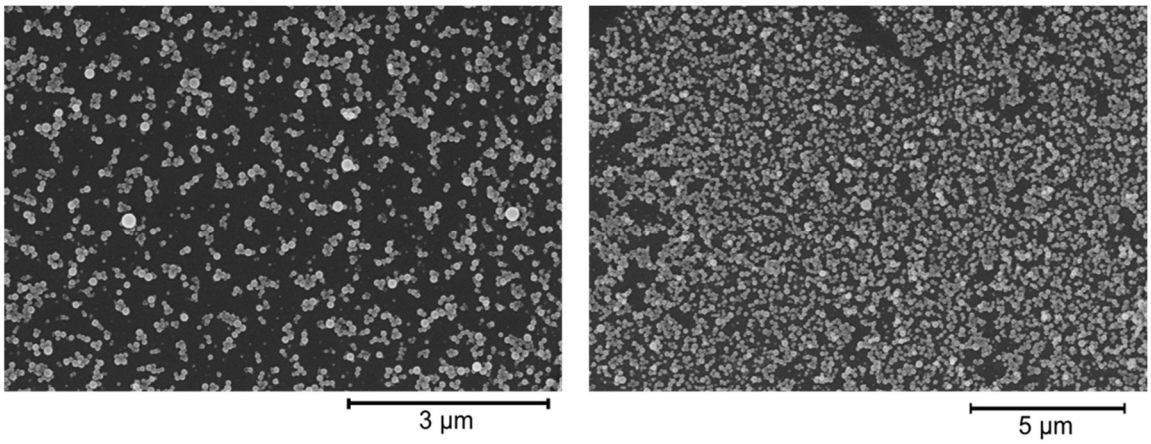

Figure 4.6: SEM image of S50-PA nanoparticles spray coated onto silicon wafer chips.

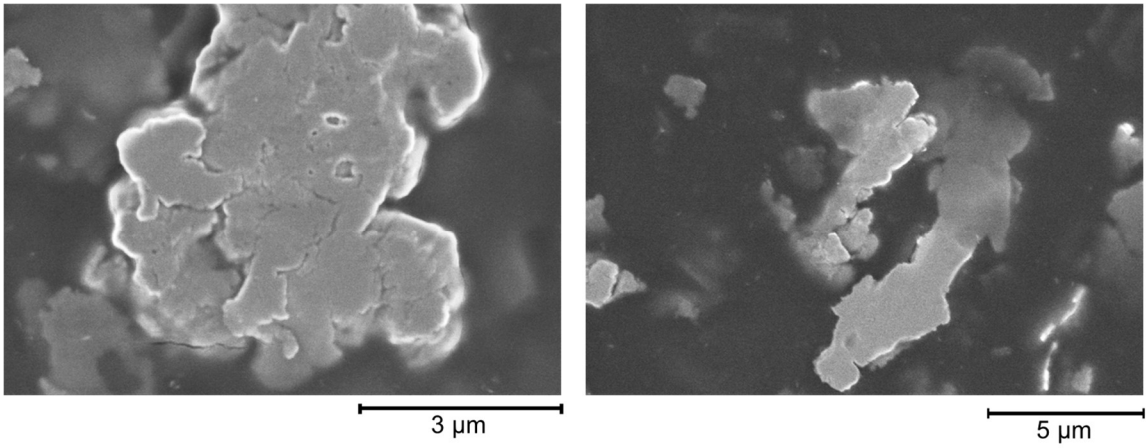

Figure 4.7: SEM image of S50-PA nanoparticles spray coated onto silicon wafer chips after heating at 140 °C for 30 minutes.

4.4.2 Coatings of Silica-Polymer Composites

High sulfur content polymer nanoparticles have the potential to be used to fabricate superhydrophobic surfaces, however, further optimisation needs to be carried out to circumvent the issue of poor adherence of particles to the substrate and poor thermal stability. Another method to fabricate surface coatings using high sulfur content polymers is to use a different nanoparticle which acts as a scaffold for the polymer to coat, this composite could then be coated onto a substrate. Wu *et al.* demonstrated that silica-gel could be coated with sulfur-limonene copolymers to form functionalised silica.[34] The coated silica was used as a filtration system for mercury and gold uptake.[34] The method of coating consisted of solubilising the copolymer followed by the addition of silica-gel. The solvent was removed by rotary evaporation, resulting in the formation of a powder. Following a similar method, fumed silica with particle average particle sizes between 200 and 400 nm (Figure 4.8) was coated with S50-PA (T_g of 34 °C). Silica and polymer ratios were varied from 90:10, 70:30 and 50:50, and the resulting composites were denoted Si(X)-S50PA(Y) where X=weight% of silica, and Y=weight% of S50-PA. The motivation behind using fumed silica was to prepare particles coated with high sulfur content polymers that could be dispersed in solvents such as water or ethanol for spray coating. The hypothesis was that the polymer would act as a 'glue' to adhere the silica particles to the surface following thermal treatment, as demonstrated by the increased adhesion of the polymeric nanoparticles to glass. Using silica as a scaffold would provide the surface with roughness, and may be able to retain that roughness after thermal treatment, as demonstrated by the ability of silica to act as a nanocrucible for gold nanoparticles.[35]

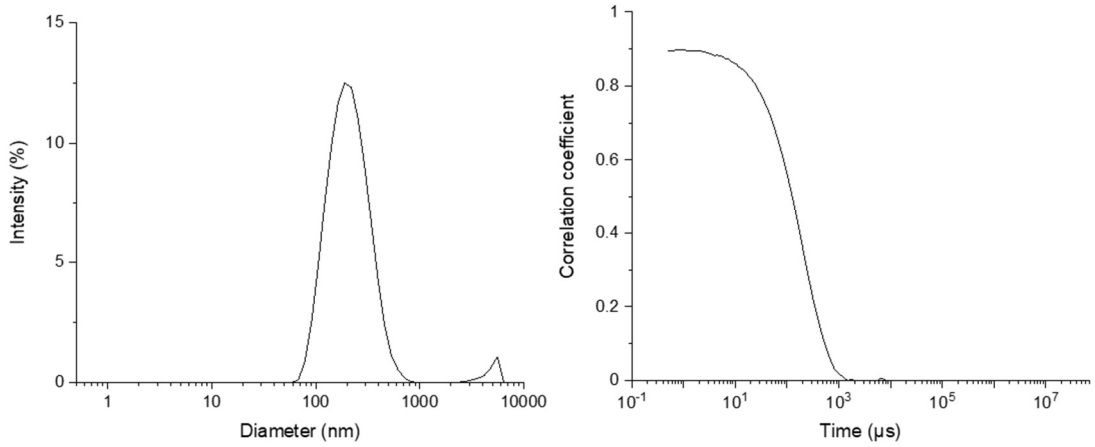

Figure 4.8: DLS trace and correlogram of as-received fumed silica dispersed in water.

As-received fumed silica and the functionalised samples with silica:S50-PA ratios of 90:10, 70:30 and 50:50 were analysed by FT-IR spectroscopy (Figure 4.9). The characteristic peaks for silica are present at approximately 1100 cm^{-1} and 790 cm^{-1} due to asymmetric and symmetric Si-O-Si stretching vibrations respectively, are present in the spectra of all samples.[36] Peaks present in the region of approximately 2800-3000 cm^{-1} are present in the spectra of the functionalised silica samples, but absent in the spectrum of as-received fumed silica. These signals are present in the FT-IR spectrum of bulk S50-PA (Figure 2.7), and may be attributed to alkane C-H stretching vibrations provided by perillyl alcohol units within the polymer. The analysis suggests successful coating of fumed silica with S50-PA. DSC analysis of Si(50)-S50PA(50) (Figure 4.10) shows a transition consistent with that of the glass transition temperature of bulk S50-PA in the region of 30 °C further confirming successful coating of silica.

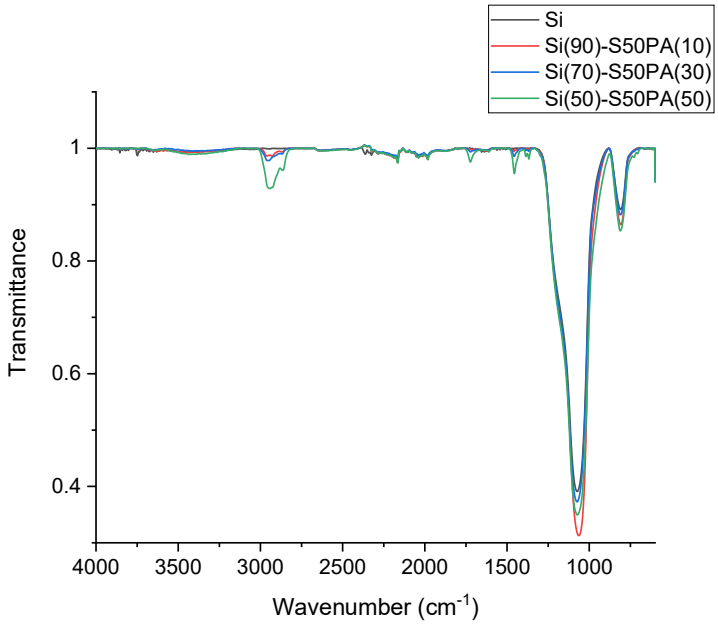

Figure 4.9: FT-IR spectra of as received silica (Si), and silica coated with S50PA, denoted Si(X)-S50PA(Y) where X and Y represent the weight % of silica and S50-PA in the composite (X=90, 70 or 50, and Y=10, 30 or 50).

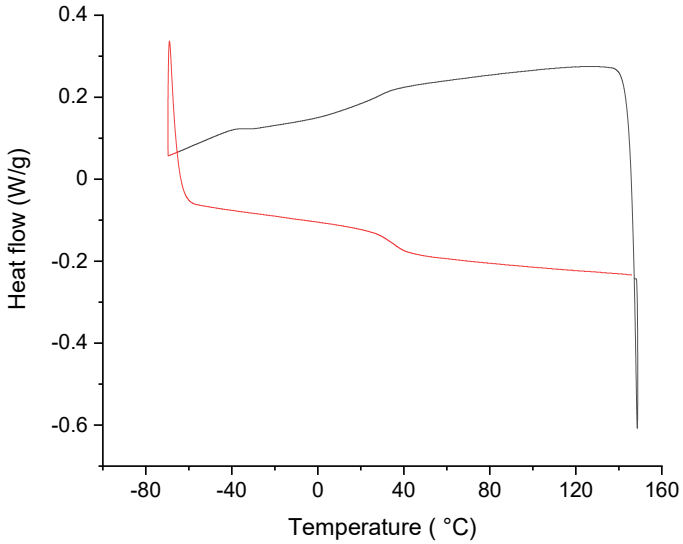

Figure 4.10: DSC trace of Si(50)-S50PA(50) composite.

Fumed silica and Si(X)-S50PA(Y) composites were dispersible in water upon sonication. Longer sonication times were required to disperse composites with higher S50-PA content, likely due to the hydrophobicity of the polymer relative to hydrophilic silica. Due to their dispersibility, the antibacterial activity of the composites and fumed silica were assessed against methicillin-resistant *S. aureus* (strain USA300) (Figure 4.11). This was done by dispersing the powdered samples to 1 and 5 mg/ml in the bacterial culture, followed by incubation for 5 h at 37 °C. At 1 mg/ml, Si(50)-S50PA(50) and Si(70)-S50PA(30) were found to inhibit *S. aureus* by >80%, whereas Si(90)-S50PA(10) was found to inhibit *S. aureus* by approximately 35% (Figure 4.11). As-received functionalised silica was found to have no inhibitory effect against *S. aureus* at 1 mg/ml. Increasing the composite concentration to 5 mg/ml in the bacterial culture resulted in an increase in the inhibitory effect of Si(90)-S50PA(10) composite, likely due to the increase in overall polymer content within the culture medium. The results show that Si(X)-S50PA(Y) composites have antibacterial activity, however, this effect is dependent on the polymer content of the composite, suggesting that it is the polymer that is responsible for the antibacterial activity of the composites.

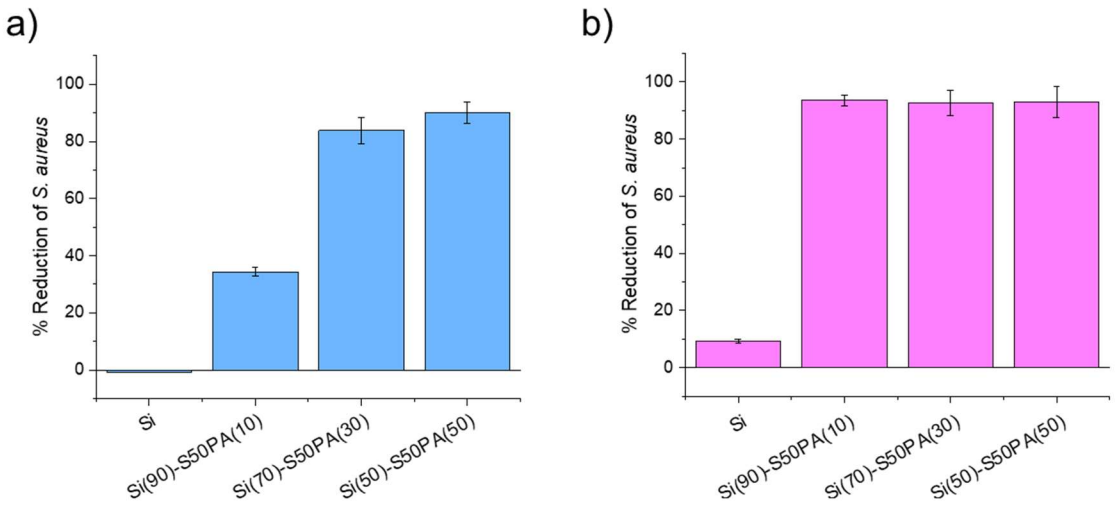

Figure 4.11: Antibacterial activity of silica and Si(X)-S50PA(Y) composite powders at a) 1 mg/ml composite in culture and b) 5 mg/ml composite in culture. Antibacterial activity is expressed as the % reduction in viable *S. aureus* compared to an untreated culture.

Due to the dispersibility of Si(X)-S50PA(Y) composite powders, the fabrication of superhydrophobic surfaces by spray deposition was investigated. The composites were dispersed in ethanol (1 mg/ml) and loaded into an airbrush attached to a compression pump. The dispersions were sprayed onto glass slides at a pressure of 2 bar and a working distance of approximately 10 cm. A simple trial was conducted to assess the hydrophobicity of the composites at varying silica:polymer ratios by spraying 4 layers of the dispersion onto glass, before assessing the water contact angles produced when dropping water onto the surface. It was found that the hydrophobicity was greatest for glass coated with Si(50)-S50PA(50), followed by Si(70)-S50PA(30) and Si(90)-S50PA(10). It is expected that the composites become more hydrophobic with increasing polymer content due to the hydrophobicity of the polymer and the hydrophilicity of the unfunctionalised fumed silica. Si(50)-S50PA(50) was chosen for further investigations into the fabrication of superhydrophobic surface coatings. The number of layers that were sprayed onto the surface were assessed by comparing 3 layers and 10 layers, along with the effect of thermal treatment at 140 °C. It was hypothesised that the silica-polymer composites may also have some mobility upon the addition of water to the surface, similar to the polymeric nanoparticles, that may be circumvented by thermal treatment. Without thermal treatment, the surfaces coated with 3 layers and 10 layers of Si(50)-S50PA(50) had very similar water contact angles of approximately 80 ° (Table 4.1). Heat treatment at 140 °C was found to increase the obtained WCA for the samples, particularly for surfaces coated with 10 layers of the dispersion. Similarly to the polymeric nanoparticles discussed in section 4.4.1, it is thought that thermal treatment enhances the adhesion of the particles to the surface, resulting in lower particle mobility and therefore increased hydrophobicity.

Table 4.1: Summary of the water contact angles (WCA) obtained from surfaces coated with different number of layers with and without thermal treatment.

	Number of layers	Cured at 140 °C	WCA (°)
1	3	X	82.2 ± 4.6
2	3	✓	97.9 ± 5.9
3	10	X	79.6 ± 8.6
4	10	✓	137.5 ± 12.5

The evaporation of nanoparticle dispersions on a surface usually results in the particles aggregating in rings, known as the coffee-ring effect.[37] Immobilised particles on a surface are not expected to form ring-like aggregates as they are unable to move as the dispersive medium evaporates. Therefore the mobility of the particles on the surface before and after thermal treatment was assessed by SEM imaging. Water droplets were added to the surfaces, which were expected to result in the formation of rings if the particles were mobile. Images of the surfaces that had not undergone thermal treatment show ring-like aggregation patterns of the coated silica particles after the addition of a water droplet to the surface, consistent with that of mobile particles (Figure 4.12). No ring-like aggregation patterns of the particles were found on the surfaces which had undergone thermal treatment (Figure 4.13). It is likely that the thermal treatment promotes better adhesion of the composite particles to the surface, which increases the hydrophobicity of the coated surface.

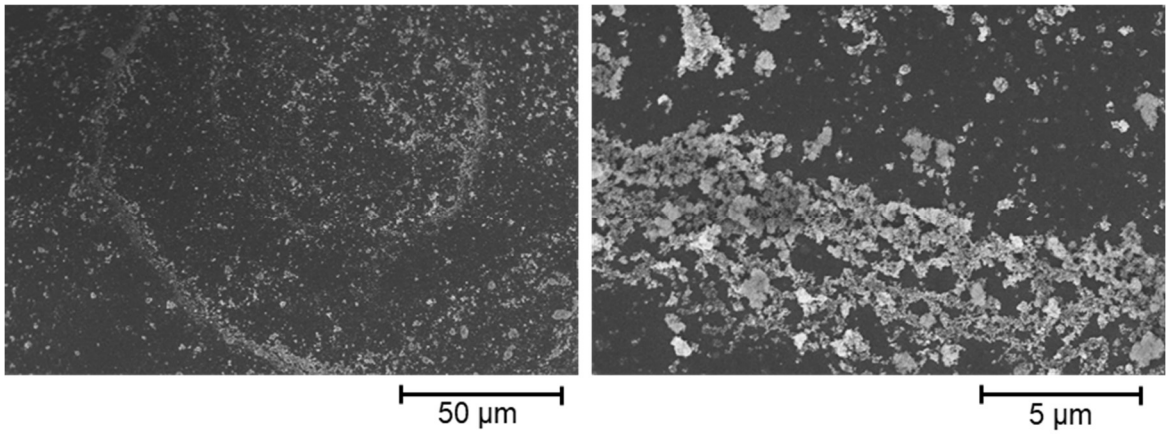

Figure 4.12: SEM images of surface coated with Si(50)-S50PA(50) with no thermal treatment after addition of a water droplet.

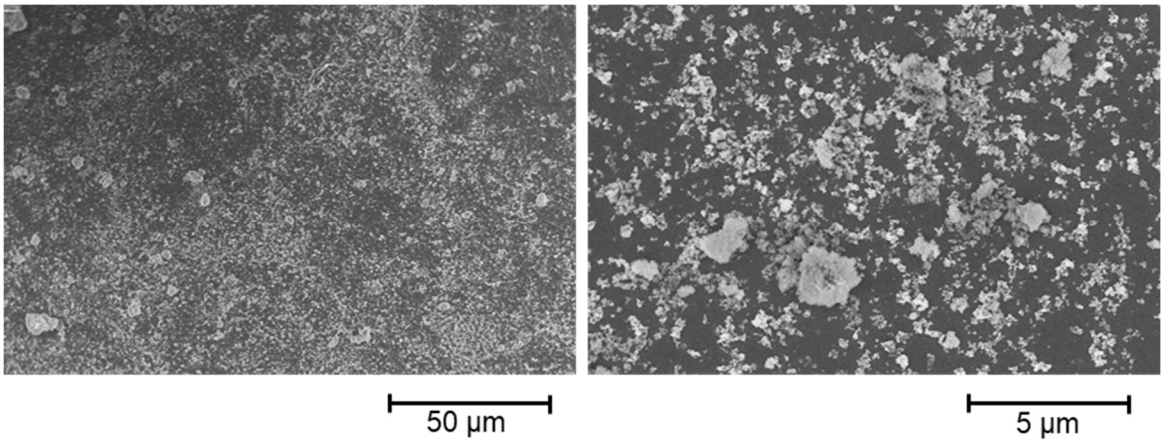

Figure 4.13: SEM images of surface coated with Si(50)-S50PA(50) with thermal treatment at 140 °C after addition of a water droplet.

Despite spraying 10 layers of Si(50)-S50PA(50) composite on glass with thermal treatment, the highest obtained WCA was (137.5 ± 12.5)°, short of what can be deemed superhydrophobic. It is likely that superhydrophobicity has not been achieved with these formulations due to incomplete coating of the silica particles with polymer, which will result in some small hydrophilic areas which will promote the wetting of the surface. We hypothesised that the composite could be made more hydrophobic by increasing the polymer content of the polymer, however, the dispersibility of the composites are compromised as larger aggregates are formed which could block the spray nozzle of the airbrush or form non-uniform surfaces. To circumvent this issue, silica was functionalised with hexamethyldisilazane (HMDS) to increase the hydrophobicity of the silica particle. HMDS increases the hydrophobicity of silica particles by replacing surface hydroxyl groups with trimethylsilyl functionality (Figure 4.14).[38,39]

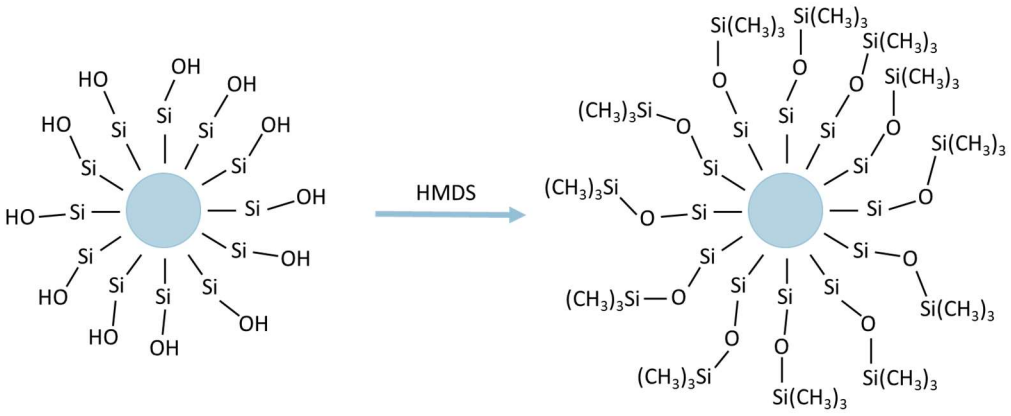

Figure 4.14: Schematic of the surface modification of silica nanoparticles with HMDS, as depicted by Zhang *et al.*[40]

FT-IR analysis of the HMDS-modified silica particles (denoted Si[HMDS]) show signals at ~850 and ~740 cm^{-1}, which can be attributed to Si-C stretching vibrations and CH_3 rocking, respectively (Figure 4.15).[41] The hydrophobicity of Si[HMDS] was crudely assessed by dispersing the powder into water. Where the unmodified fumed silica dispersed readily in water, Si[HMDS] particles did not disperse and remained at the water-air interface (Figure 4.16).

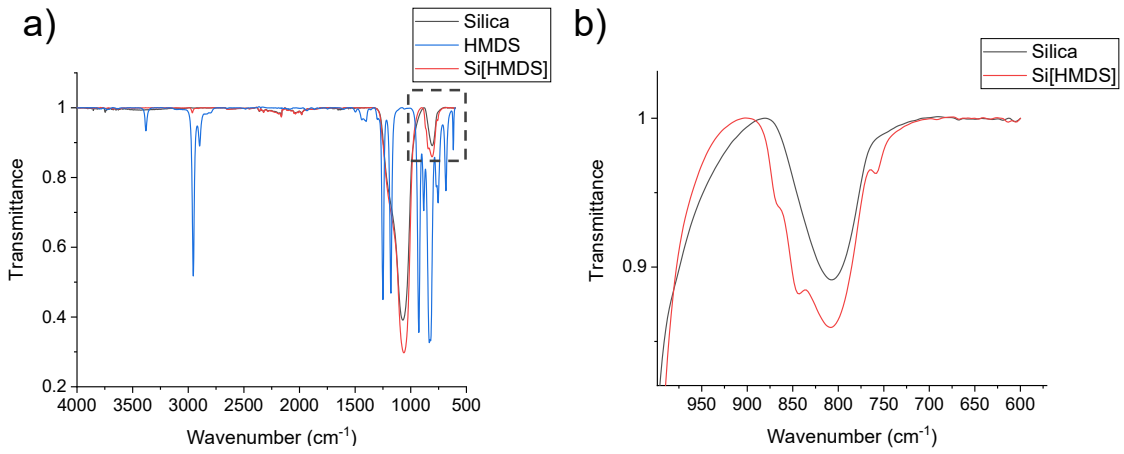

Figure 4.15: FT-IR spectra of a) silica, HMDS and Si[HMDS] and b) a zoom up of the spectra of silica and Si[HMDS] showing the new signals at ~850 and ~740 cm^{-1}, which can be attributed to Si-C stretching vibrations and CH_3 rocking, respectively.[41]

Figure 4.16: Photograph of vials containing unmodified fumed silica (left) and HMDS-modified silica (right) dispersed in water dyed with Brilliant Blue R.

In collaborative work, we reported that superhydrophobic spray coatings could be prepared by spray deposition of HMDS-modified silica and S-PA dissolved in a suitable solvent.[42] The composite coatings were prepared by grinding the polymer into a fine powder and dissolving in chloroform, to which Si[HMDS] was added. The suspensions were stirred and loaded into an airbrush gun, and sprayed onto the surface of glass at 60 °C. The highest obtained WCA of the coated surfaces were observed in general with higher sulfur content of the polymer (S70-PA > S60-PA > S50-PA). The highest achieved WCA was found for composite coatings using S70-PA, with a WCA of (169 ± 1) °.[42] Elemental sulfur was present in SEM images of the composite coating formed from S70-PA, and was proposed that the sulfur content of the polymer was too high to endure re-processing into a composite.[42] The antibacterial activity of the composite formed from S60-PA was assessed against methicillin-resistant *S. aureus*. It was found that the composite coating was more effective at inhibiting *S. aureus* on its surface than bulk S60-PA. This result was attributed to the reduced surface area as a result of the Cassie-Baxter state, leading to fewer attachment sites for bacteria on the surface.[42] The surface was also found to have photocatalytic behaviour, where, during exposure to UV radiation, resazurin dye became reduced to resorufin (colour change from blue to pink) within 40 minutes.[42]

To avoid using toxic solvents such as chloroform for spray deposition of the composites, instead of spraying a suspension of polymer and silica in chloroform as described above, Si[HMDS] was first coated with S50-PA. Coating of Si[HMDS] with S50-PA was achieved by stirring Si[HMDS] in a solution of S50-PA in THF, followed by solvent removal. Coating of Si[HMDS] with S50-PA was confirmed by FT-IR by the presence of signals corresponding to S-PA in the composite spectrum (Appendix 4.1). Si[HMDS] was coated with S50-PA polymer at a silica:polymer mass ratio of 50:50, forming a pale yellow powder denoted Si[HMDS](50)-S50PA(50), as for the unmodified silica coated composites. The hydrophobic composite powders were dispersible in ethanol after sonication for 1 minute using a probe sonicator. The dispersons were sonicated over ice to limit the evaporation of ethanol during sonication and to prevent a rise in temperature that may cause the particles to aggregate. The dispersed hydrophobic composites were loaded into an airbrush gun attached to a compression pump, as for the unmodified silica composites, and were sprayed onto glass at a working distance of ~10 cm. The glass substrates were heated on a heating block set to 100 °C, and the dispersions were sprayed directly onto the heated glass. A total of 3 layers were sprayed, allowing each previous layer to completely dry before spraying on the next. The coating of Si[HMDS] with S50-PA first requires the polymer to be dissolved in a suitable solvent such as THF or chloroform, however, the volume of toxic solvents used in the process can be reduced as spraying can be done in ethanol. Pre coating silica with polymer also offers better long-term storage of the composite. The powdered composites can be used directly in some applications as discussed above, where silica-polymer composite powders were found to be antibacterial, or it can be redispersed when it is required for spray coating. The hydrophobicity of the coated surface was assessed by adding water droplets to the surface and compared to uncoated glass (Figure 4.17). Water droplets added to the coated surface would bounce and were easily rolled off the surface by tilting the surface, consistent with the properties of a superhydrophobic surface. In

contrast, the droplets on uncoated glass smeared out onto the surface, as expected for a hydrophilic surface (Figure 4.17). The surface coated with Si[HMDS](50)-S50PA(50) was found to have contact angles of ~170 ° (Figure 4.18), and sliding angles of ~6 °. The surface can therefore be characterised as superhydrophobic.

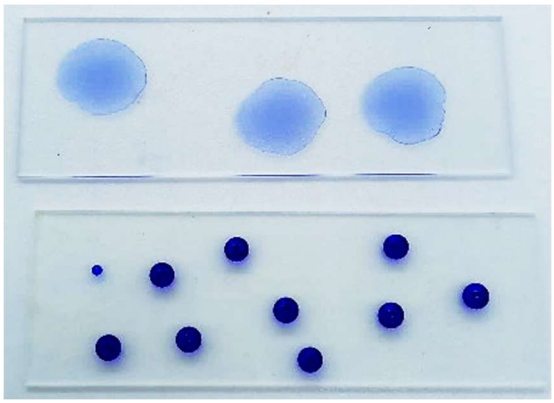

Figure 4.17: Photograph of uncoated glass (top) and glass coated with Si[HMDS](50)-S50PA(50) (bottom) after the addition of water droplets dyed with methylene blue.

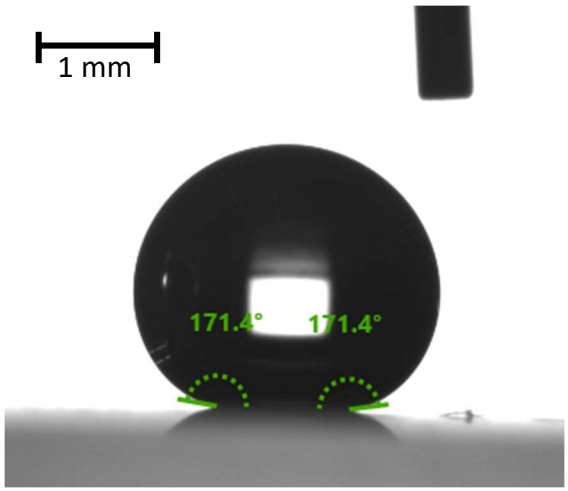

Figure 4.18: Image of a 5 µl water droplet on the surface of glass coated with Si[HMDS](50)-S50PA(50), with a water contact angle of 171.4 °.

The antibacterial activity of surfaces coated with both Si(50)-S50PA(50) and the superhydrophobic Si[HMDS](50)-S50PA(50) were assessed against methicillin-resistant *S. aureus* (Figure 4.19). The inhibition of cells on the sample surface and cells within the surrounding medium were enumerated. A 'smooth' S50-PA coating was prepared as a comparitive control for the roughness given by the nanoparticles. The smooth coating was

prepared by polymerising perillyl alcohol with sulfur, once homogeneous the mixture was poured onto glass before curing overnight. Fumed silica and Si[HMDS] were also used to coat glass by spray deposition, to investigate the influence of the polymer on the roughened surfaces. Glass coated with fumed silica did not show an inhibitory effect against viable *S. aureus* compared to uncoated glass. Si[HMDS] coating showed an approximately 1 log reduction in viable *S. aureus* on its surface, however did not show an inhibitory effect against viable cells in the surrounding medium. The hydrophobicity of the surface of Si[HMDS] coated glass may render the surface less favourable for bacterial adhesion compared to uncoated glass. Glass coated with Si(50)-S50PA(50) shows an inhibitory effect against cells on the surface and in the surrounding medium, although lower than that of the smooth S50PA control. The differences between S50PA control and Si(50)-S50PA(50) could be due to differences in the coating thickness, where the thickness of the smooth control coating was visibly much thicker than that of the spray coated surfaces. Glass coated with hydrophobic Si[HMDS](50)-S50PA(50) showed the greatest inhibition of viable cells on the surface and in the surrounding medium, despite being made of only 4 sprayed layers of composite compared to the smooth surface which was thicker.

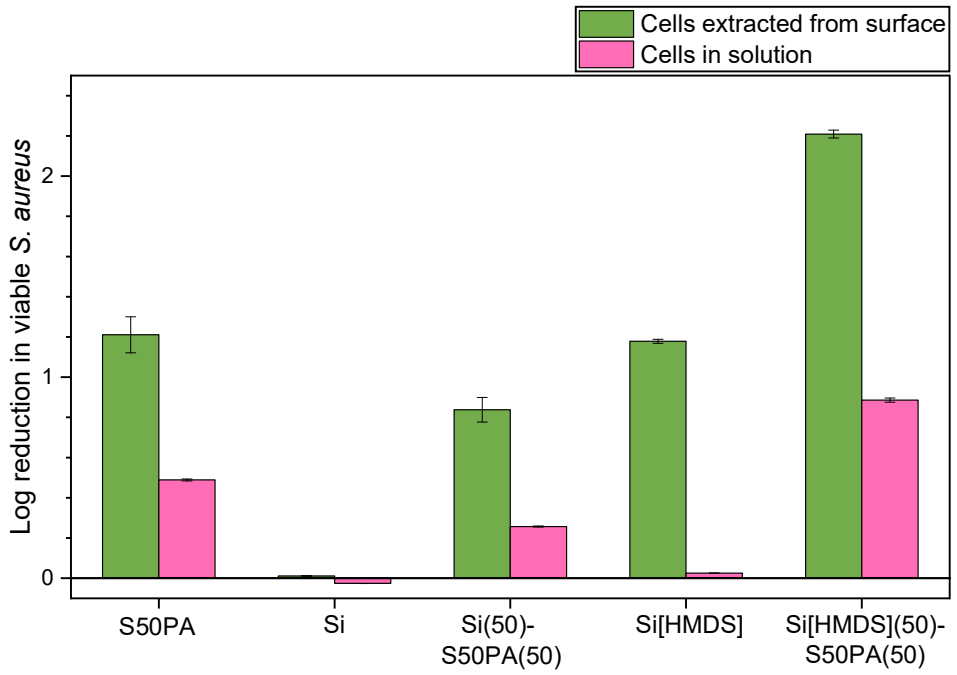

Figure 4.19: The log reduction in viable *S. aureus* on the sample surface (green) and cells surrounding the samples (pink) of several coated surfaces compared to uncoated glass.

The antibiofilm activity of the coated surfaces were assessed against *S. aureus* (USA300) (Figure 4.20) and *P. aeruginosa* (PAO1) (Figure 4.21). This was done in a similar method to that used to investigate the antibiofilm activity of 1 cm^3 bulk polymers discussed in Chapter 2. In brief, 1 cm x 1 cm surfaces were submerged in bacterial culture and were statically incubated for 5, 24 and 48 h at 37 °C. The samples were removed, rinsed with PBS and stained with crystal violet. The samples were rinsed thoroughly with water, and the crystal violet was solubilised in ethanol. The absorbance of the solubilised crystal violet was measured, higher values are indicative of more biofilms on the sample surface. At all incubation periods, uncoated glass and glass coated with fumed silica showed the largest amount of biofilm on their surface when assessed against both *S. aureus* and *P. aeruginosa*. On average, the biofilms on the surface of Si(50)-S50PA(50) and the superhydrophobic Si[HMDS](50)-S50PA(50) are lower than that of bulk S50-PA, however, these surfaces are not directly comparable as the coating thickness of S50-PA is much thicker than that of the spray coated composite coatings. It was hypothesised that the antibiofilm activity of the superhydrophobic Si[HMDS](50)-

S50PA(50) coating was greater than that of Si(50)-S50PA(50). When assessed against S. aureus, the superhydrophobic coating has greater antibiofilm activity compared to Si(50)-S50PA(50) after 5 and 24 h, however, after 48 h both surfaces show similar antibiofilm activity. The superhydrophobicity of the coating may not be resistant to submerging in liquids for prolonged periods of time, which may result in surface wetting over time. Overall, the results show that coatings of high sulfur content polymers have antibiofilm actvitiy compared to uncoated surfaces.

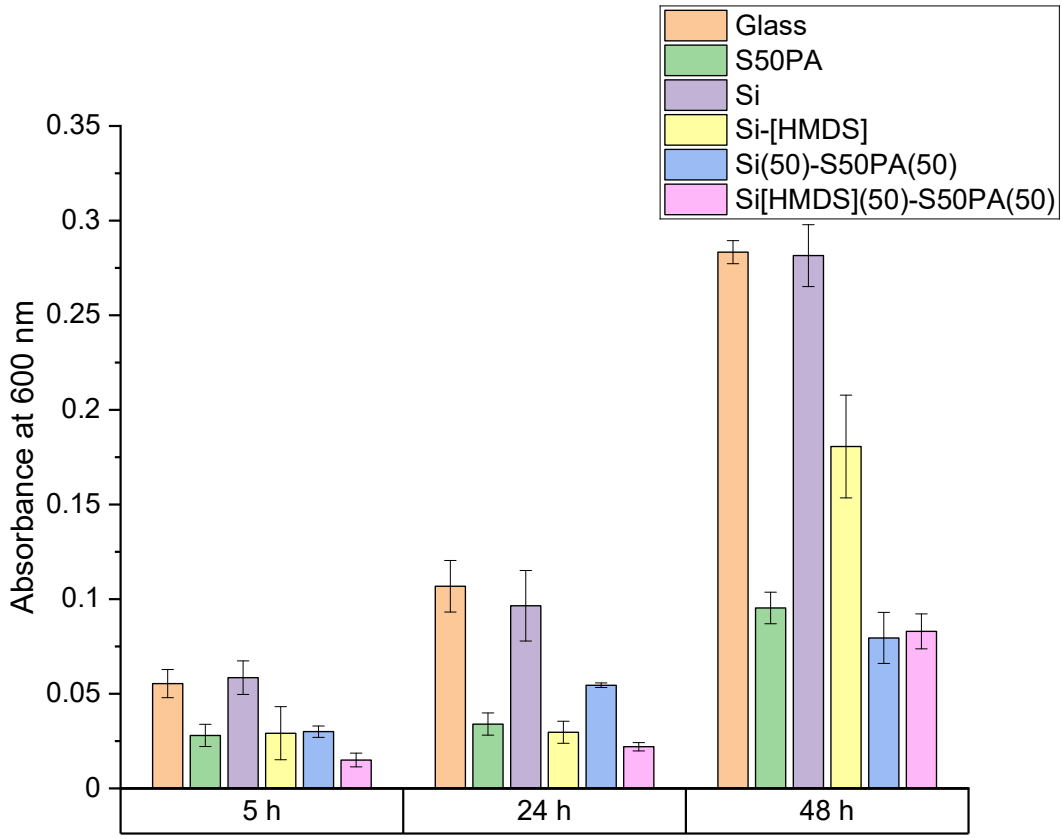

Figure 4.20: Absorbance at 600 nm for uncoated glass, and glass coated with bulk S50-PA, fumed silica (Si), hydrophobic silica (Si-[HMDS]), Si(50)-S50PA(50) and Si[HMDS](50)-S50PA(50) composites after staining with crystal violet after 5, 24 and 48 incubation with *S. aureus* (USA300).

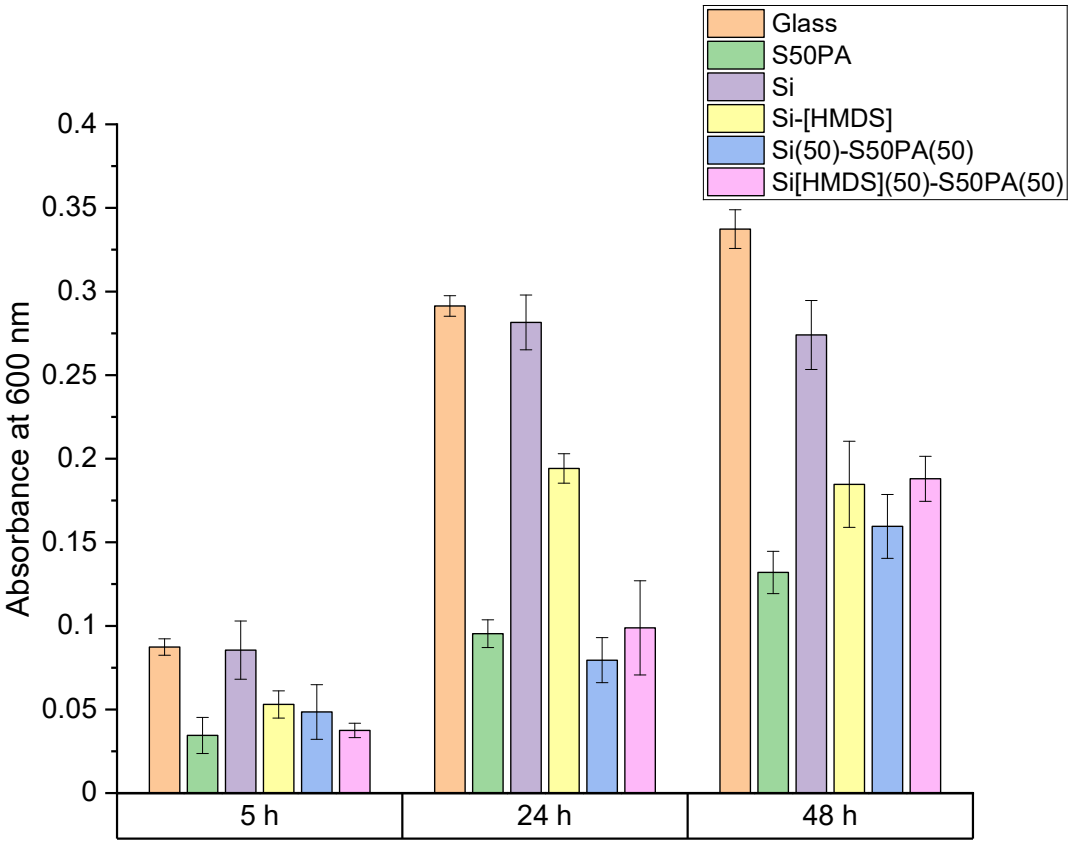

Figure 4.21: Absorbance at 600 nm for uncoated glass, and glass coated with bulk S50-PA, fumed silica (Si), hydrophobic silica (Si-[HMDS]), Si(50)-S50PA(50) and Si[HMDS](50)-S50PA(50) composites after staining with crystal violet after 5, 24 and 48 incubation with *P. aeruginosa* (PAO1).

Uncoated glass and glass coated with superhydrophobic Si[HMDS](50)-S50PA(50) were imaged by SEM before and after 5 h incubation with methicillin-resistant *S. aureus* (Figure 4.22). Pristine glass has a relatively flat surface with very few morphologies present, whereas glass coated with Si[HMDS](50)-S50PA(50) composite was found to have a roughened surface with very small particles present. After incubation with *S. aureus*, the surface of glass coated with the composite appeared unchanged. In contrast, many spherical species with approximate diameters of 500-1000 nm can be seen on the surface of glass after incubation with *S. aureus*. The spherical species are consistent with *S. aureus* cells, that often aggregate in pairs, chains and grape-like clusters, as shown in Figure 4.22.[43] This demonstrates that coating of glass with Si[HMDS](50)-S50PA(50) can reduce the prevalence of *S. aureus* on surfaces compared to an uncoated surface.

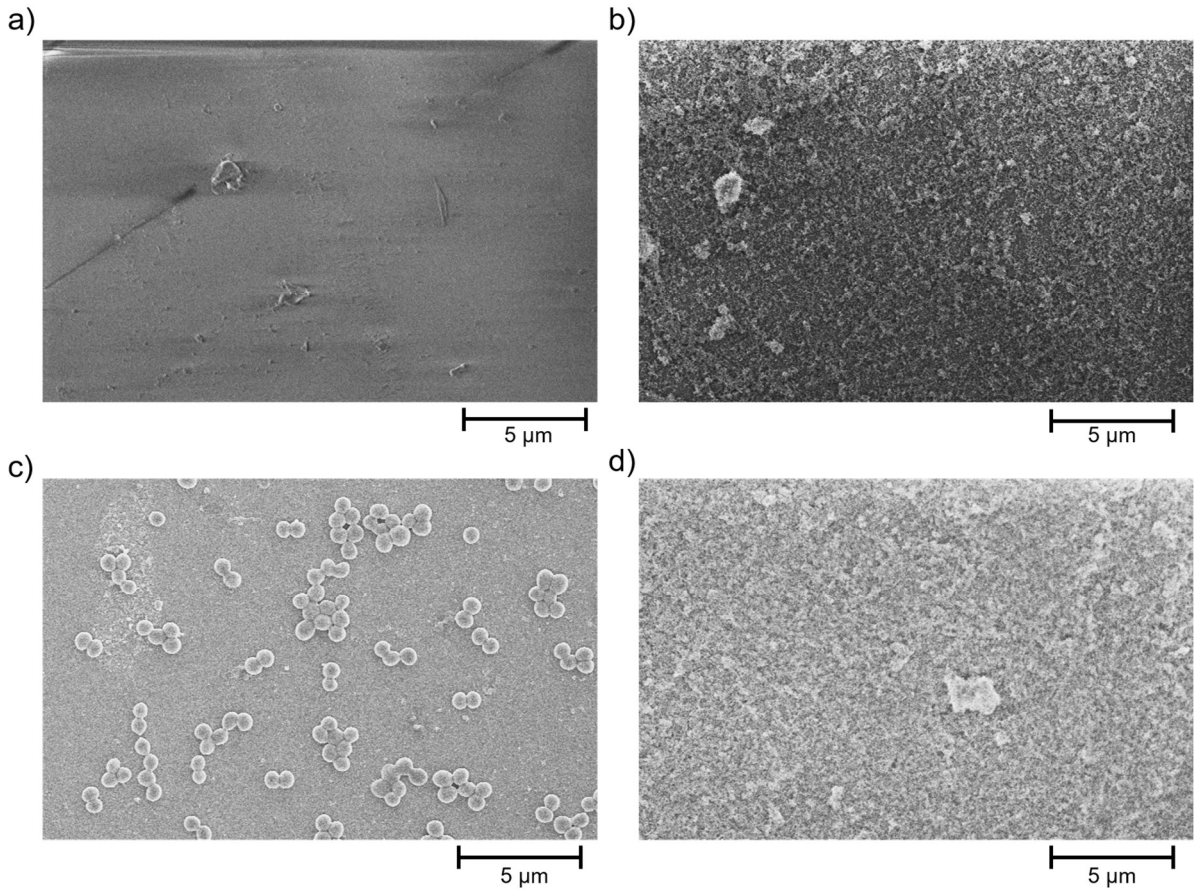

Figure 4.22: SEM images of a) uncoated glass b) glass coated with Si[HMDS](50)-S50PA(50) c) glass after 5 h incubation with *S. aureus* and d) glass coated with Si[HMDS](50)-S50PA(50) after 5 h incubation with *S. aureus*.

4.5 Conclusions

In summary it has been demonstrated that high sulfur content polymer nanoparticles can be used to fabricate coatings by spray deposition. Spray deposition of nanoparticles on glass has been shown to increase the hydrophobicity of the surface relative to uncoated glass. Adhesion of the polymeric nanoparticles to glass can be promoted by thermal treatment, although at the expense of the structure of the nanoparticles which were found to form bulk material after heating. Improving the adhesion of nanoparticles to surfaces by methods that do not compromise the nanoparticle structure should be prioritised in future work to develop their applications as surface coatings.

Spray coating of silica-polymer composites, where the silica core acts as a nanoparticle scaffold for the polymer, have been shown to form superhydrophobic coatings on glass. The composite coating was found to have WCA > 170 ° and sliding angles of < 10 °. Compared to uncoated glass, the surfaces were found to have an inhibitory effect against methicillin-resistant *S. aureus* by inhibiting the cells adhered to the surface of the material, and inhibiting cells in the surrounding medium. SEM imaging of the coated and pristine surface before and after incubation with *S. aureus* also showed that the superhydrophobic coating was able to inhibit the proliferation of *S. aureus* on its surface compared to pristine glass.

4.6 Experimental Details

4.6.1 Materials and Equipment

Materials: Ground sulfur sublimed powder reagent grade ≥99.5% was obtained from Brenntag U.K. and Ireland. (S)-(−)-perillyl alcohol food grade ≥95%, fumed silica 0.2-0.3 μm avg. particle size, Luria−Bertani broth (Miller), LB agar and phosphate buffered saline (PBS) and crystal violet were purchased from Sigma-Aldrich. Methicillin-resistant *S. aureus* strain USA300 and *P. aeruginosa* PAO1 were cultured from frozen stocks stored at the University of Liverpool.

DSC was performed using a TA Instruments Q200 DSC, programmed using a heat/cool/heat method for three cycles by heating to 150 °C, cooling to −80 °C, and reramping to 150 °C. The heating/cooling rate was set to 10 °C/min. The second heating curve was analysed and used to determine the glass transition temperature

DLS measurements were obtained at 25 °C on a Malvern Instruments Ltd. Zetasizer Nano Series Nano-ZS spectrometer using the automatic attenuator and measurement position settings. The z-average diameter was measured using 1 cm path length disposable cuvettes. Particles were dispersed at a range of concentrations to determine a size independent of the concentration.

SEM was performed using a Hitachi S-4800 cold-field emission scanning electron microscope. The particle suspensions were sprayed onto silicon wafer chips which were subsequently mounted onto SEM stubs using conductive silver paint. Prior to imaging, samples were coated with gold using a current of 120 mA for 15 s to give approximately 15 nm gold coatings using a Quorum S1505 ES sputter coater.

FT-IR spectroscopy was conducted with a Bruker Vertex V70 FT-IR spectrometer, with a germanium ATR crystal.

Static contact angle measurements were obtained using a DSA100 Expert Drop Shape Analyser (Kruss GmbH) operating with Young-Laplace fitting and using 5 µL water droplets.

4.6.2 Polymer Synthesis

S50-PA was synthesised in 40 mL glass vials placed in aluminium heating blocks. 5 g of sulfur powder was allowed to melt at 135 °C. The temperature was increased to 175 °C and 5 g of perillyl alcohol was added to the molten sulfur with stirring. The reaction mixture became viscous and increasingly dark in colour with time. Once homogenous the viscous mixture was poured into silicone moulds and cured overnight in an oven at 140 °C. The resulting material was a dark red glassy solid which was ground into a powder using a pestle and mortar.

4.6.3 Hydrophobisation of Silica

A solution of hexamethyldisilazane (HMDS, 1 mL) in toluene (100 mL) was added to a suspension of silica (fumed, 0.2 – 0.3 µm) (10 g) in toluene (250 mL) and refluxed at 120 °C for 24 h, with magnetic stirring. Silica particles were centrifuged and washed once in toluene and twice in ethanol (2000 rpm for 10 min per wash), before being dried in the oven at 80 °C overnight.[42]

4.6.4 Preparation of Silica-Polymer Composites

Silica (fumed, 0.2 – 0.3 µm) was suspended in solubilised S50-PA in THF (1 mg/ml polymer concentration) at various masses to give silica:polymer ratios of 90:10, 70:30 and 50:50. The suspensions were vortexed for 1 minute and sonicated for a minimum of 30 seconds. THF was evaporated by rotary evaporation to give powdered samples. The powders were pale yellow, but darker at increases polymer content.[34]

4.6.5 Spray Coating of Surfaces

Silica-polymer composites (4.6.4 Preparation of Silica-Polymer Composites) were dispersed in ethanol to a concentration of 1 mg/ml. The dispersions were sonicated for 30

seconds to ensure thorough mixing of the dispersions. The dispersions were loaded into an airbrush gun (Voilamart). The dispersed composites were sprayed onto glass substrates, using a compression pump at a pressure of 2 bar and a working distance of approximately 10 cm.

4.6.6 Antibacterial Testing of Si-S50PA Powders

The antibacterial efficiency of Si-S50PA powders were assessed against *S. aureus* USA300. Uncoated fumed silica and untreated bacterial cultures were used as control samples. Overnight cultured bacteria prepared in LB broth were diluted to 10^5 CFU/mL (OD600 = 0.001) in LB. Powdered samples were dispersed to 1 mg/ml and 5 mg/ml in diluted bacterial suspension in 15 ml falcon tubes. The samples were placed on an agitator and incubated at 37 °C for 5 h. After incubation, an aliquot from each sample was serially diluted in PBS and the viable cells were enumerated by the Miles and Misra method. Each sample was tested in triplicate.

4.6.7 Antibacterial Testing of Coated Surfaces

1 cm x 1 cm square glass samples coated with composite (4.6.5 Spray Coating of Surfaces) were placed into separate wells of a 24-well plate. Uncoated glass and glass coated with bulk S50-PA, fumed silica and hydrophobic silica were used as controls. 500 µl of overnight cultured bacteria (*S. aureus* USA300 and *P. aeruginosa* PAO1) prepared in LB broth diluted to 10^5 CFU/mL (OD600 = 0.001) was added to each well. Samples were statically incubated for 5 h at 37 °C, after which the surrounding bacterial solution was removed. Viable cells in the removed solution were enumerated using the Miles and Misra method using PBS as the diluent. To enumerate cells adhered to the sample surfaces, the samples were rinsed with 1 mL of PBS to remove any planktonic cells before vortexing in 1 mL of LB broth for 10 s to remove any adhered cells.

4.6.8 Biofilm Staining Assay

S. aureus USA300 and *P. aeruginosa* PAO1 were used to evaluate biofilm formation on glass (1 cm x 1 cm) coated with composite suspensions. Control surfaces were prepared by spray deposition of fumed silica on glass (1 cm x 1 cm). Surfaces were placed in separate wells of a 24-well plate. 500 µl of overnight cultured bacteria prepared in LB broth diluted to 10^5 CFU/mL (OD600 = 0.001) was added to each well. The well plate was incubated statically at 37 °C for 24 and 48 hr. After incubation the solutions from the well plate were discarded and the wells were rinsed with 1 ml PBS, which was then discarded and the plate allowed to dry. The dried wells were stained with 1 ml 0.25% crystal violet for 30 minutes. The dye was discarded, the well plate was thoroughly rinsed with water and allowed to dry. 1 ml of ethanol was added to each well in order to solubilise any remaining dye. The absorbance at 600 nm was measured using ethanol as a blank.

4.6.9 Imaging of Surfaces After Incubation

The 1 cm x 1 cm coated samples and uncoated glass were statically incubated with 500 µL *S. aureus* USA300 in LB medium (10^5 CFU/ml) in a 24-well plate. After incubation the samples were rinsed gently with PBS, and soaked overnight in glutardialdehyde. The samples were rinsed with PBS and soaked in series of ethanol dilutions (50, 70, 90, 95 and 100 % v/v) for a minimum of 5 minutes in each dilution. The samples were mounted onto SEM stubs using conductive silver paint. Prior to imaging, samples were coated with gold using a current of 120 mA for 15 s to give approximately 15 nm gold coatings using a Quorum S1505 ES sputter coater.

4.7 References

1 M. Moreno-Couranjou, R. Mauchauffé, S. Bonot, C. Detrembleur and P. Choquet, *J. Mater. Chem. B*, 2018, **6**, 614–623.

2 R. M. Donlan, *Emerg. Infect. Dis.*, 2002, **8**, 881–890.

3 K. A. Floyd, A. R. Eberly and M. Hadjifrangiskou, eds. Y. Deng and W. B. T.-B. and I. M. D. Lv, Woodhead Publishing, 2017, pp. 47–95.

4 I. Alav, J. M. Sutton and K. Rahman, *J. Antimicrob. Chemother.*, 2018, **73**, 8, 2003-2020.

5 J. Tasse, S. Trouillet-Assant, J. Josse, P. Martins-Simões, F. Valour, C. Langlois-Jacques, S. Badel-Berchoux, C. Provot, T. Bernardi, T. Ferry and F. Laurent, *PLoS One*, 2018, **13**, e0200064.

6 N. M. Maurice, B. Bedi and R. T. Sadikot, *Am. J. Respir. Cell Mol. Biol.*, 2018, **58**, 428–439.

7 R. Sarvari, B. Naghili, S. Agbolaghi, S. Abbaspoor, H. B. Baghi, V. Poortahmasebi, M. Sadrmohammadi and M. Hosseini, *Int. J. Polym. Mater. Polym. Biomater.*, 2022, **0**, 1–42.

8 S. Parvate, P. Dixit and S. Chattopadhyay, *J. Phys. Chem. B*, 2020, **124**, 1323–1360.

9 M. Yamamoto, N. Nishikawa, H. Mayama, Y. Nonomura, S. Yokojima, S. Nakamura and K. Uchida, *Langmuir*, 2015, **31**, 7355–7363.

10 R. N. Wenzel, *Ind. Eng. Chem.*, 1936, **28**, 988–994.

11 A. B. D. Cassie and S. Baxter, *Trans. Faraday Soc.*, 1944, **40**, 546–551.

12 A. Kamaraj, V. Shaw and M. Sundaram, *Novel Fabrication of Un-Coated Super-Hydrophobic Aluminum via Pulsed Electrochemical Surface Modification*, 2015, vol. 1.

13 A. Giacomello, S. Meloni, M. Chinappi and C. M. Casciola, *Langmuir*, 2012, **28**, 10764–10772.

14 H. Y. Erbil, *Langmuir*, 2020, **36**, 2493–2509.

15 L. Cao, A. K. Jones, V. K. Sikka, J. Wu and D. Gao, *Langmuir*, 2009, **25**, 12444–12448.

16 M. A. Sarshar, D. Song, C. Swarctz, J. Lee and C.-H. Choi, *Langmuir*, 2018, **34**, 13821–13827.

17 B. Chen, J. Qiu, E. Sakai, N. Kanazawa, R. Liang and H. Feng, *ACS Appl. Mater. Interfaces*, 2016, **8**, 17659–17667.

18 R. Pallye and S. Ghosh, *IOP Conf. Ser. Mater. Sci. Eng.*, 2020, **827**, 12003.

19 M. Haji-Savameri, A. Irannejad, S. Norouzi-Apourvari, M. Schaffie and A. Hemmati-Sarapardeh, *Sci. Rep.*, 2022, **12**, 17059.

20 E. J. Falde, S. T. Yohe, Y. L. Colson and M. W. Grinstaff, *Biomaterials*, 2016, **104**, 87–103.

21 V. K. Pandey, K. R. Srivastava, G. Ajmal, V. K. Thakur, V. K. Gupta, S. N. Upadhyay and P. K. Mishra, *Int. J. Mol. Sci.*, 2019, **20**, 20, 5110.

22 Z. Li, A. Milionis, Y. Zheng, M. Yee, L. Codispoti, F. Tan, D. Poulikakos and C. H. Yap, *Nat. Commun.*, 2019, **10**, 5562.

23 H. Zheng, M. Pan, J. Wen, J. Yuan, L. Zhu and H. Yu, *Ind. Eng. Chem. Res.*, 2019, **58**, 8050–8060.

24 S. M. R. Razavi, J. Oh, R. T. Haasch, K. Kim, M. Masoomi, R. Bagheri, J. M. Slauch and N. Miljkovic, *ACS Sustain. Chem. Eng.*, 2019, **7**, 14509–14520.

25 C. Sanchez-Cano and M. Carril, *Int. J. Mol. Sci.*, 2021, **21**, 3, 1007.

26 M. J. H. Worthington, C. J. Shearer, L. J. Esdaile, J. A. Campbell, C. T. Gibson, S. K. Legg, Y. Yin, N. A. Lundquist, J. R. Gascooke, I. S. Albuquerque, J. G. Shapter, G. G. Andersson, D. A. Lewis, G. J. L. Bernardes and J. M. Chalker, *Adv. Sustain. Syst.*, 2018, **2**, 1800024.

27 Z. Deng, A. Hoefling, P. Théato and K. Lienkamp, *Macromol. Chem. Phys.*, 2018, **219**, 1700497.

28 M. Mann, B. Zhang, S. J. Tonkin, C. T. Gibson, Z. Jia, T. Hasell and J. M. Chalker, *Polym. Chem.*, 2022, **13**, 1320–1327.

29 J. M. Scheiger, C. Direksilp, P. Falkenstein, A. Welle, M. Koenig, S. Heissler, J. Matysik, P. A. Levkin and P. Theato, *Angew. Chemie Int. Ed.*, 2020, **59**, 18639–18645.

30 A. P. Grimm, J. M. Scheiger, P. W. Roesky and P. Théato, *Polym. Chem.*, 2022, **13**, 5852–5860.

31 C. Miao, X. Xun, L. J. Dodd, S. Niu, H. Wang, P. Yan, X.-C. Wang, J. Li, X. Wu, T. Hasell and Z.-J. Quan, *ACS Appl. Polym. Mater.*, 2022, **4**, 4901–4911.

32 C. Miao, P. Yan, H. Liu, S. Cai, L. Dodd, H. Wang, X. Deng, J. Li, X.-C. Wang, X. Hu, X. Wu, T. Hasell and Z.-J. Quan, *Bull. Chem. Soc. Jpn.*, 2022, **95**, 1253–1262.

33 Z. Li, M. Cao, P. Li, Y. Zhao, H. Bai, Y. Wu and L. Jiang, *Matter*, 2019, **1**, 661–673.

34 X. Wu, J. Smith, S. Petcher, B. Zhang, D. Parker, J. Griffin and T. Hasell, *Nat. Commun.*, 2019, **10**, 647.

35 K. Dick, T. Dhanasekaran, Z. Zhang and D. Meisel, *J. Am. Chem. Soc.*, 2002, **124**, 2312–2317.

36 K. Panwar, M. Jassal and A. K. Agrawal, *Particuology*, 2015, **19**, 107–112.

37 K. N. Al-Milaji and H. Zhao, *J. Phys. Chem. C*, 2019, **123**, 12029–12041.

38 T. I. Suratwala, M. L. Hanna, E. L. Miller, P. K. Whitman, I. M. Thomas, P. R. Ehrmann, R. S. Maxwell and A. K. Burnham, *J. Non. Cryst. Solids*, 2003, **316**, 349–363.

39 X. Zhang, F. Zheng, L. Ye, P. Xiong, L. Yan, W. Yang and B. Jiang, *RSC Adv.*, 2014, **4**, 9838–9841.

40 X. Zhang, F. Zheng, L. Ye, P. Xiong, L. Yan, W. Yang and B. Jiang, *RSC Adv.*, 2014, **4**, 9838–9841.

41 S. Haukka and A. Root, *J. Phys. Chem.*, 1994, **98**, 1695–1703.

42 R. L. Upton, R. A. Dop, E. Sadler, A. M. Lunt, D. R. Neill, T. Hasell and C. R. Crick, *J.*

Mater. Chem. B, 2022, **10**, 4153–4162.

43 J.-A. Hennekinne, M.-L. De Buyser and S. Dragacci, *FEMS Microbiol. Rev.*, 2012, **36**, 815–836.

4.8 Appendix

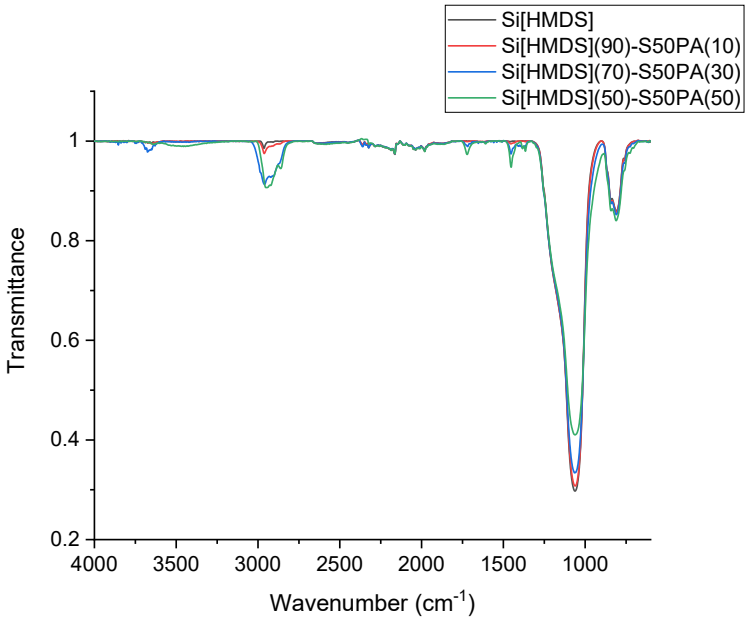

Appendix 4.1: FT-IR spectra of Si[HMDS] and Si[HMDS](X)-S50PA(Y) composites, where X=wt.% of silica and Y=wt.% S50-PA.

Chapter 5

Conclusions and Future Work

5.1 Conclusions

Antimicrobial resistance is one of the most serious global threats of the century. In particular, antibacterial resistance is of most concern due to the high rates of resistance in bacteria that cause common infections and diseases.[1] All current approved antibiotics have come across resistance by atleast some of their target pathogens.[2] Infections caused by multidrug-resistant bacteria are becoming more common and present a threat to global public health by reducing the probability of effective treatment, and increasing the mortality rate associated with common bacterial infections.[3] Of particular concern are infections caused by *Enterococcus faecium, S. aureus*, *Klebsiella pneumoniae*, *Acinetobacter baumannii*, *P. aeruginosa*, and *Enterobacter* species, also known collectively as the ESKAPE pathogens.[4] Resistance of bacteria to antibiotics is continuing to emerge, whereas the rate at which novel antibiotics are being developed are decreasing.[3] The need for alternative therapies and methods to treat and control multidrug-resistant pathogens is of utmost importance.

Sulfur and its organic and inorganic compounds are known to have several biological activities such as antioxidant, anticancer, antimicrobial and radical-scavenging properties.[5] The biological applications of elemental sulfur are often limited due to its hydrophobicity and low water solubility.[6] Sulfides and polysulfides have reported antimicrobial activities, which is thought to be due to the S-S bond within sulfide containing compounds, and is thought that higher order sulfides such as polysulfides have greater antimicrobial activities compared to lower order polysulfides.[7] Polysulfur, formed by ring opening polymerisation of elemental sulfur is unstable and will revert back to S_8, limiting the use of polysulfur.[8] Inverse vulcanisation is a method to produce high sulfur content polymers that are stable to depolymerisation.[8] Prior to this work, inverse vulcanised polymers were found to have antimicrobial activity, however only two comonomers had been studied, where the antibacterial properties of the polymers were poorly understood.[9,10] The aims of this work in summary, was

to further understand the antibacterial properties of high sulfur content polymers synthesised by inverse vulcanisation, and to investigate their potential application as surface coatings.

Further investigations into the antibacterial properties of inverse vulcanised polymers was discussed in Chapter 2. A small library of polymers was synthesised by varying the type of comonomer and the sulfur:comonomer ratios within the reaction feedstock. The antibacterial activity of the polymers were assessed against Gram-positive methicillin-resistant *S. aureus* and Gram-negative *P. aeruginosa*. Polymers which have not been previously reported for their antibacterial activity was investigated. Furthermore, the antibacterial activity of high sulfur content polymers synthesised by inverse vulcanisation have not been previously investigated against *P. aeruginosa*. The antibacterial properties of the materials were effected by the comonomer type and the sulfur content of the polymer. Furthermore, it was found that the incubation temperature at which the polymers were tested effected their antibacterial properties. Polymers tested at temperatures above their T_g had increased antibacterial activity compared to at temperatures below their T_g. The polymers were found to have an inhibitory effect against both surface-associated cells, and cells in the surrounding medium, both of which were effected by the physical state of the polymer. The materials were also found to inhibit *S. aureus* and *P. aeruginosa* biofilm formation on their surfaces. This demonstrates that high sulfur content polymers have an inhibitory effect against Gram-positive and Gram-negative pathogens and that the antibacterial properties of the polymers are influenced by their comonomer type and sulfur:comonomer ratio, which ultimately alters their T_g. These findings were not previously known in the literature regarding the antibacterial properties of high sulfur content polymers prepared by inverse vulcanisation.

Elemental sulfur has poor water solubility, to circumvent this issue, sulfur nanoparticles have been reported which exhibit antibacterial activity.[5,11,12] Similarly to elemental sulfur, high sulfur content polymers prepared by inverse vulcanisation often have poor water solubility and

dispersibility, which may limit their use for biological applications. Sulfur polymer nanoparticles prepared by inverse vulcanisation contain organic moieties due to the comonomers used, which may provide sites for further functionalisation, where functionalisation of pure sulfur nanoparticles may be difficult. In Chapter 3, the preparation and biological properties of high sulfur content polymer nanoparticles was discussed. The nanoparticles were found to be water dispersible, with average hydrodynamic radii of approximately 200 nm. Nanoparticles prepared in the presence of Tween80 were found to be salt-stable, demonstrating that particle aggregation in biological media can be prevented. The nanoparticles exhibited an inhibitory effect against methicillin-resistant *S. aureus* and *P. aeruginosa,* and were shown to inhibit *S. aureus* biofilm formation over 48 h. Nanoparticle-bacteria charge interactions were found to be an important factor for the evaluation of the antibacterial activity of the particles, as demonstrated by an increased inhibitory effect against less-negatively charged *P. aeruginosa* strain LESB65, compared to a more negatively charged mutant. A dual-therapy of tobramycin combined with nanoparticles was assessed against a multidrug-resistant *P. aeruginosa* strain B9, demonstrating the potential of using the polymer nanoparticles in combination with other drugs, an application that has not been previously reported. This may enable use of lower antibiotic concentrations, for antimicrobial stewardship, or help alleviate the side effects of long term, high dose, antimicrobial therapy. Furthermore, no dose-dependent toxicity was observed after treatment of mammalian liver cells with particles, demonstrating that high sulfur polymer nanoparticles may exhibit low cytotoxicity. In the presence of thiols such as cysteine, H_2S was generated, suggesting that one potential mechanism of action of the polymer nanoparticles may be due to interaction of particles with cellular thiols. In summary, the work discussed in Chapter 3 demonstrates that sulfur polymer nanoparticles have antibacterial activity along with low cytotoxicity, along with good water

dispersibility and stability makes the particles good candidates for further development for biological applications.

Hospital-acquired infections (HAIs) are defined by the World Health Organization as infections that develop after 48 h of hospitalisation and that were not present or incubating at the time of admission.[13] In recent years, there has been interest in employing antimicrobial surfaces to help limit microbial contamination. Surfaces can act as microbial reservoirs, which upon being touched can be spread to other healthcare workers or patients and, in turn, lead to HAIs. Any method that can reduce the prevalence or viability of microbes on a surface could help to reduce the frequency of HAIs.[14] The fabrication of surface coatings of high sulfur content polymers was investigated and discussed in Chapter 4. Spray deposition of sulfur polymer nanoparticles was shown to increase the hydrophobicity of glass, however, the particles showed poor adhesion to glass. Thermal treatment of the coated substrate improved the adhesion of the particles, however at the expense of loss of surface topography which is important to achieve superhydrophobicity. Silica-polymer composite powders were prepared and found to have good water dispersibility and antibacterial activity, spray deposition of the composite resulted in increased hydrophobicity, but did not achieve superhydrophobicity. Hydrophobisation of the silica-polymer composite resulted in superhydrophobic surfaces which were found to inhibit both *S. aureus* and *P. aeruginosa*. This demonstrates that sulfur polymers have the potential to be used as coatings that are water-repellent and inhibit bacterial adhesion.

5.2 Future Work

Despite the progress made to investigate the antibacterial properties of high sulfur content polymers prepared by inverse vulcanisation, as demonstrated in this thesis, there remains unanswered questions and gaps in understanding the origin of the properties. Many sulfur containing compounds, in particular, sulfide containing compounds are known to have antibacterial activity.[15] Few of these compounds have been used in antibacterial treatment and clinical therapy due to poorly defined mechanisms of action, specificity and biocompatibility.[15] This issue also stands for sulfur polymers prepared by inverse vulcanisation as discussed in this thesis. Concerning both bulk polymers and polymer nanoparticles, the mechanism of action of sulfur polymers remains poorly understood. In Chapter 3 it was discussed that the polymer nanoparticles may exert an antibacterial effect by reaction with cellular thiols, however, this may not be the only mechanism of action, and during this study we are unable to conclude that reaction with thiols results in an inhibitory effect or not. Furthermore, it is not understood why the polymeric nanoparticles show an inhibitory effect against bacterial cells, but do not show a dose-dependent toxicity effect against mammalian liver cells. If interaction of the particles with cellular thiols results in inhibition of bacteria, as has been reported for other sulfide containing molecules, this inhibitory effect should be non-selective.[16] Determining whether any species are leaching out of the polymeric material is an important consideration for future work, as this may influence the longevity of the antibacterial activity of the materials, or may have implications for their safety. It has been demonstrated that the polymers show an inhibitory effect against both Gram-positive *S. aureus* and Gram-negative *P. aeruginosa*, however, all studies were done using single strain species, rather than a culture containing mixed species. Investigating the behaviour of the materials in mixed species cultures would be important to show if there is selective inhibition against a particular species within a mixture, which has important implications for the use of the materials under real conditions. In summary,

investigating the mechanism of action of sulfur polymers prepared by inverse vulcanisation should be a priority for future work, as this will have important implications for the materials applicability and for investigating resistance mechanisms that bacteria may evolve in response to the materials.

The findings presented in this thesis open up further questions regarding the biological applications of sulfur polymers. Concerning the polymer nanoparticles discussed in Chapter 3, there is scope to develop the nanoparticles for drug delivery methods. The hydrophobicity of the polymers makes the particles good candidates to aid the delivery of hydrophobic drugs that often have poor water solubility and low bioavailability.[17] Future work could be conducted to investigate the potential of the polymer nanoparticles for drug delivery. The polymer nanoparticles may also have the potential to be used in wound dressings or as biomedical coatings such as for catheter coatings. Chapter 4 discussed the fabrication of surface coatings using sulfur polymer nanoparticles and silica-polymer composites. Further work is required to improve the durability of the coatings, as particles showed poor adhesion to the surface following spray deposition. Glass was chosen as the main substrate to investigate the fabrication of coatings, however, other substrates would need to be investigated such as plastics, fabrics and metals.

5.3 References

1 F. Prestinaci, P. Pezzotti and A. Pantosti, *Pathog. Glob. Health*, 2015, **109**, 309–318.

2 D. G. J. Larsson and C.-F. Flach, *Nat. Rev. Microbiol.*, 2022, **20**, 257–269.

3 A. H. Elmaidomy, N. H. Shady, K. M. Abdeljawad, M. B. Elzamkan, H. H. Helmy, E. A. Tarshan, A. N. Adly, Y. H. Hussien, N. G. Sayed, A. Zayed and U. R. Abdelmohsen, *RSC Adv.*, 2022, **12**, 29078–29102.

4 S. K. Panda, S. Buroni, S. S. Swain, A. Bonacorsi, E. A. da Fonseca Amorim, M. Kulshrestha, L. C. N. da Silva and V. Tiwari, *Front. Microbiol.*, 2022, **13**, 1029098.

5 S. Saedi, M. Shokri and J.-W. Rhim, *Arab. J. Chem.*, 2020, **13**, 6580–6588.

6 S. G. Bolton and M. D. Pluth, *Chem. Sci.*, 2020, **11**, 11777–11784.

7 J. Kim, J. Huh, S. Kyung and K. Kyung, *Food Sci. Biotechnol*, 2004, **13**, 235–239.

8 W. J. Chung, J. J. Griebel, E. T. Kim, H. Yoon, A. G. Simmonds, H. J. Ji, P. T. Dirlam, R. S. Glass, J. J. Wie, N. A. Nguyen, B. W. Guralnick, J. Park, Á. Somogyi, P. Theato, M. E. Mackay, Y. E. Sung, K. Char and J. Pyun, *Nat. Chem.*, 2013, **5**, 518–524.

9 J. A. Smith, R. Mulhall, S. Goodman, G. Fleming, H. Allison, R. Raval and T. Hasell, *ACS Omega*, 2020, **5**, 5229–5234.

10 Z. Deng, A. Hoefling, P. Théato and K. Lienkamp, *Macromol. Chem. Phys.*, 2018, **219**, 1700497.

11 S. Shivalkar, F. Arshad, A. K. Sahoo and M. P. Sk, *ACS omega*, 2022, **7**, 33358–33364.

12 S. Shankar, R. Pangeni, J. W. Park and J.-W. Rhim, *Mater. Sci. Eng. C*, 2018, **92**, 508–517.

13 B. J. Hensley and J. R. T. Monson, *Surg.*, 2015, **33**, 528–533.

14 K. Page, M. Wilson and I. P. Parkin, *J. Mater. Chem.*, 2009, **19**, 3819–3831.

15 H. Cao, Q. Wang, X. Wang, L. Chen, J. Jiang and L. Gao, *Accounts Mater. Res.*, 2023, **4**, 115–132.

16 A. Müller, J. Eller, F. Albrecht, P. Prochnow, K. Kuhlmann, J. E. Bandow, A. J. Slusarenko and L. I. O. Leichert, *J. Biol. Chem.*, 2016, **291**, 11477–11490.

17 T. Gunasekaran, T. Haile, T. Nigusse and M. D. Dhanaraju, *Asian Pac. J. Trop. Biomed.*, 2014, **4**, S1-7.